GL-TR-89-0272

Active Probing of Space Plasmas

Chang Chan
Michael B. Silevitch
Elena Villalon

Northeastern University
360 Huntington Avenue
Boston, MA 02115

1 September 1989

Final Report
25 October 1985-30 September 1989

GEOPHYSICS LABORATORY
AIR FORCE SYSTEMS COMMAND
UNITED STATES AIR FORCE
HANSCOM AIR FORCE BASE, MASSACHUSETTS 01731-5000

"This technical report has been reviewed and is approved for publication"

WILLIAM J. BURKE
Contract Monitor

NELSON C. MAYNARD
Branch Chief

FOR THE COMMANDER

RITA C. SAGALYN
Division Director

This report has been reviewed by the ESD Public Affairs Office (PA) and is releasable to the National Technical Information Service (NTIS)

Qualified requestors may obtain additional copies from the Defense Technical Information Center. All others should apply to the National Technical Information Service.

If your address has changed, or if you wish to be removed from the mailing list, or if the addressee is no longer employed by your organization, please notify GL/DAA, Hanscom AFB, MA 01731. This will assist us to maintain a current mailing list.

Do not return copies of this report unless contractual obligations or notices on a specific document requires that it be returned.

Unclassified

SECURITY CLASSIFICATION OF THIS PAGE

REPORT DOCUMENTATION PAGE

Form Approved OMB No. 0704-0188

1a. REPORT SECURITY CLASSIFICATION
Unclassified

1b. RESTRICTIVE MARKINGS

2a. SECURITY CLASSIFICATION AUTHORITY

2b. DECLASSIFICATION/DOWNGRADING SCHEDULE

3. DISTRIBUTION/AVAILABILITY OF REPORT
Approved for public release;
Distribution unlimited

4. PERFORMING ORGANIZATION REPORT NUMBER(S)

5. MONITORING ORGANIZATION REPORT NUMBER(S)
GL-TR-89-0272

6a. NAME OF PERFORMING ORGANIZATION
Northeastern University

6b. OFFICE SYMBOL *(If applicable)*

7a. NAME OF MONITORING ORGANIZATION
Geophysics Laboratory

6c. ADDRESS (City, State, and ZIP Code)
360 Huntington Avenue
Boston, MA 02115

7b. ADDRESS (City, State, and ZIP Code)
Hanscom AFB, MA 01731-5000

8a. NAME OF FUNDING/SPONSORING ORGANIZATION

8b. OFFICE SYMBOL *(If applicable)*

9. PROCUREMENT INSTRUMENT IDENTIFICATION NUMBER
F19628-85-K-0053

8c. ADDRESS (City, State, and ZIP Code)

10. SOURCE OF FUNDING NUMBERS

PROGRAM ELEMENT NO	PROJECT NO	TASK NO	WORK UNIT ACCESSION NO
62101F	7661	14	BE

11. TITLE *(Include Security Classification)*
Active Probing of Space Plasmas

12. PERSONAL AUTHOR(S)
Chang Chan; Michael B. Silevitch; Elena Villalon

13a. TYPE OF REPORT	13b. TIME COVERED	14. DATE OF REPORT (Year, Month, Day)	15. PAGE COUNT
Final Report	FROM 10-25-85 TO 9-30-89	1989/09/01	114

16. SUPPLEMENTARY NOTATION

17. COSATI CODES

FIELD	GROUP	SUB-GROUP

18. SUBJECT TERMS *(Continue on reverse if necessary and identify by block number)*
Electron acceleration; Wave particle interaction; Substorm dynamics; Spacecraft interactions. (EDC)

19. ABSTRACT *(Continue on reverse if necessary and identify by block number)*

During the course of the research period our efforts were focused on the following areas:

I. An Examination of Stochastic Acceleration Mechanisms in the Ionosphere;

II. A Study of Nonequilibrium Dynamics of the Coupled Magnetosphere - Ionosphere System, (3).

III. Laboratory Studies of Active Space Experiments. Reprints include: Dynamics of charged particles in the [illegible] wake of a very negatively charged body; --1 Laboratory experiment and numerical simulation; [illegible] study of the electron temperature in the near wake of a conducting body; [illegible] for auroral breakup during substorms. Substorm breakup on closed field lines; New [illegible] substorm onsets; --1 The pre-breakup and triggering [illegible]; [illegible] of the westward traveling surge and the [illegible] of Pi 2 pulsations; [illegible] electron acceleration by electromagnetic waves near regions of plasma resonances; Relativistic particle acceleration by oblique propagating electromagnetic fields. Some consequences [illegible] intense electromagnetic wave [illegible]

20. DISTRIBUTION/AVAILABILITY OF ABSTRACT
☐ UNCLASSIFIED/UNLIMITED ☐ SAME AS RPT ☐ DTIC USERS

21. ABSTRACT SECURITY CLASSIFICATION
Unclassified

22a. NAME OF RESPONSIBLE INDIVIDUAL
William J. Burke

22b. TELEPHONE *(Include Area Code)*

22c. OFFICE SYMBOL
GL/PHG

DD Form 1473, JUN 86 — *Previous editions are obsolete.*

SECURITY CLASSIFICATION OF THIS PAGE
Unclassified

TABLE OF CONTENTS

Publication Reprints

1. W.L. Burke, E. Villalon, P.L. Rothwell and M.B. Silevitch, *Some Consequences of Electromagnetic Wave Injection into Space Plasmas*, TPL - Publication 86-49 (NASA Jet Propulsion Lab, California Inst. Tech.) p. 213 (1986).

2. E. Villalon, *Ionospheric Electron Acceleration by Short Wavelength Electrostatic Waves*, Physics of Space Plasma, SPI *Conference Proceedings and Reprint Series* 7, 317 (1987).

3. E. Villalon and W.L. Burke, *Relativistic Particle Acceleration by Obliquely Propagating Electromagnetic Fields*, Phys. Fluids 30, (1987).

4. E. Villalon, *Ionospheric Electron Acceleration by Electromagnetic Waves Near Regions of Plasma Resonances*, J. Geophys. Res., 94, 2717 (1989).

5. P.L. Rothwell, M.B. Silevitch and L.P. Block, *Pi2 Pulsations and the Westward Travelling Surge*, J. Geophys Res. 91, 6921 (1986).

6. P.L. Rothwell, M.B. Silevitch, L.P. Block and P. Tanskanen, *A Model of the Westward Travelling Surge and the Generation of Pi2 Pulsations*, Geophys Res. 93, 8613 (1988).

7. M. Silevitch, P.L. Rothwell and L.P. Block, *Magnetosphere-Ionosphere Coupling and Substorm Dynamics. Physics of Space Plasmas SPI Conference Proceedings*, Vol. 7, T. Chang editor, Cambridge, MA (1987).

8. P.L. Rothwell, L.P. Block, M.B. Silevitch and C-G Falthammar, *A New Model for Substorm Onsets: The Prebreak up and Triggering Regimes*, Geophys Res. Lett. 15, 1279 (1988).

9. P.L. Rothwell, L.P. Block, M.B. Silevitch, and C-G Falthammar, *Substorm Breakup on Closed Field Lines*, Adv. Space Res. 8 p. (9) 437 (1988).

10. P.L. Rothwell, L.P. Block, M.B. Silevitch and C-G Falthammar, *A New Model for Auroral Breakup During Substorms* IEEE Trans Plasma Sci. 17, 150 (1989).

11. C. Chan, M.A. Morgan and R.C. Allen, *Electron Dynamics in the Near Wake of a Conducting Body*, IEEE Trans. Plasma Sci PS-14, 915 (1986).

12. M.A. Morgan, C. Chan and R. Allen, *A Laboratory Study of the Electron Temperature in the Wear Wake of a Conducting Body*, Geophys, Res. Lett., 14, 1170 (1987).

13. M.A. Morgan, C. Chan, D.L. Cooke, and M.F. Tautz, *The Dynamics of Charged Particles in the Near Wake of a Very Negatively Charged Body - Laboratory Experiment and Numerical Simulation*, IEEE Trans. Plasma Sci., 17, 220 (1989).

INTRODUCTION

This document is the final report of the investigation "Active Probing of Space Plasmas". During the course of the research period, we concentrated our efforts into the three areas:

I. An Examination of Stochastic Electron Acceleration Mechanisms in the Ionosphere.

II. A Study of the Nonequilibrium Dynamics of the Coupled Magnetosphere-Ionosphere System.

III. Laboratory Studies of Active Space Experiments

In the remainder of this report, we shall briefly summarize the results associated with each of the above three research areas.

We also include reprints of all journal publications which resulted through the auspices of this contract. These articles are contained at the end of this report.

DESCRIPTION OF RESEARCH

Let us turn now to a discussion of each of the three research areas.

I. Electron Acceleration by Intense EM waves

Throughout the contract period we have studied in detail the theory of the interaction of oblique high-frequency electromagnetic (EM) waves with plasma particles. We have published two major papers which contain most of the theory we developed; in addition we have also published two articles in conference proceedings. This analysis is of interest to ionospheric modification research which uses the ionosphere as a natural plasma laboratory without walls, to study high power radiowave propagation and associated non-linear phenomena. The EM fields can be radiated either from the ground or from satellites or rockets. These waves interact with the ambient electrons and may accelerate them to high energies. Suitable ground- based high power facilities are located at HIPAS-UCLA (Alaska), Arecibo-Cornell (Puerto Rico), and Tromso (Norway). They have produced interesting observations on the propagation of the radiowaves and the plasma response to them. Experiments from satellites or rockets such as the WISP/HP colThe

effectiveness of this mechanism is largely dependent on the value of the incident frequency. Calculations on single particle acceleration show that initially cold electrons can gain 1 or 2 keV for moderate power levels ($1 mW/m^2$) if the wave frequency is chosen equal to the second harmonic of the cyclotron frequency.

The following publications (reprinted herein) have resulted from this aspect of our research.

E. Villalon, *Ionospheric Electron Acceleration by Short Wavelength Electrostatic Waves*, Physics of Space Plasma, SPI *Conference Proceedings and Reprint Series* 7, 317 (1987).

E. Villalon and W.L. Burke, *Relativistic Particle Acceleration by Obliquely Propagating Electromagnetic Fields*, Phys. Fluids 30, (1987).

E. Villalon, *Ionospheric Electron Acceleration by Electromagnetic Waves Near Regions of Plasma Resonances*, J. Geophys. Res., 94, 2717 (1989).

II. Nonequilibrium Dynamics of a Coupled Magnetosphere-Ionosphere System

We have initiated a new line of research and published a first article in the proceedings of the TPL conference (1986). It studied the dynamics of the interaction of Radiation Belt particles with electromagnetic waves. An important motivation for this line of investigation is the need to develop an analytical framework for dynamic Radiation Belt models which can be used to support the upcoming CRRES active experiment mission. Based on the ideas of the "Alfven Maser" by Bespalov and Trakhtengerts we have proposed a theoretical scheme for dumping both electrons and protons from the Belts. The magnetosphere can be consided as a gigantic maser where whistler and Alfven waves are trapped between the ionospheric mirrors and grow in amplitude as they cross back and forth across the equatorial regions. We have derived a set of equations based on the Fokker-Planck theory of pitch-angle diffusion, which describe the evolution in time of the number of particles in the flux tube and the energy density of waves. The reflection of waves in the ionosphere is very relevant to the efficiency of the Alfven maser. We may use RF energy to heat the ionosphere at the foot of the flux tube to raise the height integrated conductivity and improve wave reflection. In addition to external ionospheric perturbations particle precipitation also raises ionospheric conductivity. At present we are preparing a longer article with these ideas which will be submitted to the Journal of Geophysical Research.

We have also focussed our attention on the propagation of ionospheric disturbences during substorms including associated magnetospheric waves. This work has been reported in the following papers (which are reported herein).

P.L. Rothwell, M.B. Silevitch and L.P. Block, *Pi2 Pulsations and the Westward Travelling Surge*, J. Geophys Res. 91, 6921 (1986).

W.L. Burke, E. Villalon, P.L. Rothwell and M.B. Silevitch, *Some Consequences of Electromagnetic Wave Injection into Space Plasmas*, TPL - Publication 86-19 (NASA Jet Propulsion Lab, California Inst. Tech.) p. 213 (1986).

P.L. Rothwell, M.B. Silevitch, L.P. Block and P. Tanskanen, *A Model of the Westward Travelling Surge and the Generation of Pi2 Pulsations*, J. Geophys Res 93, 8613 (1988).

M. Silevitch, P.L. Rothwell and L.P. Block, *Magnetosphere-Ionosphere Coupling and Substorm Dynamics*, *Physics of Space Plasmas SPI Conference Proceedings*, Vol. 7, T. Chang editor, Cambridge, MA (1987).

P.L. Rothwell, L.P. Block, M. B. Silevitch and C-G Falthammar, *A New Model for Substorm Onsets: The Prebreak up and Triggering Regimes*, Geophys Res. Lett. 15, 1279 (1988).

P.L. Rothwell, L.P. Block, M.B. Silvetich, and C-G Falthammar, *Substorm Breakup on Closed Field Lines*, Adv. Space Res. 8 p. (9)137 (1988).

P.L. Rothwell, L.P. Block, M.B. Silevitch and C-G Falthammar, *A New Model for Auroral Breakup During Substorms* IEEE Trans Plasma Sci. 17, 150 (1989).

III. Laboratory Studies of Active Space Experiments

During the past three years we have successfully achieved a large volume, low density plasma that is suitable for simulations of certain space phenomena in the "Jumbo" chamber at the Air Force Geophysical Laboratory, Hanscom, MA. Much time has been spent in characterizing the baseline plasma parameters for this plasma.

The plasma can be produced by two techniques. The first technique consists of two large arrays of hot filament cathodes. This system produced a cylindrical plasma of roughly 1m in radius and 1.5 m in length. We have so far achieved the following plasma parameters:

Electron density	$N_e \simeq 10^4 \rightarrow 10^9\ cm^{-3}$
Neutron density	$N_0 \simeq 10^{11} \rightarrow 6x10^{12} cm^{-3}$
Electron Temperature	$T_e = 1 \rightarrow 4eV$
Ion Temperature	$T_i \simeq 0.1 \rightarrow 0.3eV$
Magnetic Field	$B \simeq 0 \rightarrow 60G$

This plasma has been utilized in preliminary studies of the sheath effects of an electric field antenna which was employed in the ECHO 6 mission and also in the studies of ion beam propagation across magnetic fields in the presence of a low density ambient ionospheric plasma.

The second technique consists of the use of an ion thruster to produce a flowing plasma that is suitable for studying the effects of spacecraft charging and multibody interaction in the wake. The parameters of the ion thruster produced plasma are of the following:

ion energy	E_b = 100eV at 35mA
ion flow velocity	$V_b \simeq 2 \times 10^6$ cm/s
ion energy spread	$\Delta E_b \simeq$ 10eV
electron temperature	$T_e \simeq$ 5 - 7eV
Plasma density	$N_e = 10^9 - 10^7 cm^{-3}$
Uniform beam width	$\Delta d_\beta \simeq$ 40 cm

We have also teamed up with Dr. Dave Cook of the Spacecraft Interactions Branch AFGL at Hanscom MA, and Dr. Maurice Tantz of Radex Inc. MA, to compare our laboratory results with their numerical simulations. We have also utilized our laboratory at Northeastern University to study the temporal evolution of the near wake of small objects to provide further electron transport physics to their simulations. This collaboration has been very fruitful and resulted in our recent joint publication of the first effort to compare the results of a laboratory experiment and a numerical simulation that employed the same physical and boundary conditions for wake studies.

In the first year of the contract, we have successfully achieved a uniform, large volume plasma for our antenna study. Our experiments on an electric field antenna have yielded unexpected results. We have found out that the antenna detects a strong enhancement in the fluctuation spectrum corresponding to the antenna sheath-plasma resonances rather than the ambient plasma oscillations. As the antenna sheath changes (e.g. as a result of charging during particle beam injection) the antenna responses to the changes in the sheath plasma resonances rather than changes in the ambient plasma characteristics caused by the particle beam injection. Such results may have important consequences to the interpretation of wave data during active space experiments.

In the second year, we studied the propagation of a neutralized ion beam across a magnetic field. We have found the following results:

a) The initial beam energy density should exceed the energy density necessary to set up a polarized electric field $E_p = -v_b \times B$ where v_b is the ion beam velocity and B the magnetic field strength. This is equivalent to the condition $\epsilon = 1 + \omega_{pi}^2/\omega_{ci}^2 \gg 1$ where ϵ is the static dielectric constant of the beam in the magnetic field, ω_{pi} is the ion plasma frequency and ω_{ci} is the ion cyclotron frequency. If the ion beam is propagated initially from a field-free region, the condition is stronger i.e. $\epsilon \gg (m_i/m_e)^{1/2}$ where m_i and m_e are the ion and electron mass, respectively. This condition arises from the possible charge separation at the sharp magnetic-field boundary and thus the presence of a longitudinal electric field at the beam front.

b) The thickness D_p of the polarization charge layers must be much less than the ion beam radius r_b so that the beam would not lose a considerable fraction of beam particles as it propagates. This is equivalent to the condition of $\rho_i/\epsilon \ll r_b$ where ρ_i is the ion Larmor radius.

c) The potential at the positive surface of the beam cannot exceed the ion accelerating potential. Lindberg has pointed out that if the radius of the beam is too large, the potential difference across the beam will exceed the beam energy and the adiabatic approximation will be violated. This condition sets an upper-bound on the beam radius or

$$r_b < \frac{1}{4}\ \rho_i \left[1 + 2\,\frac{k(T_i + T_e)}{m_i v_b^2}\right]$$

d) The slowing of the beam in the magnetic field can occur due to the transverse expansion of the beam in the direction parallel to the magnetic field. This is equivalent to the condition of $\ell_B/r_B < \epsilon$ where ℓ_B is the axial distance that the beam has propagated.

We have performed preliminary experiments using an ion beam with energy $E_b \leq 1.2$ keV, ion current of $I_i \leq 150$ mA and a uniform magnetic field of $B \leq 20$G. Experiments have been performed both with and without a low density background plasma. In our experiments, the dielectric constant of the beam varied form $\epsilon \sim 10^3$ to 5×10^4 which is in the regime of marginal propagation (i.e. $(m_i/m_e)^{1/2} \sim 270$). However, this regime has not been studied much previously but corresponds to the active space experimental conditions where very high energy ion beams, thus very low beam density, are expected to be used. The present

experiment can also contribute to our understanding of using low energy ion beams for active space environmental controls e.g. discharging of spacecraft.

In our experiments, conditions (a) through (b) are satisfied initially so that we expected the beam to propagate across the transverse magnetic field to the end of the chamber. However, at the highest beam current (e.g. I_b ~ 120 mA) we have only measured a polarization electric field of the order of $|E_p| \leq 0.005$ V/cm which is much less than the theoretical value of $|E_p| \leq 1$V/cm. We believe the slowing of the ion beam comes from the following reasons:

(i) The magnetic field lines were terminated at both ends with conducting walls such that the ion beam was depolarized by current flow to both ends. We will install two insulated boundaries for a proper termination of the magnetic field lines.

(ii) Although we have performed experiments under background neutral pressure as low as 2×10^{-6} torr, the condition of $\nu_i/\omega_{ci} << 1$, where ν_i is the ion-neutral collision frequency, is not well satisfied as a result of the low magnetic field nature of this experiment. This is because conditions (a) through (d) are derived based on the guiding center approximation which assumes that the collision frequencies of particles are much less than their cyclotron frequencies. In the present experiment, the charge exchange frequency is the order of $10^3 \rightarrow 10^4$ Hz which makes ν_i/ω_{ci} the order of one. However, the charge exchange collision cross-section decreases rapidly with ion beam energy and this condition would be satisfied at the proposed $E_i > 10$KeV experiments.

(iii) The divergence angle of the present ion beam source is quite large ($\phi > 5^c$) so that condition (a) is marginal at large distances from the beam. As the beam expands, the beam density decreases rapidly while the magnetic field strength remains constant thus, ϵ decreases as ω_{pi}^2.

In the third year, we have begun to setup a flowing plasma which is suitable to simulate wake of large and small spacecrafts. We have compared laboratory results with numerical simulations using realistic boundary conditions to understand the ion trajectories in the wake of a negatively biased small object. The results are detailed in the following publications (which are reprinted herein).

C. Chan, M.A. Morgan and R.C. Allen, *Electron Dynamics in the Near Wake of a Conducting Body*, IEEE Trans. Plasma Sci PS-14, 915 (1986).

M.A. Morgan, C. Chan and R. Allen, *A Laboratory Study of the Electron Temperature in the Near Wake of a Conducting Body*, Geophys, Res. Lett., 14, 1170 (1987).

M.A. Morgan, C. Chan, D.L. Cooke, and M.F. Gantz, *The Dynamics of Charged Particles in the Near Wake of a Very Negatively Charged Body - Laboratory Experiment and Numerical Simulation*, IEEE Trans. Plasma Sci., 17, 220 (1989).

References

1. E. Villalon and W.L. Burke, Phys. Fluids 30, 3695, 1987.

2. E. Villalon, T. Geophys. Res., 94, 2717, 1989.

3. W.L. Burke, E. Villalon, P.L. Rothwell and M.B. Silevitch, TPL - Publication 86-49 (NASA Jet Propulsion Lab, California Inst. Tech.) p. 213 Oct. 1, 1986.

4. E. Villalon, Physics of Space Plasma, *SPI Conference Proceedings and Reprint Series* 7, 317, 1987.

Refereed Publications

1. W.L. Burke, E. Villalon, P.L. Rothwell and M.B. Silevitch, *Some Consequences of Electromagnetic Wave Injection into Space Plasmas*, TPL - Publication 86-49 (NASA Jet Propulsion Lab, California Inst. Tech.) p. 213 (1986).

2. E. Villalon, *Ionospheric Electron Acceleration by Short Wavelength Electrostatic Waves*, Physics of Space Plasma, SPI *Conference Proceedings and Reprint Series* 7, 317 (1987).

3. E. Villalon and W.L. Burke, *Relativistic Particle Acceleration by Obliquely Propagating Electromagnetic Fields*, Phys. Fluids 30, (1987)

4. E. Villalon, *Ionospheric Electron A* [illegible] *Waves Near Regions of Plasma Resonances*, J. Geophys. Res., 9[illegible]

5. P.L. Rothwell, M.B. Silevitch an[illegible] *and the Westward Travelling Surge*, J. Geophys Res. 91, 6921 (1986).

6. P.L. Rothwell, M.B. Silevitch, L.P. Bloc[illegible] Tanskanen, *A Model of the Westward Travelling Surge and the Generation of Pi2 Pulsation*[illegible] Res. 93, 8613 (1988).

7. M. Silevitch, P.L. Rothwell and L.P. Block, *Magnetosphere-Ionosphere Coupling and Substorm Dynamics, Physics of Space Plasmas SPI Conference Proceedings*, Vol. 7, T. Chang editor, Cambridge, MA (1987).

8. P.L. Rothwell, L.P. Block, M.B. Silevitch and C-G Falthammar, *A New Model for Substorm Onsets: The Prebreak up and Triggering Regimes*, Geophys Res. Lett. 15, 1279 (1988).

9. P.L. Rothwell, L.P. Block, M.B. Silevitch, and C-G Falthammar, *Substorm Breakup on Closed Field Lines*, Adv. Space Res. 8 p. (9) 437 (1988).

10. P.L. Rothwell, L.P. Block, M.B. Silevitch and C-G Falthammar, *A New Model for Auroral Breakup During Substorms* IEEE Trans Plasma Sci. 17, 150 (1989).

11. C. Chan, M.A. Morgan and R.C. Allen, *Electron Dynamics in the Near Wake of a Conducting Body*, IEEE Trans. Plasma Sci PS-14, 915 (1986).

12. M.A. Morgan, C. Chan and R. Allen, *A Laboratory Study of the Electron Temperature in the Near Wake of a Conducting Body*, Geophys, Res. Lett., 14, 1170 (1987).

13. M.A. Morgan, C. Chan, D.L. Cooke, and M.F. Tautz, *The Dynamics of Charged Particles in the Near Wake of a Very Negatively Charged Body - Laboratory Experiment and Numerical Simulation*, IEEE Trans. Plasma Sci., 17, 220 (1989).

The Dynamics of Charged Particles in the Near Wake of a Very Negatively Charged Body–Laboratory Experiment and Numerical Simulation

M. Alvin Morgan
Chung Chan
David L. Cooke
Maurice F. Tautz

Reprinted from
IEEE TRANSACTIONS ON PLASMA SCIENCE
Vol. 17, No. 2, April 1989

The Dynamics of Charged Particles in the Near Wake of a Very Negatively Charged Body—Laboratory Experiment and Numerical Simulation

M. ALVIN MORGAN, CHUNG CHAN, SENIOR MEMBER, IEEE, DAVID L. COOKE, AND MAURICE F. TAUTZ

Abstract—A numerical simulation that is cylindrical in configuration space and 3-D (v_r, v_θ, v_z) in velocity space has been initiated to test a model for the near-wake dynamics of a very negatively charged body. The simulation parameters were closely matched to those of a laboratory experiment so that the results may be compared directly. It was found from the laboratory study that the electrons and ions can display different temporal features in the filling-in of the wake; and that they both can be found in the very near-wake region (within one body diameter) of an object with a highly negative body potential. We have also found that the temperature of the electrons in the very near wake could be somewhat colder than the ambient value, suggesting the possibility of a filtering mechanism being operative there.

The simulation results to date largely corroborate the density findings in terms of the presence of an enhancement for both ions and electrons and in its location. There is reason to think too that additional agreements can be realized if two key elements—the inclusion of a 2-component, source electron distribution in the simulation and an understanding of the perturbation imposed by the diagnostic probe itself on the experiment—can be achieved. This is an ongoing process. Results from both the laboratory experiment and the numerical simulation will be presented, and a model that accommodates these findings will be discussed.

I. Introduction

THE need to further understand the plasma environment surrounding spacecrafts has been recognized for sometime now. With the resumption of shuttle flights into near-earth orbit, and the wide variety of experiments that are to be carried out in its wake or within that of the planned space station, it is becoming imperative that this information be acquired. Hester and Sonin [1], Samir *et al.* [2], and Stone [3] are foremost among those who have reported on experiments that seek to relate laboratory wake phenomena to the space environment. Others, including Martin [4] and Parker [5] have sought to gain some insight into the physics of plasma wakes by means of numerical simulation. To date, however, there has not been much attention given to corroborating numerical simulation results with laboratory findings. A key reason for wanting to do this would be to obtain some assurance that a numerical model can indeed provide results that are realistic: one could actually test the code with some known parameters and compare the results. Conversely, if the model's efficacy is established, then one might want to see how well the laboratory results conform to the model.

This paper is an update of our ongoing effort to understand the dynamics of charged particles in the near wake of a very negatively charged body. In previous publications, we reported on the temporal evolution of electron and ion streams within one body radius in the wake of a metallic disc placed in a flowing plasma [6]; and on the variability of the electron temperature in the same region depending on the characteristics of the surrounding plasma [7]. Here, we briefly review these recent and entirely unanticipated findings, present some results from a steady-state numerical simulation (that incorporated much of the experimental parameters, including the finite boundary and the wall potential) which corroborate the steady-state, electron, and ion density findings, and propose a model that links these results together. The organization of the subsequent material is as follows: Section II contains a brief description of the experimental configuration and the experimental results. Section III describes in short order the numerical model and technique that were used to carry out a computer simulation of the experimental scenario. The simulation results achieved to date are also presented. A discussion of the laboratory and simulation results then follow, in the closing Section IV.

II. Experimental Configuration and Results

Our experiments were performed in a pulsed plasma stream that was produced in the modified double plasma device shown in Fig. 1. The object used was a thin (thickness < 0.5 cm) aluminum disc of radius $\cong 3.25$ cm. It was suspended in the middle of the stream 5.0 cm from the plasma entrance into the target chamber. Readers are referred to previous publications for details on the experimental set-up and diagnostics [6], and on the specifics of the generated plasma [7]. For the particle density studies, the typical operating parameters were: Plasma source density $n_e \cong 10^9$ cm^{-3}; average plasma stream (target)

Manuscript received August 27, 1988; revised January 23, 1989. The work of M.A. Morgan and C. Chan was partially supported by NASA under Grant no. NAGW 1572 and by the Air Force Geophysics Laboratory under Contract no. F19628-85-K-0053.

M. A. Morgan and C. Chan are with the Center for Electromagnetics Research, Department of Electrical and Computer Engineering, Northeastern University, 235 Forsyth Bldg., Boston, MA 02115.

D. L. Cooke is with the Air Force Geophysics Laboratory, Space Physics Division, Spacecraft Interactions Branch, Hanscom Air Force Base, Bedford, MA 01731.

M. F. Tautz is with Radex, Inc., 192 Log Hill Road, Carlisle, MA 01741.

IEEE Log Number 8927086.

0093-3813/89/0400-0220$01.00 © 1989 IEEE

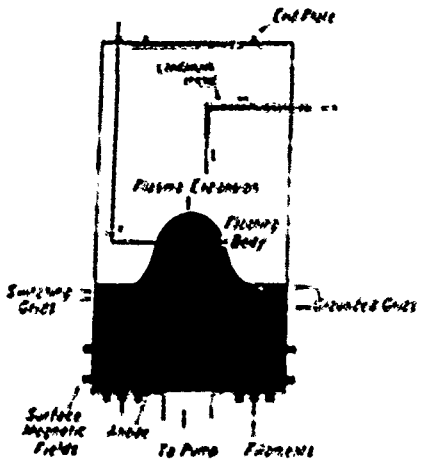

Fig 1 Schematic of the experimental device

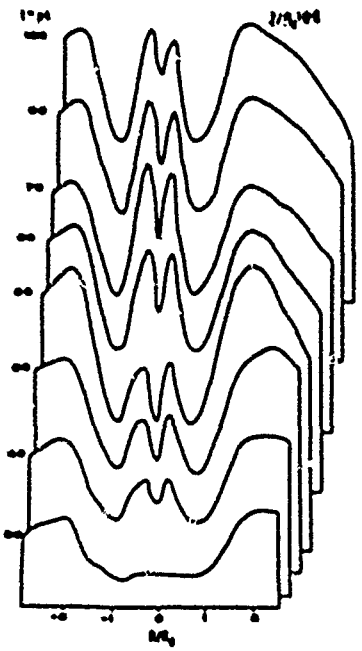

Fig 2 $A < 1$. Time evolving measured electron current density profiles at $Z/R_0 = 0.8$

density $n_i \cong 10^5$–10^7 cm^{-3}; ambient electron temperature $T_e \cong 2$–4 eV and ion temperature $T_i \lesssim 0.3$ eV; ion flow velocity $(v_i) \approx 1 \rightarrow 2c_i$, where c_i is the ion-acoustic velocity; Debye length $(\lambda_D) \cong 0.33$ cm; and the steady-state floating potential of the object was $\cong -20 \rightarrow -25$ V. The ratio of the ion flow energy to the object potential energy—subsequently referred to as the A parameter—was < 1.0.

Figs. 2 and 3 are illustrative of the results obtained for electron and ion current density in this plasma regime. The figures both infer particle density at a fixed location $(Z/R_0 = 0.8)$ in time, from 30 to 100 μs for the electrons and to 500 μs for the ions. The salient points here are that 1) a strong enhancement in density for both particles in the wake is evident at this location. Indeed, it can be seen that at 70 μs for the electrons and 55 μs for the ions, the wake density exceeds the ambient density in magnitude,

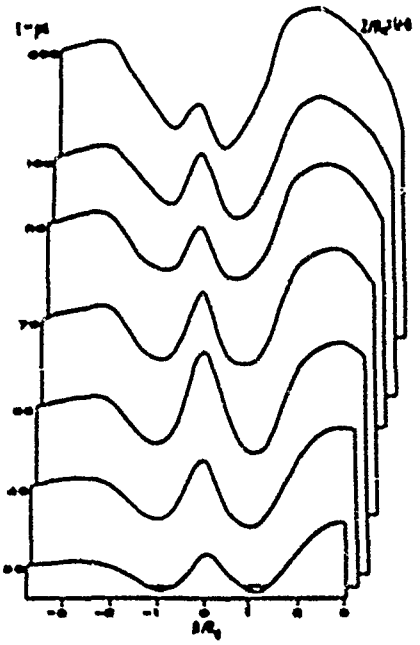

Fig 3 $A < 1$. Time evolving measured ion current density profiles at $Z/R_0 = 0.8$

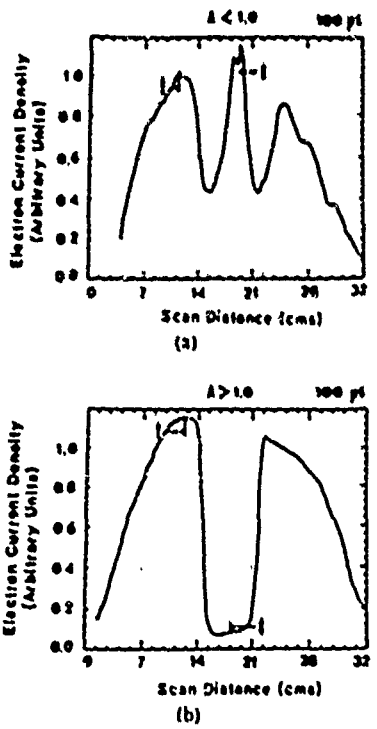

Fig 4 (a) $A < 1.0$; Transverse electron current density profile at 100 μs and 3.0 cm $(Z/R_0 = 0.9)$ behind disc. (b) $A > 1.0$; Transverse electron current density profile at 100 μs and 3.0 cm $(Z/R_0 = 0.9)$ behind disc. (†) Energy analyzer probe location for ambient data. (‡) Energy analyzer probe location for wake data.

2) the electrons' profile exhibits a double peaking feature, suggestive of crossing electron streams but which may be due to other factors that are absent in the ion profiles. Only a single ion enhancement peak was ever observed in these experiments, 3) it is noted that whereas the electron profiles exhibit an electron void in the wake at 30 μs, the

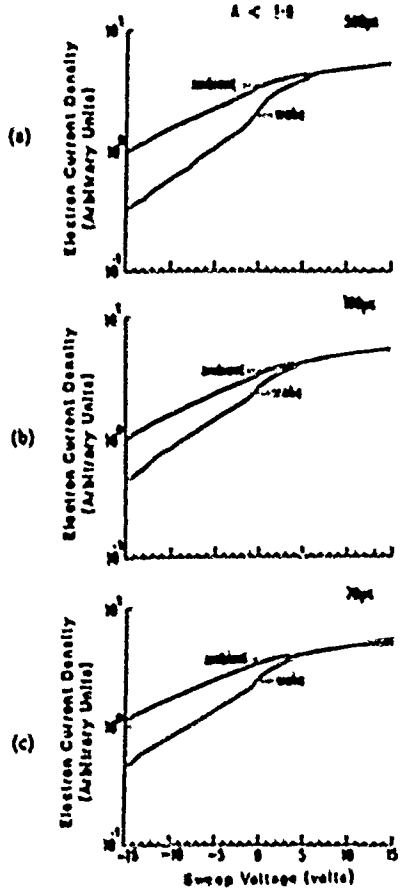

Fig. 5. $A < 1.0$; Energy analyzer probe traces of ambient and wake, electron data at 3.0 cm ($Z/R_0 = 0.9$) and time (a) 500 μs; (b) 100 μs; and (c) 70 μs.

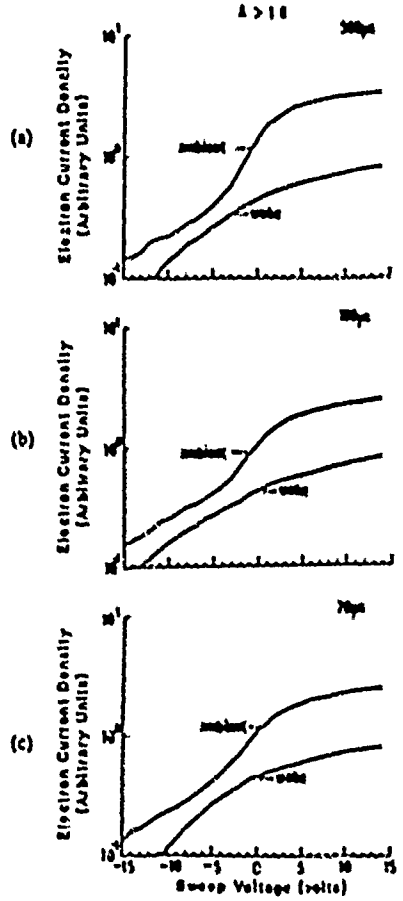

Fig. 6. $A < 1.0$; Energy analyzer probe traces of ambient and wake, electron data at 3.0 cm ($Z/R_0 = 0.9$) and time (a) 500 μs, (b) 100 μs, and (c) 70 μs.

equivalent ion profile displays a significant ion enhancement. This strongly suggests that particle enhancement occurs first with the ions and subsequently with the electrons.

In the electron temperature experiments two plasma regimes were investigated. One regime corresponded to that used for the aforementioned temporal studies as outlined above. In the other, v_i was increased to $3 \rightarrow 5c_s$ and ϕ_B was ≈ -10 V, such that $A = 2.0 \rightarrow 3.0$, or $A > 1.0$. Fig. 4(a) for the $A < 1.0$ regime and Fig. 4(b) for $A > 1.0$ effectively summarize the contrast between the two plasma regimes in terms of the near-wake density. They show the electron current density profiles as obtained by scanning transversely at 3.0 cm ($Z/R_0 = 0.9$) behind the disc; as can be seen in Fig. 4(b), the density profile displays a void in the wake with respect to the ambient density. This is in sharp contrast to the profile shown in Fig. 4(a) for which a density enhancement in the region is clearly evident.

Figs. 5 and 6 show the electron energy distribution for the $A < 1.0$ and $A > 1.0$ regimes, respectively, at the location ($Z/R_0 = 0.9$) of Fig. 4. It was found that in both regimes the energy distribution consists of a Maxwellian bulk population at the plasma potential, and another population of hotter-tail electrons. However, the location at which this is true is different for the two regimes. As a result, while the ambient temperature is clearly colder than that of the wake region in the $A > 1.0$ regime, the converse is true in the $A < 1.0$ instance. It is seen then that for $A < 1$, a large-density enhancement in the near wake corresponds to cold ambient electrons being drawn into the region. On the other hand, in the absence of any near-wake density enhancement the electron temperature in the region could be even hotter than the ambient value due to the presence of a hot-tail component in the bulk electron distribution of the flowing plasma.

III. Numerical Model, Simulation Technique, and Simulation Results

In order to further verify the results that were achieved in the experiments, a full computer simulation of the experimental scenario was initiated. The approach taken was to model the plasma kinetically; that is, the net motion of many interacting particles was regarded as the determining factor in the plasma flow. The laws of mechanics are therefore applied to the individual particles of the ensemble, and statistical techniques are then used to determine the net movement of the bulk plasma. As such, the relevant equations that govern particle behavior in a rarefied plasma flow with singly ionized ions and electrons sur-

rounding an object are 1) the Vlasov equations for both ions and electrons which provide the local values of both species, and 2) Poisson's equation, which governs the electric potential. Since the thermal velocity of the electrons ($v_{th_e} \equiv 10^8$ cm/s) significantly exceeds the plasma-streaming velocity, which is on the order of the ion-acoustic velocity (i.e., $v_p \approx 2c_s = (5)10^5$ cm/s, where c_s = ion-acoustic velocity), it is therefore usual to consider the electrons to be in thermal equilibrium and to have a Maxwell-Boltzmann energy distribution so that

$$f_e(x, v, t) = n_0\left(\frac{m_e}{2\pi kT}\right)^{1/2} \cdot \exp\left[\left(e\Phi(x, t) - \frac{1}{2} m_e v^2\right)\Big/ KT_e\right] \quad (1)$$

where n = initial stream electron density, and v = electron thermal velocity.

The local electron density is then given by

$$n_e(x, t) = n_0 \exp\left[(e\Phi(x, t)/KT_e)\right]. \quad (2)$$

The ion-energy distribution cannot be as easily specified, for there is no ready form in which the ion density can be expressed. The local ion density is thus expressed as

$$n_i = \int_{-\infty}^{+\infty} f_i\, dv \quad (3)$$

where f_i is to be determined.

Substituting (2) and (3) into Poisson's equation, one gets

$$\nabla^2\Phi = 4\pi e\left[n_0 \exp\left(e\Phi/KT_e\right) - \int f_i\, dv\right] \quad (4)$$

which is solved along with the Vlasov equation for ions,

$$\frac{\partial f_i}{\partial t} + v_i \cdot \nabla f_i + \frac{e}{m_i} \nabla\Phi \cdot \nabla_v f_i = 0. \quad (5)$$

It is then necessary to solve (4) and (5), subject to the appropriate boundary conditions, to get self-consistent values for n_e, n_i, and Φ.

In general, four boundary conditions are required to obtain a solution. These are as follows:

1) The potential on the body; i.e., $\Phi(R) = \Phi_s$, where R = body radius, and Φ_s = surface potential.
2) The potential far away from the object, usually expressed as $\Phi(\infty, t)$, but necessarily the boundary potential in a bounded plasma.
3) The distribution function for ions, far away from the object $f_i(\infty, v)$; also, it is just the distribution function for ions at the edge in a bounded plasma.
4) The distribution that describes the charged ions leaving the surface of the object—$f_i(R, v_R > 0)$, where v_R = velocity of the emitted ion at the boundary of the object; i.e., at the body radius R.

Generally, all of the above information cannot be readily known and some assumptions must be made. For boundary condition 4, for example, it was assumed that the object surface is perfectly conducting to incident ions and secondary emission was ignored; $f_i(R, v_R > 0)$ was therefore set to zero. $f_i(\infty, V)$, on the other hand, was specified to be a drifting Maxwellian, given by

$$f_\infty = \left(\frac{m}{2\pi KT}\right) \exp - \left(\frac{m}{2KT}(v_i - v_s)^2\right)$$

where v_s is the plasma flow velocity.

The boundary potential was set at $-1\ KT_e$, which roughly corresponded to the actual experimental chamber-wall sheath value and the object body potential was set at a steady-state value of -20 V.

The actual solution technique used was the "inside out" method [8]. Particles were followed from a point within the wake, then back outside into the ambient plasma in a time-independent fashion. With no time dependency the distribution function along the particle tracks is constrained to be whatever it is specified to be in the source region, thus affording a means of solving Vlasov's equation to obtain particle densities. The program used was the Mesothermal Auroral CHarging (MACH) program. It is an adaptation of TDWAKE, a program originally developed for the National Aeronautics and Space Administration (NASA). Currently in the possession of the Space Physics Division of the U.S. Air Force Geophysics Laboratory, MACH was developed in part to study the sheath structures surrounding large bodies in space. It is 2-D (R, Z) in configuration space and 3-D (v_r, v_y, v_z) in velocity space.

Computations were carried out in a cylindrical mesh centered on the object, and the Vlasov and Poisson equations were solved to produce electron density, ion density, total density, and electric potential at each iteration node point. The machine on which the program was executed was a RIDGE-32 supermini computer.

The steady-state results for the electron and ion density, as obtained by inputting the parameters for the $A < 1.0$ regime of the experimental study and iterating in a cylindrical space scaled to the dimensions of the plasma chamber, are shown in Figs. 7 and 8, respectively. Corresponding plots from data taken at 500 μs (the longest time for which experimental data was available, and which is essentially steady state in the experiment) are shown in Figs. 9 and 10. It is clearly seen in the experimental results that a density enhancement occurs in the wake region of both species; in addition, the location at which this is true is roughly equivalent, for it occurs between $Z/R_0 \approx 0.6 \rightarrow 1.2$ for the electrons, and between $Z/R_0 \approx 0.5 \rightarrow 1.0$ for the ions. In the simulation results, some density enhancement is also seen in the wake region. The location at which this occurs, however, is a little further downstream from that of the experimental results, at $Z/R_0 = 1.6 \rightarrow 2.1$ for ions and $Z/R_0 \approx 1.7 \rightarrow 2.1$ for electrons. It is noted too that in the electron profiles of Fig. 7 there

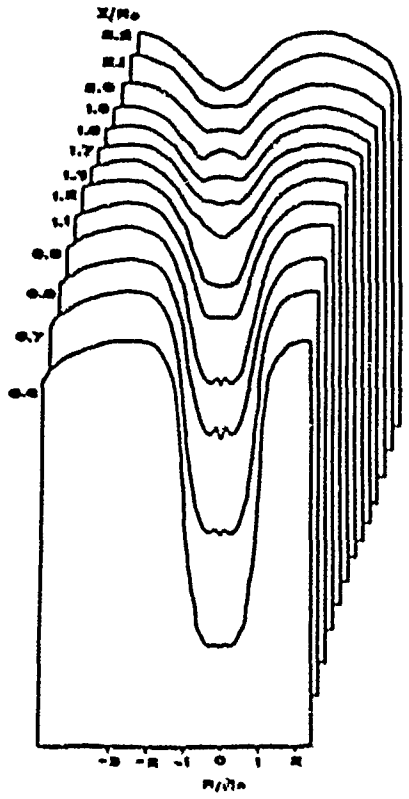

Fig. 7. $A < 1$. Two-dimensional electron number density profiles from simulation in the steady state

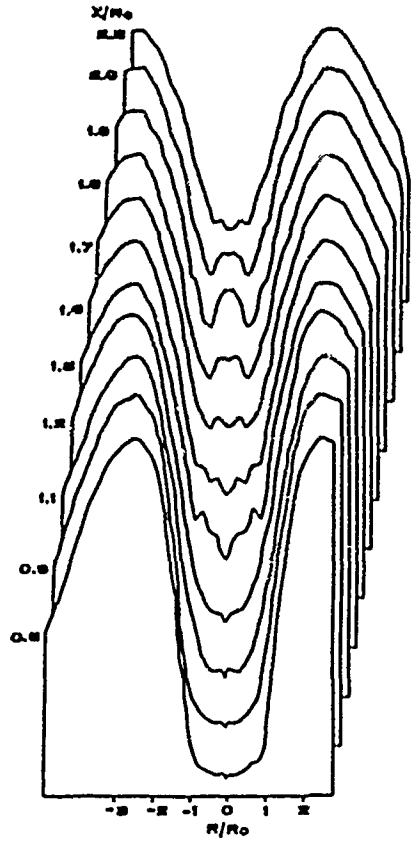

Fig. 8. $A < 1$. Two-dimensional ion number density profiles from simulation in a steady state

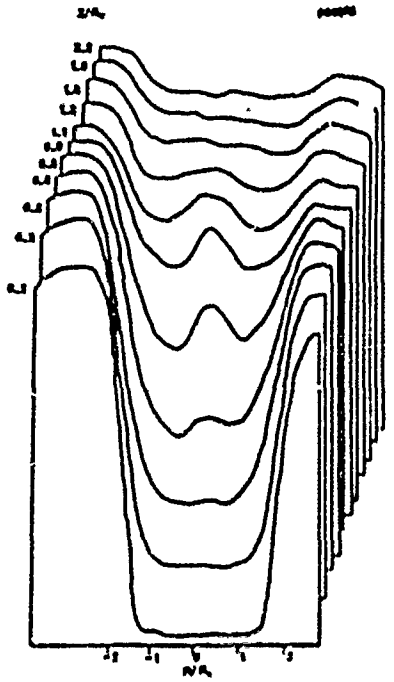

Fig. 9. $A < 1$. Two-dimensional electron current density profiles from experiment at 500 μs

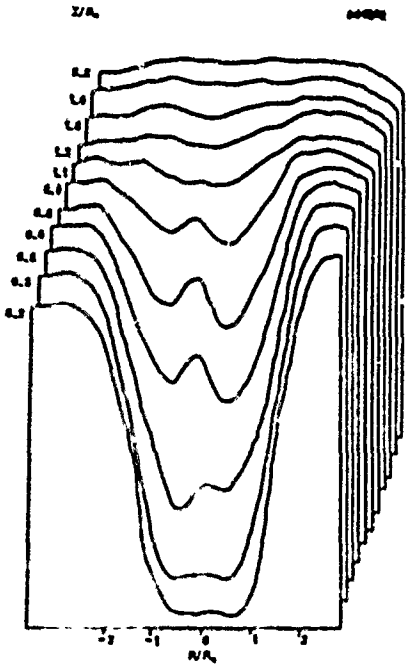

Fig. 10. $A < 1$. Two-dimensional ion current density profiles from experiment at 500 μs

is some apparent enhancement at $Z/R_0 \approx 0.7 \rightarrow 1.0$ which is in very close accord with the experimental results. The amplitude of this feature with respect to the ambient density is considerably less than was observed in the corresponding experimental result however, and further effort is required to fully resolve this feature in order to determine exactly what is occurring there. One possible

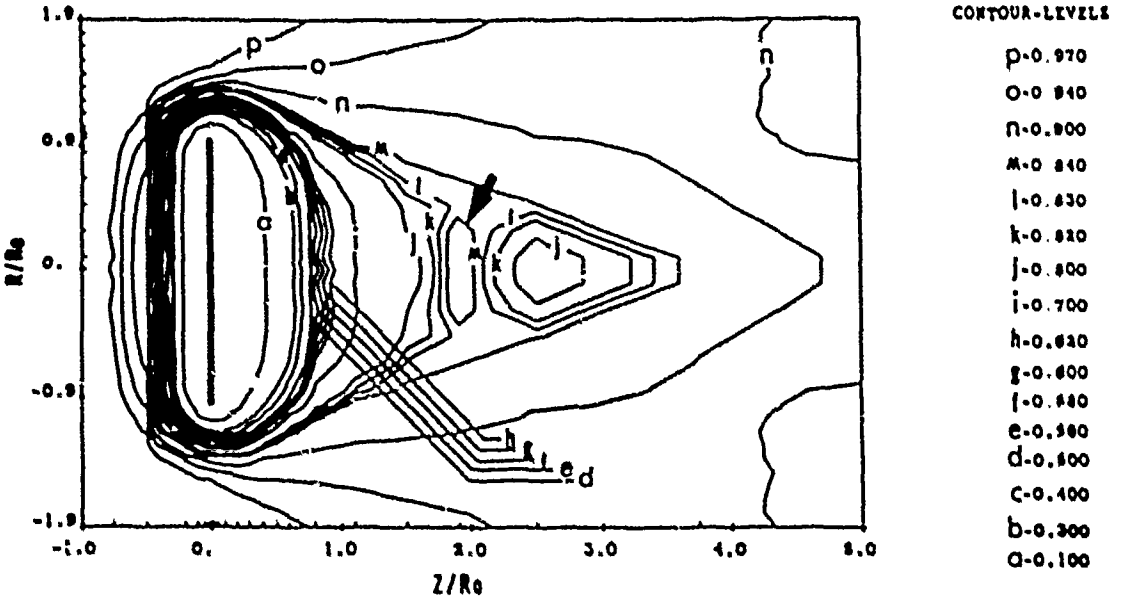

Fig. 11 $A < 1$. Two-dimensional electron density contours from simulation in a steady state.

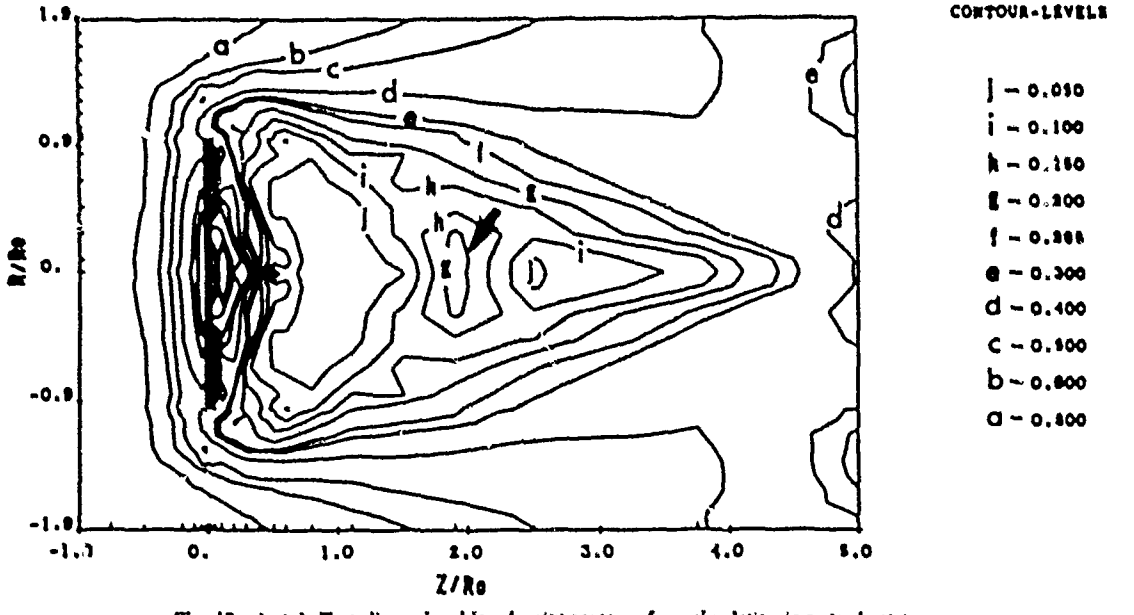

Fig. 12. $A < 1$. Two-dimensional ion density contours from simulation in a steady state.

explanation could lie in the fact that actual number densities were calculated in the simulation, while current density was the actual quantity measured in the experiments.

A different perspective of the information in Figs. 7 and 8 is shown in Figs. 11 and 12. These figures essentially show the 2-D density contours of the electrons and ions, respectively; in both, the density-enhancement regions (indicated by an arrow) can be clearly seen. The unnumbered contours to the left of $Z/R_0 \approx 0.5$ are indicative of ions impinging directly onto the backside of the object and creating a region of significant density enhancement in the process. Such a feature could not be observed in the experimental results because of the single-sided nature of the Langmuir probe that was used to make the density measurements. This is due to the fact that the trajectories of the particles that give rise to it would have impacted directly onto the backside of the probe which was covered with an insulating ceramic coating. This does serve to illustrate very nicely, however, how numerical simulations can direct experimental work, for the presence of such impinging ions will certainly be allowed for and possibly be detected in subsequent laboratory investigations.

IV. Discussion of Laboratory and Simulation Results

Although the experimental ion and electron current density profiles are similar in their essential features to

the numerical profiles, there is a significant difference in their magnitudes. To begin with, the experimental data shows a much larger electron current density enhancement in the wake when compared to the electron-density enhancement seen in the numerical data. This might be explained by the fact that: a) Electron current density was the quantity measured in the experiment, while the actual electron number density was calculated in the simulation. As such, then, the velocity of the wake electrons could play a role in the observed differences in magnitude, b) there could also be some secondary electron emission from the backside of the disc, which is being impacted by ions. These electrons would contribute additionally to the enhancement of the wake electron current density as measured in the laboratory. Since secondary emission was not considered in the numerical simulation, this added enhancement effect would therefore not be a factor in the simulation results; c) another matter that could have some bearing on the observed differences is that the physical presence of a probe in the wake region of an object will influence to some extent the very parameters which the probe seeks to measure. Perturbations of this type are particularly noteworthy in these experiments, for the physics of Langmuir probes in the wake of a larger object is currently not well understood. To illustrate, it is noted that the wake of the probe could conceivably interact with the wake of the disc in such a manner that some of the observed difference between the experiment and simulation data might be attributed to the perturbing influence of the probe. We are currently engaged in studying how such effects could potentially arise by comparing the obtained I–V characteristic of a Langmuir probe that is physically immersed in a plasma (supported on a conducting probe shaft) with those obtained from numerical simulations of a probe-like object that is biased at varying potentials to collect electron current in the wake of a larger object. It is hoped that along with the wall effects, which have also been included in the simulation parameters, we will arrive at a better understanding of laboratory wake dynamics in the presence of diagnostic probes.

The picture that emerges from the experimental and simulation data then, regarding the dynamics of electrons and ions in the near wake, is a somewhat more involved process than that depicted in what has become the standard view of the near-wake environment. From that perspective, ions follow straight line or "ballistic" trajectories in going past an object immersed in a collisionless plasma flow and cross the geometric axis of the object somewhere in the mid- to far-wake region. The near wake (the region in the immediate vicinity of the object and extending out to roughly $Z/R_0 < 4$) is thought to be ion free. These are the underlying assumptions in the works of several authors, including Taylor [9], Martin [10], Konemann [11], and Stone [12].

One difficulty with this standard viewpoint is the fact that for plasma-flow regimes in which the potential energy of the object exceeds the kinetic flow energy of the plasma stream—i.e., when $A < 1.0$—ion trajectories will not follow ballistic paths, and as seen in Figs. 2–6, 9, and 10—ions do enter into the near-wake region. Such conditions could arise from the charging of a spacecraft during the emission of a charged-particle beam or during an auroral event.

The results indicate that if an $A < 1.0$ scenario suddenly comes about, ions will be attracted to the object, and under the influence of the surrounding charge sheath, which initially is large in extent (on the order of the object radius prior to the arrival of the main bulk plasma), will follow a curved trajectory into the region behind the object. This focusing action is enhanced by the fact that the sheath contracts as the plasma density increases at the object location (the final Debye length is $\simeq 0.33$ cms in our experiment), for the contracting sheath serves to pull ions even closer to the object. Indeed, it is seen from the simulation data that some ion trajectories impinge directly onto the backside of the object, even in a steady state.

The excess positive space charge generated by the buildup of ions just behind the object—clearly seen in Fig. 12—subsequently serve to attract more electrons to the area. This is supported by the experimental data in Figs. 2 and 3. As was pointed out in Section II, not only do the ions move into the wake region before the electrons, but the electron density is at a maximum at a later time than the corresponding time for the ions, it is this mechanism that is thought to bring about a colder-than-ambient electron temperature in the near-wake region.

Of course, the electrons can never directly impact the object, as the ions easily can, unless they possess energy sufficient to overcome the object's potential barrier. It can be expected that the electrons will be ultimately reflected at the point where the potential barrier equals their kinetic energy. For an electron population that is perfectly Boltzmann in distribution, the $1\ KTe$ potential contour will be roughly the closest that electrons can be expected to approach the object. For an electron distribution that has a hot tail component, as was the case in the experiments, it might be expected that electrons would approach even closer to the object. With electron densities on the order of 10^7 cm^{-3}, the Debye length was ≈ 0.3 cm, which corresponded to a location of $Z/R_0 \approx 0.1$. It would therefore seem possible for electrons to approach to within $Z/R_0 < 1.0$, even in steady state, and that both ions and electrons would be present in the near wake. The steady-state results seem to indicate this to be true.

Acknowledgment

The authors would like to acknowledge the contribution of Prof. U. Samir, whose suggestions provided the initial impetus for this work, Dr. W. Burke, for his support and encouragement in this endeavor, and Dr. K. Wright for some helpful discussions along the way. We would also like to thank J. Genevich and R. Allen for their technical assistance in carrying out the experiments.

REFERENCES

[1] S. D. Hester and A. A. Sonin, "A laboratory study of the electrodynamic influences on the wakes of ionospheric satellites," *AIAA J.*, vol. 8, pp. 1090-1098, 1969.

[2] U. Samir, W. A. Oran, and N. H. Stone, "Laboratory simulation of space aerodynamic phenomena: Satellite wake studies," *Rarefied Gas Dynamics*, vol. 2, 1974.

[3] N. H. Stone, "The aerodynamics of bodies in a rarefied ionized gas, with applications to spacecraft environmental dynamics," NASA, TP-1933, 1981.

[4] A. R. Martin, "Numerical solutions to the problem of charged particle flow around an ionospheric spacecraft," *Planet. Space Sci.*, vol. 22, pp. 121-141, 1974.

[5] L. W. Parker, "Computation of collisionless steady-state plasma flow past a charged disk," NASA, Washington, DC, CR-144159, 1976.

[6] C. Chan, M. A. Morgan, and R. C. Allen, "Electron dynamics in the near wake of a conducting body," *IEEE Trans. Plasma Sci.*, vol. PS-14, no. 6, pp. 915-924, 1986.

[7] M. A. Morgan, C. Chan, and R. C. Allen, "A laboratory study of the electron temperature in the near wake of a conducting body," *Geophys. Res. Lett.*, vol. 14, no. 11, pp. 1170-1173, 1987.

[8] L. W. Parker, "Computation of collisionless steady-state plasma flow past charged disks," NASA, CR-133159, 1976.

[9] J. C. Taylor, "Disturbance of a rarefied plasma by a supersonic body on the basis of the Poisson-Vlasov equations—I," *Planet. Space Sci.*, vol. 15, pp. 155-187, 1967.

[10] A. R. Martin, "Numerical solutions to the problem of charged particle flow around an ionospheric spacecraft," *Planet. Space Sci.*, vol. 22, pp. 121-141, 1974.

[11] B. Könemann, "The collisionless flow of unmagnetized plasmas around bodies," *J. Plasma Phys.*, vol. 20, pp. 17-30, 1978.

[12] N. H. Stone, "The plasma wake of mesonic conducting bodies, part I: An experimental parametric study of ion focusing by the plasma sheath," *J. Plasma Phys.*, vol. 25, pp. 351-371, 1981.

M. Alvin Morgan was born on Montserrat, in the British West Indies, on May 19, 1956. He received the B.S.E.E and M.S.E.E degrees from Northeastern University, Boston, MA, in 1984 and 1988, respectively. He is currently a Research Assistant in the Department of Electrical and Computer Engineering at Northeastern, where he is working towards the Ph.D. degree. His research interests are in collisionless plasma dynamics, diagnostics and simulation in general, and wake phenomena in particular.

Chung Chan (S'80-M'81-SM'88) was born in Canton, China, on October 23, 1956, and received the B.S. degree in electrical engineering from North Dakota State University, Fargo, in 1978, and the M.S. and Ph.D. degrees in electrical and computer engineering from the University of Iowa, Iowa City, in 1980 and 1981, respectively.

From 1981 to 1984 he served as a Research Scientist in the Phaedrus Tandem Mirror at the University of Wisconsin in Madison. In September 1984, he joined the faculty of Northeastern University, Boston where he currently holds the rank of Associate Professor. He is currently the Director of the Plasma Science and the Microelectronic Laboratories at Northeastern University. He is also a principal investigator on research projects supported by the National Science Foundation, the Air Force, the Office of Naval Research, Sematech, the Department of Energy, the National Aeronautics and Space Administration, and a number of industrial companies.

Dr. Chan received the IEEE Outstanding Graduate Student Award in 1981 for his research work on laboratory plasmas. He has published 40 refereed papers and presented more than 40 conference papers on topics related to novel plasma devices, space plasma simulations, nonlinear plasma phenomena, plasma processing, microelectronic fabrication, and novel plasma diagnostic techniques. He holds membership in Tau Beta Pi, AVS, APS, AGU and NY Academy of Science.

David L. Cooke was born in Abilene, TX, on December 17, 1951. He received the B.A. degree from McMurry College, Abilene, in 1974. Both M.S. (1977) and Ph.D. (1980) degrees were received from Rice University, Houston, TX.

He is currently working in Spacecraft Interactions, on the staff in the Space Physics Division at the Air Force Geophysics Laboratory, Hanscom AFB, MA. His research interests include plasma kinetics, plasma-spacecraft interactions, plasma kinetic simulations, ionization phenomena, and time travel.

Maurice F. Tautz was born in Victoria, BC, Canada, on October 29, 1941. He received the B.Sc. and M.Sc. degrees from the University of Victoria in 1964 and 1968, respectively. He obtained the Ph.D. degree from Northeastern University, Boston, in 1976, in the field of elementary particle physics.

He worked for a few years as a Postdoctoral Fellow at Northeastern, on physics experiments being carried out at Fermilab. Since then, he has been at the Air Force Geophysics Laboratory, where his main research interest is in computer simulations of spacecraft charging problems.

GEOPHYSICAL RESEARCH LETTERS, VOL. 14, NO. 11, PAGES 1170-1173, NOVEMBER 1987

A LABORATORY STUDY OF THE ELECTRON TEMPERATURE IN THE NEAR WAKE OF A CONDUCTING BODY

M. A. Morgan, Chung Chan and Ryne C. Allen

Center for Electromagnetics Research and
Department of Electrical and Computer Engineering,
Northeastern University

Abstract. The temporal evolution of the electron energy distribution in the near wake of a conducting object has been studied experimentally, using a pulsed plasma stream. We have found that depending on the electron energy distribution of the incident plasma stream and on the extent to which the ion flow energy is greater or lower than the potential energy of the object, the electron temperature may be hotter or colder than the ambient value in the region.

Introduction

The issue of whether or not the electron temperature in the near wake of a conducting body is hotter or colder than the ambient value has been the concern of several authors over the past few years. The Gemini/Agena satellite data reported by Medved [1969], was among the first to provide evidence of an enhanced electron temperature in the near wake. Subsequently, Samir and Wrenn [1972] reported a temperature enhancement of 50 – 100% from their analysis of the Explorer 31 data. Since the advent of the space shuttle, the electron temperature issue has become less clear. Siskind et al. [1984] and Raitt et al. [1984], report no temperature enhancement in the near wake of the shuttle. Siskind [1984] in fact mentions that from their analysis, the electron temperature actually decreased in the wake of the space shuttle Orbiter by almost 2000°K from the ambient value. On the contrary, Murphy et al. [1986] report measuring a factor of 4 – 5 increase in electron temperature, in a different experiment, in the wake of the same STS-3 shuttle mission.

The issue is equally controversial in laboratory investigations. Intriligator and Steele [1985] report no enhancement in their experiment using a very high energy (≈ 1KeV) plasma stream; while Illiano and Storey [1974], Oran et al. [1975] and Shuvalov [1980], found an enhanced electron temperature in the wake using a much lower energy plasma stream. Samir et al. [1986], and others, have speculated that the electrons could be energized in the negative potential sheath of the wake by some wave-particle interaction. Gurevich et al. [1966] and Gurevich and Meshcherkin [1981b] offer two other possible theories for enhanced electron temperature in the near wake. The first is associated with the expansion of the ambient plasma into the void of the near wake, and the resulting counterstreaming electrons that can contribute to the heating of the wake electrons. A recent numerical simulation by Singh et al. [1987] indicates that this is indeed a possible mechanism for electron heating. The second theory postulates that jump discontinuities exist in the plasma parameters in the wake region and this serves to excite ion acoustic waves. As the damping of these waves occur through Landau absorption by the electrons, an enhancement in the electron temperature in that region, is again suggested. However, the fact that a colder electron temperature is observed in the near wake of the STS-3 shuttle mission for example, is not predicted by either theory.

In this letter, we provide laboratory results which show that the electron temperature in the near wake can be either colder or hotter than the ambient value. We have found that key influencing factors are the nature of the electron distribution in the plasma stream and a dimensionless variable A - which is defined as the ratio of the ion flow energy to the magnitude of the negative body potential energy. When $A > 1.0$, only the tail population of the bulk electron distribution can penetrate into the near wake. For a bulk electron distribution with a relatively energetic tail, the wake electron temperature would appear hotter - by a factor of two in our experiment for example, than the ambient value. On the other hand, for $A < 1.0$ it was found that a significant number of cold electrons - which probably entered via the ion space charge electric field, are present in the near wake; and the electron temperature in the region can be even colder than the ambient value.

Experimental Considerations

Our experiments were carried out in a modified double plasma device, which has been described in a previous publication [Chan et al., 1986]. The body used was a thin (thickness < 0.5cm) aluminium disc, with radius R_o = 3.25cm, which was suspended in the middle of the stream, 5.0cm from the plasma entrance into the target chamber.

Paper number 7L6639D
0094-8276/87/007L-6639$03.00

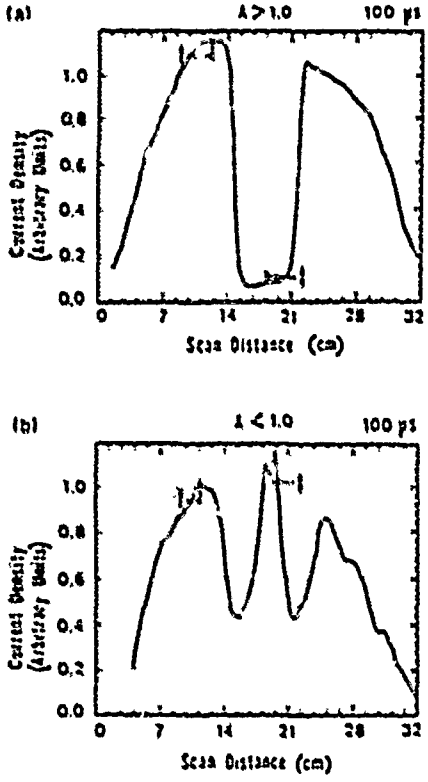

Fig. 1. (a) A > 1.0; Transverse electron current density profile at 100μs and 3 0cm (Z/R_0 – 0.9) behind disc. (b) A < 1.0; Transverse electron current density profile at 100μs and 3.0cm (Z/R_0 – 0.9) behind disc.
↑ Energy Analyzer Probe location for ambient data
↓ Energy Analyzer Probe location for wake data

We have found that the near wake electron temperature can either be hotter or colder than the ambient value, depending on the variable A. Two different plasma regimes were studied. Typical parameters for the first regime were: Source density (n_0) ≈ $10^9 cm^{-3}$; Target density (n_s) ≤ $10^8 cm^{-3}$; Ion flow velocity (u_0) ≈ 3 – $5c_s$, where c_s is the ion acoustic velocity; Debye length (λ_D) ≈ 0.33cm. The steady state floating potential of the body ϕ_s was ≈ -3 to -3 A – 2.0 ≈ 3 V.

In the second regime, the ion flow velocity was reduced to 1 – $2c_s$. Source and target densities were about the same as the first regime, but ϕ_s was ≈ -25V. The major difference here was that A decreased to 0.45 – 0.52 or A < 1.0.

The electron distribution function measurements were made with an electrostatic energy analyzer of radius < 0.5cm. The front grid was biased at slightly above the local plasma potential of 1.0 – 2.0V, to ensure that it was not seen as a barrier to the ambient electrons; and it also ensured that the swept voltage on the discriminator did not penetrate into the plasma.

Experimental Results

The electron density profile obtained by scanning transverse to the plasma flow, at 3.0cms (Z/R_0 – 0.9) behind the disc, is seen in Figure 1a for the A > 1.0 regime, and in Figure 1b for A < 1.0. Compared to the ambient density in Figure 1a, the wake is a relative void. Contrastingly, a density enhancement in the wake of Figure 1b is clearly evident

Differences in density are also apparent for the three time periods shown in Figure 2 and Figure 3, where the electron energy distribution for the A > 1.0 and A < 1.0 regimes respectively, are indicated on semi-log plots. It is noted also from the profiles in Figure 2 and Figure 3, that while the ambient temperature is clearly colder than that of the wake region in the A > 1.0 regime, the converse is true for A < 1.0. Indeed in Figure 3 it is seen that the wake profile displays a somewhat colder characteristic than the ambient profile. We have found that in both regimes, the electron energy distributions consist of a

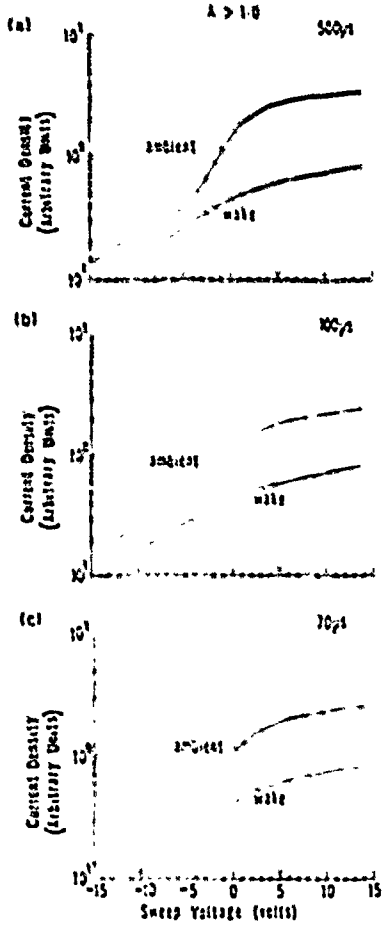

Fig. 2. A > 1.0; Energy Analyzer Probe traces of ambient and wake data at 3.0cm (Z/R_0 – 0.9), and time a) 500μs; b) 100μs; c) 70μs.

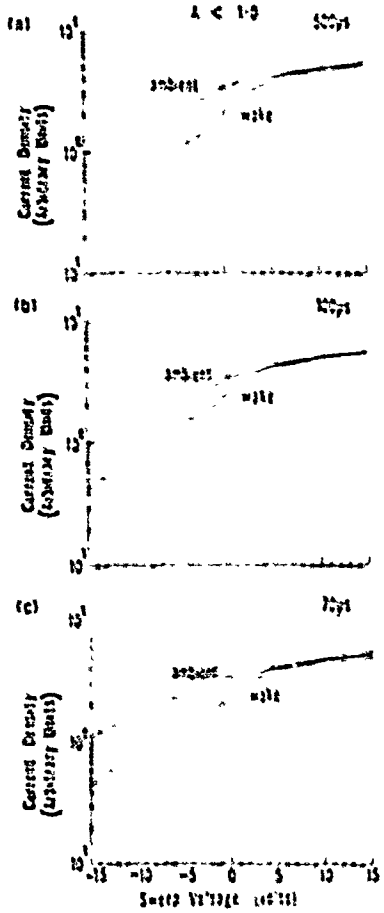

Fig. 3 $\Lambda < 1.0$; Energy Analyzer Probe traces of ambient and wake data at 3.0cm ($Z/R_o \sim 0.9$) and time a) 500μs; b) 100μs; c) 70μs.

Maxwellian bulk electron population at the plasma potential and another population of hotter tail electrons. This tail electron population originates from three probable sources. These are. 1)the switching process at the grids [Chan et al., 1986]; 2)degraded primary electrons from the hot filaments; and 3)other heating process associated with the flowing plasma.

For $\Lambda > 1.0$, the ambient temperature T_e around the plasma potential is approximately 4eV and the tail population is hotter at 10eV. The wake temperature in the same regime however is clearly different, with a value of $T_e \approx 10$eV at the plasma potential and no obvious tail. On

Table 1 Summary of Ambient and Wake temperature values, at location and times indicated in Figure 2

	Ambient Location		Wake Location	
Time (μs)	Bulk Temp (eV)	Tail Temp (eV)	Bulk Temp (eV)	Tail Temp (eV)
70	3 - 4	≈ 10	8 - 9	none
100	4 - 5	9 - 10	≈ 10	none
500	4 - 5	10 - 11	8 - 9	none

Table 2 Summary of Ambient and Wake temperature values at location and times indicated in Figure 3

	Ambient Location		Wake Location	
Time (μs)	Bulk Temp (eV)	Tail Temp (eV)	Bulk Temp (eV)	Tail Temp (eV)
70	13 - 16	none	4 - 5	9 - 10
100	12 - 13	none	5 - 6	8 - 10
500	12 - 13	none	4 - 5	8 - 9

the other hand, the wake electron distribution for the $\Lambda < 1.0$ regime consists of a colder bulk electron population of $T_e = 4$eV as well a tail population, which is on average hotter at approximately 9eV. It is noted from Figure 3 also, that the ambient plasma is fairly Maxwellian - i.e a straight line on the semilog plot, with $T_e = 10 - 13$eV and no distinct tail population present. A listing of the particular electron temperatures as obtained from analyzing the slopes of the distributions in Figure 2 and Figure 3 is presented in Tables 1 and 2 respectively.

Discussion

As the major difference between the regimes $\Lambda > 1.0$ and $\Lambda < 1.0$ is that the ion trajectory is almost ballistic in passing by the object in the former case while this is not true in the latter instance, our experimental results suggest the following hypothesis for the electron behaviour, and the resulting temperature in the near wake. In the $\Lambda < 1.0$ instance, the ions are attracted into the near wake of the body as a result of the high negative body potential of the object and the relatively low flow energy. They in turn, attract in the relative cold ambient electrons via their space charge electric field. The net effect is that a significant enhancement in ion and electron density occurs in the near wake, with the cold ambient electrons being transferred to the wake, evidenced by the cold bulk electron population with $T_e = 4$eV, that was observed. This is much colder than the ambient value. In fact, the ambient temperature now depleted of it's cold population, can be expected to be hotter than usual, and it does display a hotter temperature of $Te \geq 10$eV. When $\Lambda > 1.0$, the floating potential of the object is small in comparison with the kinetic energy of the ions, implying that the ions are not as strongly attracted into the near wake. Since the ion trajectory is essentially ballistic, one would expect only energetic tail electrons which can overcome the sheath electric field, to get into the wake, and the temperature there should be on the order of that for the ambient tail. The data seems to support these expectations.

The results therefore suggest the operation of a velocity filtering mechanism in the near wake electron dynamics, and as

such, appears to contradict the simulation results of Singh et al. [1987]; for the counterstreaming electron populations that interact to produce a single warm electron population reported in that work, were not observed by us when $A > 1.0$ - the regime that corresponds to their simulation conditions. Rather, the warm electron population in the near wake region comes from the tail portion of the ambient electron distribution. It is noted that of the previously mentioned laboratory experiments in which a temperature enhancement was observed, the plasma streams all originated from discharge plasmas which contained a population of energetic tail electrons. Our results are therefore consistent with these observations.

Acknowledgements. We would like to thank Dr. Uri Samir for suggesting this experiment and J. Genevich for his technical assistance.

References

Chan, C., M. A. Morgan and R. C. Allen, Electron dynamics in the near wake of a conducting body, IEEE Trans. on Plasma Science, PS-14, No.6, 915-924, 1986

Gurevich, A. V., and A. P. Meshcherkin, Jump discontinuity on the front of a rarefaction wave front in a plasma, Sov. Phys. JETP, Engl. Transl., 54, 688-706, 1981b.

Gurevich, A. V., L. V. Pariiskaya and L. P. Pitaevskii, Self similiar motion of a rarefied plasma, Sov. Phys. JETP, Engl. Transl., 22, 449-454, 1966.

Illiano, J. M. and L. R. O. Storey, Apparent enhancement of electron temperature in the wake of a spherical probe in a floving plasma, Planet Space Sci., 22, 873-878, 1974.

Intriligator, D. S. and G. R. Steele, Analysis of experimental observations of electron temperatures in the near wake of a large spherical model in a laboratory simulated solar wind plasma, J. Geophys. Res., 90, 4027-4034, 1985

Medved, D. B., Measurements of ion wakes and body effects with the Gemini/Agena satellite, Rarefied Gas Dynamics, 1, 1525-1540, 1969.

Murphy, G., J. Ficket, N. D'Angelo and W. A. Kurth, Measurements of plasma parameters in the vicinity of the space shuttle, Planet. Space Sci., 34, 993-1004, 1986.

Oran, W. A., U. Samir, N. H. Stone and E. G. Fontheim, Laboratory observations of electron temperature in the wake of a sphere in a streaming plasma, Planet. Space Sci., 23, 1081-1083, 1975.

Raitt, W. J., D. E. Siskind, P. M. Banks and P. R. Williamson, Measurements of the thermal plasma enviroment of the space shuttle, Planet. Space Sci., 32, 457-467, 1984.

Samir, U., N. H. Stone and K. H. Wright, Jr., On plasma disturbances caused by the motion of the space shuttle and small satellites: A comparison of In-Situ observations, J. Geophys. Res., 91, 277-285, 1986

Shuvalov, V. A., Structure of the near wake behind a cylinder in a non-equilibrium rarefied plasma, Geomag. and Aeron., 20, 293-295, 1980.

Singh, S., U. Samir, K. H. Wright, Jr. and N. H. Stone, A possible explanation of the electron temperature enhancement in the wake of a satellite, J. Geophys. Res., 92, 6100-6106, 1987.

Siskind, D. E., W. J. Raitt, P. M. Banks and P. R. Williamson, Interactions between the orbiting space shuttle and the ionosphere, Planet. Space Sci., 32, 881-896, 1984.

M. A. Morgan, Chung Chan and Ryne C. Allen, Center for Electromagnetics Research and Department of Electrical and Computer Engineering, Northeastern University, Boston, MA 02115.

(Received August 4, 1987;
revised September 9, 1987;
accepted September 15, 1987.)

Electron Dynamics in the Near Wake of a Conducting Body

C. Chan
M. A. Morgan
R. C. Allen

Reprinted from: IEEE TRANSACTIONS ON PLASMA SCIENCE, Vol. PS-14, No. 6, DEC. 1986.

IEEE TRANSACTIONS ON PLASMA SCIENCE, VOL. PS-14, NO. 6, DECEMBER 1986

Electron Dynamics in the Near Wake of a Conducting Body

CHUNG CHAN, MEMBER, IEEE, M. A. MORGAN, AND RYNE C. ALLEN

Abstract—The temporal behavior of the near wake of an electrically floating disc is studied experimentally using a pulsed plasma stream. The time evolution of the electron and ion current density profiles, revealed the presence of electron and ion streams within one body radius downstream of the disc during the early stage of the wake formation process. The trajectory of the electron streams depends on the body potential and is found to be more complicated than that of the ions. Since the ions appear inside the wake at an earlier time than the electrons, the electron streams may be associated with the space charge of the ions which are attracted into the near wake by the highly negative body potential.

I. Introduction

THE physics associated with a body moving rapidly through a plasma and a plasma streaming past a stationary body are essentially similar. In the most commonly considered case, the body acts as a sink for the charged particles which strike it and leave behind a wake where the particle densities are disturbed from their ambient values. Although most of the disturbances are created in the vicinity of the body, the disturbed zones can reach large distances downstream. The study of plasma wakes has long been a subject of interest in space physics, especially in the context of solar wind/planetary body interactions [1], aerodynamics of spacecrafts in the ionosphere [2], and the structuring of comet tails [3].

Since it is difficult to obtain detailed measurements of plasma-wake regions in space, laboratory experiments [4]–[7] have been utilized to simulate the various wake phenomena. Most laboratory experiments in the past have employed steady-state plasma streams and stationary bodies. These so-called plasma wind tunnel experiments have revealed a number of interesting effects, including the focusing [5] of ion streams onto the wake axis by the electric fields within the sheath of a floating body, and the excitation [5]–[7] of wave-like disturbances downstream of the body. However, there is still a dearth of knowledge with regard to the temporal behavior of the wake region. Such information has become even more important in the space shuttle era with the large size of the shuttle and the variety of active experiments taking place within the shuttle wake. Significant temporal variations of plasma parameters (i.e., fluctuations in plasma potentials) in the shuttle wake may also affect the operation of some diagnostic instruments [8] (e.g., ac electric field antennas and particle analyzers) which may be placed within such regions of disturbed plasma. In this paper, we present laboratory results on the temporal evolution of the wake region behind a conducting disc using a pulsed plasma stream. An additional advantage of using a pulsed plasma stream instead of a steady-state stream, is that the plasma potential and density profiles in a steady state are determined by a balance of the electron and ion loss to the body and the chamber walls. As such, the measured profiles of the wake in a steady-state experiment may depend on the conditions at the boundaries, as well as the confinement characteristics of the device in which the experiment is performed.

By pulsing the plasma stream on and off at a frequency of 100 Hz, we are able to examine the very early stage of the wake formation process (i.e., before the main plasma stream reaches the chamber walls). Our initial investigation has been concentrated on the electron and ion dynamics in the near wake. This study is motivated by our recent observations [9] of significant electron temperature variations in the near wake of an electrically floating body. Since there have been a number of conflicting observations [10]–[17] in laboratory and space plasmas regarding the issue of electron temperature enhancement in the near wake of a floating body, a detailed study of the electron and ion dynamics in that region seemed to be in order.

Unlike most previous results [5], [6] which report an ion void region one to two body radii R_0 downstream of the body, we have found the presence of both electron and ion streams in that region. The electron streams have rather complicated flow patterns and are present only when the body potential ϕ_0 is negative with respect to the plasma potential, indicating that they may be associated with the positive sheath electric field of the negatively floating disc. To our knowledge, the data presented here is the only attempt so far to investigate the temporal dynamics of the electrons in the near wake of a body. The organization of the paper is as follows. Section II contains a brief description of the experimental apparatus. Section III presents data on the temporal and spatial evolution of the electron and ion current density profiles in the near wake. A comparison of our results with previous work and our conclusions are given in Section IV.

Manuscript received April 4, 1986, revised August 8, 1986. This work was supported in part by the National Science Foundation under Grant ECS 86 09906, and by the Air Force Geophysical Laboratory.

The authors are with the Department of Electrical and Computer Engineering, Center for Electromagnetics Research, Northeastern University, Boston, MA 02115.

IEEE Log Number 8610915

0093-3813/86/1200-0915$01.00 © 1986 IEEE

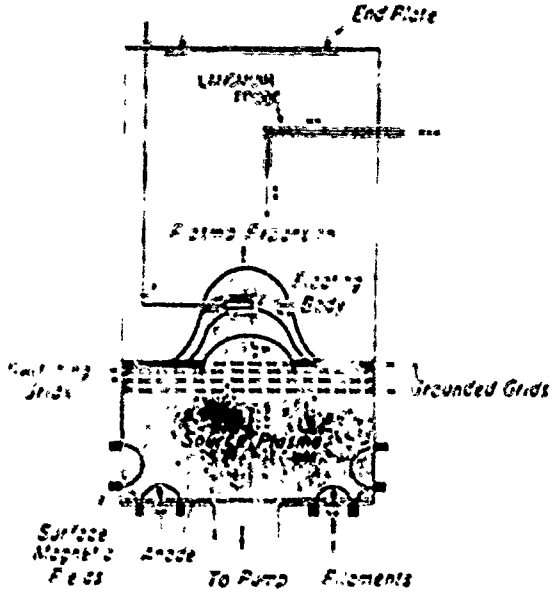

Fig. 1. Schematic of the modified double plasma device.

II. Experimental Considerations

Our experiments were performed in a modified double plasma device shown in Fig. 1. An argon plasma was produced by hot filaments placed inside a multidipole surface magnetic field [18] in the source chamber. The target chamber was separated from the source chamber by four fine mesh grids (≥60-percent transparency each). The two outermost grids were always held at ground so that all of the chamber walls and the plasma boundaries were at the same potential (i.e., at ground). The two inner grids were biased at +50 V and −100 V, respectively, in order to prevent the source ions and electrons from entering the target chamber (which was a vacuum with neutral argon pressure $P_0 < 1.5 \times 10^{-4}$ torr) at time $t < 0$. The plasma potential of the source can be adjusted by the bias on the source anodes. At time $t = 0$, both inner grids were switched to ground and source plasma expanded freely into the target chamber. Since the source plasma potential was always positive ($\phi_s \cong 5$–20 V) with respect to ground and the target plasma potential ($\phi_T \cong 2$ V), the source electrons entered the target chamber with no directed energy. On the other hand, ions entering the target chamber were accelerated by the potential difference between the source and target plasmas, i.e., with directed energy $E_i \cong e(\phi_s - \phi_T)$. By adjusting the anode bias voltage and hence ϕ_s, the ions stream into the target chamber with an adjustable range of Mach number M (i.e., $M = u_0/c_i$ where u_0 is the velocity of the ion flow and c_i is the ion acoustic velocity). Since the two outermost grids are at ground potential, pulsing the inner grids does not affect the boundary conditions of the target and the source plasma (i.e., they are not seen as effective anodes for either plasma). The characteristics of the expanding plasma stream with $M \geq 1$ have been described in some detail in a previous publication [19]. In that experiment, the motion of the plasma was found to be self-similar [20] except at very early times ($t \lesssim 40$ μs) when an ion front was observed. At the expanding front, the electrons moved ahead of the ions and the resultant ambipolar electric field accelerated a few ions to velocities a few times the ion acoustic velocity c_i. In the main plasma stream, the electrons moved along with the ions at approximately the ion flow velocity.

In the present experiment, the source plasma potential ϕ_s was set at 10–20 V above ground which resulted in a plasma stream velocity of $u_0 \cong 3$–$5c_i$. Typical operating parameters were plasma source density $n_0 \cong 10^{9}$ cm^{-3}, average plasma stream (target) density $n_i \cong 10^{8}$–10^{9} cm^{-3}, ambient electron temperature $T_e \cong 2$–4 eV, and ion temperature $T_i \cong 0.3$ eV. There also appeared to be a very small population of higher energy electrons and ions at the front of the plasma stream. We believe that these particles were originally trapped between the two inner switching grids at $t < 0$ and acquired a directed energy when the grids were switched to ground at $t = 0$. These ballistic particles are therefore similar to the so-called pseudowave effects observed in other plasma experiments when the potential of a grid immersed in a plasma was changed abruptly. Although the density of these particles is very low (less than 1 percent of the ambient density) they can contribute to the initial charging of the floating body in our experiment. One obvious evidence of this effect is the dependence of the floating potential of the body on the bias voltage of the switching grid at very early times $t < 10$ μs. In this paper, we will concentrate on wake data which utilize thin aluminum discs (thickness ≤0.5 cm) with a radius ranging from 1 to 5 cm as floating bodies. The parameter regime in our experiment is quite similar to the ionospheric plasma condition with the exception of a higher electron-to-ion temperature ratio in our experiment.

A series of experiments has been performed in order to study the electron dynamics in the near-wake region. Although the boundary conditions are almost the same for each set of the experiment, the initial conditions were slightly different (i.e., the source plasma potential may differ by a few volts from day to day even though the operating parameters are kept the same). As such, the details of the wake region varied somewhat in each experiment, but the overall results remain essentially the same.

In order to minimize the effect of the radial walls on the wake formation, an aluminum aperture with a 20-cm radius was placed onto the grid that is closest to the target chamber (i.e., the top grid in Fig. 1). The presence of the aperture limited the radius of the plasma stream to approximately 20 cm. In previous experiments [21], we have studied the expansion of a plasma stream through such an aperture and found that almost no radial transport of the plasma stream had occurred for $t < 100$ μs due to the high velocity of the plasma in the streaming (axial) direction.

The electron current density profile measurements were obtained by scanning a single-sided Langmuir probe (a tantalum disc with a 0.1-cm radius) in the transverse di-

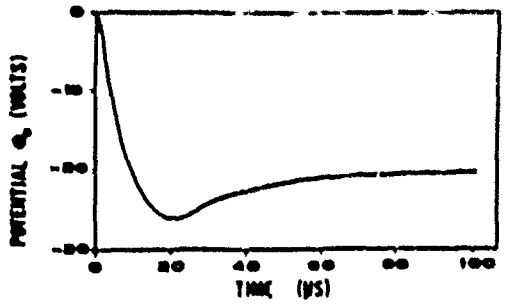

Fig. 2. The temporal behavior of the floating potential of the disc.

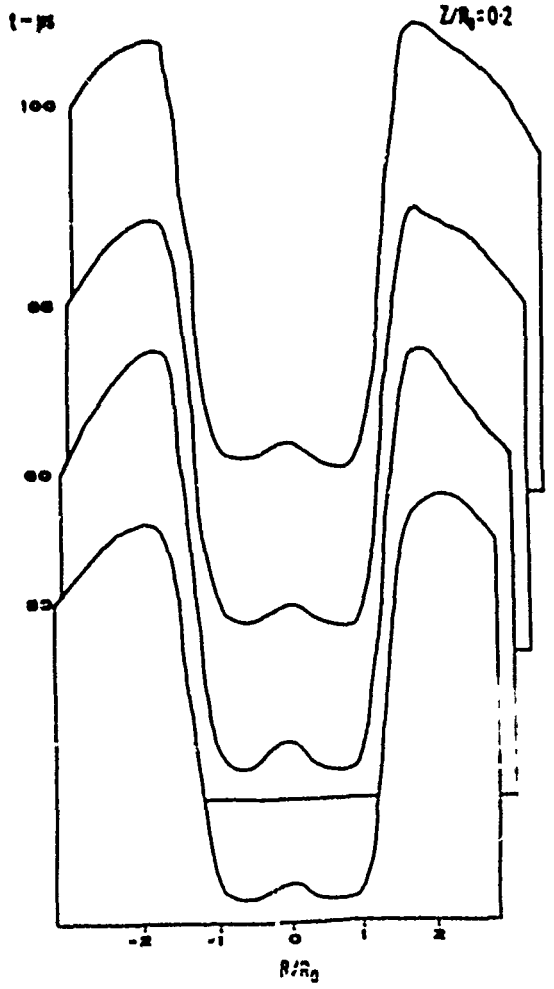

Fig. 3. Time-evolving electron current density profiles at $z/R_0 = 0.2$ (the disc with $R_0 = 3.3$ cm is placed at $z/R_0 = 0$)

rection. The probe had a specially designed inner shaft made with spring steel tubing. By externally adjusting the length of the inner shaft, the probe can be placed at various distances downstream of the body (see Fig. 1). This design eliminated the use of mechanical maneuvering systems inside the plasma and significantly minimized the perturbations created by the probe. Faraday cups and electrostatic energy analyzers can also be placed on this probe shaft for obtaining particle measurements in two spatial dimensions.

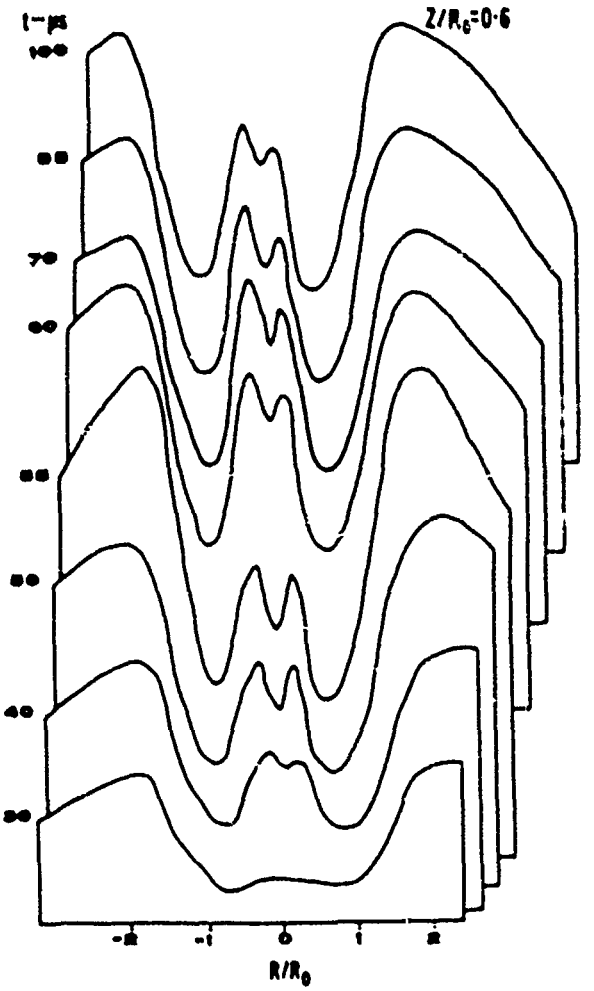

Fig. 4. Time-evolving electron current density profiles at $z/R_0 = 0.6$

III. Experimental Results

At time $t = 0$, the source plasma was allowed to enter the target chamber with an average ion flow velocity $u_0 \approx 4c_s$. An electrically floating disc with radius $R_0 = 3.3$ cm was placed on the axis of the device, 5 cm away from the aperture grid. The ratio of body radius to Debye length was on the order of 10 in steady state. In Fig. 2, we show the temporal behavior of the disc potential ϕ_0. As the plasma stream expands past the disc, the floating potential of the disc first decreases rapidly to $\phi_0 = -25$ V and then settles back to a steady-state value of $\phi_0 = -20$ V for $t > 50$ μs. The initial high negative value of ϕ_0 is possibly caused by the existence of some ballistic electrons after the switching of the grid as discussed in Section II. The ratio of the body potential to the electron thermal energy ($e\phi_0/T_e$) was on the order of 10 in steady state.

Figs. 3, 4, 5, and 6 show the temporal evolution of the transverse electron current density profiles at successive axial distances $z/R_0 = 0.2$, 0.6, 0.8, and 1.1 downstream of the disc, respectively. The electron current density profiles were obtained by scanning the Langmuir probe in the transverse (R) direction with collector surface facing the

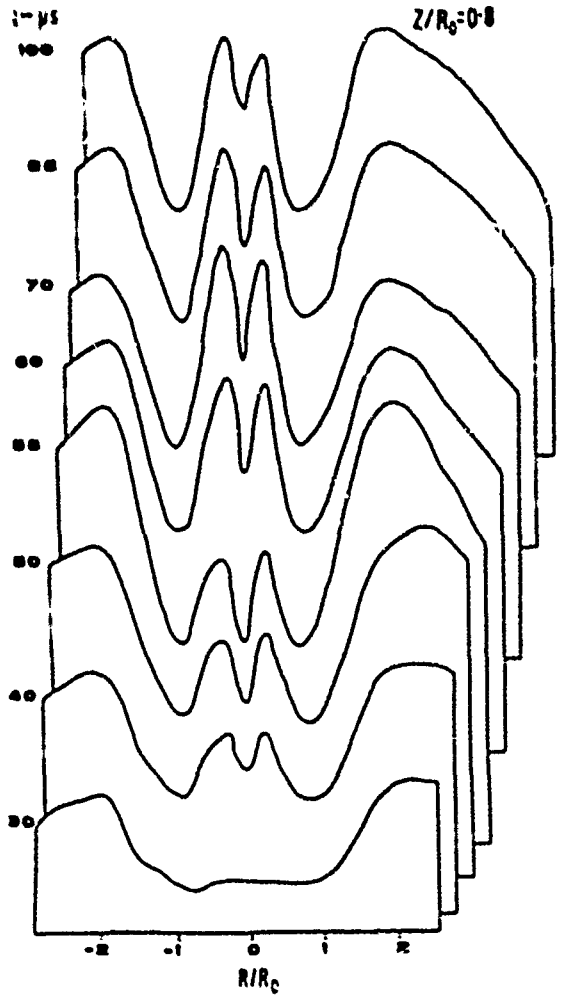

Fig. 5. Time-evolving electron current density profiles at $z/R_0 = 0.8$.

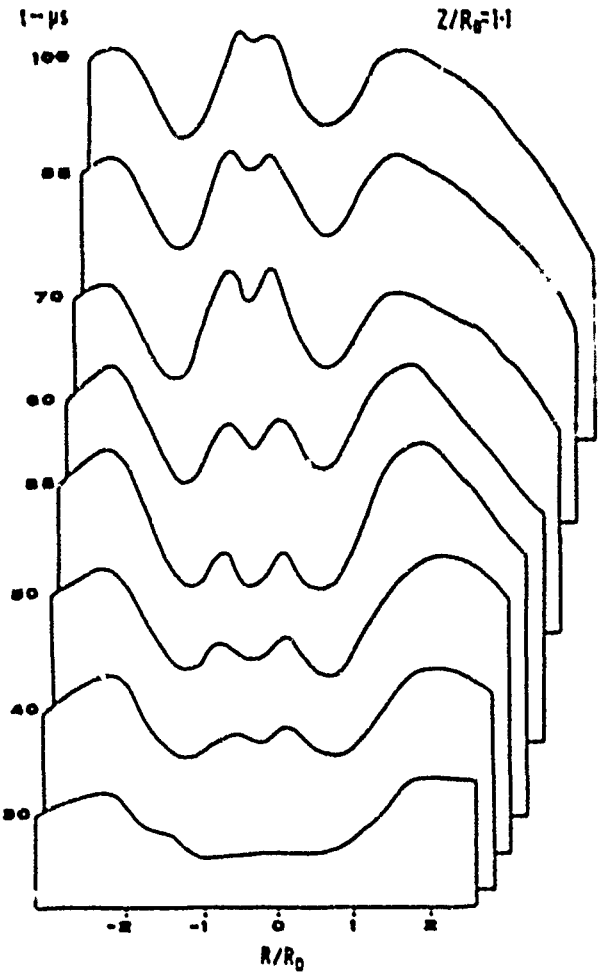

Fig. 6. Time-evolving electron current density profiles at $z/R_0 = 1.1$.

plasma source. A Boxcar interferometer averaging technique [19] was used to obtain the time resolved current density profiles. The Langmuir probe was biased positively (5-30 V) with respect to the target plasma potential so that the probe collected electron saturation current. We have obtained essentially identical electron current density profiles for a probe bias voltage range of 3-50 V when $t > 20$ μs. This indicates that the biasing on the probe has not altered the electron trajectories nor the plasma potential contours significantly. The higher positive bias voltage, e.g., 30 V, is needed to prevent the ballistic ions from reaching the probe right after the switching of the grids.

As the plasma stream expands into the target chamber, the plasma density at a fixed axial location increases with time and reaches a steady state at time $t \sim 100$ μs. This effect is shown clearly in Figs. 3-6 where the density of the plasma stream is higher near the source (i.e., at smaller z/R_0 values) and increases in time. The wake boundary is also found to narrow in time. The narrowing of the wake boundary may be attributed to the following effects. 1) The increase of the plasma density in time results in a decrease of the Debye length λ_D, and therefore the shielding distance of the disc potential, in time. As such, one would expect the extent of the perturbation created by the body to also decrease in time. 2) The wake region may be filled by a radial expansion of the ambient plasma stream into the void region [22].

The transverse electron current density profiles at early time (e.g., $t < 40$ μs) in Figs. 3-6 resemble that of an electron void. However, for time $t \geq 40$ μs, two distinct electron streams are observed to emerge inside the wake at axial distance $z/R_0 \geq 0.6$ downstream of the disc. The two electron streams appear to be more separated when they are further away from the body; i.e., at $t = 50$ μs, the two electron peaks are further apart at $z/R_0 = 1.1$ than at $z/R_0 = 0.6$. On the other hand, the two peaks also appear to merge together as time increases; i.e., at $z/R_0 = 1.1$, the two peaks are closer at $t = 85$ μs then at $t = 40$ μs. The amplitudes of the electron streams also increase with time and become even higher than the ambient value for $t = 70$ μs and $z/R_0 \approx 0.8$.

In Figs. 7 and 8, we show the two-dimensional profiles of the near wake at time $t = 55$ μs and $t = 70$ μs, respectively. The data were obtained in a different experiment under similar conditions. Since the Langmuir probe can only see electrons which have a velocity component

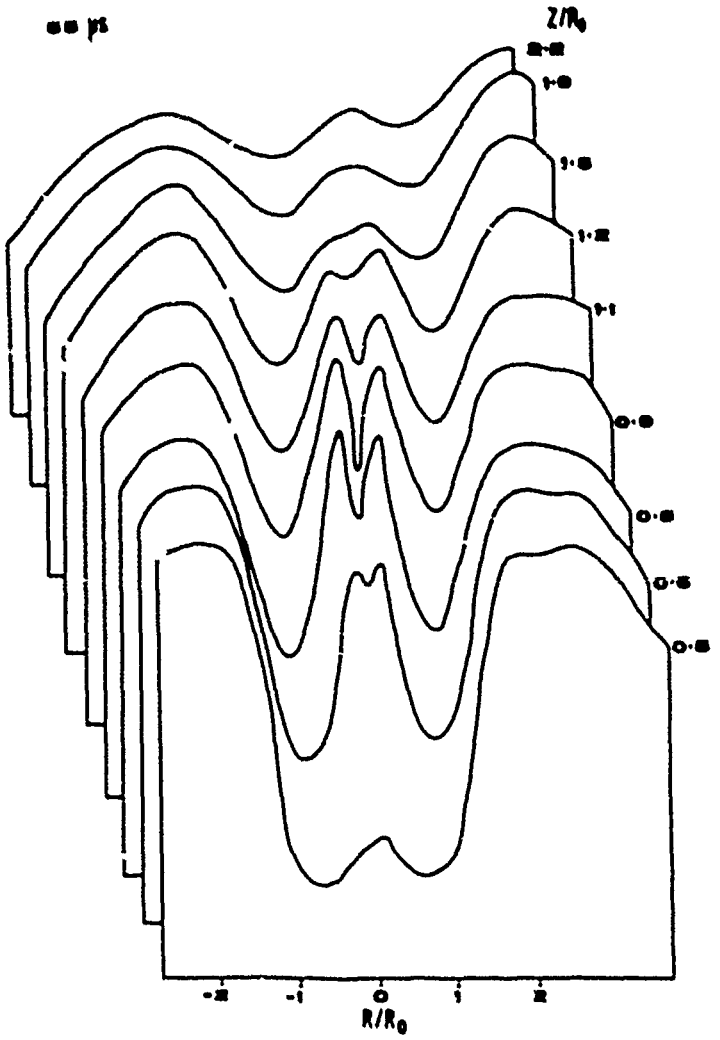

Fig. 7 Two-dimensional electron current density profiles at time t = 55 μs

in the +z direction, the electron streams appear to evolve immediatley behind the disc (i.e., as a single stream at $z \approx 1.5$ cm or $z/R_0 \approx 0.5$) and then diverge as they propagate downstream. The trajectory of the electron streams at distances $z/R_0 < 2$ resembles that of a "trailing-V wave" reported in the ion wake experiment by Stone [5]. However, the trailing-V wave in that experiment actually consisted of ion streams focused by the sheath electric field into the wake. When the focusing ion streams crossed each other, they emerged as a trailing-V structure many body radii downstream (i.e., at $z/R_0 > 15$). The trailing-V structure in our experiment actually appears almost right behind the disc and seems to propagate downstream in time (i.e., compare the stream trajectories at $t = 55$ μs and $t = 70$ μs). Note that the floating potential of the disc had reached a steady-state value of $\phi_0 = -20$ V at $t > 50$ μs so that the changes in the stream trajectories cannot be caused by the change of the body potential. Moreover, instead of diverging even further apart as one would expect for the trailing-V wave, the electron streams actually merge together again at $z/R_0 > 2$. In Figs. 7 and 8, the gradient of the wake boundary is observed to decrease in distance and in time, indicating a filling-in process [22], [27] with the ambient plasma expanding radially inward into the wake. In steady state ($t > 150$ μs), the two streams are observed to merge together with very small amplitudes.

The origin of the electron streams is not yet understood but is clearly associated with the sheath electric field. As shown in Fig. 9, the electron streams disappear when the disc is grounded or biased positively. Since the target plasma potential is also close to ground, the sheath electric field is negligible in the former case and is pointing radially outward in the latter. The dependence of the separation of the electron streams on the potential of the disc is also illustrated in Fig. 9 where a more negative disc potential is found to result in a wider separation of the streams. We have performed experiments with discs of various sizes (R_0 varies from 1 to 5 cm) and found that the separation of the electron streams also increased with the body radius. The above evidence indicates the importance of the sheath electric field to the existence of the

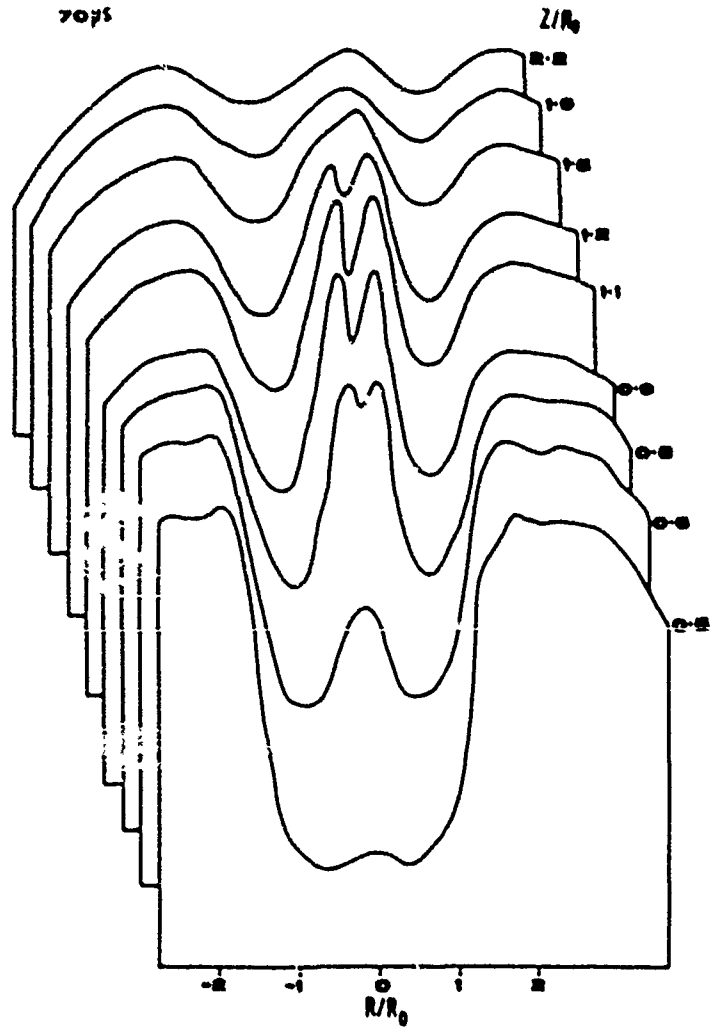

Fig. 8. Two-dimensional electron current density profiles at time $t = 70$ μs.

electron streams. This result is quite unexpected because the sheath electric field of the floating disc (which is directed towards the disc) should deflect electrons outward from the wake region. As such, one would expect an electron void in the very near wake of the body [17].

The behavior of the ions in the present experiment was found to be quite different from that of the electrons. As shown in Fig. 10, the two-dimensional ion current density profile at $t = 70$ μs shows the presence of only a single ion stream inside the wake while the corresponding electron profile shown in Fig. 8 clearly reveals the complicated electron flow pattern. The ion current density measurements were made with the same scanning Langmuir probe and the results were confirmed with a gridded Faraday cup. The ion profile in the present experiment resembles the steady-state profiles reported by Hall *et al.* [23] and those of Fourier and Pigache [6] to a large extent. In Figs. 11 and 12, we show the temporal evolution of the transverse ion current density profiles at two axial locations in order to facilitate a direct comparison with the electron data already shown in Figs. 4 and 5. It is clear from these ion data that only a single ion enhancement peak is present inside the wake. We have detected neither detached-focusing ion streams nor trailing-V waves in this experiment.

Furthermore, the ion stream appears to be present in the wake at an earlier time than the electron streams. For example, the electron profile exhibits a void at $t = 30$ μs in Fig. 5 while the corresponding ion profile in Fig. 12 clearly shows an ion enhancement peak inside the wake. On the other hand, both the electron and the ion streams reach their maximum amplitudes at $t \approx 70$ μs and $z/R_0 \approx 0.8$–0.9. We also note that the ratio of the ion enhancement peak to the ambient density decreases at a later time ($t > 100$ μs) in agreement with the electron data. For example, at steady state (e.g., $t = 500$ μs) the ion current density profile in Fig. 11 resembles that of an ion void even though the initial ion enhancement density (i.e., at $t = 40$ μs) is comparable to the ambient density.

IV. Conclusion

By studying the temporal evolution of the near wake of a conducting disc, we have found the presence of electron and ion streams in regions less than one body radius

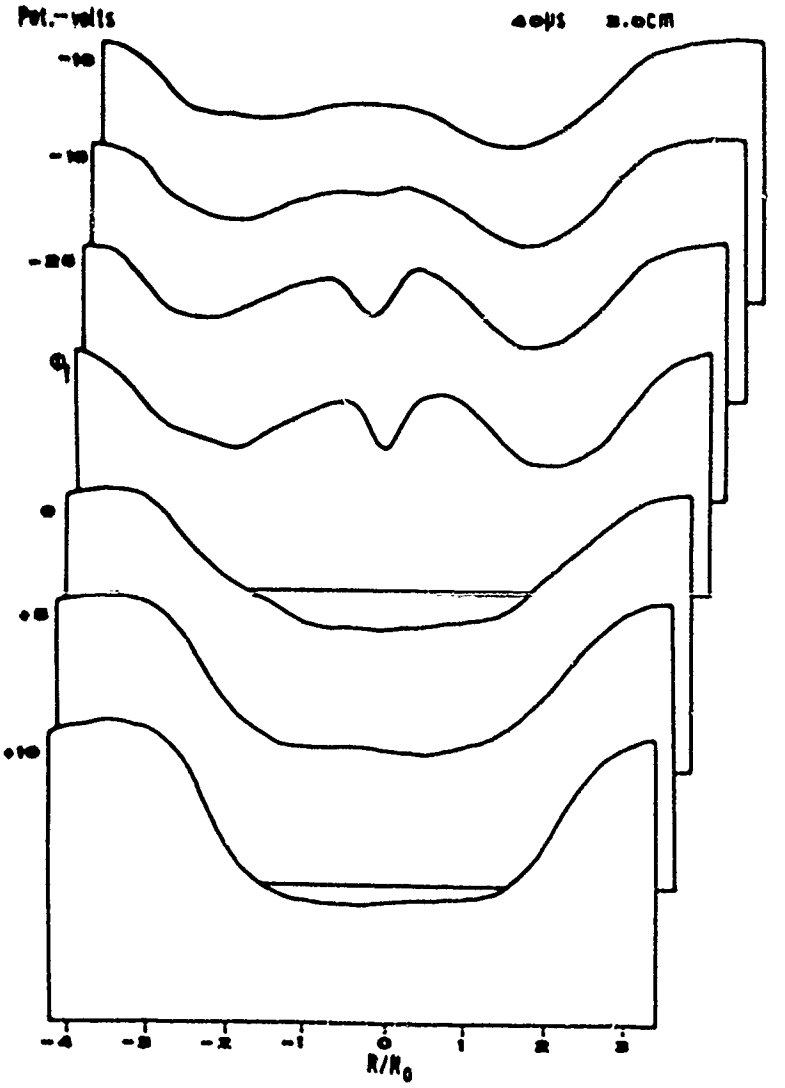

Fig. 9. The dependence of the electron current density profile (at $z/R_0 \approx 0.91$) on the disc potential ϕ_0 at $t = 40\ \mu s$.

downstream. The flow patterns of the electron streams are more complicated than that of the ions and their origin is not yet fully understood. The dependence of the electric streams on the sheath electric field indicates their possible association with the focusing ion streams which are free-streaming ions that are attracted by the sheath electric field and are focused onto the wake axis. Previous experiments [4]-[7] have investigated only the ion current density profiles in steady-state plasma streams and found an ion void in the region of $z/R_0 < 5$. For example, in the experiments by Stone [5] and Stone *et al.* [4], there was no measurable ion current in the void and the effects of the focusing ions began to show up at $z/R_0 = 10$, as a small ion enhancement on each side between the void and the ion rarefaction wave. The ion streams converged and formed a single ion enhancement region at the crossing point ($z = z_d$) and a trailing-V structure appeared for distance $z > z_d$. The trailing-V structure was actually diverging ion streams, which emerged from the focusing ions at the crossing point with very little collective interaction. Several authors [25], [26] have estimated the location of the crossing point as

$$z_d = M \sqrt{\frac{R_0/\lambda_D}{e\phi_0/T_e}}\, R_0. \tag{1}$$

For the present experiment, $M \geq 4$, $R_0 = 3.3$ cm, $\lambda_D \leq 1$ cm, $\phi_0 = 20$ V, and $T_e \approx 2.4$ eV, which results in $z_d/R_0 \geq 2.2$ or $z_d \geq 7.3$ cm. On the other hand, most previous experimental and theoretical results [5], [19] seem to indicate that $z_d \approx MR_0$ which implies that $z_d \approx 14$ cm in the present experiment. Both estimates indicate that the ion focusing point is further downstream from the observed locations of the electron streams in our experiment.

A possible explanation of this discrepancy is that most previous studies [4]-[7], [24]-[26] were concerned with conditions in which the similarity parameter A, defined as the ratio of the ion stream flow energy to the magnitude of the negative body potential, was greater than one. In

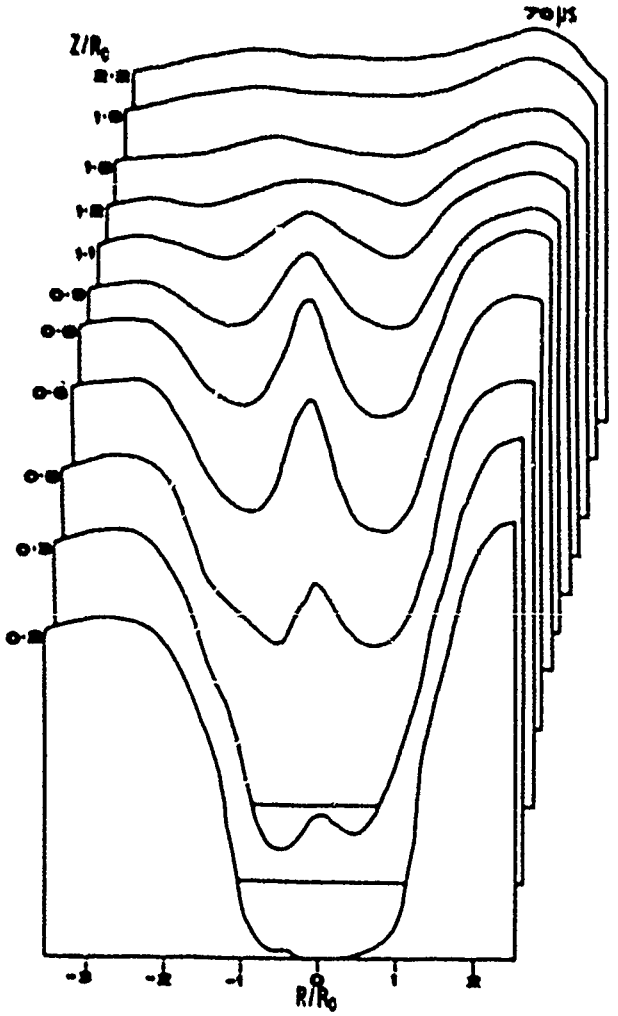

Fig. 10 Two dimensional ion current density profiles at time $t = 70\ \mu s$

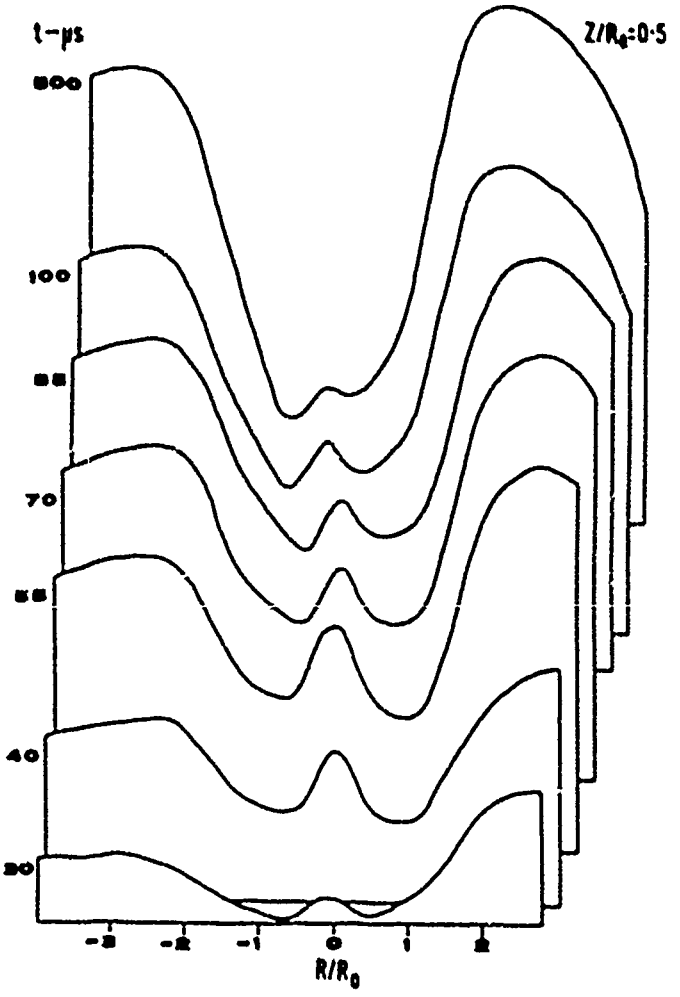

Fig. 11 Time-evolving ion current density profiles at $z/R_0 = 0.5$

our present experiment, $A \approx 0.7$ and our ion data are actually consistent with the only other reported $A < 1$ experiment by Hall *et al.* [23]. Using a steady-state plasma flow, they found that ions always appear right behind the body and in cases of sufficiently high negative body potentials, ions can even strike the rear surface of the body. As such, the presence of electron and ion streams in the near wake is probably caused by the highly negative floating potential of the disc in the present experiment.

The fact that we have not observed any detached ion streams and trailing-V waves indicates a more complicated trajectory of the ions than the ballistic ion trajectory assumed in (1). The behavior of the electron streams is also shown to be much different from that of the ions and cannot be explained by the assumption that the electron follows the ion trajectory because no focusing ion streams were observed to precede the ion enhancement region. From the temporal evolution of the ion and electron current density profiles, the ions were found to appear inside the wake at an earlier time than the electrons. This suggests that the ions enter the void due to the highly negative body potential and their corresponding space charge attracts the electrons into the void. Since the sheath electric field of the floating disc should deflect the electrons outward from the wake region, the presence of the electron streams in the near wake must be induced by the ion motion.

Additionally, the thermal velocity of the streaming ions is small (with $T_i \leq 0.3$ eV) and the streaming ions could only then be attracted into the wake at distances $z < z_s$ by the sheath electric field. The void can also be filled by charge-exchange cold ions that are attracted into the void by the sheath electric field and by the radial expansion of the ambient plasma into the void. For the present range of neutral pressure (5×10^{-5}–1.5×10^{-4} torr), the charge-exchange time is considerably longer than 100 μs, thus charge exchange cannot affect the wake formation process for times $t < 100\ \mu s$. On the other hand, electrons can enter the void due to their high thermal velocity but would be expelled from the void by the sheath electric field. As such the trajectory of the ions and the electrons depends on the potential profile in that region and therefore can be influenced by the body potential ϕ_0 as shown in Fig. 9. It is not yet clear whether these processes can account for the observed electron streams at $z/R_0 \leq 1$. However, their presence will affect the measurement of

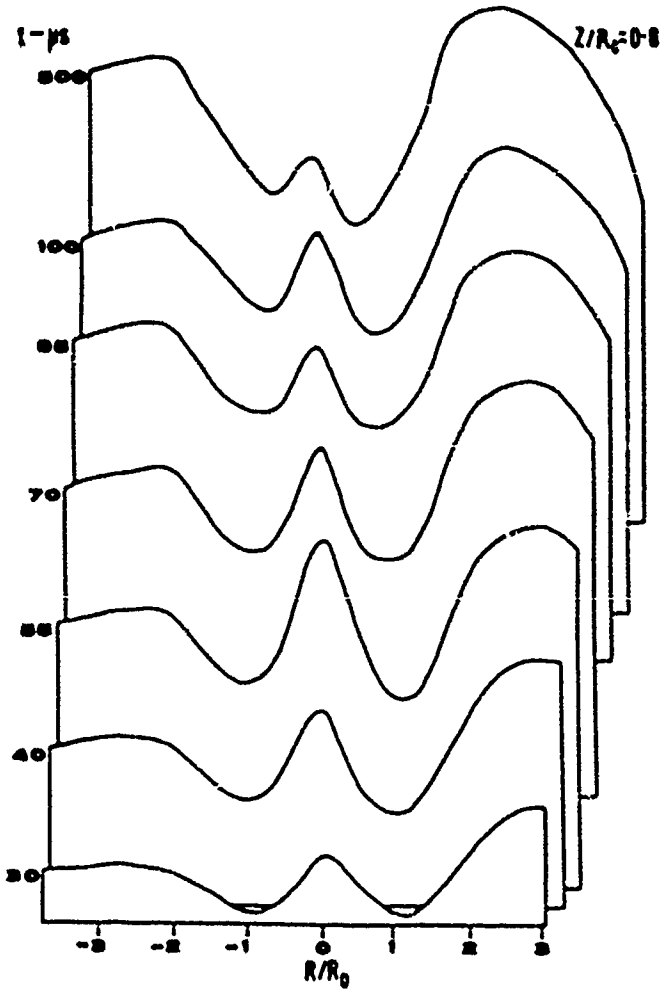

Fig. 12. Time-evolving ion current density profiles at $Z/R_c = 0.8$.

electron temperature in that region. A complete understanding of their origin awaits data on the temporal behavior of the potential profile in future experiments.

Acknowledgment

The authors are grateful to Dr. U. Samir, Dr. M. Silevitch, Dr. N. Stone, and K. H. Wright, Jr. for discussions and suggestions. We thank J. Genevich for constructing much of the apparatus.

References

[1] I. M. Podgorny and Yu. V. Andrianov, "Simulation of the solar wind interaction with non-magnetic celestial bodies," *Planet. Space Sci.*, vol. 26, pp. 99-109, 1978.

[2] A. V. Gurevich, L. P. Pitaevskii, and V. V. Smirnova, "Ionospheric aerodynamics," *Space Sci. Rev.*, vol. 9, p. 805, 1969.

[3] I. M. Podgorny, E. M. Dubinin, and P. L. Israelevich, "Laboratory simulation of the induced magnetospheres of comets and venus," *Moon and Planets*, vol. 23, pp. 323-338, 1980.

[4] N. H. Stone, W. A. Oran, and U. Samir, "Collisionless plasma flow over a conducting sphere," *Planet. Space Sci.*, vol. 20, p. 1787, 1972.

[5] N. H. Stone, "The plasma wake of mesosonic conducting bodies, Part I, An experimental parametric study of ion focusing by the plasma-sheath," *J. Plasma Phys.*, vol. 25, p. 351, 1981.

[6] G. Fournier and D. Pigache, "Wakes in collisionless plasma," *Phys. Fluids*, vol. 18, p. 1443, 1975.

[7] J. P. M. Schmit, "Wake past an obstacle in a magnetized plasma flow," *Plasma Phys.*, vol. 15, p. 677, 1973.

[8] N. H. Stone, U. Samir, and K. H. Wright, Jr., "Plasma disturbances created by probes in the ionosphere and their potential impact on ion energy measurements considered for spacelab," *J. Geophys. Res.*, vol. 83, p. 1668, 1978.

[9] C. Chan, M. A. Morgan, and R. C. Allen, "Dynamics of the plasma wake region in the laboratory," *IEEE Trans. Geosci. Remote Sensing*, vol. 66, p. 1041, 1985.

[10] U. Samir and G. L. Wrenn, "Experimental evidence of an electron temperature enhancement in the wake of an ionospheric satellite," *Planet. Space Sci.*, vol. 20, p. 959, 1972.

[11] U. Samir, N. H. Stone, and K. H. Wright, Jr., "On plasma disturbances caused by the motion of the space shuttle and strand satellites: A comparison of in situ observations," *J. Geophys. Res.*, vol. 91, p. 227, 1986.

[12] D. B. Medved, "Measurement of ion wakes and body effects with the Gemini/Agena satellite," *Rarefied Gas Dyn.*, vol. 1, p. 1525, 1969.

[13] J. M. Illiano and L. R. O. Storey, "Apparent enhancement of electron temperature in the wake of a spherical probe in a flowing plasma," *Planet. Space Sci.*, vol. 22, p. 873, 1974.

[14] U. Samir, P. J. Wildman, F. Rich, H. C. Brinton, and R. C. Sagalyn, "About the parametric interplay between ions mach number, body size, and satellite potential in determining the ion depletion in the wake of the S3-2 satellite," *J. Geophys. Res.*, vol. 86, pp. 11 and 161, 1981.

[15] B. E. Troy, Jr., E. J. Maier, and U. Samir, "Electron temperature in the wake of an ionospheric satellite," *J. Geophys. Res.*, vol. 80, p. 993, 1975.

[16] D. E. Siskind, W. J. Raitt, P. M. Banks, and P. R. Williamson,

interactions between the orbiting space shuttle and the ionosphere," *Planet. Space Sci.*, vol. 3?, p. 881, 1983.

[17] D. S. Intriligator and G. R. Steele, "Analysis of experimental observations of electron temperatures in the near wake of a large spherical model in a laboratory simulated solar wind plasma," *J. Geophys. Res.*, vol. 91, p. 2?? 1986.

[18] S. Hershkowitz, J. DeKock, P. Coakley, and S. Cartier, "Surface trapping of primary electrons by multi-dipole magnetic fields," *Rev. Sci. Instrum.*, vol. 51, p. 64, 1980.

[19] C. Chan *et al.*, "Experimental observations of self-similar plasma expansion," *Phys. Fluids*, vol. 27, p. 266, 1984.

[20] A. V. Gurevich, L. V. Pariiskaya, and L. P. Pitaevskii, "Ion acceleration upon expansion of a rarefied plasma," *Soviet Phys. JETP*, vol. 36, p. 274, 1973.

[21] C. Chan, "Laboratory experiments on plasma expansion," *Ion Acceleration in the Magnetosphere and Ionosphere* (Geophys. Monograph 38), p. 249, 1986.

[22] U. Samir, K. H. Wright, and N. H. Stone, "The expansion of a plasma into a vacuum: Basic phenomena and processes and applications to space plasma physics," *Rev. Geophys. Space Phys.*, vol. 21, p. 1631, 1983.

[23] D. F. Hall, R. F. Kemp, and J. M. Sellen, "Plasma vehicle interaction in a plasma stream," *AIAA J.*, vol. 2, p. 1032, 1964.

[24] U. Samir, "A possible explanation of an order of magnitude discrepancy in electron wake measurements," *J. Geophys. Res.*, vol. 75, p. 855, 1970.

[25] A. R. Martin, "Numerical solutions to the problem of charged particle flow around an ionospheric spacecraft," *Planet. Space Sci.*, vol. 22, p. 121, 1974.

[26] J. C. Taylor, "Disturbance of a rarefied plasma by a supersonic body on the basis of the Poisson–Vlasov equations I and II," *Planet. Space Sci.*, vol. 15, pp. 155 and 463, 1967.

[27] S. Raychaudhuri *et al.*, "An experiment on the plasma expansion into a wake," *Phys. Fluids*, vol. 29, p. 29, 1986.

A New Model for Auroral Breakup During Substorms

Paul L. Rothwell
Lars P. Block
Michael B. Silevitch
Carl-Gunne Fälthammar

Reprinted from
IEEE TRANSACTIONS ON PLASMA SCIENCE
Vol. 17, No. 2, April 1989

A New Model for Auroral Breakup During Substorms

PAUL L. ROTHWELL, LARS P. BLOCK, MICHAEL B. SILEVITCH, SENIOR MEMBER, IEEE, AND CARL-GUNNE FÄLTHAMMAR

Abstract—A model for substorm breakup is developed, based on 1) the relaxation of stretched (closed) dipolar field lines, and 2) the formation of an incipient current wedge within a single arc structure. It is argued that the establishment of a coupled current structure within a single arc leads to a quasi-stable system; i.e., the pre-breakup regime. Perturbation of the pre-breakup structure leads to an instability criterion. It is found, consistent with observations, that narrower auroral arcs at lower L shells undergo the most explosive poleward expansion. According to this model, the precise location at which breakup occurs depends on the O^+ density in the plasma sheet, the level of magnetic activity (K_p), and the intensity of the substorm westward electrojet in the ionosphere. An enhancement of any of these features will cause breakup to occur at lower L shells. Comparison of our model with the Heppner-Maynard polar-cap potential model indicates that breakup is restricted to the west of the Harang discontinuity consistent with recent observations from the Viking satellite.

I. Introduction

THERE is considerable evidence [1]-[5] that a substorm, as first seen in the auroral region, may start earthward of any associated near-earth neutral line. This leads to the following possible physical scenario: Tail magnetic field lines reconnect to a stretched dipolar configuration through a near-earth neutral line. The relaxation of these stretched dipolar field lines requires a decrease in the cross-tail current by Maxwell's equations. Presumably, part of the required current decrease can occur self-consistently (Kaufmann [6]) through the effect of dipolarization on ion gradient and curvature drifts. On the other hand, part of the current decrease occurs due to a diversion of the cross-tail current through the ionosphere, forming what is commonly called a substorm current wedge (McPherron *et al.* [7]). The dipolar collapse proceeds by the conversion of magnetic energy that is stored in the stretched magnetic field lines into ionospheric Joule heating via this current wedge.

One basic question that we address in this paper is the location where the wedge can self-consistently exist within a single arc structure for given magnetospheric and ionospheric conditions. This provides an enhanced yet quiescent coupling between the magnetosphere and the ionosphere. A simple stability analysis shows that narrow-arc structures that form at lower L shells may be unstable to poleward expansion, while wider arcs structures at higher L shells are stable. This, in our model, is the cause for substorm breakup being observed well inside the discrete arc region. We also find that breakup should occur more equatorward the higher the O^+ concentration in the plasma sheet, a finding which connects our work with the recent results of [8]-[11] that indicate that the ionosphere seeds the inner edge of the plasma sheet with energetic O^+ during times of high magnetic activity. The obtained instability also depends on the presence of a tailward electric field component in the equatorial plane which maps to a poleward component in the ionosphere. (According to our model, this allows the kinetic energy of earthward convecting plasma to generate electrical energy that drives the instability.) Such an electric field component is present in the Heppner-Maynard model [12] just west of the Harang discontinuity, which is consistent with the preferential location for breakup as observed by Shepherd *et al.* [13]. Although our model is first formulated for a dipole field, we rescale the results using the Tsyganenko 1987 [14] model for various K_p values. We find that for higher K_p values, breakup should occur even more equatorward. A key feature of our model is, therefore, that although the formation of a near-earth neutral line is required to create the stretched dipolar field lines, substorm breakup may occur much closer to the earth through the formation of a substorm current wedge.

It should be pointed out that another recent model for substorm onsets has been proposed by Kan *et al.* [15] based on the earlier work of Kan and Sun [16]. In their model, substorm onset is directly caused by an enhancement in the magnetosphere-ionosphere coupling due to an enhancement of magnetospheric convection following a southward turning of the IMF. This produces a narrow belt of intense upward field aligned current that can, in their model, lead to substorm onset. The major difference between our approach [17] and that of Kan *et al.* [15] is that we treat the stability of a single arc structure, while they examine the global effects of enhanced convection. Both models consider auroral breakup to be directly related to enhanced magnetosphere-ionosphere coupling which does not explicitly depend on the formation of a near-earth neutral line. However, in our model we can predict the location of substorm breakup as a function of arc size, while Kan *et al.* [15] cannot.

Manuscript received August 12, 1988; revised November 8, 1988. This work was partially supported by the U.S. Air Force under Contract no. F19628-85-K-0053.

P. L. Rothwell is with the Air Force Geophysics Laboratory, Hanscom Air Force Base, Bedford, MA 01731.

L. P. Block and C.-G. Fälthammar are with the Department of Plasma Physics, Royal Institute of Technology, S100 44 Stockholm 70, Sweden.

M. B. Silevitch is with the Department of Electrical and Computer Engineering and the Center for Electromagnetics Research, Northeastern University, Boston, MA 02115.

IEEE Log Number 8926490

0093-3813/89/0400-0150$01.00 © 1989 IEEE

Substorm breakup, as observationally defined, is the sudden brightening of a previously quiescent auroral arc near local midnight. Once it is "triggered," the arc dynamics is characterized by a rapid poleward and westward expansion [2], [3], [5]. Hallinan [5], using real-time TV imaging techniques, observed a new arc forming poleward of the diffuse aurora, rapidly followed by the sequential formation of up to three more arcs, each poleward of its predecessor. As one arc formed, Hallinan [5] observed another one fading. This process lasted between 15 s and 10 min until one of the arcs established dominance, brightened explosively, then initiated the poleward surge. Auroral intensifications with characteristics similar to those of substorm breakup can occur in the evening sector, as detected on Viking [13]. They expand poleward and eastward, abruptly stopping at local midnight. Triggering generally occurs on the poleward boundary of the diffuse aurora, which can be at invariant latitudes which correspond to dipolar L shells as low as 5-6. The purpose of this paper is to establish the quiescent pre-breakup conditions which are necessary for triggering to occur at such low latitudes and to examine the dynamics of the breakup in the first few seconds before inductive effects become important.

The basic idea in our model is that the pre-breakup arc is an arc in which two coupled electrical circuits are established between the ionosphere and the magnetosphere; i.e., it is the incipient formation of a substorm current wedge similar to the one proposed some time ago by McPherron *et al.* [7] that distinguishes the breakup arc from adjacent arcs and leads to the observations described by [5]. As such, it has the basic features of the Westward Traveling Surge (WTS) current system that we have previously used [18]-[21] and as used by Coroniti and Kennel [22]. As implied from Fig. 1, the physical picture is of two current sheets: One flowing upward on the poleward boundary and another flowing downward on the equatorward boundary of an enhanced conductivity region in the ionosphere. Our approach is comparable to one used some years ago by Coroniti and Kennel [22]. However, we treat a nonzero polarization field in the magnetosphere which is considered essential for the breakup instability. Moreover, our approach depicts the L shells at which a self-consistent quiescent current wedge can form over a wide range of dimensions, while Coroniti and Kennel [22] treated breakup as occurring over the entire auroral oval. In the present model we examine the possibility of breakup occurring in arc structures from the size of an individual arc to the size of the WTS.

II. The Two Circuit Model

The extended east-west orientation of the breakup arc motivates an approach which models the system as two coupled circuits, one north-south and the other east-west. In our model these circuits close in the magnetosphere via field-aligned currents which are calculated from the model of Fridman and Lemaire [23]. The field-aligned currents,

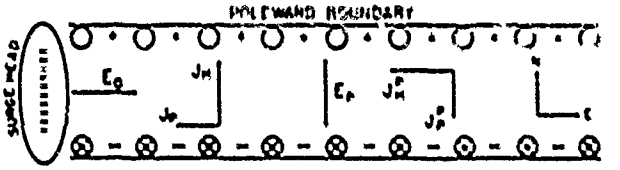

Fig. 1. The Inhester-Baumjohann current system for substorm breakup that is used in the model

in turn, are the continuation of magnetospheric currents in the equatorial plane and are dependent on the plasma characteristics there. In particular, in the MHD approximation enhanced earthward convection of magneto-tail plasma and the attached magnetic field lines that are associated with dipolar collapse are the primary energy sources for both circuits. It is the consistency of this earthward convection and the field-aligned currents with the ionospheric configuration that determines where quiescent current systems can be established between the ionosphere and the magnetosphere. The associated auroral arcs are the most likely candidates for auroral breakup.

Fig. 1 shows the ionospheric elements of the two circuits. Briefly, a westward-directed electric field drives both a westward Pedersen current and a poleward Hall current in a highly conducting slab. The lack of full continuation of the Hall current into the magnetosphere creates positive charges along the poleward boundary, generating a southward-pointing polarization field. This field drives a southward Pedersen current and a westward Hall current, thereby creating a Cowling channel. As previously stated, we believe that the establishment of this Cowling channel is an essential element of the breakup mechanism. Fig. 2(a) and (b) shows the mapping of the ionospheric circuits into the equatorial plane. The magnetospheric westward electric field, E_{W_e}, is mapped, consistent with field-aligned potential drops in the east-west circuit, to the ionosphere as E_0 in Fig. 1.

We denote W and H circuits as containing the ionospheric westward and poleward currents, respectively, as shown in Fig. 2. The W circuit (henceforth denoted WC) is a current wedge connected to the near-earth cross tail or ring current, which is correspondingly weakened within the wedge in the night sector. The H circuit (HC) is closed by an earthward current, J_{H_e}, in the equatorial plane between the upward and downward current sheets. We explicitly derive J_{H_e} below.

The Cowling channel is a dissipative structure. In Fig. 1 the dissipation is driven by the Pedersen currents only. This is simply due to the fact that the "Hall" terms-of-power balance out. In the ionosphere the WC load (westward Hall current parallel to the westward electric field) exactly equals the HC generator (northward Hall current antiparallel to southward polarization field). When we refer, therefore, to the ionospheric Hall generator in the HC circuit we do not mean to imply that the ionosphere is an energy source. The ultimate energy source is the magnetospheric portion of the WC. This electrical energy trans-

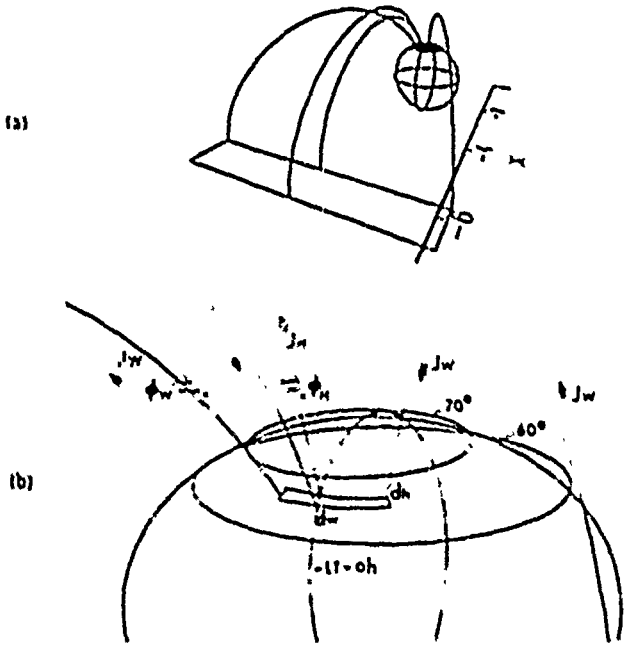

Fig. 2. (a) The substorm current wedge looking towards the earth from the magneto-tail. Note the mapping of the currents of Fig. 1 to the equatorial plane. (b) A closeup near the earth of the wedge current system. d_h and d_w denote the north-south and east-west dimensions of the breakup region in the ionosphere.

fer from the *WC* to the *HC* contributes to the power required to sustain a field-aligned potential drop in the *HC*. However, narrower breakup arcs may also require the presence of a magnetospheric generator in the *HC* to sustain a field-aligned potential along the poleward boundary. As discussed below, this situation is inherently unstable and is associated with the triggering of substorm breakup.

One of the key elements of our model regards how the *HC* current is closed in the magnetosphere. The north-south extent, d_h, of the ionospheric system shown in Fig. 1 is mapped to the equatorial plane as $d_{he} = d_h/F_r$, where F_r is a scaling factor equal to $\Delta\Lambda/\Delta L$. F_a is the azimuthal ionosphere-magnetosphere scaling factor which, in a dipole field, is equal to $L^{-3/2}$ (see Fig. 2). We choose a coordinate system in the equatorial plane such that x points towards the sun (earthward), y points towards dusk, and z points northward. Over the interval, d_{he}, the magnetospheric current, J_{He}, causes the bulk plasma to be accelerated in the $-y$ direction:

$$J_{He} \times B_e = d_{\parallel} d(\rho V_y)/dt = d_{\parallel} \Delta(\rho V_y)/\Delta t \qquad (1)$$

where B_e is the equatorial value of the magnetic field and $d_{\parallel} \simeq LR_E/3$ is the assumed field-line segment over which J_{He} is nonzero and ρ is the plasma mass density. We replace the derivatives with differentials. The plasma crosses d_{he} in a time equal to $\Delta t = d_{he}B_e/E_{We}$, where E_{We} is the dawn-to-dusk electric field in the equatorial plane. We must now make some assumptions regarding the initial plasma velocity in the y direction. If it is negative (eastward) there is a load, since both the electric field, E_{pe}, and the current density, J_{He}, are directed earthward. If the initial plasma velocity has a positive y component, however, there is a generator ($E_{pe} < 0$) and the bulk plasma motion is decelerated. For the load case, we assume that the *initial* y velocity is zero. For the generator case, we assume the *final* y velocity to be zero. Thus, $\Delta(\rho V_y) = \pm\rho E_{pe}/B_e$, where the plus and minus signs refer to the load and generator cases, respectively. Therefore, J_{He} is given by

$$J_{He} = \pm\rho E_{pe} E_{We} d_{\parallel}/(d_{he} B_e^2) \qquad (2)$$

where E_{We} and E_{pe} can be expressed in terms of the ionospheric electric fields and field-aligned potential drops, Φ_W and Φ_H, according to Kirchhoff's law

$$E_{We} = F_a(E_0 + \Phi_W/d_w) \qquad (3a)$$

$$E_{pe} = F_r(E_p - \Phi_H/d_h). \qquad (3b)$$

III. Description of Quiescent Solutions

We assume (see Fig. 2) that a field-aligned potential drop, Φ_W, exists in the western leg of the east-west circuit and that a field-aligned potential drop, Φ_H, exists in the poleward leg of the north-south circuit. Knowing the expression for J_{He} as given in (2), we can determine all the relevant parameters needed in our model to define the structure of the pre-breakup regime.

Fig. 3 shows a flowchart of the logic used. Assume that in the equatorial plane there is a plasma with an ion density n_i, an ion mass m_i, an electron density $n_e = n_i$, and the electrons have a parallel temperature $T_{\parallel e}$ and a perpendicular temperature of $T_{\perp e}$. The model of Fridman and Lemaire [23] is then used to calculate the precipitation flux (current density) at the ionosphere for both the east-west and north-south circuits for given field-aligned potential drops. Current continuity at the ionosphere is then invoked to calculate the ionospheric westward and poleward currents J_W and J_N. They are

$$J_W = E_0\Sigma_p + E_p\Sigma_H = j_{\parallel W}\, 1 \times 10^5 \qquad (4a)$$

$$J_N = E_0\Sigma_H - E_p\Sigma_p = j_{\parallel H} R_b \qquad (4b)$$

where Σ_H and Σ_p are the ionospheric height-integrated Hall and Pedersen conductivities inside the arc region. For lack of a detailed model for current continuity at the western boundary, we scale the precipitating flux so that 1 μA/m^2 of precipitation current corresponds to 0.1 A/m of ionospheric current. This corresponds to a circular hot spot at the western boundary with a radius of 64 km. R_b is the extent of the poleward boundary and is estimated from auroral studies as being about 20 km. The ionospheric conductivities are calculated using the model of Robinson *et al.* [24]. The electric fields inside the Inhester-Baumjohann current system shown in Fig. 1 are then found by inverting (4a) and (4b). Equations (3a) and (3b) are now used to find the corresponding electric fields in the equatorial plane. These results are inserted into (2). Current continuity, however, requires that $J_{He} = F_a J_N$, where J_N is the net poleward ionospheric current density (A/m) in-

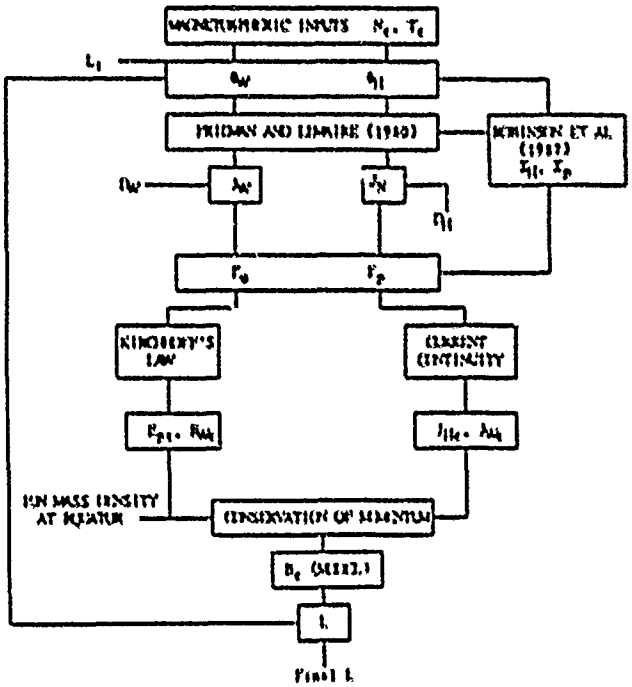

Fig. 3. A flowchart for the method of solution used in the model.

side the pre-breakup arc. The equatorial B field is assumed to be dipolar ($\sim L^{-3}$). Therefore, L is determined. Note, however, that in order to initiate the calculation an L shell had to be assumed for the scaling factors in the Fridman and Lemaire model [23]. Usually, this initial assumption differs from the value of L finally obtained. Fortunately, convergence is obtained by successively iterating the calculation using the final L value for the initial assumption in the Fridman and Lemaire model [23].

We now want to give a numerical example of our model. Unfortunately, the large number of parameters involved precludes an exhaustive exploration here. We assume that the plasma sheet moves sufficiently inward during magnetically disturbed times [25] so that plasma sheet values apply. Thus we set $n_i = 1\ \mathrm{cm}^{-3}$ and $T_{e\perp} = T_{e\parallel} = 1$ keV. The substorm current wedge is able to form when the field-aligned potentials can accelerate electrons to the E layer (~ 4 keV, [26]). On the other hand, we choose 32 kV as a reasonable upper limit to the field-aligned potential drop which corresponds to a precipitation current of $\sim 30\ \mu\mathrm{A/m}^2$. Using this range for Φ_H (see Fig. 2(b)) corresponds to a net westward ionospheric current, J_W, of ~ 0.3–3.0 A/m according to (4a). By using the four values of 4, 8, 16, and 32 kV for Φ_W, our results are thereby parameterized according to the intensity of the westward electrojet. For purposes of illustration, the east-west extent of the breakup arc is fixed at 200 km.

Fig. 4(a)-(d) depicts the quiescent arc structures as a function of the ionospheric north south extent of the enhanced conductivity breakup region and in terms of invariant latitude for three values of Φ_H, 2.5, 5.0, and 10.0 kV. These first three runs assume 50 percent O^+ in the equatorial plane (this affects J_{He} as given in (2)). Fig. 4(d) is discussed below. All curves in this figure were generated by incrementing d_h in 5-km steps. The peaks in the curves correspond to the magnetospheric portion of the *HC*, switching from a generator load as d_h increases. When this happens all the energy in the *HC* is supplied by the Hall generator. As discussed below, the transition from a *HC* load to a generator is inherently unstable. Thus, the peaks in our model will be closely associated with the triggering of breakup. These peaks occur at smaller values of d_h for smaller values of Φ_H. This is due to the fact that smaller field-aligned potentials are smaller loads in the *HC*, so that the ionospheric Hall generator can support these loads at smaller values of d_h. The figure shows that self-consistent quiescent solutions occur closer to the earth the stronger the westward electrojet (Φ_W) is. The magnitude of Φ_H seems to have little effect on the location at which pre-breakup solutions ($d_h \approx 15$–20 km) may occur. But both Φ_H and Φ_W do affect the transition point at which the magnetosphere becomes a generator in the *HC*. Note that the model predicts that larger quiescent current structures can be formed at higher latitudes, as seen from the figure.

Fig. 4(a)-(c) also indicates that incipient breakup regions (15–20 km in the N-S direction versus 200 km in the E-W direction) can occur on invariant latitudes corresponding to dipolar L shells below 6 ($\Lambda \approx 65.9°$) as observed by [3] and [27]. We have found that solutions can occur on even lower L shells if the oxygen concentration is increased or a more realistic field model is used. The solutions are also consistent for surge-type quiescent structures ($d_h \sim$ 100's km). That is, the surge counterpart to breakup is predicted to occur at higher L shells, as observed.

Fig. 4(d) is the same as (b) except that there is no oxygen in the plasma sheet. A higher concentration of O^+, presumably originating in the ionosphere, allows a pre-breakup arc to form at lower L shells. This is because the magnitude of J_{He} is fixed by Φ_H through the Fridman and Lemaire model [23], which implies by (2) that $nn_i L^{10} F_*^3$ is constant. If the magnitude of the O^+ seeding of the plasma sheet by the ionosphere [8] is dependent on the duration of the growth phase, then our model predicts that breakup associated with these prolonged growth phases should occur more equatorward.

It is also found that the arc location is relatively insensitive to the plasma-sheet electron temperatures above 1 keV.

IV. Stability of Quiescent Solutions

Recall from (3b) and Fig. 4 that the magnetospheric part of *HC* is a generator if $\Phi_H / d_h > E_p$. Now, if Φ_H increases, as between Fig. 4(a) and (b), then for some auroral arcs the magnetospheric portion of the *HC* switches from a load to a generator. (Note that in the earlier approach of Coroniti and Kennel [22] this generator does not exist, since they assumed the magnetospheric polarization electric field to be zero.) We now show that this leads to instability and the triggering of breakup. Let us

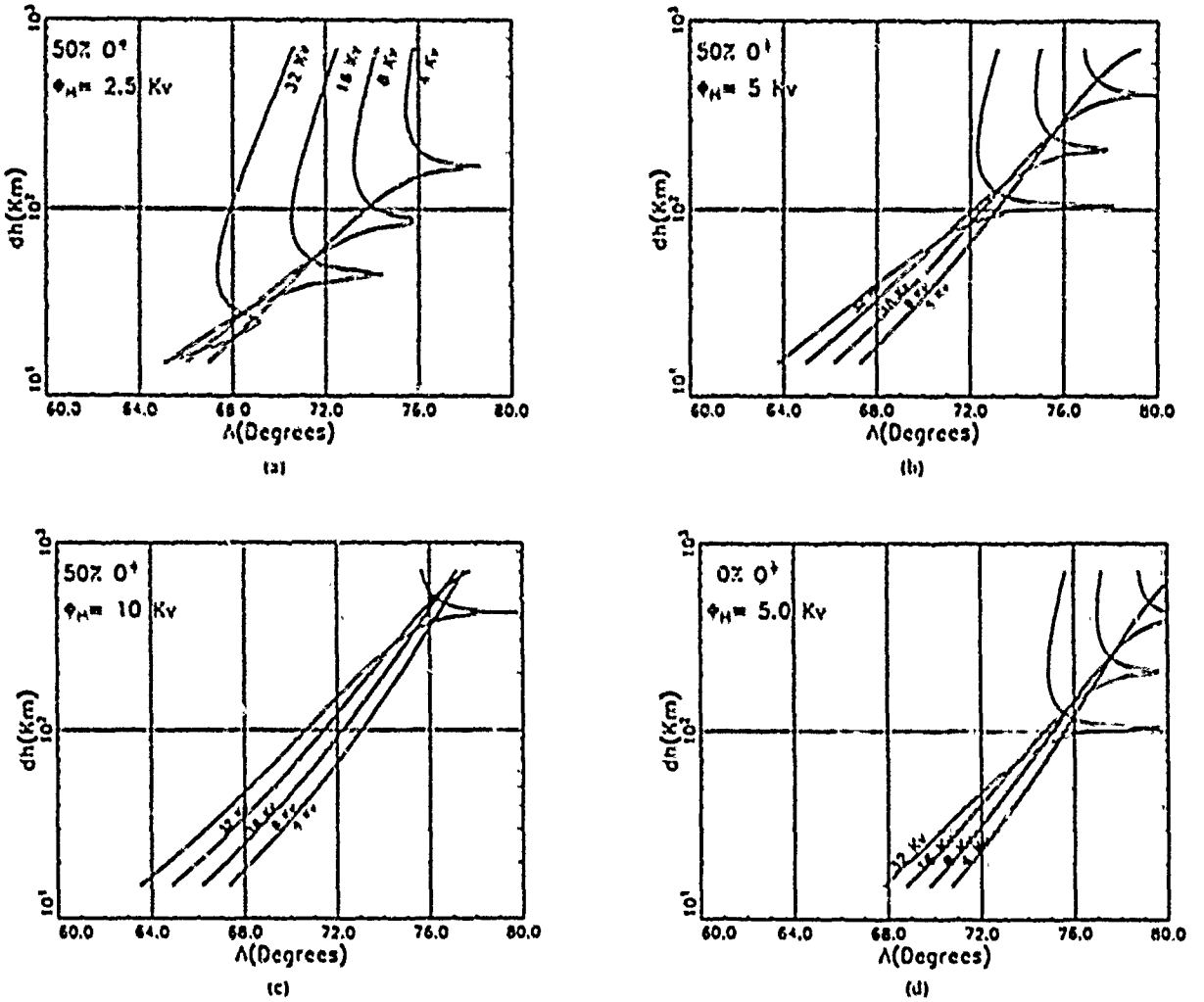

Fig. 4. Quiescent solutions for the location of substorm breakup as a function of invariant latitude. d_h is the north-south extent of the breakup region in the ionosphere. The four voltages (4, 8, 16, and 32 kV) are values for the field-aligned potential drop along the western leg of the circuit. (See Fig. 2.) The field-aligned potential drop along the poleward arc boundary, $\Phi_{//}$, increases from 2.5 to 10 kV as shown in Fig. 4(a)-(c). The peaks denote the switching of the magnetospheric portion of the // circuit from a generator to a load as d_h increases. The generator (unstable) region expands as $\Phi_{//}$ increases. All examples assumed a 50 percent O^+ concentration in the plasma sheet except in Fig. 4(d), which is 0 percent. Note that an enhancement of the O^+ concentration shifts the breakup region equatorward.

do this by considering the effect of poleward expansion on $\Phi_{//}$ itself. We assume that inductive effects keep $J_{//}$ approximately constant during the initial stages. By solving equation (3b) for $\Phi_{//}$, it is easy to show, using (2) (with the plus sign), for E_p, that $\delta\Phi_{//}$ increases with δd_h as long as $\Phi_{//} > E_p d_h/2$. That is, even when the magnetospheric portion of HC is a weak load, $\Phi_{//}$ increases as the breakup arc expands poleward. In Rothwell *et al.* [20], we showed that the speed of the poleward expansion is proportional to the electron precipitation energy along the poleward boundary or $\Phi_{//}$. Therefore, in our model there is a positive feedback between poleward expansion and the field-aligned potential drop along the poleward boundary. This inherent (global) instability initiates breakup.

In more detail, the dynamical equation for d_h, the north-south extent of the breakup arc in the ionosphere, is given by

$$\delta d_h = C\Phi_{//}^{1.2}\delta t \qquad (5)$$

from [20] and where $C = 5\alpha E_0/B_i$. Here, B_i is the value of the earth's magnetic field at the ionosphere, E_0 is as defined in Fig. 1, and α is the closure parameter as defined in [20]. Basically, it is the fraction of the poleward Hall current (Fig. 1) that is continued into the magnetosphere by the electron precipitation along the poleward boundary. The dynamical equation for $\Phi_{//}$, the field-aligned potential drop along the poleward boundary, is given by

$$\delta\Phi_{//} = C(2\Phi_{//}/d_h - E_p)\,\Phi_{//}^{1.2}\delta t. \qquad (6)$$

We will now look at some numerical solutions.

Figs 5(a) and 6(a) show the time evolution of $\Phi_{//}$ as normalized to its initial value at $t = 0$ as the arc (surge) expands. Figs 5(b) and 6(b) are the corresponding curves for d_h. Five initial values for d_h are listed (20, 50, 100, 200, and 400 km) in Figs. 5(a) and 6(a). The associated L-shell locations are also listed for the quiescent, pre-

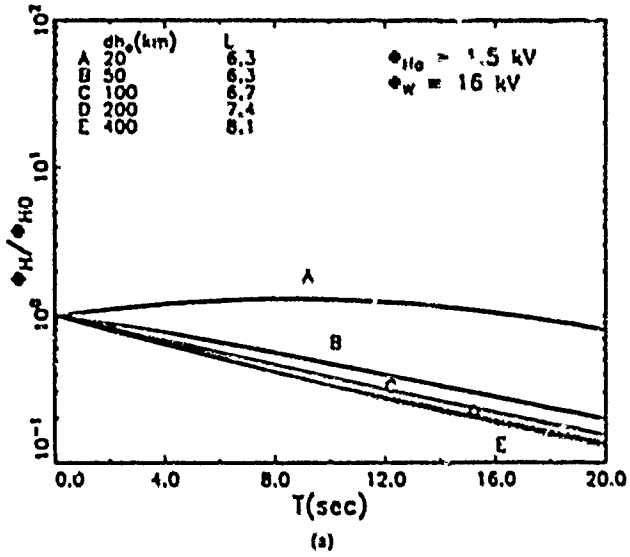

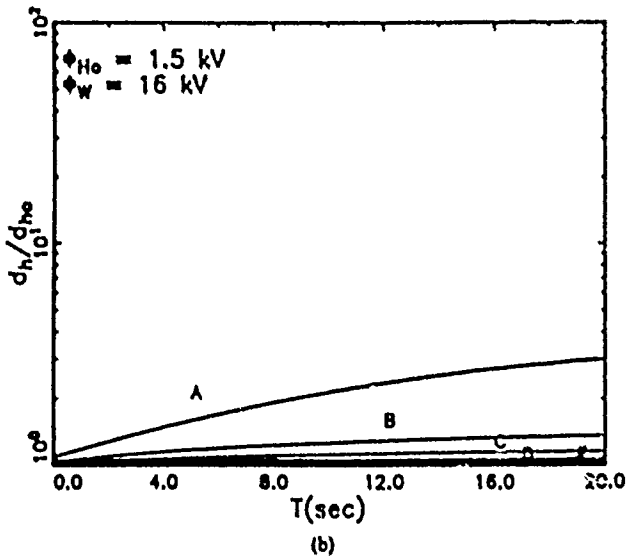

Fig. 5. (a) The time evolution of the field-aligned potential drop along the poleward arc (surge) boundary for an initial value of 1.5 kV and for various initial values for d_h of 20, 50, 100, 200, and 400 km, respectively. These initial values correspond to curves A, B, C, D, and E. The L values at which the quiescent arc (surge) structures can form according to Fig. 3 and the dipole approximation are also given. Note here and in (b) that all cases are relatively stable. (b) The corresponding time evolution of d_h for the same initial values as used in (a).

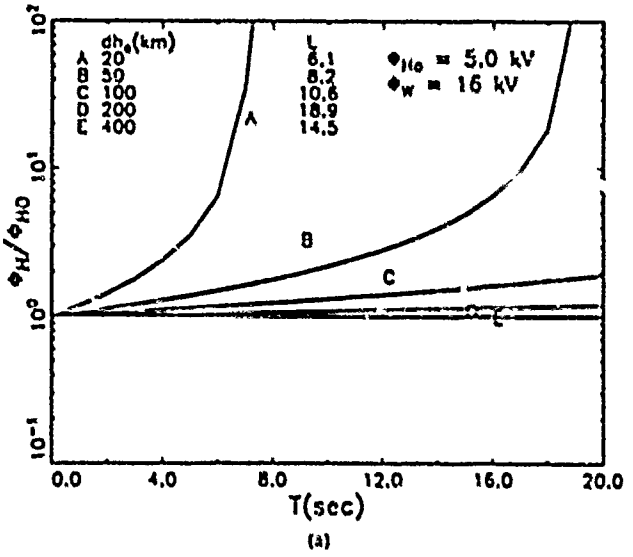

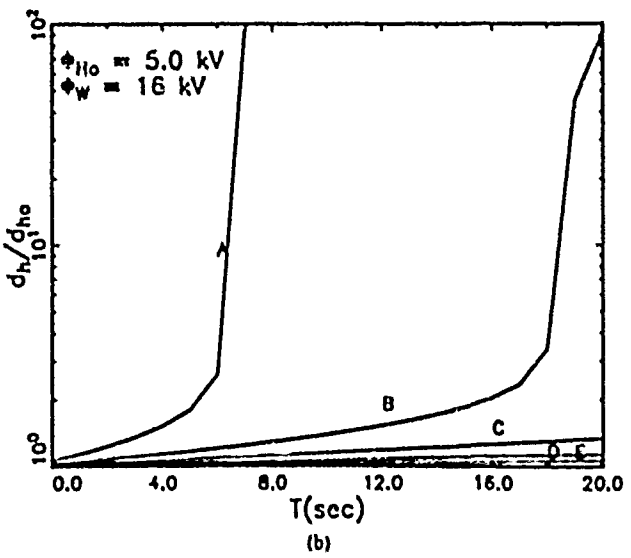

Fig. 6. (a) The same as for Fig. 5(b) except that the initial value of Φ_H has increased to 5.0 kV. This changes the location of the pre-breakup quiescent arc (surge) structures, as calculated in the dipole approximation, and causes the narrower arc structures (20–50 km) to be explosively unstable. (b) Time evolution of d_h for an initial value of 5.0 kV for Φ_H, as in (a).

breakup arc structures as determined by the method shown in Fig. 3. The related curves are denoted by the letters A through E. We chose a value of 16 kV for Φ_W as being representative. Note that when the initial field-aligned potential is weak (1.5 kV), as in Fig. 5a, the poleward expansion as seen in Fig. 5(a) and (b) is weak and finite. However, if Φ_H(initial) increases to 5.0 kV, then the smaller arcs (20- to 50-km wide) become successively unstable to poleward expansion, as seen in Fig. 6(a) and (b). Physically, this implies that a brightening along the poleward boundary of a previously quiescent narrow arc that is located at fairly low L shells (see Fig. 4) will render the arcs unstable to rapid poleward expansion. The value of E_0 (see Fig. 1) obtained for the examples shown in Fig. 6(a) and (b) is on the order of 16 mV/m. The location of the pre breakup quiescent arc was determined using a dipole field model and, therefore, the actual location may be different. For example, L = 8.2 (the 50-km case in Fig. 6(a) and (b)) corresponds to an invariant latitude of 69.6°. Using the Tsyganenko field model [14] as described below and as shown in Fig. 7, this corresponds to magnetic latitudes between 66° and 68°, depending on the value of K_p. Thus, our model can predict where breakup will be observed for a given arc size and closely reflects the observed dynamical features of this phenomenon. In terms of our previous comments, the enhancement of Φ_H causes a transition from the stable regime (a large magnetospheric load in *HC*) to the unstable regime (a weak magnetospheric load or a magnetospheric

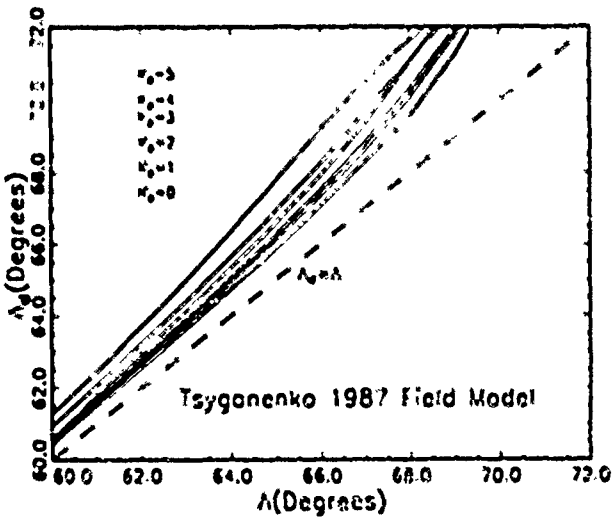

Fig. 7. The magnetospheric closure current J_{Hc} (see text), depends on a specific magnetic field model through the equatorial value of the magnetic field and the scaling factors between the ionosphere and equatorial plane. The Tsyganenko [14] magnetic field model was used to calculate this parameter and then equated with an equivalent dipole latitude. In this way our model can be scaled to a more realistic field model. The highest curve denotes K_p = 5 while the lowest curve denotes K_p = 0. This figure shows that breakup arcs will tend to form at lower latitudes during periods of higher magnetic activity (K_p), consistent with observations.

generator in the *HC*). We presently believe that the instability eventually saturates due to electron-ion recombination in the ionosphere and the presence of inductive effects over longer time scales.

The solutions shown in Fig. 4 were obtained using a dipole magnetic field model. These results have been scaled to the Tsyganenko [14] model as shown in Fig. 7 using the fact that the magnetospheric closure current, J_{Hc}, depends on a specific magnetic-field model (see (2)). The ordinate is the value of the invariant latitude for a dipole field. The abscissa is the equivalent latitude for the same solution but calculated according to the Tsyganenko model. The six scaling curves correspond to different K_p values, with the largest K_p value (= 5) at the top and the lowest (= 0) at the bottom. The results imply that a pre-breakup arc structure as calculated from a dipole field model will form at lower L shells at higher K_p values. This is also consistent with observations.

V. Conclusions

We have shown, by taking the ionospheric current system shown in Fig. 1 and mapping it to the equatorial plane, that two coupled circuits can form. One is north-south (*HC*) the other is east-west (*WC*). The *HC* is closed in the equatorial plane by a current which is consistent with the $J \times B$ force there. The ultimate energy source for both circuits is earthward-convecting plasma from the magneto-tail and the electrical power generated by the dipolar collapse. The *WC* transfers energy to the *HC* through an ionospheric Hall generator. By inputting reasonable values into the solution method described above and shown in Fig. 3, we are able to predict the locations (L shells) at which self-consistent quiescent arc structures may occur as a function of the north-south extent of the enhanced conductivity region in the ionosphere.

The major results of our breakup model are the following: 1) Pre-breakup structures can occur on fairly low L shells (5), (6), consistent with observations. 2) A higher concentration of O^+ in the plasma sheet and/or a stronger westward electrojet shifts the conditions favorable to breakup to lower L shells. This implies that an O^+ seeding of the plasma sheet by the ionosphere during a prolonged growth phase would cause breakup to occur closer to the earth. The concurrent unloading of the enhanced magnetic energy stored in the tail lobes would also imply that this particular breakup would be very explosive. 3) The location of the pre-breakup structure is relatively insensitive to the electron temperature in the plasma sheet. 4) We find a positive feedback between poleward expansion and Φ_H and presently speculate that this instability can trigger substorm breakup. 5) We find for the cases studied that the predicted values for the *WC* equatorial electric fields, E_{M_e}, are between 3 and 11 mV/m at geosynchronous. This compares favorably with the substorm electric field values measured at geosynchronous orbit by Pedersen *et al.* [28] on GEOS-2. 6) Narrower auroral arcs that form an incipient substorm current wedge at lower shells undergo the most violent breakup. Using the Tsyganenko 1987 [14] model, we find that breakup should occur on even lower L shells as the magnetic activity index, K_p, increases.

Finally, let us consider the following speculative idea. We assume that the ionospheric current system is as shown in Fig. 1 and is mapped to the equatorial plane as shown in Fig. 2. We also assume that the magnetospheric electric field, E_{M_e}, in the *HC* coincides with that produced by a global two-cell polar-cap convection pattern [12], [29]. If E_{M_e} is negative (points tailward), it is antiparallel to J_{H_e} and the magnetospheric *HC* is a generator (see (2) and (3b)). This can occur only west of the Harang discontinuity. East of the Harang discontinuity, E_{M_e} is earthward and the magnetospheric *HC* is a load. We speculate that this feature could abruptly stop the eastward expansion at midnight, as observed by Viking [13].

Acknowledgment

It is with pleasure that we acknowledge the helpful comments of N. Maynard, W. Burke, F. Rich, H. Singer and M. Heinemann from the Air Force Geophysics Laboratory (AFGL), and of E. Whipple, who is visiting AFGL from UCSD. The clerical assistance of L. Silva is also appreciated.

References

[1] A. T. Y. Lui and J. R. Burrows, "On the location of auroral arcs near substorm onsets," *J. Geophys. Res.*, vol. 83, pp. 3342-3348, 1978.
[2] S.-I. Akasofu, "A study of auroral displays photographed from the DMSP-2 satellite and from the Alaska meridian chain of stations," *Space Sci. Rev.*, vol. 16, pp. 617-725, 1974.

[3] P. Tanskanen *et al.*, "Different phases of a magnetospheric substorm on June 23, 1979," *J. Geophys. Res.*, vol. 92, pp. 7443-7457, 1987.
[4] R. J. Pellinen and W. J. Heikkila, "Observations of auroral fading before breakup," *J. Geophys. Res.*, vol. 83, pp. 4207-4217, 1978.
[5] T. J. Hallinan, "The dynamics of substorm onset," *EOS*, vol. 68, p. 1420, 1987.
[6] Richard L. Kaufmann, "Substorm currents: Growth phase and onset," *J. Geophys. Res.*, vol. 92, pp. 7471-7486, 1987.
[7] R. L. McPherron, C. T. Russell, and M. P. Aubrey, "Satellite studies of magnetospheric substorms on August 15, 1968, 9: Phenological model for substorm," *J. Geophys. Res.*, vol. 78, pp. 3131-3149, 1973.
[8] Charles L. Chappell, "The terrestrial plasma source: A new perspective in solar-terrestrial processes from Dynamic Explorer," *Revs. of Geophys.*, vol. 26, pp. 229-248, 1988.
[9] J. L. Burch, "Energetic particles and currents: Results from Dynamic Explorer," *Revs. of Geophys.*, vol. 26, pp. 215-228, 1988.
[10] W. Lennartsson and E. G. Shelley, "Survey of 0.1 to 16-keV/e plasma sheet ion composition," *J. Geophys. Res.*, vol. 91, pp. 3061-3076, 1986.
[11] J. B. Cladis, "Parallel acceleration and transport of ions from polar ionosphere to plasma sheet," *Geophys. Res. Lett.*, vol. 13, pp. 893-896, 1986.
[12] J. P. Heppner and N. C. Maynard, "Empirical high-latitude electric field models," *J. Geophys. Res.*, vol. 92, pp. 4467-4489, 1987.
[13] G. G. Shepherd, C. D. Anger, J. S. Murphree, and A. Vallance-Jones, "Auroral intensification in the evening sector observed by the Viking ultra violet imager," *Geophys. Res. Lett.*, vol. 14, pp. 395-398, 1987.
[14] N. A. Tsyganenko, "Global quantitative models of the geomagnetic field in the cislunar magnetosphere for different disturbance levels," *Planet. Space Sci.*, vol. 35, pp. 1347-1358, 1987.
[15] J. R. Kan, L. Zhu, and S.-I. Akasofu, "A theory of substorm: Onset and subsidence," *J. Geophys. Res.*, vol. 93, pp. 5624-5640, 1988.
[16] J. R. Kan and W. Sun, "Simulation of the Westward Traveling Surge and Pi 2 pulsations during substorms," *J. Geophys. Res.*, vol. 90, pp. 10911-10922, 1985.
[17] P. L. Rothwell, L. P. Block, M. B. Silevitch, and C.-G. Fälthammar, "A new model for substorm onsets: The pre-breakup and triggering regimes," *Geophys. Res. Lett.*, vol. 15, pp. 1279-1282, 1988.
[18] H. W. Iabester, W. Baumjohann, R. W. Greenwald, and E. Nielsen, "Joint two-dimensional observations of ground magnetic and ionospheric electric fields associated with auroral zone currents, 3: Auroral zone currents during the passage of a Westward Traveling Surge," *J. Geophys. Res.*, vol. 49, pp. 155-162, 1981.
[19] P. L. Rothwell, M. B. Silevitch, and L. P. Block, "A model for the propagation of the Westward Traveling Surge," *J. Geophys. Res.*, vol. 89, pp. 8941-8948, 1984.
[20] P. L. Rothwell, M. B. Silevitch, and L. P. Block, "Pi 2 pulsations and the Westward Traveling Surge," *J. Geophys. Res.*, vol. 91, pp. 6921-6928, 1986.
[21] P. L. Rothwell, M. B. Silevitch, L. P. Block, and P. Tanskanen, "A model of the WTS and the generation of Pi 2 pulsations," *J. Geophys Res.*, vol. 93, pp. 8613-8624, 1988.
[22] F. V. Coroniti and C. F. Kennel, "Polarization of the auroral electrojet," *J. Geophys. Res.*, vol. 77, pp. 2835-2850, 1972.
[23] M. Fridman and J. Lemaire, "Relationships between auroral electron fluxes and field-aligned potential differences," *J. Geophys. Res.*, vol. 85, pp. 664-670, 1980.
[24] R. M. Robinson, R. R. Vondrak, K. Miller, T. Dabbs, and D. Hardy, "On calculating ionospheric conductances from the flux and energy of precipitating electrons," *J. Geophys. Res.*, vol. 92, pp. 2565-2569, 1987.
[25] C. E. McIlwain, "Substorm injection boundaries," in *Magnetospheric Physics*, B. M. McCormac, Ed. Dordrecht, Holland: Reidel, 1974, pp. 153-154.
[26] M. H. Rees, "Auroral ionization and excitation by incident energetic electrons," *Planet. Space Sci.*, vol. 29, pp. 225-247, 1963.
[27] G. Kremser *et al.*, "Coordinated balloon satellite observations of energetic particles at the onset of magnetospheric substorms," *J. Geophys. Res.*, vol. 87, pp. 4445-4453, 1982.
[28] A. Pedersen *et al.*, "Electric fields in plasma sheet and plasma sheet boundary layer," *J. Geophys. Res.*, vol. 90, pp. 1231-1242, 1985.
[29] J. R. Kan and L. C. Lee, "Theory of imperfect magnetosphere-ionosphere coupling," *Geophys. Res. Lett.*, vol. 7, pp. 633-636, 1980.

Paul L. Rothwell was born in Norwood, MA, on April 2, 1938. He received the A.B. degree from Harvard College, Cambridge, MA, in 1960. The M.S. and Ph.D. degrees were obtained in 1962 and 1967, respectively, from Northeastern University, Boston, MA.

He is currently a Research Physicist at the Air Force Geophysics Laboratory at Hanscom Field, Bedford, MA. His research interests are primarily in the field of space physics, particularly the earth's radiation belts and the dynamics of substorm onsets. Other research interests have included experimental particle physics, solar isotopes, particle dynamics in the earth's magnetotail, spacecraft charging, and single event upsets in microelectronic devices flown on-board spacecraft.

•

Lars P. Block was born in Stockholm, Sweden, on April 19, 1925. He received the B.S. degree in electrical engineering in 1948 and the degree of Dr. of Technology in plasma physics in 1958, both from the Royal Institute of Technology (KTH) in Stockholm, Sweden.

Until 1967 he did research on thermonuclear fusion at the Atomic Energy Company of Sweden. Since 1967 he has been engaged in space plasma physics research at the KTH. He has been a Visiting Scientist for periods of 1–10 months at the Stevens Institute of Technology in Hoboken, NJ, at the Jet Propulsion Laboratory in Pasadena, CA, at the University of Iowa in Iowa City, IA, at Stanford University, at the University of Texas at Dallas, and at the Air Force Geophysics Laboratory in Bedford, MA. Currently he is a Research Professor at the KTH, doing magnetospheric research with instruments carried by balloons, rockets, and satellites, most recently with the ones carried by the first Swedish research satellite Viking.

•

Michael B. Silevitch (S'67–M'72–SM'84) was born in 1942. He received the B.S.E.E., M.S.E.E., and Ph.D. degrees from Northeastern University, Boston, MA, in 1965, 1966, and 1971, respectively. He also received the M.S. degree in physics from Brandeis University, Waltham, MA, in 1970.

He is currently a Professor of Electrical and Computer Engineering at Northeastern University. In addition, he is also the Director of Northeastern's Center for Electromagnetics Research, an NSF-Industry University Center. His research interests are focused on the temporal dynamics of space plasmas, plasma sheaths and double layers, and plasma statistical mechanics.

•

Carl-Gunne Fälthammar was born in Markaryd, Sweden, on December 4, 1931. He received from the Royal Institute of Technology, Stockholm, the degree of Civilingenjör (graduate engineer) in 1956, the Tekn. lic. (approx. Ph.D.) degree in 1960, and the Docent (approx. assistant professor) in 1966.

In 1969 he was appointed as Associate Professor of Plasma Physics at the Royal Institute of Technology. In 1973 he was called on to succeed Hannes Alfvén as Professor of Plasma Physics. Since 1967 he has been Chairman of the Department of Plasma Physics of the Royal Institute of Technology. His research interests include fundamental aspects of plasma electrodynamics, with application to space and astrophysical plasmas, especially in the context of auroral and magnetospheric physics.

Prof. Fälthammar has served in several international scientific organizations, including the Executive Committee of IAGA, the Space Science Committee of the European Science Foundation, and the Council of the European Geophysical Society. He is Associate Editor of *Astrophysics Space Science*, and *Annales Geophysicae*. Since 1975 he has been a Full Member of the Royal Swedish Academy of Sciences.

[illegible] Vol. X, No. X, pp. [illegible], 1986
Printed in the U.S.A.

[illegible] Special Issue No.
Copyright [illegible] COSPAR

SUBSTORM BREAKUP ON CLOSED FIELD LINES

P. L. Rothwell,* L. P. Block,** M. B. Silevitch*,*** and C.-G. Fälthammar**

*Air Force Geophysics Laboratory, Hanscom AFB, Bedford, MA 01731, U.S.A.
**Department of Plasma Physics, Royal Institute of Technology, S100 44 Stockholm 70, Sweden
***Department of Electrical and Computer Engineering and the Center for Electromagnetics Research, Northeastern University, Boston, MA 02115, U.S.A.

ABSTRACT

This model explains why breakup has been observed as low as L = 5-6 and predicts that a higher concentration of O^+ in the plasma sheet will permit breakup at such low L values. It is argued that the establishment of a coupled current structure within a single arc leads to a quasi-stable system i.e. the pre-breakup regime. Perturbation of the pre-breakup structure leads to an instability criterion. Certain quiescent configurations are inherently unstable. Thus transitions from a stable to an unstable situation can trigger a rapid poleward expansion of the quiescent arc or substorm breakup. In our model the kinetic energy of injected plasma from the magnetotail supplies the energy for breakup.

INTRODUCTION

Substorm breakup is usually preceded by the sudden brightening of a previously quiescent auroral arc near local midnight. Once it is "triggered" the arc dynamics in the classical model is characterized by a by rapid poleward and westward expansion /1/, /2/. Auroral intensifications with characteristics similar to those of substorm breakup can occur in the evening sector as detected on Viking by Shepherd /3/. Triggering generally occurs on the poleward boundary of the diffuse aurora which can be at invariant latitudes which correspond to dipolar L-shells as low as 5-6.

The purpose of this paper is to establish the quiescent pre-breakup conditions which are necessary for triggering to occur at such low latitudes. The basic idea in our model is that the pre-breakup arc is an arc in which two coupled electrical circuits are established between the ionosphere and the magnetosphere. I.e. it is the incipient formation of a substorm current wedge /4/. As such it has the basic features of the Westward Traveling Surge (WTS) current system that we have previously used /5/, /6/ and as used by Coroniti and Kennel /7/. As implied from Figure 1, the physical picture is of two current sheets; one flowing upward on the poleward boundary and another flowing downward on the equatorward boundary of an enhanced conductivity region in the ionosphere. Our approach is comparable to one used some years ago by /7/. However, we treat a nonzero polarization field in the magnetosphere which we consider essential for the breakup instability.

THE TWO CIRCUIT MODEL

The extended east-west orientation of the breakup arc motivates an approach which models the system as two coupled circuits, one north-south and the other east-west. In our model these circuits close in the magnetosphere via field-aligned currents which are calculated from the model of /8/. The field aligned currents, in turn, are the continuation of magnetospheric currents in the equatorial plane and are dependent on the plasma characteristics there. In particular, enhanced quasi-steady earthward convection of magnetotail plasma is the primary energy source for both circuits. It is the consistency of this earthward convection and the field aligned currents with the ionospheric configuration that determines where quiescent current systems can be established between the ionosphere and the magnetosphere. The associated auroral arcs are the likely candidates for auroral breakup.

The ionospheric elements of the two circuits is described in detail in /6/. Figures 2a and 2b show the mapping of the ionospheric circuits into the equatorial plane. It is assumed that the magnetospheric westward electric field, E_{WG}, associated with the earthward convection from the magnetotail is mapped, consistent with field-aligned potential drops in the east-west circuit, to the ionosphere.

We denote W and H circuits as containing the ionospheric westward and poleward currents, respectively, as shown in Figure 1. The W-circuit, (henceforth denoted WC) is a current wedge connected to the near earth cross-tail or ring current, which is correspondingly weakened within the wedge in the night sector. The H-circuit (HC) is closed by an earthward current, J_{He}, in the equatorial plane.

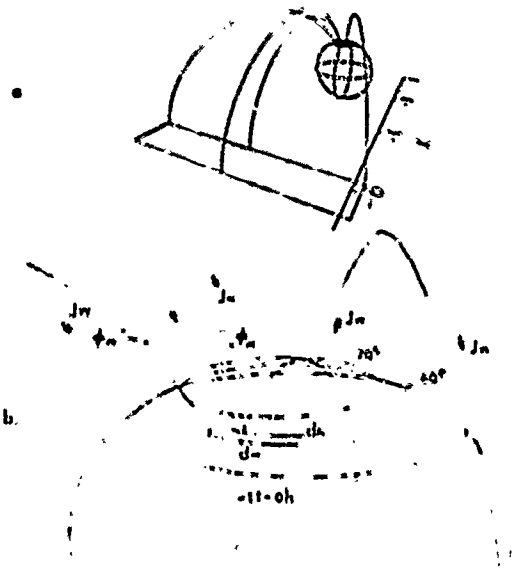

Figure 1. a) The substorm current wedge looking towards the earth from the magnetotail. Note the mapping of the ionospheric currents of Ref. /6/ to the equatorial plane. b) A closeup near the earth of the wedge current system. d_H and d_W denote the north-south and east-west dimensions of the breakup region in the ionosphere.

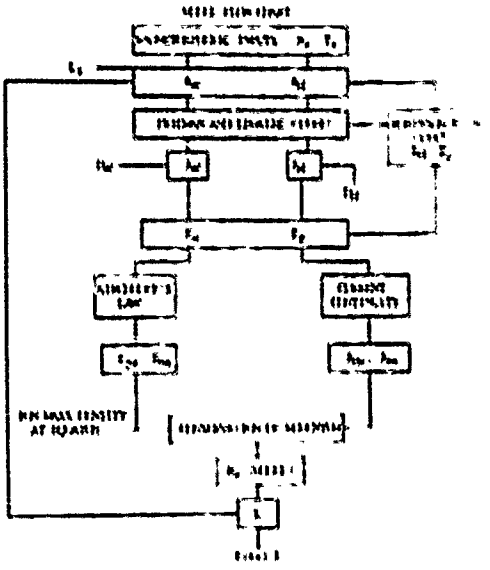

Figure 2. A flow chart the method of solution used in the model.

One of the key elements of our model is how the HC current is closed in the magnetosphere. The north-south extent, d_H, of the ionospheric current system shown in Figure 1 is mapped to F_r and F_a are the radial and azimuthal ionosphere-magnetosphere scaling factors, see Figure 2. We choose a coordinate system in the equatorial plane such that x points towards the sun (earthward), y points towards dusk and z northward. Over the interval, d_{He}, the magnetospheric current, J_{He}, causes the bulk plasma to be accelerated in the -y direction. The derivation of J_{He} is given elsewhere /9/ and will not be repeated.

$$J_{He} = \rho E_{pe} E_{We} d_H / (d_{He} B_z^2) \qquad (1)$$

where E_{We} and E_{pe} can be expressed in terms of the ionospheric electric fields and field-aligned potential drops, ϕ_W and ϕ_H, according to Kirchhoff's law

$$E_{We} = F_a(E_o + \phi_W/d_W) \qquad (2a)$$

$$E_{pe} = F_r(E_p - \phi_H/d_H) \qquad (2b)$$

DESCRIPTION OF QUIESCENT SOLUTIONS

We assume (see Figure 1) that a field-aligned potential ϕ_W drop exists in the western leg of the east-west circuit and that a field-aligned potential, ϕ_H, exists in the poleward leg of the north-south circuit. Knowing the expression for J_{He} as given in equation (1) we can determine all the relevant parameters needed in our model to define the structure of the pre-breakup regime. Figure 2 shows a flow chart of the logic used. Assume that in the equatorial plane there is a plasma with ion density n_i, ion mass m_i, electron density n_e =

n_i, and the electrons have a parallel temperature $T_{\|e}$ and a perpendicular temperature of $T_{\perp e}$. Unfortunately, the large number of parameters involved precludes an exhaustive exploration here. We assume that the plasma sheet moves sufficiently inward during magnetically disturbed times /10/ so that plasma sheet values apply. Thus we set n_i = 1 cm^{-3} and $T_{e\perp}$ = $T_{e\|}$ = 1 keV. The substorm current wedge is able to form when the field-aligned potentials can accelerate electrons to the E-layer (~ 4 keV, /11/). On the other hand, we choose 32 kV as a reasonable upper limit to the field-aligned potential drop which corresponds to a precipitation current of ~ 30 mA/m^2. Using this range for Φ_H (see Figure 2b) corresponds to a net westward ionospheric current, J_H, of ~ 0.1 - 1.0 A/m. By using the four values of 4 kV, 8 kV, 16 kV and 32 kV for Φ_H our results are thereby parameterized according to the intensity of the westward electrojet. For purposes of illustration the east-west extent of the breakup region is fixed at 200 km.

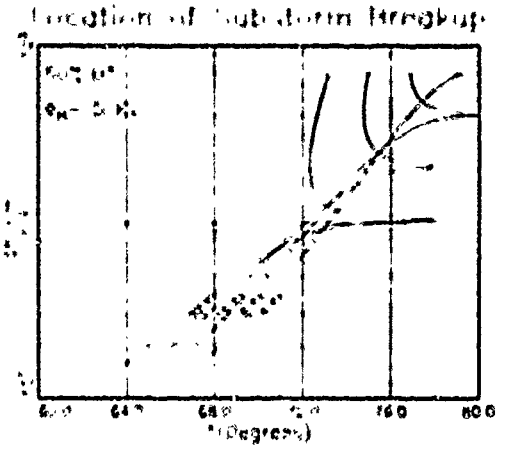

Figure 3. Quiescent solutions for the location of substorm breakup as a function of invariant latitude. $d_\|$ is the north-south extent of the breakup region. The four voltages are values for the field aligned potential drop along the western leg of the circuit. See Figure 1. The peaks denote when the magnetospheric portion of the H-circuit switches from being a generator to being a load as d_h increases.

Figure 3 depicts the quiescent arc structures as a function of the ionospheric north-south extent of the enhanced conductivity breakup region and in terms of invariant latitude for $\Phi_\|$ equal to 5.0. These assume 90° in the equatorial plane (this affects $J_{\|e}$ as given in equation (3)). All curves in this Figure were generated by incrementing $d_\|$ in 5 km steps. The peaks in the curves correspond to the magnetospheric portion of the HC switching from a generator to a load as $d_\|$ increases. When this happens all the energy in the HC is supplied by the Hall generator. As discussed below the transition from an HC load to a generator is inherently unstable. Thus the peaks in our model will be closely associated with the triggering of breakup. These peaks occur at smaller values of $d_\|$ for smaller values of $\Phi_\|$. This is due to the fact that smaller field-aligned potentials are smaller loads in the HC so that the ionospheric Hall generator can support these loads at smaller values of d_h. All figure show that self-consistent quiescent solutions occur closer to the earth the stronger the westward electrojet (Φ_H). The magnitude of $\Phi_\|$ seems to have little effect on the location at which pre-breakup solutions ($d_\|$ = 15-20 km) may occur. But both $\Phi_\|$ and Φ_H do affect the transition point at which the magnetosphere becomes a generator in the HC. Note that the model predicts that larger quiescent current structures can be formed at higher latitudes as seen from the figure.

Figure 3 also indicates that incipient breakup regions (15-20 km in the N-S direction vs. 200 km in the E-W direction) can occur on invariant latitudes corresponding to dipolar L-shells below 6 (Λ = 65.9°) as observed by /2/. We have found that solutions can occur on even lower L-shells if the oxygen concentration is increased or a more realistic field model is used. The solutions are also consistent for surge type quiescent structures (d_h ~ 100's km). That is, the surge counterpart to breakup is predicted to occur at higher L-shells as observed.

STABILITY OF QUIESCENT SOLUTIONS

Recall from Figure 3 that the magnetospheric part of HC is a generator if $\Phi_\|/d_h > E_p$. Now if $\Phi_\|$ increases then for some auroral arcs the magnetospheric portion of the HC switches from a load to a generator. (Note that in the earlier approach of Coroniti and Kennel (1972) this generator does not exist since they assumed the magnetospheric polarization electric field to be zero). We now show that this leads to instability and the triggering of breakup. Let us do this by considering the effect of poleward expansion on $\Phi_\|$ itself. We assume that inductive effects keep $J_\|$ approximately constant during the initial stages. By solving equation 3b for $\Phi_\|$ it is easy to show using equation 1 (with the plus sign) that $\delta\Phi_\|$ increases with δd_h as long as $\Phi_\| > E_p d_h/2$. That is, even when the magnetospheric portion of HC is a weak load $\Phi_\|$ increases as the breakup arc expands poleward. In /6/ we showed that the speed of the poleward expansion is proportional to $\Phi_\|$. Therefore, in our model there is a positive feedback between poleward expansion and the field-aligned potential drop along the poleward boundary. This inherent instability initiates breakup as shown in /9/.

CONCLUSIONS

The major results of our pre-breakup model are the following. (1) Pre-breakup structures can occur on fairly low L-shells (5-6) consistent with observations. (2) A higher concentration of O^+ in the plasma sheet and/or a stronger westward electrojet shifts the conditions favorable to breakup to lower L-shells. (3) The location of the pre-breakup structure is relatively insensitive to the electron temperature in the plasma sheet. (4) We find a positive feedback between poleward expansion and Φ_M and presently speculate that this instability can trigger substorm breakup. (5) We find for the cases studied that the predicted values for the MC equatorial electric fields, E_{MC}, are between 3 and 11 mv/m at geosynchronous. This compares favorably with the substorm electric field values measured at geosynchronous orbit by Pedersen et al. /12/ on GEOS-2.

Finally, let us consider the following speculative idea. We assume that the magnetospheric electric field, E_{pe}, in the MC coincides with that produced by a global two-cell polar cap convection pattern /13/. If E_{pe} is negative (points tailward) it is antiparallel to $J_{\|e}$ and the magnetospheric MC is a generator (see equations 1 and 2b). This can occur only west of the Harang discontinuity. East of the Harang discontinuity E_{pe} is earthward and the magnetospheric MC is a load. We speculate that this feature could abruptly stop the eastward expansion at midnight as observed by Viking /3/.

ACKNOWLEDGEMENTS

It is with pleasure that we acknowledge the helpful comments of Nelson Maynard, William Burke, Frederick Rich, Howard Singer and Michael Heinemann from the Air Force Geophysics Laboratory. One of the authors (MRS) would like to acknowledge the support of U.S. Air Force contract F19628-85-K-0053.

REFERENCES

1. S.-I. Akasofu, A study of auroral displays photographed from the DMSP-2 satellite and from the Alaska meridian chain of stations, Space Sci. Rev. 16, 617-725 (1974)
2. P. Tanskanen, J. Kangas, L. Block, G. Kremser, A. Korth, J. Woch, I.B. Iversen, K. H. Torkar, W. Riedler, S. Ullaland, J. Stadsnes, K.-H. Glassmeir, Different phases of a magnetospheric substorm on June 23, 1979, J. Geophys. Res. 92, 7443-7457 (1987)
3. Shepherd, G. G., C. D. Anger, J. S. Murphee, and A. Vallance Jones, Auroral intensification in the evening sector observed by the Viking ultra violet imager, Geophys. Res. Ltrs. 14, 395-398 (1987)
4. McPherron, R. L., C. T. Russell, and M. P. Aubrey, Satellite studies of magnetospheric substorms on August 15, 1968, 9, Phenological model for substorm, J. Geophys. Res. 78, 3131-3149 (1973)
5. Inhester, B. W., W. Baumjohann, R. W. Greenwald, and E. Nielsen, Joint two-dimensional observations of ground magnetic and ionospheric electric fields associated with auroral zone currents, 3 auroral zone currents during the passage of a Westward Traveling Surge, J. Geophys. 49, 155-162 (1981)
6. Rothwell, Paul L., Michael B. Silevitch, and Lars P. Block, A model for the propagation of the Westward Traveling Surge, J. Geophys. Res. 89, 8941- 8948 (1984)
7. Coroniti F. V., and C. F. Kennel, Polarization of the auroral electrojet, J. Geophys. Res., 77, 2835-2850 (1972)
8. Fridman M., and J. Lemaire, Relationships between auroral electron fluxes and field-aligned potential differences, J. Geophys. Res. 85, 664-670 (1980)
9. Rothwell, P. L., L. P. Block, M. B. Silevitch, and C.-G. Falthammar, A new model for substorm onsets: The pre-breakup and triggering regimes, accepted for publication, Geophys. Res. Ltrs., (1988)
10. McIlwain, Carl E., Substorm injection boundaries, Magnetospheric Physics, ed. B. M. McCormac, 153-154, D. Reidel Publ., Dordrecht-Holland, 1974.
11. Rees, M. H., Auroral ionization and excitation by incident energetic electrons, Planet. Space Sci. 29, 225-247 (1963)
12. Pedersen A., C. A. Cattell, C.-G. Falthammar, K. Knott, P.-A. Lindqvist, R. H. Manka, and F. S. Mozer, Electric fields in plasma sheet and plasma sheet boundary layer, J. Geophys. Res. 90, 1231-1242, (1985)
13. Kan, J. R., and L. C. Lee, Theory of imperfect magnetosphere-ionosphere coupling, Geophys. Res. Ltrs., 7, 633-636 (1980)

GEOPHYSICAL RESEARCH LETTERS, VOL. [illegible], NO. 11, PAGES [illegible], OCTOBER 1988

A NEW MODEL FOR SUBSTORM ONSETS: THE PRE-BREAKUP AND TRIGGERING REGIMES

P. L. ROTHWELL[1], L. P. BLOCK[2], M. B. SILEVITCH[2] AND C.-G. FALTHAMMAR[3]

Abstract. This model explains why breakup has been observed as low as $L = 5.6$ and predicts that a higher concentration of O^+ in the plasma sheet will permit breakup at such low L values. The establishment of a coupled current structure within a single arc leads to a quasi-stable system i.e. the pre-breakup regime. Perturbation of the pre-breakup structure leads to an instability criterion. Certain quiescent configurations are inherently unstable. Transitions from a stable to an unstable situation can trigger a rapid poleward expansion of the quiescent arc or substorm breakup. The kinetic energy of injected plasma from the magnetotail supplies the energy for breakup.

I. INTRODUCTION

Substorm breakup is usually preceded by the sudden brightening of a previously quiescent auroral arc near local midnight. Once it is "triggered" the arc dynamics in the classical model is characterized by a by rapid poleward and westward expansion [Akasofu, 1974; Tanskanen et al., 1987] Auroral intensifications with characteristics similar to those of substorm breakup can occur in the evening sector as detected on Viking by Shepherd et al. [1987]. They expand poleward and eastward, abruptly stopping at local midnight. Triggering generally occurs on the poleward boundary of the diffuse aurora which can be at invariant latitudes which correspond to dipolar L-shells as low as 5.6. This paper establishes the quiescent pre-breakup conditions which are necessary for triggering to occur at such low latitudes.

The basic idea is that the pre-breakup arc consists of two coupled electrical circuits between the ionosphere and the magnetosphere, i.e. it is the incipient formation of a substorm current wedge [McPherron et al., 1973]. As such it has the basic features of the Westward Traveling Surge (WTS) current system that we have previously used [Inhester et al., 1981; Rothwell et al., 1984] and as used by Coroniti and Kennel [1972]. As implied from Figure 1, the physical picture is of two current sheets; one flowing upward on the poleward boundary and another flowing downward on the equatorward boundary of an enhanced conductivity region in the ionosphere. Our approach is comparable to one used some years ago by Coroniti and Kennel [1972]. However, we treat a nonzero polarization field in the magnetosphere which we consider essential for the breakup instability.

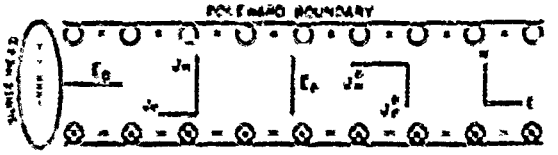

Fig. 1. The Inhester-Haerendel current system for substorm breakup that is used in the model.

II. THE TWO CIRCUIT MODEL

The extended east-west orientation of the breakup arc motivates an approach which models the system as two coupled circuits, one north-south and the other east-west. In our model these circuits close in the magnetosphere via field-aligned currents which are calculated from the model of Fridman and Lemaire [1980]. The field-aligned currents, in turn, are the continuation of magnetospheric currents in the equatorial plane and are dependent on the plasma characteristics there. In particular, enhanced quasi-steady earthward convection of magnetotail plasma is the primary energy source for both circuits. It is the consistency of this earthward convection and the field-aligned currents with the ionospheric configuration that determines where quiescent current systems can be established between the ionosphere and the magnetosphere, i.e. the quasi-stable breakup arcs.

Figure 1 shows the ionospheric elements of the two circuits which are described in Rothwell et al. [1984]. We believe that the establishment of a Cowling channel is an essential element of the breakup mechanism. Figures 2a and 2b show the mapping of the ionospheric circuits into the equatorial plane. It is assumed that the magnetospheric westward electric field, E_{W_e}, associated with the earthward convection from the magnetotail is mapped, consistent with field-aligned potential drops in the east-west circuit, to the ionosphere as E_x in Figure 1.

We denote the W and H circuits as containing the ionospheric westward and poleward currents, respectively, as shown in Figure 2. The W-circuit, (henceforth denoted WC) is a current wedge connected to the near earth cross-tail or ring current, which is correspondingly weakened within the wedge in the night sector. The H-circuit (HC) is closed by an earthward current, J_{H_e}, in the equatorial plane between the upward and downward current sheets. We explicitly derive J_{H_e} below.

The Cowling channel is a dissipative structure due to the Pedersen currents. This is simply due to the fact that the "Hall" terms of power balance out. In the ionosphere the

[1]Air Force Geophysics Laboratory
[2]Dept. of Plasma Physics, Royal Institute of Technology, Sweden
[3]Dept. of Electrical and Computer Engineering and the Center for Electromagnetics Research, Northeastern University

Paper number 88GL03581.
0094-8276/88/88GL-03581$03.00

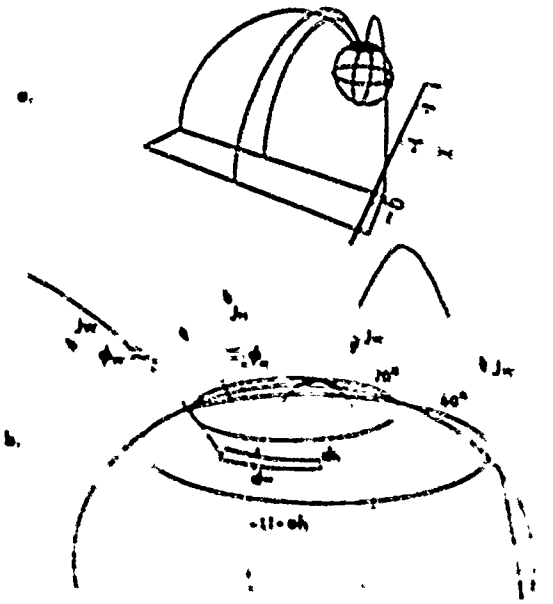

Fig. 2. a) The substorm current wedge looking towards the earth from the magnetotail. Note the mapping of the currents of Figure 1 to the equatorial plane. b) A closeup near the earth of the wedge current system. d_A and d_w denote the north-south and east-west dimensions of the breakup region in the ionosphere.

WC load (westward Hall current parallel to the westward electric field) exactly equals the IIC generator (northward Hall current antiparallel to southward polarization field). When we refer, therefore, to the ionospheric Hall generator in the IIC circuit we do not mean to imply that the ionosphere is an energy source. The ultimate energy source is the magnetospheric portion of the WC. This electrical energy transfer from the WC to the IIC contributes to the power required to sustain a field-aligned potential drop in the IIC. However, narrower breakup arcs may also require the presence of a magnetospheric generator in the IIC to sustain a field-aligned potential along the poleward boundary. As discussed below this situation is inherently unstable and is associated with the triggering of substorm breakup.

One of the key elements of our model is how the IIC current is closed in the magnetosphere. The north-south extent, d_A, of the ionospheric current system shown in Figure 1 is mapped to the equatorial plane as $d_{A_e} = d_A/F_r$ where F_r is a scaling factor equal to $\Delta\Lambda / \Delta L$. F_a is the azimuthal ionosphere-magnetosphere scaling factor which, in a dipole field, is equal to $L^{-3/2}$. See Figure 2. We choose a coordinate system in the equatorial plane such that x points towards the sun (earthward), y points towards dusk and z northward. Over the interval, d_{A_e}, the magnetospheric current, J_{M_e}, causes the bulk plasma to be accelerated in the -y direction.

$$J_{M_e} \times B_e = d_{\parallel} d(\rho V_y)/dt = d_{\parallel} \Delta(\rho V_y)/\Delta t \qquad (1)$$

where B_e is the equatorial value of the magnetic field and $d_{\parallel} \simeq L\, R_E / 3$ is the assumed field line segment over which J_{M_e} is nonzero and ρ is the plasma mass density. We replace the derivatives with differentials. The plasma crosses d_{A_e} in a time equal to $\Delta t = d_{A_e} B_e / E_{W_e}$ where E_{W_e} is the dawn to dusk electric field in the equatorial plane. We assume that if the initial plasma velocity is negative (eastward) there is a load since both the electric field, E_{P_e}, and the current density, J_{M_e}, are directed earthward. If the initial plasma velocity has a positive y-component, however, there is a generator ($E_{P_e} < 0$) and the bulk plasma motion is decelerated. For the load case we assume an *initial* y velocity of zero. For the generator case we assume the *ending* y-velocity to be zero. Thus, $\Delta(\rho V_y) = \pm \rho E_{P_e}/B_e$ where the plus and minus signs refer to the load and generator cases, respectively. Therefore, J_{M_e} is given by

$$J_{M_e} = \pm \rho E_{P_e} L_{W_e} d_{\parallel} / (d_{A_e} B_e^2) \qquad (2)$$

where E_{W_e} and E_{P_e} can be expressed in terms of the ionospheric electric fields and field-aligned potential drops, Φ_W and Φ_M, according to Kirchhoff's law

$$E_{W_e} = F_a (E_w + \Phi_W / d_w) \qquad (3a)$$

$$E_{P_e} = F_r (E_P - \Phi_M / d_A) \qquad (3b)$$

III. DESCRIPTION OF QUIESCENT SOLUTIONS

We assume (see Figure 2) that a field-aligned potential Φ_W drop exists in the western leg of the east-west circuit and that a field-aligned potential, Φ_M, exists in the poleward leg of the north-south circuit. Knowing the expression for J_{M_e} as given in equation (2) we can determine all the relevant parameters needed to define the structure of the pre-breakup regime.

Figure 3 shows a flow chart of the logic used. Assume that in the equatorial plane there is a plasma with ion density n_i, ion mass m_i, electron density n_e ($= n_i$), and the

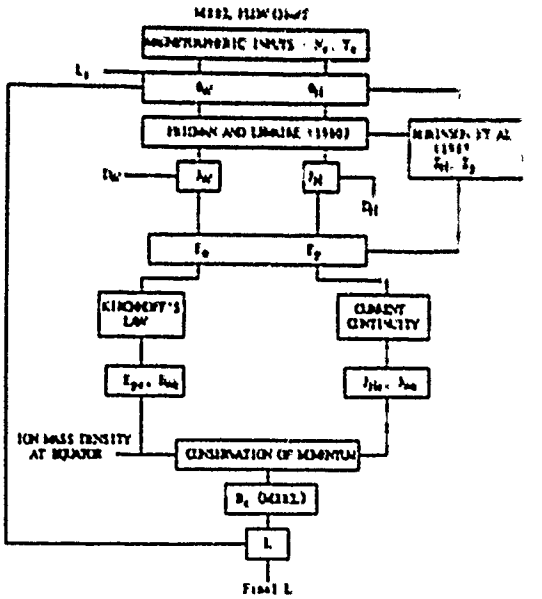

Fig. 3. The method of solution used in the model.

electrons have a parallel temperature $T_{\parallel}$ and a perpendicular temperature of $T_{\perp}$. The model of Fridman and Lemaire [1980] is then used to calculate the precipitation flux (current density) at the ionosphere for both circuits. Current continuity for the ionospheric westward and poleward currents J_W and J_N gives

$$J_W = E_x\Sigma_P + E_y\Sigma_H = J_{iw}l \times 10^3 \quad (4a)$$

$$J_N = E_x\Sigma_H - E_y\Sigma_P = J_{iN}l_A \quad (4b)$$

where Σ_H and Σ_P are the ionospheric height-integrated Hall and Pedersen conductivities inside the arc region. For lack of a detailed model at the western boundary we scale the precipitating flux so that 1 $\mu A/m^2$ of precipitation current corresponds to 0.1 A/m of ionospheric current. This corresponds to a circular hot spot at the western boundary with a radius of 64 km. R_A is the extent of the poleward boundary and is estimated from auroral studies as being about 20 km. The ionospheric conductivities are calculated using the model of Robinson et al. [1987]. The electric fields inside the Iijima-Baumjohann current system shown in Figure 1 are then found by inverting equations (4a) and (4b). Equations (3a) and (3b) are now used to find the corresponding electric fields in the equatorial plane. These results are inserted into equation (2). Current continuity, however, requires that $J_{N_i} = F_s J_N$, where J_N is the net poleward ionospheric current density (A/m) inside the pre-breakup arc. The equatorial B-field is assumed to be dipolar ($\sim L^{-3}$). Therefore, L_i is determined. Note, however, that in order to initiate the calculation an L_i-shell had to be assumed for the scaling factors in the Fridman and Lemaire [1980] model. Convergence is obtained by successively iterating the calculation over L_i.

The plasma sheet is assumed to move sufficiently inward during magnetically disturbed times [Mellwain, 1974] so that plasma sheet values apply. We set $n_i = 1$ cm^{-3} and $T_{i\perp} = T_{i\parallel} = 1$ keV. The substorm current wedge is able to form when the field-aligned potentials can accelerate electrons to the E-layer ($\sim$ 4 keV, Rees [1963]). On the other hand, we choose 32 kV as a reasonable upper limit to the field-aligned potential drop which corresponds to a precipitation current of $\sim$ 30 $\mu A/m^2$. Using this range for Φ_W (see Figure 2b) corresponds to a net westward ionospheric current, J_W, of $\sim$ 0.3 -3.0 A/m according to equation 4a. By using the four values of 4 kV, 8 kV, 16 kV and 32 kV for Φ_W our results are thereby parameterized according to the intensity of the westward electrojet. For purposes of illustration the east-west extent of the breakup region is fixed at 200 km.

Figure 4 depicts the quiescent arc structures as a function of the ionospheric north-south extent of the enhanced conductivity breakup region and in terms of invariant latitude for Φ_H = 5.0 kV. This run assumes 50% O^+ in the equatorial plane. All curves in this Figure were generated by incrementing d_A in 5 km steps. The peaks in the curves correspond to the magnetospheric portion of the HC switching from a load to a generator as d_A decreases. As discussed below this transition is inherently unstable. It is seen that self consistent quiescent solutions occur closer to the earth the stronger the westward electrojet (Φ_W). The magnitude of Φ_H seems to have little effect on the location

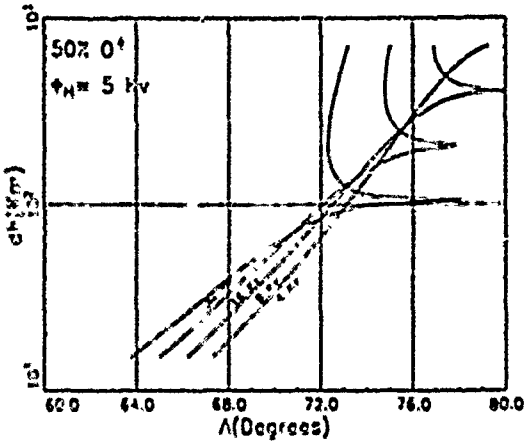

Fig. 4. Quiescent solutions for the location of substorm breakup as a function of invariant latitude. d_A is the north-south extent of the breakup region. The four voltages are values for the field aligned potential drop along the western leg of the circuit. See Figure 2. The peaks denote when the magnetospheric portion of the H-circuit switches from being a generator to being a load as d_A increases.

at which pre-breakup solutions ($d_A \simeq$ 15- 20 km) may occur. Both Φ_H and Φ_W affect the transition point at which the magnetosphere becomes a generator in the HC.

Figure 4 also indicates that incipient breakup regions (15-20 km in the N-S direction vs. 200 km in the E-W direction) can occur on invariant latitudes corresponding to dipolar L_i-shells below 6 ($\Lambda \simeq 65.9°$) as observed for example by Tanskanen et al. [1987]. We have found that solutions can occur on even lower L_i-shells if the oxygen concentration is increased or a more realistic field model is used. This is because the magnitude of J_{N_i} is fixed by Φ_H through the Fridman and Lemaire [1980] expression which implies by equation (2) that $[\, n\, m_i\, L^{10}\, F_s^2\,]$ is constant. The solutions are also consistent for surge type quiescent structures ($d_A \sim$ 100's km). That is, the surge counterpart to breakup is predicted to occur at higher L_i-shells as observed. It is also found that the arc location is relatively insensitive to the plasma sheet electron temperatures above 1 keV.

IV. STABILITY OF QUIESCENT SOLUTIONS

Recall from Figure 4 that the magnetospheric part of HC is a generator if $\Phi_H/d_A > E_y$. As Φ_H increases some auroral arcs will become unstable as the magnetospheric portion of the HC switches from a load to a generator. (Note that in the earlier approach of Coroniti and Kennel [1972] this generator does not exist since they assumed the magnetospheric polarization electric field to be zero). Let us examine this instability by considering the effect of poleward expansion on Φ_H itself. We assume that inductive effects keep J_H approximately constant during the initial stages. By solving equation 3b for Φ_H it is easy to show using equation 2 (with the plus sign) that $\delta\Phi_H$ increases with δd_A as long as $\Phi_H > E_y d_A/2$. That is, even when the magnetospheric portion of HC is a weak load Φ_H increases

as the breakup arc expands poleward. In Rothwell et al. [1984] we showed that the speed of the poleward expansion is proportional to Φ_H. Therefore, in our model there is a positive feedback between poleward expansion and the field-aligned potential drop along the poleward boundary. This inherent instability initiates breakup.

V. CONCLUSIONS

We have shown, by taking the ionospheric current system shown in Figure 1 and mapping it to the equatorial plane, that two coupled circuits can form. One is north-south (HC) the other is east-west (WC). The HC is closed in the equatorial plane by a current which is consistent with the JxB force there. The ultimate energy source for both circuits is earthward convecting plasma from the magnetotail and the WC transfers energy to the HC through an ionospheric Hall generator.

The major results of our pre-breakup model are the following. (1) Pre-breakup structures can occur on fairly low L-shells (5-6) consistent with observations. (2) A higher concentration of O^+ in the plasma sheet and/or a stronger westward electrojet shifts the conditions favorable to break up to lower L-shells. (3) The location of the pre-breakup structure is relatively insensitive to the electron temperature in the plasma sheet. (4) We find a positive feedback between poleward expansion and Φ_H and presently speculate that this instability can trigger substorm breakup. (5) We find for the cases studied that the predicted values for the WC equatorial electric fields, E_{WC}, are between 3 and 11 mv/m at geosynchronous. This compares favorably with the substorm electric field values measured by Pedersen et al. [1985] on GEOS-2.

Finally, consider the following speculative idea. We assume that the magnetospheric electric field, E_{HC}, in the HC coincides with that produced by a global two-cell polar cap convection pattern. If E_{HC} is negative (points tailward) it is antiparallel to J_H, and the magnetospheric HC is a generator (see equations 2 and 3b). This occurs west of the Harang discontinuity. East of the Harang discontinuity E_{HC} is earthward and the magnetospheric HC is a load. We speculate that this feature could abruptly stop the eastward expansion at midnight as observed by Viking [Shepherd et al., 1987].

Acknowledgements. We acknowledge helpful comments of N. Maynard, W. Burke, F. Rich, H. Singer and M. Heinemann of AFGL. One of the authors (MBS) acknowledges the support of Air Force contract F19628-85-K-0053.

References

Akasofu, S.-I., A study of auroral displays photographed from the DMSP-2 satellite and from the Alaska meridian chain of stations, *Space Sci. Rev., 16*, 617-725, 1974.

Coroniti F. V., and C. F. Kennel, Polarization of the auroral electrojet, J. Geophys. Res., 77, 2835-2850, 1972.

Fridman M., and J. Lemaire, Relationships between auroral electron fluxes and field-aligned potential differences, *J. Geophys. Res., 85*, 664-670, 1980.

Inhester, B. W., W. Baumjohann, R. W. Greenwald, and E. Nielsen, Joint two-dimensional observations of ground magnetic and ionospheric electric fields associated with auroral zone currents, 3 auroral zone currents during the passage of a Westward Traveling Surge, *J. Geophys., 49*, 155 - 162, 1981.

McIlwain, Carl E., Substorm injection boundaries, *Magnetospheric Physics*, ed. B. M. McCormac, 153-171, D Reidel Publ., Dordrecht-Holland, 1974.

McPherron, R. L., C. T. Russell, and M. P. Aubrey, Satellite studies of magnetospheric substorms on August 15, 1968, 9, Phenological model for substorm, *J. Geophys. Res., 78*, 3131-3149, 1973.

Pedersen A., C. A. Cattell, C.-G. Fälthammar, K. Knott, P.-A. Lindqvist, R. H. Manka, and F. S. Mozer, Electric fields in plasma sheet and plasma sheet boundary layer, *J. Geophys. Res., 90*, 1231-1242, 1985.

Robinson, R. M., R. R. Vondrak, K. Miller, T. Dabbs, and D. Hardy, On calculating ionospheric conductances from the flux and energy of precipitating electrons, *J. Geophys. Res., 92*, 2565 - 2569, 1987.

Rees, M. H., Auroral ionization and excitation by incident energetic electrons, *Planet. Space Sci., 29*, 225-247,1963.

Rothwell, Paul L., Michael B Silevitch, and Lars P. Block, A model for the propagation of the Westward Traveling Surge, *J. Geophys. Res., 89*, 8941- 8948, 1984.

Shepherd, G. G., C. D. Anger, J. S. Murphee, and A. Vallance Jones, Auroral intensification in the evening sector observed by the Viking ultra violet imager, *Geophys. Res. Ltrs., 14*, 395-398, 1987.

Tanskanen, I , J. Kangas, L. Block, G. Kremser, A. Korth, J. Woch, I.B. Iversen, K. M. Torkar, W. Riedler, S. Ullaland, J. Stadsnes, K.-H. Glassmeir, Different phases of a magnetospheric substorm on June 23, 1979, *J. Geophys. Res., 92*, 7443-7457, 1987.

L P Block and C.-G Fälthammar, Department of Plasma Physics, Royal Institute of Technology, S100 44 Stockholm 70, Sweden.

P. L. Rothwell, Air Force Geophysics Laboratory, Hanscom AFB, Bedford MA 01731.

M. B. Silevitch, Department of Electrical and Computer Engineering and the Center for Electromagnetics Research, Northeastern University, Boston, MA, 02115.

(Received June 22, 1988;
revised Aug 8, 1988;
accepted Aug 18, 1988)

PHYSICS OF SPACE PLASMAS (1987)
SPI Conference Proceedings and Reprint Series, Vol. 7

MAGNETOSPHERE-IONOSPHERE COUPLING AND SUBSTORM DYNAMICS

Michael B. Silevitch
Center for Electromagnetics Research
Northeastern University
Boston, MA, 02115

Paul L. Rothwell
Air Force Geophysics Laboratory
Hanscom AFB, Bedford, MA, 01731

Lars P. Block
Department of Plasma Physics
The Royal Institute of Technology
S100 44 Stockholm 70, Sweden

ABSTRACT

A brief review is given of dynamical coupling models between the ionosphere and magnetosphere for auroral phenomena. The models presented include local and global effects as well the temporal and steady-state aspects of the westward traveling surge. Details will be presented of how the generation of Pi 2 pulsations and the motion of the surge are related.

I. INTRODUCTION

In this paper we will review various approaches to the problem of magnetosphere-ionosphere (M-I) coupling during the formation and propagation of the Westward Travelling Surge (WTS). There are various ionospheric signatures which are associated with this temporally active portion of the substorm. For example, it is observed that enhanced conductivity regions can sometimes propagate with speeds between 1 and 30 km/s. Other features include energetic precipitating electrons (1-10 keV), generation of Pi 2 pulsations, and distortion of the global convection patterns. It is also important to point out that the high temporal resolution (1 min) imaging systems on the Viking Satellite have just begun to provide a wealth of observational information which must be integrated into any model for substorm dynamics.

The next section of the paper gives a summary of a local model of WTS propagation developed by the authors [1,2]. This discussion will be used to define various mechanisms and terminology and it will provide a frame of reference for comparing different works. Following this, we consider global steady state models for calculating the ionospheric polarization electric field using empirical current blockage criteria. Next we develop temporal models wherein we consider the role of the active ionospheric feedback as a mechanism for propagation of conductivity regions and the generation of Pi 2 pulsations. In

Scientific Publishers, Inc., Cambridge, MA 02139

discussing the various temporal and steady state models we will utilize a block diagram format which should allow the reader to quickly see their similarities and differences. Let us now turn to a discussion of the local model due to [1,2].

II. DESCRIPTION OF THE LOCAL MODEL

The Westward Traveling Surge is a large region of auroral brightening that occurs near local midnight during substorm onsets. This region generally moves in a northwestward direction but at times is seen to move even eastward. The WTS has also been identified as the source of Pi 2 pulsations [3]. What we have tried to do over the past few years is to develop a unified model for the WTS that explains both the motion of the surge and the generation of the Pi 2 pulsations [2,3]. Our approach has been to model the ionospheric response to the precipitating electrons rather than first identifying a promising magnetospheric mechanism and then determining its effect upon the ionosphere. While this may appear to be a somewhat backward approach it has the advantage of starting with a tractable portion of the problem whose solution imposes conditions on the far less tractable magnetospheric source. It is implicitly assumed in our model that the Inhester-Baumjohann current model [4,5] represents the ionospheric currents inside the surge region, (see Figure 1).

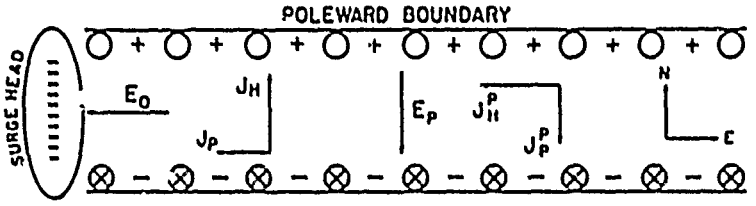

Figure 1. Inhester-Baumjohann ionospheric current system model for the WTS

We will consider the motion of this current system and its coupling to the magnetosphere that is the subject of this paper. While the recent Viking results indicate that the formation of a surge may be far more complex than previously thought [6], the present model is still considered applicable for individual "hot spots". The surge is created by an external electric field, E_0 (Fig. 1). This field drives a westward Pedersen current and a poleward Hall current. The Hall current is closed off into the magnetosphere by precipitating electrons along the poleward WTS boundary. Closure is governed by the parameter, α. In our context, full closure ($\alpha = 1$) implies the full continuation of the ionospheric Hall current into the magnetosphere via field-

aligned currents. In [1] we found that the WTS motion in the midnight sector is controlled by (1) the energy and flux of the precipitating electrons, (2) the electron-ion recombination rate, and (3) the degree of current closure on the poleward boundary of the surge.

On the basis of work by [3,7] there is clearly an observed relationship between the WTS and the generation of Pi 2 pulsations during substorm onsets. It is natural, therefore, to look for ways in which this could occur using the current system shown in Figure 1. It was determined in [2] that the north-south current in the WTS could produce standing waves due to the reflection from conductivity gradients along the surge boundaries. The surge serves as an AC port to an equivalent transmission line [8] formed by the attached magnetic field lines. Under the right conditions this port can resonate with the transmission line and Pi 2 pulsations will be generated from the ionosphere into the magnetosphere.

One basic idea in our model is that there is a quasi-steady state (DC) component of electron precipitation that is dependent upon the temperature and density of the plasma sheet boundary as well as on a potential difference along the field line. This DC component modulates the ionospheric conductivity and controls the speed and direction of the surge motion [1]. The interior of the surge has a higher conductivity than the surroundings due to the enhanced precipitation. The current carried by precipitating energetic electrons in the interior surge region is assumed to be precisely balanced by upward flowing lower energy ionospheric electrons. Therefore, ionospheric current closure into the magnetosphere is assumed to occur only at the north-south boundaries.

During substorm onsets there is a transient injection of electrons into the ionosphere from the plasma sheet. The associated transient current is assumed in our model to coincide with a transverse Alfven wave that initiates a feedback instability between the magnetosphere and the ionosphere in the surge region. This instability produces a complicated first-order AC component in the precipitation current that rides on top of the DC component as discussed above. The frequency of these oscillations tend to fall within the Pi 2 band (40 - 160 sec in period). The first and zero order effects are not decoupled. The DC precipitation flux and energy controls the frequency and damping rate of the Pi 2 pulsations.

The ionospheric ionization density is governed by the continuity equation as given by

$$\frac{\partial N}{\partial t} = Q j_{11}/e - \alpha_r N^2 \qquad (1)$$

where Q is the energy-dependent ionization efficiency as given by [9], j_{11}/e is the electron precipitation flux, α_r is the

electron-ion recombination rate in the ionosphere and N is the ionization density in the ionosphere. The current closure on the poleward boundary is given by

$$J_{11} = - a \frac{\partial J}{\partial x} \qquad (2)$$

where J is the poleward Hall current and a is the closure parameter along the poleward boundary. J is related to N by $J = \Sigma_H E_o$ where Σ_H is the Hall conductivity. Now $\Sigma_H = eN/B$ where B is the magnetic field at the ionosphere. By combining these relationships with equation (2) then equation (1) becomes a wave equation if we momentarily ignore the recombination term. The phase velocity of this ionization wave is given by

$$V_x = QHV_d a \qquad (3)$$

where H is the ionospheric height over which Q is significant and $V_d = E_o/B$. We use a coordinate system in which x points north, y points west and z points to the zenith. A solution for the case including electron-ion recombination has also been obtained by [1]. It was found by [10] that the surge motion is modulated by the ratio of the interior precipitating current and the closure current on the boundaries. If the upward current density required by current closure is larger than the current needed to sustain the zero order level of ionization (N_o) in the surge interior then the surge moves poleward. If it is less than the surge moves equatorward and the surge is stationary if the two upward current densities are equal. Our model, therefore, predicts an auroral brightening along the poleward surge boundary coincident with the poleward leaps as observed.

Equations (1) and (2) can be expanded into zero and first-order terms. The zero-order terms reproduce the results in of [1] and the first-order terms now include the effect of the Alfven wave propagating along the field lines. This is seen at the ionosphere as an equivalent AC impedance [8].

$$Z = i Z_o \cot(\omega_r L/V_A - n\pi) \qquad (4)$$

where $Z_o = \mu_o V_A$ is the characteristic impedance of the equivalent transmission line. ω_r is the frequency of the Alfven wave, n is the mode number, L is the length of the field line between the ionosphere and the equator and V_A is the Alfven speed (≈1000 km/s) in the magnetosphere.

The details of the first-order theory are provided elsewhere [2]. It is important to note, however, that one obtains the scaling relation

$$\lambda_{ns} = V_x/f_r \qquad (5)$$

where λ_{ns} is the north-south wavelength of the Pi 2 mode having the a frequency f_r. V_x is proportional to the zero-order speed of the propagating gradient. This relation implies that λ_{ns} is roughly 100 km for V_x about 10 km/s and f_r is about 100 s. This is a realistic value characterizing the enhanced conductivity strip of the WTS region.

III. GLOBAL STEADY STATE MODELS

Let us turn now to generalizations of the local model presented here. In this section we will discuss the global steady state

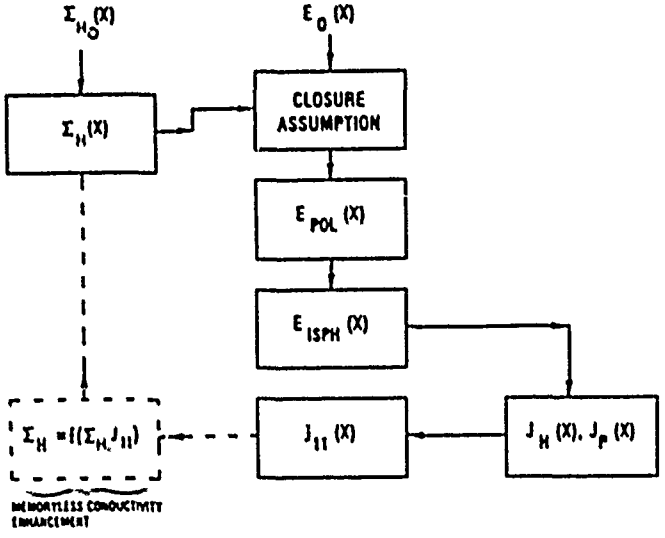

Figure 2. Global steady state models

models of Kan et al.[11], Marklund et al. [12] and Kan and Kamide [13]. All three of these works can be represented

schematically by the block diagram shown in Figure 2.

There it is seen that an assumed enhanced oval conductivity distribution, $\Sigma_{H_0}(x)$, and an ambient two-celled convection electric field $E_0(x)$ is used to calculate the polarization field via a closure condition. The parameter x denotes longitude and latitude variables. As in the local model of Figure 1, Kan et al. [11] and Kan and Kamide [13] use the assumption that only global Hall current is partially closed at the conductivity boundaries. Marklund et al. [12] argue that Hall current closure is not sufficiently general especially when one considers the duskside of the auroral oval. The ambient electric field drives a Northward Hall current that gives rise to a southward polarization electric field and current. As a result Marklund et al. [12] introduce a closure assumption that focuses upon "Type II" currents that flow as a result of conductivity gradients. In both the work of Kan et al. and Marklund et al. the calculations show that strong polarization effects tend to impose a clockwise rotation on the two-celled convection pattern. This feature is consistent with observations and is a generalization of the simple case shown in Figure 1. Note that Marklund et al. assume a uniform conductivity distribution whereas Kan et al use one with Gaussian profile centered at local midnight. Both models, however, produce qualitatively the same results. The reader is referred to the two papers for a more detailed comparison.

It is seen from Figure 2 that the field-aligned current, $j_{\parallel}(x)$, can be considered as an output of the steady state models. Kan and Kamide [13] use this current to empirically update the ambient conductivity distribution using a procedure based on the generation of energetic precipitating electrons via field-aligned potentials. These potentials are correlated to regions of upward field-aligned currents and negative ionospheric charge densities. As shown in Figure 2 via dotted lines an iterative procedure is used which results in steady state solutions which exhibit certain dynamical features of the WTS. It is important to realize, however, that the Kan and Kamide procedure is strictly a steady state model, not a temporal one. Kan and Sun [14], however, incorporated the conductivity enhancement function and the iterative procedure into a temporal schema which will be discussed in the next section.

IV. MODELS FOR TEMPORAL PROPAGATION

We now consider several methods for describing the temporal evolution of the M-I system. It is essential for this problem that an active ionosphere be included in the modeling. Figure 3 shows a block diagram which illustrates the essential features of the various approaches discussed here. A comparison of

Figures 2 and 3 reveals that the steady-state models differ from the temporal ones in the sense that an open loop system differs from one with feedback. For our application the feedback is imposed by an active ionospheric modification which is driven by the field-aligned current $j_{11}(x,t)$. The conductivity changes are governed by the same mechanism that governed the dynamics of the local model described in section II. There recall that equation (1) equates the rate of conductivity increase to the difference between the ionization driven by j_{11} and electron-ion recombination. Thus the feedback inherent in equation (1) is the major difference between steady-state and temporal models.

Another difference between Figures 2 and 3 centers upon the model used to describe the M-I coupling link. For the steady-state cases various types of closure hypotheses were used. Indeed, this methodology can also be utilized to describe the temporal evolution. Figure 4 shows an expansion of M-I block of Figure 3 using this approach. The local model described in section II is a result of the mechanisms illustrated in Figures 3 and 4. Clearly one could extend the global steady-state models of Kan et al. [11] and Marklund et al. [12] to incorporate the temporal feedback of Figure 3. Zhu and Kan [15] did this for the model of Kan et al. [11] but with the constraint of complete blockage of Hall currents via polarization electric fields. In

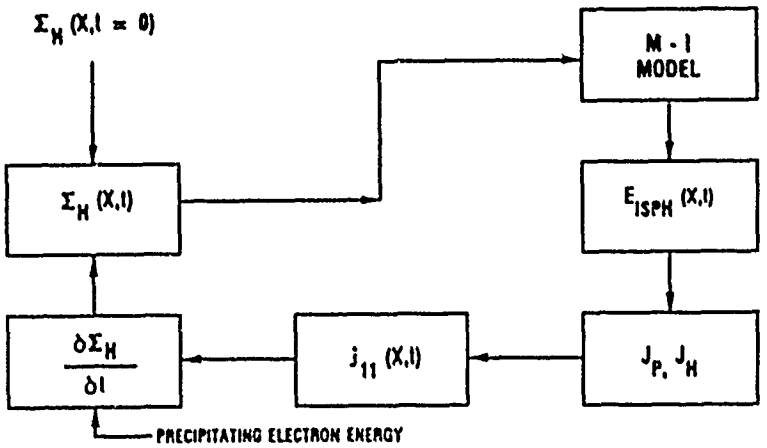

Figure 3. Models for temporal propagation

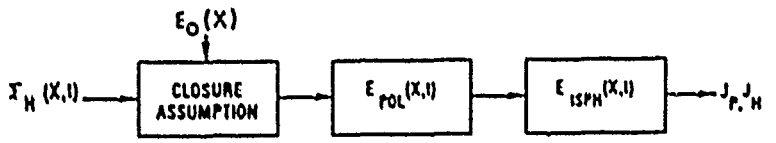

Figure 4. Magnetospheric-ionospheric coupling via current closure

the local slab model previously discussed this would correspond to assumptions which would result in a northwestward to westward propagation of the slab region. Using the same global distribution of the driving electric field, $E_0(x)$, and an initial conductivity as used by Kan et al. [11], Zhu and Kan [15] indeed find that the conductivity pattern exhibits a westward intrusion accompanied by a clockwise shift in the two cell convection pattern due to polarization effects. To date no one has yet extended the steady-state model of Harklund et al. [12] to incorporate the temporal feedback of Figure 3. This would be an interesting exercise and should be helpful in assessing the implications of the more general type II closure assumptions.

Another approach to the description of the M-I model of Figure 3 is shown in Figure 5. There it is assumed that the M-I coupling is a dynamic process. It is governed by the propagation of Alfvén waves along the flux tube connecting the ionosphere and the magnetosphere. As indicated schematically in Figure 5, magnetosphere and ionosphere input conditions provide the drivers for incident and reflected waves in the flux tube. This approach was utilized for quiet conditions by Atkinson [16], Sato [8], Miura and Sato [17] and others. In that context the global mechanism of Figure 3 was described as an ionospheric feedback instability. Miura and Sato [17] performed an extensive global simulation of the evolution of quiet time auroral arc systems. In this work it was assumed that the major component of upward field-aligned currents were carried by relatively cold electrons. Energetic particles would be produced only when the upward field-aligned current exceeded a critical threshold. Thus the characteristics of a quiet arc system are governed by the flux tube ExB drift velocity and the Alfvén wave bounce time. This results in multiple arc structures which propagate at roughly 0.2 km/s and exhibit scale sizes on the order of 10 km. This is in contrast to the local model of the substorm system described in section II which propagates at speeds of 1 to 10 km/s and exhibits scale sizes on the order of 100 km.

Generation of Pi 2 waveforms is an inherent feature in the model described by Figures 3 and 5. In the local first-order model of Rothwell et al. [2] the flux tube was assumed to act as

a uniform transmission line for Alfvén waves. Moreover,

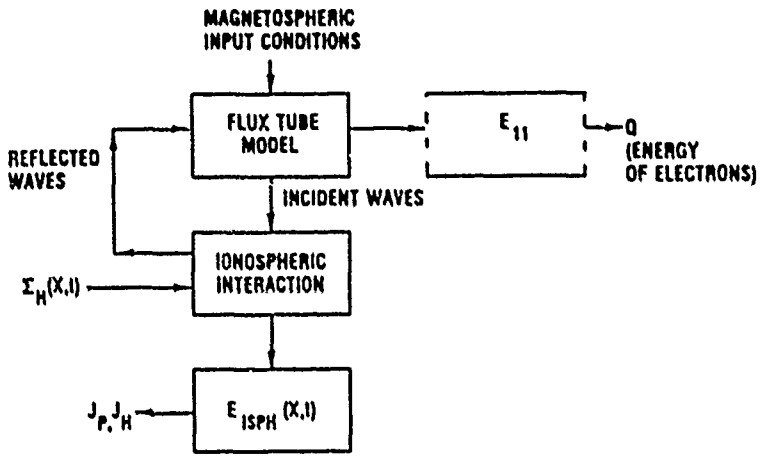

Figure 5. Magnetospheric-ionospheric coupling via Alfvén waves

properties of the Pi 2 pulsations were connected to the zeroth order propagation of the ionospheric enhanced conductivity region. Kan and Sun [14] combined the Alfvén wave M-I coupling of Figure 5 with a modification of the loop in Figure 3. In that case the temporal derivative box was replaced by the conductivity enhancement function of Kan and Kamide [13]. Their procedure results in a temporal schema involving the discrete bouncing of Alfvén waves into the ionosphere and the generation of "steplike" Pi 2 waveforms. It is relevant to note that Kan and Sun [14] discuss and review aspects of M-I coupling which are beyond the scope of this work. For more details the interested reader is referred to the references cited within the Kan and Sun [14] paper. Lysak [18] examined the implications of considering a nonuniform Alfvén transmission line mechanism as the M-I model of Figure 5. The nonuniformity can be caused by density gradients along the flux tube. It was first discussed by Hallinckrodt and Carlson [19] in the context of quiet arc systems. In his numerical study Lysak [18] showed that in addition to Pi 2 periods ($\sim$ 100 s) local reflections of Alfvén waves from density gradients could produce shorter period ($\sim$ 1 s) PiB waveforms. Moreover, it also demonstrated the importance of feedback instability and propagation mechanisms described in section II. It is interesting to note that Lysak [18] does not have to distinguish between the zeroth order role of the closure parameter α and the Alfvén wave feedback instability. In the context of his simulations Lysak is able to obtain self-

consistent propagation and expansion of an enhanced conductivity region coupled with the onset of a feedback instability. Essentially the ansatz of the α parameter is replaced by a definition of the magnetospheric generator region. In the local model of section II we have implicitly assumed that there could be different physical mechanisms present during the zeroth order initiation and conductivity propagation and the first order "ringing" of the M-I system. For example, the zeroth order mechanism could be closely coupled to the transient development of a substorm current wedge whereas the quite different steady state configuration of the wedge might determine the characteristics of the M-I flux tube/generator region during the generation of Pi 2 or PIB waves.

V. CONCLUSIONS

In this paper we have reviewed several different approaches to the problem of relating substorm dynamics to M-I coupling. At present, it is clear that more work needs to be done concerning the nature of polarization electric fields and the physical basis for the closure parameter, α. Moreover, observations can now play a critical role in helping to discriminate amongst various mechanisms. For example, one prediction of the local model of Rothwell et al. [1,2] concerns the scaling of ionospheric standing waves that arise during the feedback instability. In this case the ionospheric wavelength scales as the Pi 2 time period times the propagation velocity of the zeroth order slab region. See equation (5). In a recent work, Rothwell et al. [20] performed a preliminary comparison of this result with data of Tanskanen et al. [21] and obtained a reasonable agreement. This is perhaps one the first attempts to unify the characteristics of pulsations, which are correlated with substorms, to the dynamics of an enhanced ionospheric conductivity region. It is our opinion that such a unification is an essential ingredient for a coherent understanding of the M-I coupling processes during substorms.

ACKNOWLEDGEMENTS

It is with pleasure that we acknowledge the helpful comments of Carl-Gunne Falthammar from the Royal Institute of Technology in Stockholm, Sweden and Nelson Maynard, William Burke, Frederick Rich, H.S. Gussenhoven, Howard Singer and Michael Heinemann from the Air Force Geophysics Laboratory. One of the authors (HBS) would like to acknowledge the support of U.S. Air Force contract F19628-85-K-0053.

REFERENCES

[1] P. L. Rothwell, M. B. Silevitch, and L. P. Block, J. Geophys. Res. 89, 8941 (1984).

[2] P. L. Rothwell, M. B. Silevitch, and L. P. Block, J. Geophys. Res. 91, 6921 (1986).

[3] H. Singer, W. J. Hughes, P. J. Fougere, and D. J. Knecht, J. Geophys. Res. 88, 7029 (1983).

[4] B. W. Inhester, W. Baumjohann, R. W. Greenwald, and E. Nielsen, J. Geophys. 49, 155 (1981).

[5] W. Baumjohann, Adv. Space Res. 3, 55 (1983).

[6] Gordon Rostoker, Vallance A. Jones, R. L. Gattinger, C. D. Anger and J. S. Murphee, Geophys. Rev. Ltrs. 14, 399 (1987).

[7] J. C. Samson, and G. Rostoker, Planet. and Space Sci. 31, 435, (1983).

[8] T. Sato in Magnetospheric Plasma Physics, A. Nishida ed. (D. Reidel Publishers, Boston MA., 1982), p. 197.

[9] M. H. Rees, Planet. and Space Sci. 29, 225 (1963).

[10] P. L. Rothwell, M. B. Silevitch, and L. P. Block, Proceedings of the First Huntsville Workshop of Magnetospheric Models, T. Moore and H. Waite, eds. AGU, Washington, D. C. in press (1987).

[11] J. R. Kan, R. L. Williams and S.-I. Akasofu, J. Geophys. Res. 89, 2211 (1984).

[12] C. T. Marklund, P. A. Lindqvist and M. A. Raadu, J. Geophys. Res. 90, 10864 (1985).

[13] J. R. Kan and Y. Kamide, J. Geophys. 90, 7615 (1985).

[14] J. R. Kan and W. Sun, J. Geophys. Res. 90, 10911 (1985).

[15] L. Zhu and J. R. Kan, Planet. and Space Sci. 35, 145 (1987).

[16] G. Atkinson, J. Geophys. Res. 75, 4746 (1970).

[17] A. Miura and T. Sato, J. Geophys. Res. 85, 73 (1980).

[18] Robert L. Lysak, J. Geophys. Res. 91, 7047 (1986).

[19] A. J. Hallinekrodt and C. W. Carlson, J. Geophys. Res. 83, 1426 (1978).

[20] P. L. Rothwell, M. B. Silevitch, L. P. Block, and P. Tanskanen, accepted by the J. Geophys. Res. (1988).

[21] P. Tanskanen, J. Kangas, L. Block, G. Kremser, A. Korth, J. Woch, I. B. Iversen, K. H. Torkar, W. Riedler, S. Ullaland, J. Stadsnes, K.-H. Glassmeier, J. Geophys. Res. 92, 7443 (1987).

JOURNAL OF GEOPHYSICAL RESEARCH, VOL. 93, NO. A8, PAGES 8613-8624, AUGUST 1, 1988

A Model of the Westward Traveling Surge and the Generation of Pi 2 Pulsations

P. L. ROTHWELL,[1] M. B. SILEVITCH,[2] L. P. BLOCK,[3] AND P. TANSKANEN[4]

A model of the westward traveling surge (WTS) and the generation of Pi 2 pulsations is presented here. Previous work concentrated on the motion of the WTS as a function of the precipitating electron energy and the concurrent generation of Pi 2 pulsations via a feedback instability. Now we look in more detail at the physical assumptions used in deriving the present model and the relations between the zero-order and the first-order solutions. Constraints are placed on the electron temperature asymmetry in the plasma sheet by requiring the Pi 2 pulsations to be bounded. It is found that the electron temperature anisotropy in the plasma sheet plays a major role in determining the direction in which the surge will propagate. Narrower surges require greater electron heating parallel to the magnetic field for poleward motion. More energetic electron precipitation is predicted to produce higher-frequency Pi 2 pulsations. Pulsations occur in multiple bursts with the time interval between bursts being shorter for shorter field lines. Initial amplitude and phase conditions are crucial in determining the pulse shape. The dominant period of the Pi 2 pulsation is found to be equal to twice the north-south dimension of the surge divided by a term which is proportional to the poleward velocity of the boundary. Finally, we show that the poleward surge velocities and Pi 2 pulsation periods as measured during the magnetospheric substorm of June 23, 1979, are consistent with our model. By noting the direction of the surge motion, one can use the model to estimate the magnitude of the polarization electric field. We find that it is consistent with zero for the onsets considered.

1. INTRODUCTION

The westward traveling surge (WTS) is a large region of auroral brightening that occurs near local midnight during substorm onsets. This region generally moves in a northwestward direction but at times is seen to move even eastward. The WTS has also been identified as the source of Pi 2 pulsations. What we have tried to do over the past few years is to develop a unified model for the WTS that explains both the motion of the surge and the generation of the Pi 2 pulsations [*Rothwell et al.*, 1984, 1986] (hereinafter referred to as paper 1 and paper 2, respectively). Our approach has been to model the ionospheric response to the precipitating electrons, rather than first identifying a promising magnetospheric mechanism and then determining its effect upon the ionosphere. While this may appear to be a somewhat backward approach, it has the advantage of starting with a tractable portion of the problem whose solution imposes conditions on the far less tractable magnetospheric source.

It is implicitly assumed in our model that the Inhester-Baumjohann current model [*Inhester et al.*, 1981, *Baumjohann*, 1983] represents the ionospheric currents inside the surge region (see Figure 1). It is the motion of this current system and its coupling to the magnetosphere that are the subject of this paper. While the recent Viking results indicate that the formation of a surge may be far more complex than previously thought [*Rostoker et al.*, 1987], the present model is still considered applicable for individual "hot spots" as well as for the more classical type of surge formation. Note, however, that our model deals with the ionospheric response to electron precipitation, so that direct changes in the magnetospheric source(s), such as the creation of a new hot spot or the fading of an old one, could produce dynamic effects not explainable by the present model.

The surge is created by an external electric field E_0 (Figure 1). This field drives a westward Pedersen current and a poleward Hall current. The Hall current is closed off into the magnetosphere by precipitating electrons along the poleward WTS boundary. The parameter γ is a measure of current closure efficiency. *Lysak* [1986] has discussed the physical interpretation of the γ parameter in terms of a possible magnetospheric source and its coupling to the flux tube ionosphere system. The reader is referred to that paper for more details. In our context, full closure ($\gamma = 1$) implies the full continuation of the ionospheric Hall current into the magnetosphere via field-aligned currents. In paper 1 we found that the WTS motion in the midnight sector is controlled by (1) the energy and flux of the precipitating electrons, (2) the electron-ion recombination rate, and (3) the degree of current closure on the poleward boundary of the surge.

On the basis of work by *Rostoker and Samson* [1981], *Samson* [1982], *Samson and Rostoker* [1983], *Pashin et al.* [1982], *Lester et al.* [1984], *Singer et al.* [1983, 1985], and *Gelpi et al.* [1987], there is clearly an observed relationship between the WTS and the generation of Pi 2 pulsations during substorm onsets. It is natural therefore to look for ways in which this relationship could occur using the current system shown in Figure 1. It was determined in paper 2 that perturbations in the north-south current in the WTS could produce standing waves due to the reflection from conductivity gradients along the surge boundaries. The surge serves as an ac port to an equivalent transmission line [*Sato*, 1982] formed by the attached magnetic field lines. Under the right conditions this port can resonate with the Alfvén waves that propagate along the equivalent transmission line, and Pi 2 pulsations will be generated from the ionosphere into the magnetosphere.

One basic idea in our model is that in addition to the ac (Alfvén wave) component, there is a quasi steady state (dc)

[1]Air Force Geophysics Laboratory, Hanscom Air Force Base, Massachusetts.
[2]Center for Electromagnetics Research, Northeastern University, Boston, Massachusetts.
[3]Department of Plasma Physics, Royal Institute of Technology, Stockholm, Sweden.
[4]Department of Physics, University of Oulu, Oulu, Finland.

Paper number 7A9356.
0148-0227/88/007A-9356$05.00

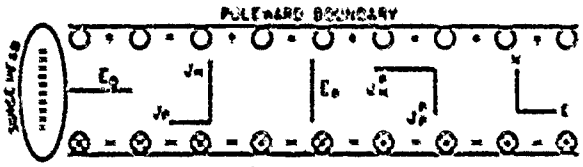

Fig. 1. Inhester-Baumjohann ionospheric current system [*Inhester et al.* 1981, *Baumjohann*, 1983] for the westward traveling surge. This model forms the basis for the model presented in this paper.

component of electron precipitation that is dependent upon the temperature and density of the plasma sheet as well as on the potential difference along the field line. This dc component modulates the ionospheric conductivity and controls the speed and direction of the surge motion (paper 1).

The interior of the surge has a higher conductivity than the exterior because of enhanced precipitation. The current carried by precipitating energetic electrons in the interior surge region is assumed to be precisely balanced by upward flowing lower-energy ionospheric electrons. Therefore ionospheric current closure into the magnetosphere is assumed to occur only at the surge boundaries.

During substorm onsets there is a transient injection of electrons into the ionosphere from the plasma sheet. The associated transient current is assumed in our model to coincide with a transverse Alfvén wave [*Baumjohann and Glassmeier*, 1984] that initiates a feedback instability between the magnetosphere and the ionosphere in the surge region. This instability produces a complicated first-order ac component in the precipitation current that rides on top of the dc component as discussed above. The period of these oscillations tends to fall within the Pi 2 band (40–160 s). Now the first- and zero-order effects are not decoupled. The dc precipitation flux and energy control the frequency and damping rate of the Pi 2 pulsations, as we will see below. This approach is significantly different from that of *Lysak* [1986], which assumes that all the electron precipitation is associated with the Alfvén wave. Also, our model considers the ionospheric response to the Alfvén wave to be localized in the surge region, not global in nature, as in the work of *Zhu and Kan* [1987]. Comparisons of our work with that of *Kan et al.* [1984], *Kan and Kamide* [1985], and *Kan and Sun* [1985] are more fully discussed in section 6.

In the work of *Rothwell et al.* [1988] the results of *Fridman and Lemaire* [1980] were used to relate the dc precipitation flux and energy to the electron temperature anisotropy in the plasma sheet and to the potential drop along the field line. It was found that the damping rate of the Pi 2 pulsations as calculated from the results of Fridman and Lemaire closely followed the envelope of the growth curves as calculated from the feedback instability theory of *Sato* [1982]. The physical constraint that the Pi 2 pulsations be damped imposes a minimum allowable value on the ratio λ_x/α, where λ_x is the north-south dimension of the surge and α is the closure parameter, as defined above. It was found that narrower surge regions (~100 km) required preferential electron heating parallel to B (the magnetic field) in order for poleward motion to take place. For thicker surge regions (~300 km), poleward motion was allowed even when the electron temperature perpendicular to B dominated the parallel temperature. The precise value of the threshold ratio, which we denote by $(\lambda_x/\alpha)_t$, depends on the electron temperature ratio $T_\perp/T_\parallel$ in the plasma sheet. In this way the dynamics of the surge motion is controlled by the electron temperature anisotropy in the plasma sheet boundary.

In section 2 we will review the zero-order WTS theory as presented in paper 1. In section 3, Pi 2 pulsations will be treated according to the first-order theory developed in paper 2. Section 4 deals with the pulse shapes and their dependence on initial conditions and on the electron precipitation energy. Section 5 compares the model with three onsets observed on June 23, 1979. Finally, section 6 summarizes and presents the conclusions of the paper. In the appendix we have constructed a very simple convection model to justify the assumptions used in interpreting the experimental data.

2. Zero-Order Equations

In this section we briefly review the motion of the poleward boundary as derived in paper 1. Along the boundary is a conductivity gradient that must be consistent with the electron precipitation from the magnetosphere. The ionospheric ionization density in the gradient region is governed by the continuity equation as given by

$$\partial N/\partial t = Q j_{\parallel e}/e - \alpha_r N^2 \tag{1}$$

where Q is the energy-dependent ionization efficiency as given by *Rees* [1963], $j_{\parallel e}$ is the electron precipitation flux, α_r is the electron-ion recombination rate, and N is the ionization density in the ionosphere. The current closure on the poleward boundary is given by

$$j_\parallel = -\alpha\, \partial J/\partial x \tag{2}$$

where J is the poleward Hall current and α is the closure parameter along the poleward boundary. We use a coordinate system in which x points north, y points west, and z points to the zenith. J is related to N by $J = \Sigma_H E_0$, where Σ_H is the height-integrated Hall conductivity. Now $\Sigma_H = eN/B$, where B is the magnetic field at the ionosphere.

By combining these relationships with (2), equation (1) becomes a wave equation if we momentarily ignore the recombination term. The phase velocity of this ionization wave is given by

$$V_x = Qh V_y \alpha \tag{3a}$$

where h is the ionospheric height over which Q is significant and $V_y = E_0/B \approx 0.25$ km/s.

A solution for the velocity of the poleward boundary including electron-ion recombination effects has also been obtained in paper 1. Under the assumption of constant closure it was found that the equations greatly simplified by transforming the system to a coordinate frame moving at the boundary speed. (A more exact treatment of boundary propagation, however, must take into account time- and space-dependent closure.) In the moving frame the conductivity profile of the boundary remained constant and matched the Hall conductivity inside the surge at $x = 0$. (Note that x is the poleward coordinate here, rather than z, as in paper 1.) In the stationary frame the poleward boundary speed as given by equation (22) in paper 1 is

$$V = V_x - G\Sigma_{H0}{}^2 E_0 \alpha j_{\parallel b} \qquad G = \alpha_r B/eh \tag{3b}$$

where $j_{\parallel b}$ is the upward closure current just where the boundary joins the surge interior and Σ_{H0} is the height-integrated Hall conductivity in the surge interior, which is maintained by a precipitating flux $j_{\parallel 0}/e$. Using $\Sigma_{H0} = ehN_0/B$, where N_0 is the zero-order ionization level inside the surge region which is

given by $[Qj_{\parallel 0}/e\alpha_r]^{1/2}$, we have

$$V = V_s'[1 - R_i/R_b] \tag{3c}$$

where $R_i = Q_i j_{\parallel 0}/e$ and $R_b = Q_b j_{\parallel 0}/e$ are the ionization rates in the surge interior and on the poleward boundary, respectively, and are approximately proportional to the energy flux. (Recall that Q_i and Q_b are the respective ionization efficiencies, which are energy dependent [*Rees*, 1963].) If the ionization rate along the poleward surge boundary is greater than the ionization rate that is required to sustain the zero-order level of ionization (N_0) in the surge interior, then the surge moves poleward. If it is less, the surge moves equatorward, and the surge is stationary if the two ionization rates are equal. The model therefore predicts an auroral brightening along the poleward surge boundary that is coincident with the poleward leading edge.

Note that in this treatment the conductivity profile has been assumed to remain stationary in the moving frame, which, in general, will not happen. A nonstationary conductivity profile leads to a time dependence in V' which more accurately reflects the surge motion [*Sileeitch et al.*, 1984]. The propagation speed of any profile, however, should increase in proportion to the excess of the ionization rate along the boundary over that of the surge interior. After all, that is what controls the propagation of the ionization wave. Therefore for short periods right after onset the measured velocities should be well represented by (3*a*) and (3*c*). This assumption is utilized below in comparing the model with data for the three substorm onsets of June 23, 1979, when data for the time evolution of the conductivity gradient are unavailable.

3. First-Order Equations

It is well documented that Pi 2 pulsations are fundamentally related to auroral breakup and substorm onsets [*Saito*, 1961; *Rostoker and Samson*, 1981; *Samson and Rostoker*, 1983; *Samson*, 1982]. As pointed out by *Samson* [1982], the Pi 2 pulsations occur simultaneously with or before all other ionospheric phenomena associated with breakup. These results are consistent with those of *Singer et al.* [1983, 1985] and *Gelpi et al.* [1987], who used magnetometer data from the Air Force Geophysics Laboratory (AFGL) magnetometer chain. Their results strongly imply that the Pi 2 source is located approximately 1 hour to the east of the western surge edge. *Pashin et al.* [1982] carried out a study on Pi 2 pulsations during the passage of the WTS under three successive auroral breakups. They found that the largest Pi 2 pulsation amplitudes were colocated in the region of the brightest auroras. In a similar study, *Baranskiy et al.* [1980] observed that the highest Pi 2 frequencies occurred near local midnight. *Stuart et al.* [1977] noted a correlation between the modulation in precipitating electron flux in the auroral zone and the coincident Pi 2 pulsations. *Multser et al.* [1974] suggested that Pi 2 pulsations were a result of the brightening of the aurora that led to an injection of an Alfvén wave from the ionosphere into the magnetosphere. This leads to field line oscillations and resonances in the Pi 2 frequency range.

On the basis of the large volume of evidence that Pi 2 pulsations and substorm onsets are related, it is therefore logical to explore whether the surge model developed in paper 1 can explain Pi 2 pulsations. We do this by looking at the first-order expansion of the basic equations. Equations (1) and (2) can be expanded into zero- and first-order terms. Along the boundary the zero-order terms reproduce the results in section 2, while the ν lead to a null result in the interior where N_0 is assumed constant. The first-order terms, on the other hand, are defined in the surge interior, where the analysis of *Sato* [1982] can be applied. They include the effect of Alfvén waves propagating along the attached field lines. Their effect at the ionosphere is seen as an equivalent ac impedance [*Sato*, 1982] which is given by

$$Z = iZ_0 \cot(\omega_r l_s/V_A' - n\pi) \tag{4a}$$

where $Z_0 = \mu_0 V_A'$ is the characteristic impedance of the equivalent transmission line, ω_r is the frequency of the Alfvén wave, n is the mode number, l_s is the length of the field line between the ionosphere and the equator, and V_A' is the Alfvén speed ($\simeq 1000$ km/s) in the magnetosphere. Equation (4*a*) assumes perfect reflection of the Alfvén wave at the equator (i.e., zero magnetospheric conductivity), in contrast to the finite magnetospheric conductivity model developed by *Lysak* [1986]. The first-order precipitation current carried by the Alfvén wave is related to Z through $Zj_{\parallel} = \nabla_\perp \cdot E_\perp$. Implicit in this equation is the transmission line assumption and the propagation/reflection of Alfvén waves within the flux tube connecting the ionosphere to the magnetosphere. Now, as shown in paper 2, this relation when combined with the first-order expansion of (1) and (2) leads to dispersion relations for the frequency and growth rates of the individual modes.

We will briefly summarize the derivation as given in paper 2, with special care being taken regarding whether the quantities are defined on the surge boundary or in the surge interior. Following paper 2, the first-order continuity equation in the surge interior gives us

$$\partial N_1/\partial t = -Qhj_{\parallel 0}/eN_{0h} - 2\kappa N_1 \tag{4b}$$

where

$$\kappa = \alpha_r N_{0h}/h$$

N_1 is the height-integrated perturbed ionization density normalized to the height-integrated zero-order density, and $j_{\parallel 0}$ is the perturbed (first-order) component of the field-aligned current, which is given by

$$j_{\parallel 0} = -J_0 \nabla N_1/(1 - Z\Sigma_{H0}) \tag{4c}$$

where $J_0 = \alpha\Sigma_{H0}E_0$ is the net zero-order poleward current in the surge interior and is considered to be constant there. On the boundary, however, J_0 closes off into the magnetosphere, giving rise to the zero-order solutions derived above. Note that α is the closure parameter as defined on the surge boundary while Σ_{H0} is defined in the surge interior. The first-order current fluctuations give rise to no net current flow in to and out of the interior region. Inserting (4*c*) into (4*b*) leads to defining the parameter $V_{s'} = \alpha Q_i h V_A'$, which is analogous to the boundary velocity parameter as defined in (3*a*) and (3*c*) and which we now call V_{sh}'. Note that $V_{si}' = V_{sh}'$ only if the energy of the zero-order precipitation is the same in the surge interior as it is on the boundary. In the absence of measurements of the electron precipitation energy we assume that the velocity of the poleward boundary gives a reasonable measure of V_{si}'. This assumption is used below in section 5 and discussed in the appendix.

The first-order dispersion relations are then given by

$$\omega_r = 2\pi(V_{si}'/\lambda_x)(1 + X^2) \tag{5}$$

$$\omega_i = \omega_r X - 2\alpha_r N_{0h}/h \tag{6}$$

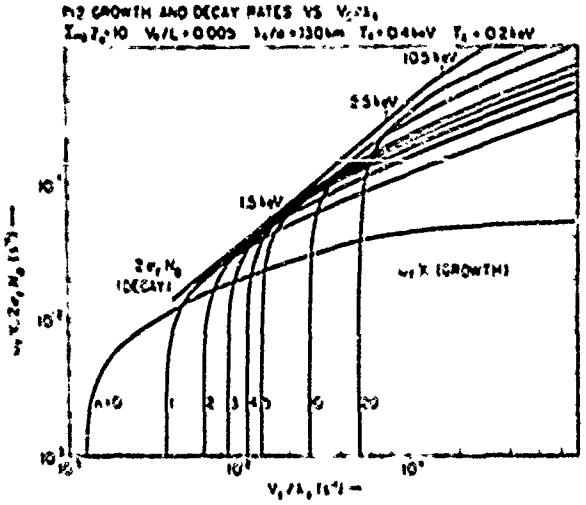

Fig. 2 Growth and damping curves for Pi 2 pulsations as derived from model. The growth curves are the nearly vertical lines, and the damping (decay) curve follows the envelope of the growth curves. The tick marks on the decay curve map the precipitating electron energies to the abscissa. The abscissa is plotted in units of V_A/λ_x, where λ_x is the north-south extent of the surge. In this example we took λ_x/α = 130 km, V_A/L = 0.005, $\Sigma_{PD}Z_0$ = 10, $T_{\parallel}$ = 0.4 keV, and $T_{\perp}$ = 0.2 keV. See text for definitions.

where ω_r and ω_i are the real and imaginary components of the frequency, respectively. X is equal to Z as defined in (4a) times the zero-order Pedersen conductivity in the ionosphere, Σ_{PD}. N_{0h} is the height-integrated equilibrium ionization density as expected from the zero-order (dc) electron precipitation inside the surge. From now on we set $N_{0h} = hN_0$, where N_0 is the local zero-order ionization density at the maximum ionization altitude for a given precipitation energy. (Note that in equation (18) of paper 2, h of equation (6) above is missing and the definition given in equation (11) of paper 2 should replace α in equations (12) and (16) of paper 2.)

Now if the zero-order electron precipitation energy inside the surge is of the order of a couple keV, then V_{Ai} is approximately a couple kilometers per second (paper 1). In addition, if the north-south surge dimensions (λ_x) are of the order of hundreds of kilometers, then the characteristic frequency ($V_{Ai}/2\lambda_x$) for ionospheric waves is close to that of Pi 2 pulsations. In order for a resonance to occur the characteristic ionospheric frequency just derived must be greater than or equal to the frequency of the fundamental toroidal mode for the attached field lines. *Singer et al.* [1981] found that the frequency of the fundamental toroidal mode was smallest at local midnight, reaching the Pi 2 range of 0.02 s^{-1} at $\Lambda = 66°$ and 0.005 s^{-1} at $\Lambda = 68°$. This suggests that the formation of a surge at auroral latitudes near local midnight sets up a resonance condition between the ionospheric waves and the magnetic field line oscillations which is triggered by the feedback instability, as described here.

There are both reactive ($+X$) and capacitive ($-X$) solutions to (5) and (6). The reactive solutions lead to growing Pi 2 pulsations from the feedback instability, while the capacitive solutions quench the instability. Reference is made to *Sato* [1982] and references therein regarding the details of these effects. *Samson* [1982] found that the Pi 2 oscillations originating from field-aligned currents are phase-shifted with respect to Pi 2 pulsations arising from the electrojet. In the present model this effect comes from the inductive nature of the field lines which allows growing solutions.

Note that the first-order dispersion relations also depend on the zero-order precipitation energy (i.e., the field-aligned potential drop) through V_{Ai}. We use the theory of *Fridman and Lemaire* [1980] to estimate the magnitude of the zero-order precipitation for various field-aligned potential differences and plasma sheet parameters.

Figure 2 shows a separate plot of the Pi 2 growth and decay terms from (6) as a function of V_A/λ_x. The growth curves are the nearly vertical lines that tend to cross over each other. The damping curve is the nearly straight line that closely follows the envelope of the growth curves. The damping curve was calculated according to the *Fridman and Lemaire* [1980] theory with electron plasma sheet temperatures of $T_{\parallel}$ = 0.4 keV and $T_{\perp}$ = 0.2 keV and with the density of the plasma sheet assumed to be 0.3 cm^{-3}. The tick marks denote the locations of various precipitation energies. Note that more energetic precipitation turns on higher-frequency modes. For Figure 2 we used Σ_{PD} = 10 mhos, Z_0 = 1 ohm, V_A/L = 0.005 s^{-1}, and λ_x/α = 130 km.

If one inserts (5) into (6) and, for the moment, ignores the decay term, then one can find the maximum growth rate as a function of X. It is $\omega_i X = \omega_r = \pi V_A/\lambda_x$ [*Rothwell et al.*, 1988]. The condition that the Pi 2 pulsations be damped (i.e., that $2\sigma_i N_0 \geq \pi V_A/\lambda_x$) leads to a minimum allowable threshold on λ_x/α, which to a high degree of accuracy is independent of the zero-order precipitation energy. This threshold depends on the plasma sheet parameters through the *Fridman and Lemaire* [1980] relation. We again set the plasma sheet number density to 0.3 cm^{-3} and calculated the threshold value of λ_x/α by assuming a linear fit to the precipitation current for field-aligned potential drops between 5 kV and 50 kV. Figure 3 shows a plot of the values $(\lambda_x/\alpha)_t$ versus the electron temperature anisotropy $T_{\perp}/T_{\parallel}$ in the plasma sheet. An analytical expression for the dependence of the threshold values on $T_{\perp}$, $T_{\parallel}$, and the plasma sheet number density N_{ps} can be found. This is done by noting that $N_{\parallel} \propto \Phi$, which leads to $(\lambda_x/\alpha)_t \propto T_{\perp}^{1/2}/(T_{\parallel}^{1/4} N_{ps}^{1/2})$, where Φ is the field-aligned potential drop.

There is a simple physical explanation for associating an enhanced $T_{\parallel}$ with poleward motion of the conductivity slab. An increase in $T_{\parallel}$ causes an increase in $J_{\parallel h}$ [*Fridman and Lemaire*, 1980]. This increases the degree of modification of the conductivity gradient along the poleward boundary, which

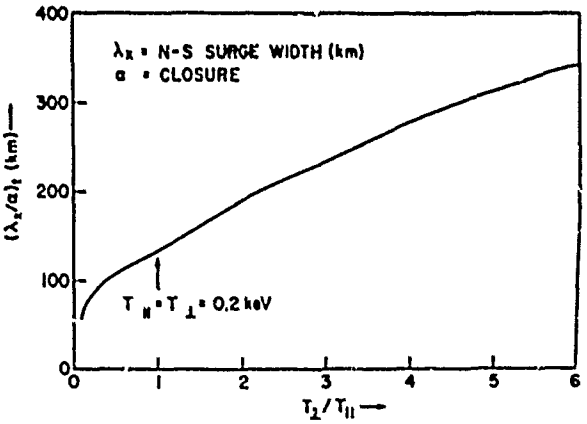

Fig. 3 The damping threshold for Pi 2 pulsations as a function of the electron temperature anisotropy in the plasma sheet using the model of *Fridman and Lemaire* [1980] for the precipitating electron flux. When the measured value of λ_x/α exceeds the threshold value, the Pi 2 pulsations are damped.

causes a faster poleward surge expansion. The net effect is that anything that increases $j_{\parallel p}$ along the poleward boundary will cause a more northward motion of the surge region. An enhancement of $j_{\parallel p}$ also reduces the north-south polarization field (see Figure 1), which decreases the westward Hall current. Now an enhancement in temperature anisotropy (if it is global) will tend to impose an increase in $j_{\parallel}$ at the surge head. In our simplified steady state model this must be offset by a compensating decrease in the field-aligned potential [*Fridman and Lemaire*, 1980] at the surge head in order for $j_{\parallel}$ there to be continuous with the diminished westward ionospheric current. Our model therefore also suggests that enhanced $T_{\parallel}$ is accompanied by a brightening along the poleward boundary and a dimming in the region near the surge head.

The opposite argument holds for preferential electron heating perpendicular to the magnetic field in the plasma sheet. In that case the westward Hall current due to the polarization electric field is increased, and therefore the field-aligned potential at the surge head must increase to maintain current continuity [*Fridman and Lemaire*, 1980]. These effects favor a more westward motion of the surge region. The corresponding arguments suggest that enhanced $T_{\perp}$ will also cause a dimming along the poleward boundary accompanied by a brightening near the surge head.

In summary, according to our model, poleward surge motion is associated with electron heating in the plasma sheet parallel to the magnetic field. This heating could be caused by Fermi acceleration as the tail field becomes more dipolar. Preferential perpendicular heating from conservation of the first invariant is associated with westward surge motion.

What happens when the surge size is below the threshold limit with $\alpha = 1$? In that case we have positive growing pulsations. The period of the wave with the fastest growth rate, and therefore the period that is characteristic of the Pi 2 pulsation is $2\lambda_x/V_x'$. In the limit of (3*a*) the surge is expanding at a velocity V_x', which means the surge triples in size in one pulsation period. The threshold for damping is quickly reached, and the pulsation has a finite amplitude. This feature validates the linear approximation used in deriving the Pi 2 pulsations. However, the rapid poleward motions mean that the zero-order parameter λ_x is changing on a time scale comparable with the first-order solutions. At the very least this leads to a time-dependent frequency which is outside the scope of our solutions. This problem is resolved if the surge moves in spurts or jumps. In that case the motion of the boundary induces a standing ionization wave inside the surge with a phase velocity which we assume to be close to the boundary velocity. From (5) this ionization wave is in resonance with the fastest growing Pi 2 mode ($X = 1$), and the present model applies between jumps. The assumption is that the jumps occur often enough that the critical surge size is reached in a timely manner and the pulsation amplitudes are not unreasonably large. A parallel resistance along the field line, such as that measured by *Weimer et al.* [1985, 1987], would also contribute to keeping the amplitudes finite (C. K. Goertz, private communication, 1987). During jumps a nonlinear treatment such as that of *Lysak* [1986, 1985], which incorporates the generation of PiB pulsations, is probably necessary. The observations of *Opgenoorth et al.* [1980] and *Bosinger et al.* [1981] suggest that PiB type pulsations lasted as long as the local onset-connected field-aligned currents were growing. On the other hand, if the multiplicative factor shown in (3*c*) is sufficiently small, then the change in frequency is adiabatic, and the present model applies in its entirety.

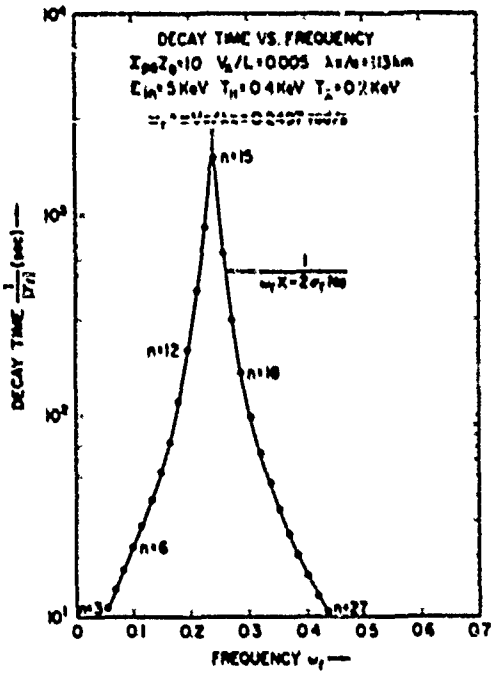

Fig. 4. Decay time of the individual modes shown in Figure 2 for a precipitating electron energy of 5 keV. The dots denote specific modes labeled *n*. Note that after several minutes the pulse will become quasi-monochromatic with the center frequency corresponding to the fastest growing mode. This is consistent with the data shown in Figure 9.

From Figure 3 we see that smaller damping threshold values for λ_x result when the plasma sheet electrons are preferentially heated parallel to the magnetic field. Now if the north-south surge dimension is below the threshold value for a given plasma sheet model, then α must be less than 1 in order for the Pi 2 pulsations to be damped. In paper 1 we showed that the direction of the surge motion is highly dependent on α. For α values less than 1, westward motion is predicted, while $\alpha \geq 1$ allows poleward or even eastward motion. Therefore according to our model the electron temperature anisotropy in the plasma sheet together with the physical requirement that the Pi 2 waves be damped plays an important role in determining which way the current system of Figure 1 is going to move. The result is that embryonic surge regions require substantial preferential heating parallel to B for poleward leaps to occur. Some specific pulse shapes will now be examined.

4. Pi 2 Pulse Shapes

Recall from Figure 2 that the net decay rate of each mode is the difference between the decay curve ($2\sigma_i N_0$) and the individual growth curves at a specific precipitation energy. Figure 4 shows the calculated decay time for each mode for an incident energy of 5 keV and a surge size of 113 km. All other parameter values are as in Figure 2.

Thirty modes are excited in this particular example, and each mode is represented by a dot. Note that the decay time as a function of frequency is highly peaked at the frequency value found in section 3 for the maximum growth rate. What Figure 4 tells us is that the higher and lower frequencies quickly become damped and that the pulse propagates around a narrower frequency band at longer times. The period of this pulsation at the peak frequency is approximately 25 s, which is consistent with the Pi 2 frequency range.

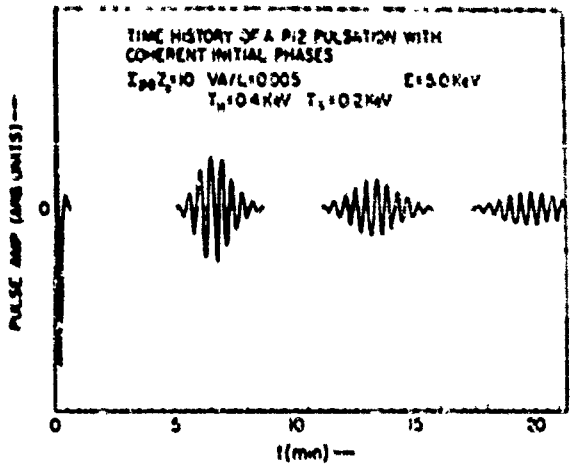

Fig. 5. A sample Pi 2 pulse shape (amplitude in arbitrary units) as a function of time for the same input parameters as shown in Figure 4. This is a linear superposition of all the modes assuming equal initial amplitudes and phases.

Figure 5 is a time history of this pulse. The initial conditions for this particular plot were chosen such that all modes were assumed to be excited with the same amplitude and at the same phase. The predicted time history as seen from Figure 5 is that of a large, initially overdamped pulse followed by series of "ringing" pulses of about 3 min in duration and 6.7 min apart. The time interval between "rings" becomes longer as the ratio l_1/l_z becomes smaller. Assuming l_1 stays constant, this implies that period between rings is proportional to the length of the magnetic field line.

The specific shape of a given pulsation therefore depends very strongly on the initial conditions of its formation. The present model does not specify what these conditions are, but it does give the time evolution of the pulse once the initial conditions are given.

Despite this uncertainty, however, one can speculate on various possibilities. We redid the plot in Figure 5 using random initial phases (between 0° and 360°) for each of the 30 modes. Figure 6 shows the results. Note that the pulse has an extremely complicated shape during the first 5 min which completely masks the underlying sinusoidal dependence. In fact, one might interpret this section as a series of single pulses. The randomness, however, destroys the precise repeatability of the time profile, so that another example with the same parameter values would look somewhat different. It was found that even if the randomness in phase was as little as 20°, a difference with Figure 6 was not discernible. Given the complexity of the magnetosphere-ionosphere system and the irregularity of the driving precipitating flux, some incoherence in mode stimulation is to be expected. This incoherence destroys the precise cancellation between bursts, as seen in Figure 5, and the model simulates the actual data more closely.

Randomization of the initial amplitudes also destroys coherence and produces results similar to those seen in Figure 6 for random initial phases. Therefore Figure 6 is representative of a wide class of initial conditions. Now, regardless of the initial conditions, the selective filtering of the frequencies as seen in Figure 4 leads to a burstlike type of behavior after longer times. Therefore the precise nature of the initial conditions seems to dominate in only the first few minutes of the pulse train.

Figure 7 shows a coherent pulse train for an incident energy of 1.5 keV, $1_1/l_z = 0.001$ s^{-1}, and $z_0 = 125$ km. Note the same general features as in Figure 5: an initial overdamped pulse followed much later (30 min) by a finite pulse train. If this plot were of data, it would take a very astute observer to recognize that these two pulses are indeed one and the same. The pulsation burst evolves toward the mode with the longest decay time. (See the above discussion in regard to Figure 4.) The period of this mode is given by $T_p = 2\lambda_1 l_1$, and in this case is equal to 122 s, as opposed to 25 s for a 5-keV electron precipitation energy. Therefore one testable element of our model is that the frequency of the later, periodic portions of the Pi 2 pulsations should increase with the electron precipitation energy.

Figure 8 shows a pulsation with the same input values as in Figure 7 except that the initial phases are randomized as in Figure 6. Note that the horizontal scale is approximately one-half that of Figure 7. Randomization causes the various modes not to cancel and produces some interesting waveforms during the first few minutes. In fact, the first two peaks resemble a sequence of two overdamped single pulses, rather than a superposition of sinusoidal modes. The underlying sinusoidal structure does not become apparent until 10 min after onset. The pulsation shape is close to the measured Pi 2 waveforms shown in paper 2 and in Figure 3 in the work of *Southwood and Stuart* [1980].

It should be pointed out that the precise cancellation of the waveforms between bursts seen in Figures 5 and 7 implies a highly systematic structure for the nonlinear solutions which were obtained numerically. Investigation is proceeding as to what this structure is and whether it can be expressed in an analytical form or not.

We are also presently looking at the Fourier transform of these time profiles in order to make comparisons with data. Owing to the fact that the decay time is a function of frequency (see Figure 4), the frequency content of the wave is time dependent. This means that the Fourier transform is sensitive to the time at which the transform is taken. Nevertheless, our model predicts a spiky power density spectrum with the central spike located at the frequency corresponding to minimum damping.

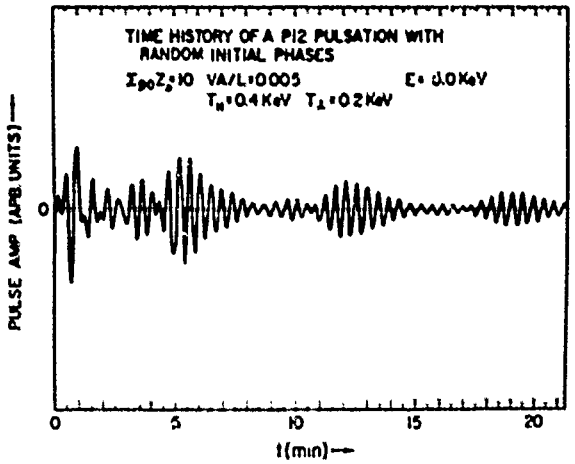

Fig. 6. The same as Figure 5 but now the linear superposition is carried out with random initial phases. Note the nonsinusoidal behavior at the beginning. This figure is more consistent with the data than Figure 5.

5. Comparison of Model With Experimental Data

A detailed study of three successive substorm onsets on June 23, 1979, was carried out using satellite-, balloon-, and ground-based particle and field data [*Tanskanen et al.*, 1987]. We now utilize these data to estimate the poleward velocity of the surge boundary and the north-south extension of the surge for each of the three onsets. These results are then used to estimate the period of the fastest growing mode, as described above. This period is then compared with the measured period of Pi 2 pulsations as seen by ground-based magnetometer stations.

For the following comparison we use Table 3 of *Tanskanen et al.* [1987]. The first onset was observed at Sodankylä (latitude 67.4°, longitude 26.6°, $L = 5.1$) at 2101 UT. Thirty seconds later, it was observed at Ivalo (latitude 68.6°, longitude 27.4°, $L = 5.7$), and 30 s beyond that, at 2102 UT, it was observed at Kevo (latitude 69.8°, longitude 27.0°, $L = 6.2$). Now Sodankylä, Ivalo, and Kevo are close together on the same meridian, so that the successive detection of the onset gives a good measure of the initial poleward surge velocity V. We find $V = 4.4$ km/s for the first onset. The westward component of the surge velocity V_w is found by noting that the onset occurs at the balloon SO622 (latitude 67.6°, longitude 5.1°, $L \simeq 6$) 10 min after it reached Sodankylä, which is along the same geographic latitude. Therefore $V_w = 1.6$ km/s for the first onset. The surge is estimated to include Sodankylä and Kevo, which gives a north-south extension λ_x of about 280 km. For a complete analysis it is necessary to know the energy and flux of the electron precipitation both inside the surge and along the poleward boundary. Unfortunately, this level of detail is not available. However, we do have riometer data which give an indication of the relative intensity of the precipitation energy. The precipitation was most intense during the first onset. Therefore for this period we make the assumption that the ionization rate along the surge boundary exceeds the ionization rate inside the surge and that $V = V_{xx} = V_{xi} = 4.4$ km/s. (See (3c), the discussion following (4c), and the appendix for more details regarding these assumptions.) In this case the period ($T_p = 2\lambda_x/V_{xi}$) of the fastest growing mode is 127 s. Now the magnetometer results are Fourier-analyzed and plotted in frequency versus time contour plots, where each contour represents a constant amplitude. The contour plot of Kevo is shown in Figure 9, with the onsets denoted by short vertical lines. Just after the first two onsets the maximum amplitude (the dense band of concentric ellipses) occurred at approximately 120 ± 10 s, with a secondary peak at ~95 s. A plot of the Ivalo magnetometer data shows similar results although at lower amplitudes. The delay of the monochromaticity relative to the substorm onsets is consistent with the model results shown in Figures 6 and 8. For the first onset the delay is approximately 6–8 min. Considering the assumptions involved in calculating V_{xi} and λ_x, the excellent agreement (127 s versus 120 ± 10 s) may be somewhat fortuitous. However, the overall agreement between the experimental observations and the model lends a great deal of credence to the model's basic veracity.

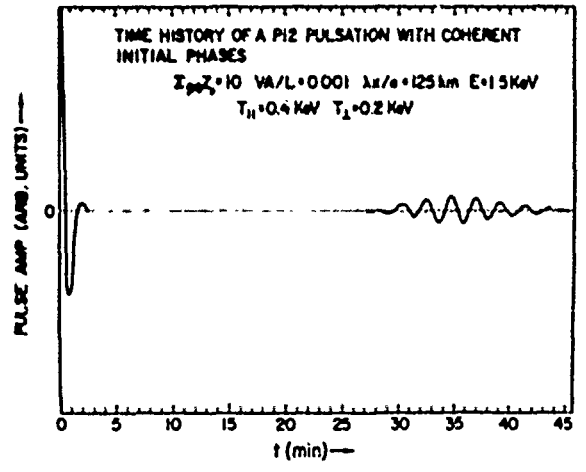

Fig. 7. Time history of a Pi 2 pulsation with coherent initial phases and 1.5 keV incident energy. Note the longer period in comparison with Figure 5. The higher the incident energy the higher the frequency of the expected pulsations.

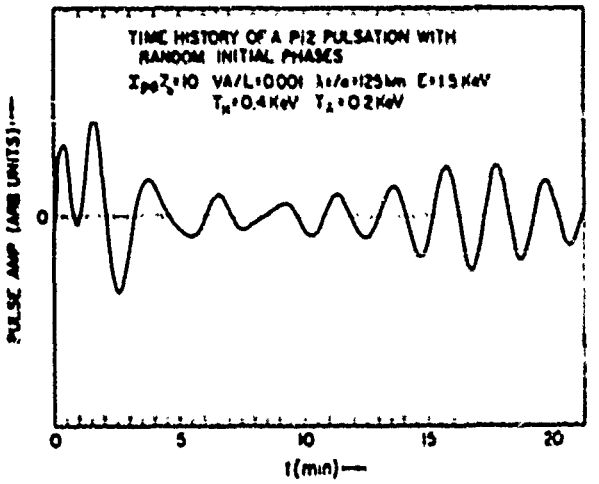

Fig. 8. Time history of a Pi 2 pulsation with random initial phases and 1.5 keV incident energy. This pulse profile is very similar to profiles observed in the data (see, for example, *Rothwell et al.* [1986]). Note once again that the pulsation becomes almost monochromatic after about 10 min.

The second onset of Sodankylä (2107:30 UT) gives similar results. The poleward velocity between Sodankylä and Ivalo (2109 UT) is 1.5 km/s, and between Ivalo and Kevo (2109:30 UT) it is 4.4 km/s. The lower velocity between Sodankylä and Ivalo is explainable by the fact that the riometer absorption at Sodankylä has dropped to 0.7 dB from 1.3 dB as in the first onset. This implies less intense precipitation and hence a slower speed according to our model. The westward velocity component is found as before and is 1.8 km/s. We take the north-south surge dimensions to be between Sodankyla and Kevo as before, which gives 286 km in geographic coordinates. Now Andenes is geographically south but magnetically north of Kevo [see *Tanskanen et al.*, 1987, Table 3]. If one prefers the surge dimensions in magnetic coordinates, then the surge should be measured between Andenes and Sodankyla. In that case we find a distance of 289 km. The period of the fastest growing mode is therefore predicted to be 131 s. Now from Figure 9 we see that the period with the maximum amplitude is around 127 s, which occurs approximately 10 min after the second onset. The agreement is again excellent.

The third onset is more complicated for two reasons. The first reason is that the poleward boundary now passes by the stations KA 0622 (latitude 70.4°, longitude −7.2°, $L \simeq 8.5$) at 2140 UT, Björnöya (latitude 74.5°, longitude 19°, $L = 9.4$) at 2143 UT, and HO 0623 (latitude 72.9°, longitude 7.6°, $L \simeq 9.2$)

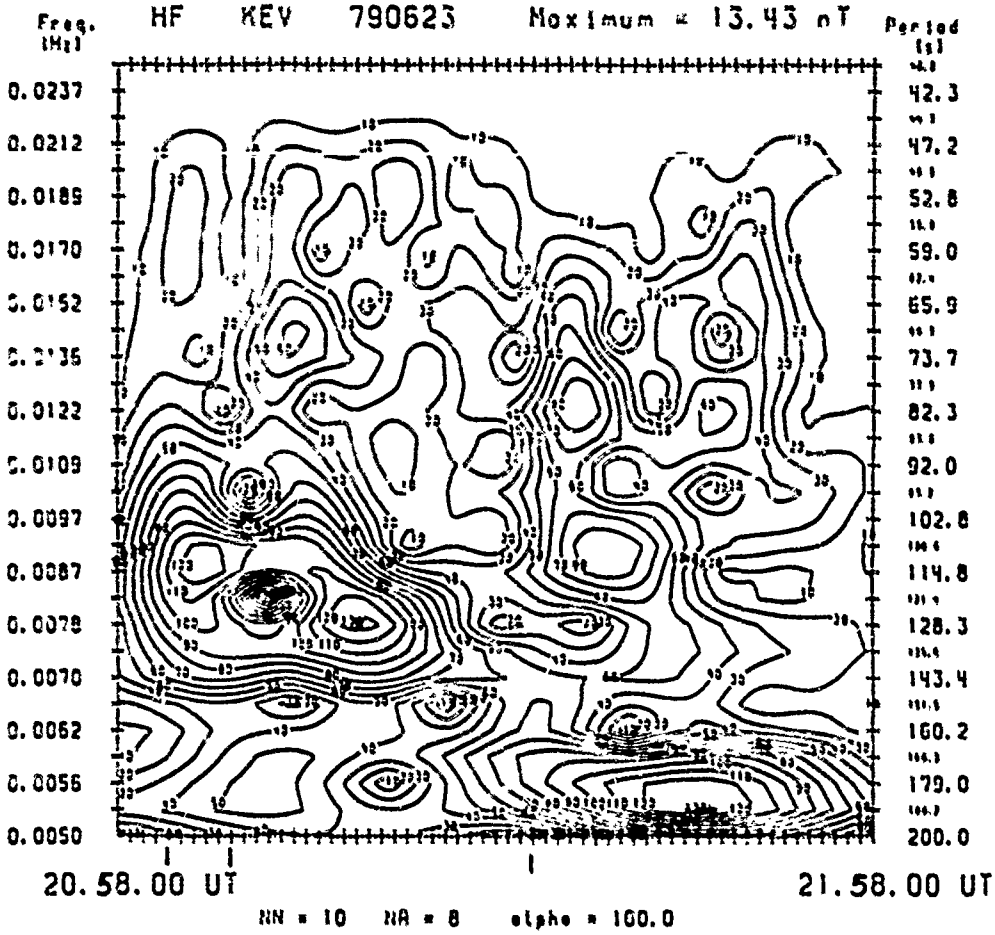

Fig. 9. A contour plot of the filtered magnetometer data taken at Kevo during the period of three substorm onsets on June 21, 1979. Each contour represents a given amplitude which is plotted as a function of frequency. The abscissa is universal time in units of minutes starting at 2058.00 UT and ending at 2158:00 UT. The three heavy tick marks show the time of the three onsets. The more concentrated areas of concentric rings denote regions of more intense wave energy. It is shown in the text that these regions are numerically very consistent with the expected Pi 2 periods as derived from our model. Also, the lengthening of the Pi 2 period with successive onsets is consistent with the poleward expansion of the surge as predicted by the model.

at 2145 UT. These stations are separated in both latitude and longitude, which complicates the determination of the velocity components. The second reason is that the third onset is much less intense than the previous two onsets according to the riometer data. This implies from our model (see (3c)) that the measured poleward velocity could be much less than the V_{x_0} parameter needed to estimate the associated Pi 2 period. We find that the measured poleward velocity is approximately equal to 0.25 km/s and the westward velocity is 2–3 km/s, where the spread is due to whether one works in geographic or magnetic coordinates. We therefore assume for the third onset that the precipitation energy is the same inside the surge as on the poleward boundary and as during the previous two onsets. According to this scenario the surge moves because of an enhancement of the boundary precipitation flux of a few percent over the precipitation flux inside the surge. The old value of 4.4 km/s for V_{x_0} will therefore be used.

The north-south extent of the surge during the third onset is also difficult to quantify because of the spatial separation of the stations. On the basis of Figure 3 of *Tanskanen et al.* [1987] we estimate the surge to be between Ivalo ($L = 5.7$) and Bjornöya ($L = 9.4$), which gives a distance of 689 km. This implies a Pi 2 period of 312 s, which is still comparable to the measured value of roughly 190 ±30 s seen 12 min after onset in Figure 9. The important thing to note from Figure 9 is the definite lengthening of the Pi 2 period as the surge expands poleward. This effect is predicted by the present model, as the period of the fastest growing mode is proportional to λ_x.

The model can be used to extract other important information about the onsets using this important data set. From the value of V_{x_0} of 4.4 km/s and noting that the measured value of E_0 was approximately 20 mV/m during the first two onsets, we use (3a) to estimate the precipitating electron energy that is responsible for the surge movement as being 1.7 keV. (Note that $QII = 5\varepsilon^{1.2}$ ions per incident electron (see paper I), where ε is the precipitating energy.) Using the direction of the surge motion, one can also estimate the magnitude of the north-south polarization electric field inside the surge. (The measured value of the north-south electric field component is 25 mV/m, which includes the convection electric field which may dominate.) Equation (12) of paper I can be rewritten as

$$\tan \gamma_s = (R - E_p/E_0)/(1 + RE_p/E_0) \qquad (7)$$

where γ_r is the angle of the surge motion relative to west, R is the ratio of the height-integrated Hall to Pedersen conductivities, and E_p (which is positive, pointing south) is the polarization electric field. (The relation $E_p = E_0 R(1 - \alpha)$ has been used in deriving (7).) Equation (7) can be rearranged as

$$E_p/E_0 = (R - \tan \gamma_r)/(1 + R \tan \gamma_r) \quad (8)$$

Grafe [1982] has noted that R ordinarily ranges between 1 and 4, with some rare cases in which R is greater than 4. It is also noted that R tends to decrease with enhanced substorm activity and widening of the electrojet. Using (8), it is found that for the first onset, -2.2 mV/m ($R = 1$) $< E_p <$ $+2.1$ mV/m ($R = 4$), which is consistent with full closure of the poleward Hall current into the magnetosphere. (A value of 2.75 was used for $\tan \gamma_r$.) The second onset is like the first, and the third is too complex to be treated here.

We conclude therefore that the three onsets discussed are consistent with our model. Not only is there quantitative agreement with the predicted Pi 2 periods, but the observed time delay for the Pi 2 pulsations to approach a monochromatic signal is compatible with a frequency-dependent decay time, as derived above. In particular, the predicted scaling of the Pi 2 periods with the surge size and poleward velocities seems convincing. The model may also be useful as a tool in separating out the polarization and convection electric fields.

6. Discussion

We have presented a unified model for the motion of the westward traveling surge and the generation of Pi 2 pulsations during substorm onsets. Using the Inhester-Baumjohann ionospheric current system shown in Figure 1, it was shown that the zero-order electron precipitation current (dc) controlled the surge motion. The dynamics of the surge boundary was found for a constant conductivity profile, which led to a constant value of the boundary propagation speed V. This value is assumed to give a reasonable estimate of the initial surge velocity, which in a more realistic treatment must be time dependent, as the conductivity profile evolves in time. The first-order equations led to dispersion equations in the Pi 2 frequency range. The present Pi 2 model was determined to be valid between surge jumps when the surge was considered quasi-stationary or when the surge moved sufficiently slowly. During jumps it is suggested that a nonlinear theory such as that of *Lysak* [1986] is more realistic, since it predicts the presence of Pi8 pulsations, which have been observed by *Opgenoorth et al.* [1980] and *Bösinger et al* [1981].

The present model leads in a natural way to using the results of *Fridman and Lemaire* [1980] and *Fälthammar* [1978] in determining the dc precipitation current, which plays a major role in damping the Pi 2 pulsations. The physical requirement that the Pi 2 pulsation be dampled puts a lower bound on the ratio of the north-south surge dimension and the closure parameter α. This bound depends on the electron temperature anisotropy in the plasma sheet and plays a crucial role in determining the direction of surge motion. Growing models were found to be quenched by the poleward expansion of the surge.

Now because of the dispersive nature of the Pi 2 pulsation, its frequency composition changes with time. The time profile of the pulsation also is very sensitive to the initial conditions. If all the modes are excited at exactly the same time (i.e., the same phase), then the time profile is that of a highly damped wave followed by periodic sinusoidal bursts. Even a small admixture of phases at $t = 0$, however, will cause the pulse to exhibit nonsinusoidal behavior just after onset which evolves into sinusoidal behavior several minutes later. This effect appears to be real, as seen from Figure 9 and from examples of the AFGL magnetometer data (paper 2).

Three onsets that were observed on June 23, 1979, were compared with the model. It was found that the poleward surge velocities and the estimated north-south surge dimensions led to predicted Pi 2 pulsation periods that were consistent with the measured values. The period of the observed Pi 2 pulsations became longer as the surge expanded, which is consistent with the model. It was also shown how the model might be used as a tool in determining the polarization electric field in the presence of a strong convection electric field.

Let us now consider a scenario for auroral breakup based on the present model. Initially, an incipient surge region of a few tens of kilometers forms near local midnight [*Akasofu*, 1974]. It consists of an enhanced ionization region in the ionosphere that contains the current system shown in Figure 1. Now if the ionization rate at the surge's poleward boundary is equal to the ionization rate in the surge interior, the surge is stationary [*Rothwell et al.*, 1988]. If the rate at the boundary is greater, then the surge moves poleward.

It is interesting to compare the present model with the experimental observations of substorm breakup described by *Akasofu* [1974, p. 647].

> The first indication of a substorm is a sudden brightening of one of the quiet arcs (discrete auroras) lying in the midnight sector or the sudden formation of an arc in that region. A typical substorm develops when this arc is located near the equatorward boundary of the belt of discrete auroras, but near the poleward boundary of the belt of diffuse auroras. In most cases, the brightening of an arc or the formation of an arc is followed by its rapid poleward motion, resulting in an 'auroral bulge' around the midnight sector. The so-called 'break-up' occurs in the bulge: a quiet curtain-like form appears to be disrupted and scattered over the sky.

In terms of our model and Akasofu's observations, auroral breakup occurs when an Inhester-Baumjohann type ionospheric current system forms near the poleward boundary of the diffuse aurora. The poleward Hall current in this embryonic system is closed off into the magnetosphere through the formation of the arc described by Akasofu.

If a field-aligned potential drop should switch on over the poleward boundary, the arc there would brighten and move poleward with a speed proportional to the magnitude of the potential drop (see papers 1 and 2 and *Rothwell et al.* [1988]). The boundary motion excites standing ionospheric waves in the surge interior which have phase velocities which are determined by the initial boundary speed. Because of their long wavelengths (~ 100 km) these ionospheric waves could be difficult to detect owing to the turbulent nature of the ionosphere over much smaller distances. If the associated frequencies of the ionospheric waves are greater than or equal to the frequency of the fundamental toroidal mode of the attached field line [*Singer et al.*, 1981], then a resonance can occur through the feedback instability.

The resonance is considered to be damped by electron-ion recombination in the ionosphere. Now the precipitating flux, which causes the damping, is a function of the electron temperature asymmetry in the plasma sheet [*Fridman and Lemaire*, 1980]. If this flux is insufficient to fully close off the

poleward Hall current in the ionosphere, then the α parameter is less than 1. This means that the surge will move predominantly westward (paper 1) and the coincident Pi 2 pulsations will be strongly damped. (For a given surge size, if α is less than 1, it is more probable that the threshold criterion for damping is met.) A value of α less than 1 implies weaker precipitation, which for a given field-aligned potential drop implies enhanced perpendicular electron heating in the plasma sheet according to the model of *Fridman and Lemaire* [1980]. Perpendicular electron heating in the plasma sheet would therefore cause predominantly westward surge motion and strongly damped Pi 2 pulsations. On the other hand, parallel electron heating in the plasma sheet is greater than or equal to 1) would cause predominantly poleward motion and, possibly, the momentary presence of growing Pi 2 pulsations. As mentioned above, the poleward expansion of the surge limits the amplitude of the pulsations when the damping threshold is reached.

Therefore according to the present model the substorm is associated with enhanced precipitation, poleward surge motion, and the generation of finite amplitude Pi 2 pulsations. All these effects are common features associated with substorms and, as shown, may be caused by preferential electron heating in the plasma sheet parallel to the magnetic field.

While the present model appears to be very successful in explaining a variety of observations during substorm onsets, it is by no means all-inclusive. It is still a linear approximation to a highly nonlinear problem where the nonlinear effects apparently are strongly damped over relatively short time scales. We have not addressed, for example, how the initial Alfvén wave transmits the information about the short circuiting of the tail current between the magnetosphere and the ionosphere during the creation of the substorm current wedge [*Baumjohann and Glassmeier*, 1984], nor have we touched upon the possibility of the Alfvén waves creating a field-aligned potential drop through turbulence [*Lysak and Dum*, 1983; *Lysak*, 1985]. Moreover, a more realistic treatment of Alfvén wave propagation in the magnetosphere and ohmic losses in the ionosphere [*Goertz and Boswell*, 1979] is needed. Finally, there may be more than one source of Pi 2 pulsations. *Edwin et al.* [1986], for example, suggest that Pi 2 pulsations arise from an impulsive source of MHD wave energy in the plasma sheet. The fast magnetoacoustic waves that are produced propagate dispersively through the plasma sheet, which gives rise to finite Pi 2 type wave packets nearer the Earth.

It is clear that an important future consideration would involve placing the mechanisms developed here into a more global framework. In this regard it should be mentioned that *Zhu and Kan* [1987] have combined the temporal propagation mechanisms of paper 1 with the global assumption of the closure parameter developed by *Kan et al.* [1984] and *Kan and Kamide* [1985]. Moreover, *Kan and Sun* [1985] have described a global model for simulating the westward surge and Pi 2 pulsations. In this model they combine steady state assumptions inherent in the work of *Kan and Kamide* [1985] with a description of Alfvén waves bouncing between a magnetospheric source and the ionosphere. Their procedure results in a temporal scheme involving the discrete bouncing of the Alfvén waves into the ionosphere and the generation of "steplike" Pi 2 waveforms. Note that in both works the ionosphere plays an active role and is a source of Pi 2 pulsations. In the present work a feedback instability is the driving mechanism, while in the work of *Kan and Sun* [1985] a feedback instability was not included. Multipoint measurements are necessary in order to determine which of these models are correct under different substorm conditions.

APPENDIX

Comparison of our model predictions for Pi 2 periods with data requires knowledge of the precipitation energy and flux both on the poleward boundary and in the surge interior. This would allow a direct calculation of V_{y_b}. Since this information was not available, it was necessary to assume that the measured velocity V of the poleward boundary was equal to V_{y_b}. Now (3c) implies that $V = V_{y_b}$ only when the ionization rate along the poleward boundary is much greater than the ionization rate in the surge interior. From (3a) we see that $V_{y_b} = V_{y_s}$ only if the electron precipitation energy in the surge interior is equal to the precipitation energy on the surge boundary. We assume that this latter condition is satisfied during the onsets considered and develop a model to ascertain the validity of assuming $R_s \sim R_b$. Now enhanced precipitation on the poleward boundary implies a depletion of the plasma associated with attached flux tubes [*Atkinson*, 1984]. Therefore as the plasma convects earthward through the surge interior, it is a weaker source of precipitation than it is on the boundary, and $V \approx V_{y_s}$ from (3c).

We now make a very simple model that illustrates the physical concepts involved. It will be shown that for reasonable substorm values of precipitation current ($\sim 10\ \mu A/m^2$) along the poleward boundary the precipitation flux in the surge interior will be sufficiently small that $V \approx V_{y_s}$ from (3c). This will validate our assumptions. Consider the equatorial plane and a plasma with a number density $N_{p_s} = 0.3\ cm^{-3}$ convecting toward the Earth at a speed $V_c \approx 50$ km/s [*Huang and Frank*, 1986]. This plasma is estimated to contribute to the electron precipitation flux over a field line length of approximately $LR_E/3$, where L is the L shell on which the precipitation takes place and $R_E = 6.37 \times 10^6$ m. Therefore the total particle flux which is available for precipitation is $N_{p_s} V_c L R_E \lambda_{y_e}/3$, where λ_{y_e} is the east-west extent of the surge region as seen in the equatorial plane. This flux is assumed to be totally depleted by precipitation along the surge's poleward boundary and in the surge interior. The total electron flux precipitated along the boundary is given by $j_{\parallel b} \lambda_{x_b} \lambda_{y_e}/e$ and in the interior by $j_{\parallel e} \lambda_{x_e} \lambda_{y_e}/e$. Here λ_{x_b} is the extent of the conductivity gradient along the poleward surge boundary (as seen at the equator), and λ_{x_e} is the north-south extent of surge (also as seen at the equator). Now particle flux conservation along the field line implies $j_{\parallel b} \lambda_{x_b} \lambda_{y_e} = j_{\parallel b} \lambda_{x_b} \lambda_{y_b}$ and $j_{\parallel e} \lambda_{x_e} \lambda_{y_e} = j_{\parallel i} \lambda_{x_i} \lambda_{y_i}$, where the quantities without the subscript e are defined at the ionosphere.

By equating the total inward convecting flux to the flux at the poleward boundary plus that in the surge interior and using flux conservation along the magnetic field lines we finally have an expression for $j_{\parallel b}$:

$$j_{\parallel b} = \frac{e N_{p_s} V_c R_E L^{3/2}}{3\lambda_{x_b}\{(U_{\parallel i}/j_{\parallel b})(\lambda_{x_i}/\lambda_{x_b}) + 1\}} \quad A/m^2 \qquad (A1)$$

where the azimuthal scaling factor for a dipole field ($\lambda_{y_e}/\lambda_{y_i} = L^{3/2}$ [*Lotko et al.*, 1987]) has been used. Now if we make the reasonable assumption that $\lambda_{x_b} = 20$ km and that $L = 6$ and $\lambda_{x_i} = 280$ km, which corresponds to the first two onsets of June 23, 1979, then (A1) can be rewritten using the numerical values

given above as

$$J_{\parallel s} = 22.5\,[1 - J_{\parallel i}/J_{\parallel s} + 1] \quad \mu A/m^2 \tag{A2}$$

Now from (3e) the surge is stationary if the current ratio is equal to 1. This corresponds to a boundary precipitation current density of 1.5 $\mu A/m^2$. For $F = F_0$ the current ratio must be approximately 0.1 or less. This implies from (A2) that $J_{\parallel s}$ should lie between 9.4 and 22.5 $\mu A/m^2$, which is easily realized. We therefore conclude, on the basis of this very simple convection model, that the assumptions used to analyze the Scandinavian data were reasonable and appropriate.

Acknowledgments. It is with pleasure that we acknowledge the helpful comments of Carl-Gunne Fälthammar from The Royal Institute of Technology in Stockholm, Sweden, and Nelson Maynard, William Burke, Howard Singer, and Michael Heinemann from the Air Force Geophysics Laboratory. One of the authors (M.B.S.) would like to acknowledge the support of U.S. Air Force contract F19628-85-K-0053. The clerical assistance of Linda Silva, Anne Rothwell, and Kathleen Sullivan is also appreciated.

The Editor thanks K.-H. Glassmeier and another referee for their assistance in evaluating this paper.

REFERENCES

Akasofu, S.-I., A study of auroral displays photographed from the DMSP-2 satellite and from the Alaska meridian chain of stations, *Space Sci. Rev.*, *16*, 617–725, 1974.

Atkinson, G., Field-aligned currents as a diagnostic tool: Result, a renovated model of the magnetosphere, *J. Geophys. Res.*, *89*, 217–226, 1984.

Baranskiy, L. N., V. A. Troitskaya, I. V. Sterlikova, M. B. Gokhberg, N. A. Ivanov, I. P. Khartchenko, J. W. Munch, and K. Wilhelm, The analysis of simultaneous observations of nighttime Pi 2 pulsations on an east-west profile, *J. Geophys.*, *48*, 1–6, 1980.

Baumjohann, W., Ionospheric and field-aligned current systems in the auroral zone: A concise review, *Adv. Space Res.*, *2*, 55–62, 1983.

Baumjohann, W., and K.-H. Glassmeier, The transient response mechanism and Pi 2 pulsations at substorm onset: Review and outlook, *Planet. Space Sci.*, *32*, 1361–1370, 1984.

Bösinger, T., K. Alanko, J. Kangas, H. Opgenoorth, and W. Baumjohann, Correlations between PiB type magnetic micropulsations, auroras and equivalent current structures during two isolated substorms, *J. Atmos. Terr. Phys.*, *43*, 933–945, 1981.

Edwin, P. M., B. Roberts, and W. J. Hughes, Dispersive ducting of MHD waves in the plasma sheet: A source of Pi 2 wave bursts, *Geophys. Res. Lett.*, *13*, 373–376, 1986.

Fälthammar, C.-G., Problems related to macroscopic electric fields in the magnetosphere, *Astrophys. Space Sci.*, *55*, 179–201, 1978.

Fridman, M., and J. Lemaire, Relationships between auroral electron fluxes and field-aligned potential differences, *J. Geophys. Res.*, *85*, 664–670, 1980.

Gelpi, C., H. J. Singer, and W. J. Hughes, A comparison of magnetic signatures and DMSP auroral images at substorm onset: Three case studies, *J. Geophys. Res.*, *92*, 2417–2430, 1987.

Goertz, C. K., and R. W. Boswell, Magnetosphere-ionosphere coupling, *J. Geophys. Res.*, *84*, 7239–7246, 1979.

Grafe, A., Estimated conductivity ratio Σ_H/Σ_P in the auroral electrojets in connection with the electrojet width and field-aligned currents, *Planet. Space Sci.*, *30*, 525–536, 1982.

Huang, C. Y., and L. A. Frank, A statistical study of the central plasma sheet: Implications for substorm models, *Geophys. Res. Lett.*, *13*, 652–655, 1986.

Inhester, B. W., W. Baumjohann, R. W. Greenwald, and E. Nielsen, Joint two-dimensional observations of ground magnetic and ionospheric electric fields associated with auroral zone currents, 3, Auroral zone currents during the passage of a westward traveling surge, *J. Geophys.*, *49*, 155–162, 1981.

Kan, J. R., and Y. Kamide, Electrodynamics of the westward traveling surge, *J. Geophys. Res.*, *90*, 7615–7619, 1985.

Kan, J. R., and W. Sun, Simulation of the westward traveling surge and Pi 2 pulsations during substorms, *J. Geophys. Res.*, *90*, 10,911–10,922, 1985.

Kan, J. R., R. L. Williams, and S.-I. Akasofu, A mechanism for the westward traveling surge during substorms, *J. Geophys. Res.*, *89*, 2211–2216, 1984.

Lester, M., W. J. Hughes, and H. J. Singer, Longitudinal structure in Pi 2 pulsations and the substorm current wedge, *J. Geophys. Res.*, *89*, 5489–5494, 1984.

Lotko, W., B. U. Ö. Sonnerup, R. L. Lysak, Nonsteady boundary layer flow including ionospheric drag and parallel electric fields, *J. Geophys. Res.*, *92*, 8635–8648, 1987.

Lysak, R. L., Auroral electrodynamics with current and voltage generators, *J. Geophys. Res.*, *90*, 4178–4190, 1985.

Lysak, R. L., Coupling of the dynamic ionosphere to auroral flux tubes, *J. Geophys. Res.*, *91*, 7047–7056, 1986.

Lysak, R. L., and C. T. Dum, Dynamics of magnetosphere-ionosphere coupling including turbulent transport, *J. Geophys. Res.*, *88*, 365–380, 1983.

Maltsev, Yu. P., S. V. Leontyev, and W. B. Lyatsky, Pi 2 pulsations as a result of an Alfvén impulse originating in the ionosphere during the brightening of aurora, *Planet. Space Sci.*, *22*, 1519–1533, 1974.

Opgenoorth, H. J., R. J. Pellinen, H. Maurer, F. Kuppers, W. J. Heikkila, K. U. Kaila, and P. Tanskanen, Ground-based observations of an onset of localized field-aligned currents during auroral breakup and around local midnight, *J. Geophys.*, *48*, 101–115, 1980.

Pashin, A. B., K.-H. Glassmeier, W. Baumjohann, O. M. Raspopov, A. G. Yahnin, H. J. Opgenoorth, and R. J. Pellinen, Pi 2 magnetic pulsations, auroral break-up, and the substorm current wedge: A case study, *J. Geophys.*, *51*, 223–233, 1982.

Rees, M. H., Auroral ionization and excitation by incident energetic electrons, *Planet. Space Sci.*, *11*, 1209–1218, 1963.

Rostoker, G., and J. C. Samson, Polarization characteristics of Pi 2 pulsations and implications for their source mechanisms: Location of the source regions with respect to the auroral electrojets, *Planet. Space Sci.*, *29*, 225–247, 1981.

Rostoker, G., A. Vallance Jones, R. L. Gattinger, C. D. Anger, and J. S. Murphree, The development of the substorm expansive phase: The "eye" of the substorm, *Geophys. Res. Lett.*, *14*, 399–402, 1987.

Rothwell, P. L., M. B. Silevitch, and L. P. Block, A model for the propagation of the westward traveling surge, *J. Geophys. Res.*, *89*, 8941–8948, 1984.

Rothwell, P. L., M. B. Silevitch, and L. P. Block, Pi 2 pulsations and the westward traveling surge, *J. Geophys. Res.*, *91*, 6921–6928, 1986.

Rothwell, P. L., M. B. Silevitch, and L. P. Block, The motion of the WTS as a function of electron anisotropy in the plasma sheet, in *Modeling Magnetospheric Plasma*, *Geophys. Monogr. Ser.*, vol. 44, edited by T. E. Moore and J. H. Waite, AGU, Washington, D. C., in press, 1988.

Saito, T., Oscillation of the geomagnetic field with the progress of pt-type pulsation, *Sci. Rep. Tohoku Univ., Ser. 5*, *13*, 53, 1961.

Samson, J. C., Pi 2 pulsations: High latitude results, *Planet. Space Sci.*, *30*, 1239–1247, 1982.

Samson, J. C., and G. Rostoker, Polarization characteristics of Pi 2 pulsations and implications for their source mechanism: Influence of the westward travelling surge, *Planet. Space Sci.*, *31*, 435–458, 1983.

Sato, T., Auroral physics, in *Magnetospheric Plasma Physics*, edited by A. Nishida, pp. 197–243, D. Reidel, Hingham, Mass., 1982.

Silevitch, M. B., L. P. Block, C.-G. Fälthammar, G. Marklund, and M. A. Raadu, On the temporal evolution of enhanced conductivity regions associated with the westward traveling surge (abstract), *Eos Trans. AGU*, *65*, 1065, 1984.

Singer, H. J., D. J. Southwood, R. J. Walker, and M. G. Kivelson, Alfven wave resonances in a realistic magnetospheric magnetic field geometry, *J. Geophys. Res.*, *86*, 4589–4596, 1981.

Singer, H. J., W. J. Hughes, P. J. Fougere, and D. J. Knecht, The localization of Pi 2 pulsations: Ground-satellite observations, *J. Geophys. Res.*, *88*, 7029–7036, 1983.

Singer, H. J., W. J. Hughes, C. Gelpi, and B. G. Ledley, Magnetic disturbances in the vicinity of the substorm current wedge: A case study, *J. Geophys. Res.*, *90*, 9583–9589, 1985.

Southwood, D. J., and W. F. Stuart, Pulsations at substorm onset, in *Dynamics of the Magnetosphere*, edited by S.-I. Akasofu, pp. 341–355, D. Reidel, Hingham, Mass., 1980.

Stuart, W. F., C. A. Green, and T. J. Harris, Correlation between modulation of the intensity of precipitating electrons in the auroral zone and a coincident Pi 2, *J. Atmos. Terr. Phys.*, *39*, 631–635, 1977.

Tanskanen, P., et al., Different phases of a magnetospheric substorm on June 23, 1979, *J. Geophys. Res.*, *92*, 7443–7457, 1987.

Weimer, D. R., C. K. Goertz, D. A. Gurnett, N. C. Maynard, and J. L. Burch, Auroral zone electric fields from DE 1 and 2 at magnetic conjunctions, *J. Geophys. Res.*, 90, 7479–7494, 1985.
Weimer, D. R., D. A. Gurnett, C. K. Goertz, J. D. Menietti, J. L. Burch, and M. Sugiura, The current-voltage relationship in auroral current sheets, *J. Geophys. Res.*, 92, 187–194, 1987.
Zhu, L., and J. R. Kan, Time evolution of the westward-traveling surge, *Planet. Space Sci.*, 35, 145–151, 1987.

I. P. Block, Department of Plasma Physics, Royal Institute of Technology, S10044 Stockholm 70, Sweden
P. L. Rothwell, Air Force Geophysics Laboratory, PHG, Hanscom AFB, Bedford, MA 01731
M. B. Silevitch, Center for Electromagnetics Research, Northeastern University, Boston, MA 02115
P. Tanskanen, Department of Physics, University of Oulu, SF-90570, Oulu, Finland

(Received October 22, 1987,
revised January 22, 1988;
accepted February 25, 1988.)

JOURNAL OF GEOPHYSICAL RESEARCH, VOL. 91, NO. A6, PAGES 6921-6928, JUNE 1, 1986

Pi 2 Pulsations and the Westward Traveling Surge

PAUL L. ROTHWELL

Air Force Geophysics Laboratory, Hanscom Air Force Base, Massachusetts

MICHAEL B. SILEVITCH

Department of Electrical Engineering, Northeastern University, Boston, Massachusetts

LARS P. BLOCK

Department of Plasma Physics, Royal Institute of Technology, Stockholm

A model is developed that relates the poleward leaps of the westward traveling surge (WTS) and the generation of Pi 2 pulsations. The feedback instability developed by Sato and coworkers is combined with the dynamic surge model of Rothwell et al. [1984]. We find that our previous results on the motion of the WTS are related to the zero-order terms in the Sato formulation. The linearized first-order terms give rise to a dispersion relation with solutions in the Pi 2 frequency range. The lth frequency, f_l, is found to be turned on in integer multiples of one-half the Alfvén bounce frequency between the ionosphere and the plasma sheet. Most important, however, is that the lth frequency is turned on only when the precipitating electron energy exceeds a certain value. As previously shown, the velocity of the poleward surge boundary also increases when the energy of the precipitating electrons is enhanced. Therefore the poleward leap of the surge during substorm onsets is accompanied by the generation of higher Pi 2 frequency components. The time evolution of the composite Pi 2 pulse is obtained using the calculated decay rates, and agreement with data is shown.

INTRODUCTION

A recent review of Pi 2 pulsations and substorm onsets has been given by *Baumjohann and Glassmeier* [1984]. On the basis of previous work by *Rostoker and Samson* [1981] and *Samson and Rostoker* [1983] there is clearly an observed relationship between the westward traveling surge (WTS) and the generation of Pi 2 pulsations during substorm onsets. In particular, the WTS marks the longitudinal transition from the equatorward to poleward Pi 2. A poleward Pi 2 exists within the surge head and to the east. An equatorward Pi 2 predominates equatorward and to the west of the surge [*Rostoker and Samson*, 1981]. The maximum intensities of the Pi 2 pulsations were found along the equatorward boundaries of the electrojets. This led *Rostoker and Samson* [1981] and *Samson and Rostoker* [1983] to suggest that the resonance region of the Pi 2 pulsations is localized within the surge region and is constrained to remain on closed field lines. *Rostoker and Samson* [1981] also suggest that the Harang discontinuity is the energy source region for the Pi 2. *Samson and Harrold* [1983], using the University of Alberta magnetometer chain, found that within the WTS the Pi 2 polarization patterns are clockwise (CW) as viewed downward. On the other hand, *Lester et al.* [1984] found with the mid-latitude Air Force Geophysics Laboratory (AFGL) chain, at the same longitude but equatorward, that the polarization ellipticity is predominantly counterclockwise (CC). These results are consistent with the fact that equatorward and poleward of the WTS the polarizations are counterclockwise while far to the east and west of the WTS they are CW. The Pi 2 polarizations relative to the WTS are therefore quite complex.

Paper number 5A8793.
0148-0227/86/005A-8793$05.00

Causes of the observed east-west north-south transitions in the Pi 2 polarizations are an open question. According to *Pashin et al.* [1982], the Pi 2 current system is primarily located in the upward current at the surge head, and the westward movement of the surge causes linearly polarized Alfvén waves to appear elliptically polarized on the ground. *Samson* [1982], on the other hand, explains the observed polarization patterns in terms of a longitudinal distribution of oscillating current sheets. *Lester et al.* [1983, 1984] interpret the mid-latitude Pi 2 pulsations as arising from the field-aligned currents that form the substorm current wedge. *Ellis and Southwood* [1983] have examined the reflection of Alfvén waves from ionospheres with a discontinuity in either the Hall or the Pedersen conductivity. The reflection properties of the Alfvén wave depend not only on the discontinuity type but also on the orientation of the incident electric field vector. In two of the four cases studied, the field aligned current sheets act as subsidiary surface waves centered on the field lines connected to the discontinuity. The subsidiary waves are circularly polarized and suppress any net flow of Hall current across the discontinuity. *Glassmeier* [1984] has extended the work of Ellis and Southwood to include arbitrary distributions in the height-integrated conductivity. Recently, *Southwood and Hughes* [1985] have suggested that two oppositely traveling east-west surface waves parallel to the conductivity gradients could give a combined signal that reproduces many of the observed features of the Pi 2 pulsations. An important unresolved question is the relation of the Pi 2 current system to the overall current system that forms the substorm current wedge.

It is assumed that the initial diversion of the cross-tail current is carried by a transverse Alfvén wave [*Baumjohann and Glassmeier*, 1984]. The subsequent reflection of the wave [*Mallinckrodt and Carlson*, 1978; *Nishida*, 1979; *Kan et al.*, 1982] between the conjugate ionospheres and the triggering of secondary Alfvén waves in the ionosphere [*Maltsev et al.*, 1974;

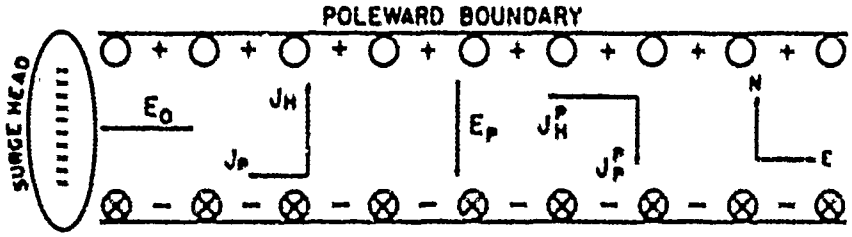

Fig. 1. Idealized model of the WTS as proposed by *Inhester et al.* [1981]. The total external electric field E_0 drives a westward Pedersen and a northward Hall current. If the northward Hall current is not fully continued by field-aligned currents into the magnetosphere, polarization charges build up on the poleward surge boundary, producing a southward directed electric field E_p. This southward electric field produces a Hall current in the same direction as the Pedersen current from the original electric field E_0.

Tamao and Miura, 1982] both contribute to the Pi 2 pulsation time profile. As pointed out by *Baumjohann and Glassmeier* [1984], it is important to treat the ionosphere as an active part of the ionosphere-magnetospheric coupling rather than just a reflecting boundary.

The purpose of this paper is to relate Pi 2 pulsations to the dynamics of the westward traveling surge (WTS). A dynamical surge model has been developed by *Rothwell et al.* [1984] using the Inhester-Baumjohann [*Inhester et al.*, 1981; *Baumjohann*, 1983] representation. Here the feedback instability analysis [*Sato and Holzer*, 1973; *Hoh and Sato*, 1973; *Sato*, 1982] is applied to the Inhester-Baumjohann model of the WTS used by *Rothwell et al.* [1984], hereinafter called paper 1. The equations are linearized in the standard fashion, and it is shown that the zero-order terms recover the poleward motion of the surge boundary as derived in paper 1. The first-order terms give rise to a dispersion relation for the feedback instability. This relation is solved for the allowed frequencies and their associated growth rates. It is found that the number of frequencies generated is related to the speed of the WTS boundaries. The resulting composite pulse shapes are shown to be very similar to those measured by *Singer et al.* [1985] at mid-latitudes. The physical picture presented is that the initial precipitation caused by the onset in the magnetotail triggers the feedback instability in the coupled ionosphere-magnetospheric system, thereby producing Pi 2 pulsations [*Baumjohann and Glassmeier*, 1984]. In the next section we relate the feedback instability to the Inhester-Baumjohann WTS model.

The Inhester-Baumjohann Model and the Feedback Instability

The Inhester-Baumjohann model is shown in Figure 1. A uniform westward electric field E_0 produces a northward Hall current that closes into the magnetosphere via field-aligned currents along the poleward surge boundary. If the precipitation is insufficient to close off this Hall current, then an effective polarization charge builds up along the conductivity gradient, producing a southward directed electric field. This electric field creates a southward Pedersen current opposite to the original Hall current and a westward Hall current that adds to the original westward Pedersen current driven by E_0.

As noted above, the Pi 2 current system and the substorm current system inside the wedge are not always the same. In this paper we initially assume that both current systems are colocated, which is true approximately 65% of the time [*Lester et al.*, 1983].

The feedback instability [*Ogawa and Sato*, 1971; *Sato and Holzer*, 1973] has its foundation in earlier work by *Atkinson* [1970]. The feedback instability was originally developed for the quiet arc, which has a much larger extension in the east-west direction than in the north-south direction, similar to the surge region. A downward field-aligned current on the equatorward edge of the arc closes via a northward Pedersen current to an upward field-aligned current on the poleward boundary. According to *Atkinson* [1970] a local ionospheric conductivity enhancement causes a local decrease of the electric field. The resulting divergence of the magnetospheric polarization currents produces precipitation that increases the original conductivity enhancement. If one visualizes a north-south ionospheric wave in the model in Figure 1, then one will have periodic conductivity enhancements which could lead to multiple arcs. The analysis for the quiet arcs as given by *Sato and Holzer* [1973] and *Holzer and Sato* [1973] is similar to the analysis presented here. In their analysis, active and passive ionospheric regions are conjugately connected by the same field line. The active ionosphere acts as an ac generator which produces an Alfvén wave that is damped in the passive ionosphere. *Sato* [1978, 1982] dispensed with the conjugately connected active and passive ionospheres and required that the Alfvén waves reflect upon reaching the equatorial plane. *Sato* [1978] also notes that the theory of quiet arcs must be self-consistent with the presence of a westward electric field. This is also a feature of the WTS as seen in Figure 1.

The feedback instability works because electrons tend to flow toward the positive part of the potential perturbation along the field lines. The inductive reactance of the magnetosphere, however, causes a phase lag in the precipitation such that it adds to the original ionization enhancement, causing the instability to grow. Should the magnetosphere have a capacitative reactance, then the precipitating electron flux coincides with the valley of the density distribution, and the perturbation decays. The magnetosphere must have an inductive response for the feedback instability to occur. By inductive and capacitative reactance we refer to the effective terminated transmission line impedance for Alfvén waves along the magnetic field lines [*Sato*, 1982]. This work has been extended by *Miura and Sato* [1980] to the global formation of multiple auroral arcs.

Tamao and Miura [1982], *Miura et al.* [1982], and *Tamao* [1984] considered a nonuniform magnetosphere coupling to the ionosphere. Negative Joule dissipation in the ionosphere is accompanied by a growing oscillation and an outflowing Poynting flux from the ionosphere. Damped oscillations occur when energy is supplied from the magnetosphere to the ionosphere. A large-scale uniform electric field in the ionosphere is required to drive the growing instability.

In the present work the generation of Pi 2 pulsations is

considered as follows. The injection of hot electrons from the plasma sheet during a substorm onset initiates the feedback instability in the ionosphere-magnetosphere system. This assumption is based on the satellite observations of *Sakurai and McPherron* [1983] that the Pi 2 burst is superimposed on a dc shift in the azimuthal component of the magnetic field which is caused by field-aligned currents. From their Figure 18 the Pi 2 occurs at the beginning of the dc shift. The parallel (precipitating) current is therefore considered to be decomposable into ac and dc components. The dc component is the primary injection from the distant magnetotail, and the ac component arises from the initial injection transient and the feedback instability. It will be shown below that the number of modes that are stimulated is dependent on the energy of the zero-order precipitation. It is argued that the feedback instability does not reach the nonlinear stage examined by *Sato* [1978] and *Miura et al.* [1982] since the flux associated with $j_{\parallel}$(dc) raises the ionization level within a time $\approx (\alpha_r N_0)^{-1}$, where α_r is the electron-ion recombination rate and N_0 is the zero-order ion density. After this time, electron-ion recombination dominates, and the composite pulsation decays.

Kan et al. [1982] consider the Pi 2 wave form to arise from the superposition of the reflected and incident Alfvén waves impinging on a passive ionosphere. They neglect polarization and Hall current effects. Here, on the other hand, we consider the natural modes arising from a self-consistent ionosphere-magnetosphere interaction (i.e., the feedback instability).

Formulation of the Model

In paper 1 [*Rothwell et al.*, 1984] the solutions to the time-dependent zero-order equations along the surge boundary conductivity gradients were solved. On the other hand, in *Sato's* [1982] theory the zero-order enhanced ionization density N_0 is taken as constant in space and time, which is consistent with the Inhester-Baumjohann model inside the surge region.

In formulating the present Pi 2 pulsation model we first connect the magnetospheric transverse Alfven wave with the ionospheric drift wave [*Tamao and Miura*, 1982]. The Alfvén wave is probably kinetic. However, the perpendicular scale lengths considered here are much larger than the ion gyroradius so that the Alfvén dispersion relation is essentially the same as in the MHD case. It is permissible, therefore, in the present context to use the MHD dispersion relation. An Alfvén wave carries parallel current which is related to the divergence of the transverse electric wave field by

$$Z_0 j_{\parallel} = \nabla \cdot E_{\perp} \tag{1}$$

where Z_0 is the characteristic impedance of an equivalent transmission line terminated at both ends by the impedance Z_0 and $j_{\parallel}$ is in the same direction as the ambient magnetic field B_0. It can be shown [see *Kan et al.*, 1982] that $j_{\parallel}$ and $\nabla \cdot E_{\perp}$ satisfy the transmission line equations. *Sato* [1982] used the transmission line analogy to impose the ionospheric and equatorial boundary conditions. As seen at the ionosphere, the magnetospheric impedance is given by

$$Z = iZ_0 \cot(\omega l / V_A) \tag{2}$$

where V_A is the magnetospheric Alfvén speed and l is the length of the field line between the ionosphere and the equator. This expression also assumes that $j_{\parallel}$ is zero at the equatorial plane. Z_0 is given by $\mu_0 V_A$. Then (1) holds at the ionosphere if Z in (2) replaces Z_0 in (1).

The northward ionospheric current component in the Inhester-Baumjohann model is given by

$$J_x = E_y \Sigma_H + E_x \Sigma_P \tag{3}$$

where Σ_H and Σ_P are the Hall and Pedersen conductivities, respectively, and E is the electric field. The conductivities are normalized to their zero-order values by

$$\begin{aligned} \Sigma_H &= \Sigma_{H0} N \\ \Sigma_P &= \Sigma_{P0} N \end{aligned} \tag{4}$$

where Σ_{H0} and Σ_{P0} are uniform inside the surge region and N is the height-integrated ionospheric ionization density normalized to the uniform density within the surge region [*Sato*, 1982]. Now we similarly have for the westward (y) current component

$$J_y = \Sigma_P E_y - \Sigma_H E_x \tag{5}$$

Equations (3), (4), and (5) are linearized as follows.

$$\begin{aligned} E_x &= E_{x0} + \bar{E}_x \\ E_y &= E_{y0} + \bar{E}_y \\ N &= 1 + \bar{N} \end{aligned} \tag{6}$$

where the values with overbars are of first order. E_{x0} is the primary electric field that drives the substorm current wedge, and E_{y0} is the primary north-south polarization electric field. Both E_{x0} and E_{y0} are assumed constant inside the surge region. Now the constancy of N_0 and E_0 inside the surge region implies that there is no net zero-order field-aligned current closing into the magnetosphere inside the surge. However, there is still a zero-order energetic electron precipitation that maintains the high conductivity inside the surge region. The current carried by the energetic electrons must be precisely balanced by a flux of upward flowing ionospheric electrons of lower energy. In this manner a high conductivity level is maintained with no net current closure. The divergence of J is given by

$$\nabla \cdot \bar{J} = J_0 \cdot \nabla \bar{N} + \Sigma_{P0} \nabla \cdot \bar{E} + \Sigma_{H0} (\nabla \times \bar{E})_z \tag{7}$$

where J_0 is the zero-order two-dimensional ionospheric current. The ionosphere is considered a source of transverse Alfvén waves so that $(\nabla \times E)_z = 0$ [*Maltzer et al.*, 1974] excludes magnetoacoustic waves in the ionosphere. The first-order field-aligned current density is given by

$$j_{\parallel} = \nabla \cdot \bar{J} - J_0 \cdot \nabla \bar{N} - \Sigma_{P0} \nabla \cdot \bar{E} \tag{8}$$

We assume that the first-order current is being carried by hot electrons. Note that we have a coordinate system with the upward current as positive, which means that we have a minus sign in the following relation.

$$Z j_{\parallel} = -\nabla \cdot \bar{E}_{\perp} \tag{9}$$

and upon combining (8) and (9) we have

$$j_{\parallel} = -J_0 \cdot \nabla \bar{N} (1 - Z \Sigma_{P0}) \tag{10}$$

Now the first-order continuity equation gives us

$$\begin{aligned} \partial \bar{N} / \partial t &= -Q h j_{\parallel} / e N_0 - 2 \bar{\alpha} \bar{N} \\ \bar{\alpha} &= \alpha_r N_0 / h \end{aligned} \tag{11}$$

where Qh is the height-integrated ion production efficiency

[*Rees*, 1963]. The insertion of (10) into (11) gives

$$\partial N/\partial t = -\mathbf{V}\cdot\nabla N\,(1 - Z\Sigma_{Pa}) - 2\alpha N \tag{12}$$

where the components of V are given by

$$\begin{aligned} V_x &= Qh\Sigma_2 V_z \\ V_y &= QhV_z^2[1 + R^2(1-\alpha)]^{-1}R \end{aligned} \tag{13}$$

The parameter α is the closure parameter as defined in the paper by *Rothwell et al.* [1984]. V_z is the $E \times B$ drift velocity taken as ≈ 0.25 km s, and R is the ratio of the height-integrated Hall to Pedersen conductivities, which we take to be ≥ 3. These are the components of the surge velocity as derived by *Rothwell et al.* [1984] without the electron-ion recombination term. This velocity term was derived in (12) by noting that

$$QhJ_\theta \cdot eN_\theta = Qh\,eN_\theta(\Sigma \cdot E) \tag{14}$$

where $\Sigma \approx eN_\theta B_\theta$ leads to equations (9) and (11) in the paper by *Rothwell et al.* [1984].

It is assumed in the usual manner that

$$N \approx \exp[i(k_x x + k_y y - \omega t)] \tag{15}$$

where ω is considered complex ($\omega = \omega_r + i\omega_i$) and k is the wave vector for the ionospheric wave. Taking $X = \Sigma_{Pa}/Z_0$ cot $[\omega_r l/V_x - n\pi]$, we have

$$-i\omega_i + \omega_r = -i\mathbf{V}\cdot\mathbf{k}(1 + iX)(1 + X^2) - 2\alpha \tag{16}$$

which leads to

$$\omega_r = \mathbf{V}\cdot\mathbf{k}(1 + X^2) \tag{17}$$

for the frequency dispersion and

$$\omega_i = \omega_r X - 2\alpha_p N_0 \tag{18}$$

for the growth rate.

Sato [1978, 1982] has argued that the maximum growth rate occurs for $X = 1$. However, X is not a free parameter, and its value must be consistent with the solutions to (17). For each value of n ($n = 0, 1, 2, \cdots$) one obtains two solutions to (17). One root corresponds to a negative transmission line impedance or a capacitative reactance and is highly damped. The other root corresponds to a positive (inductive) reactance and gives positive growth. This result is consistent with the views of *Sato* [1978]. In the following discussion we consider only the inductive roots of ω_r.

One can view the substorm current wedge as forming a box-shaped region of enhanced conductivity. The ionospheric waves associated with the Pi 2 pulsations partially reflect off the conductivity gradients on the boundaries forming standing waves in the x and y directions. In the following calculations it is assumed that the waves are dominated by the fundamental modes, i.e., the wavelengths in each component are of the same order as the scale size in that direction.

Now the $\mathbf{k}\cdot\mathbf{V}$ term in (17) can be expressed as (see (13))

$$W = \lambda_y \mathbf{k}\cdot\mathbf{V}/(2\pi QlV_z) = \{\gamma\alpha + [1 + R^2(1-\alpha)]/R\} \tag{19}$$

where $\gamma = \lambda_x/\lambda_y$. λ_y is the length of the surge wedge in the east-west direction, and λ_x is the surge width in the north-south direction. Figure 2 shows a plot of the right-hand side of (19) for various values of α and R. The long dashes in this figure represent the product $\gamma\alpha$. Note that for most cases, $\gamma\alpha$ is a reasonable approximation, which means that except for very small α (zero closure) the north-south surge dimensions dominate the Pi 2 frequency characteristics. In the following example, therefore, we set λ_y to infinity and treat the north-south case. Note also that for larger α the Pi 2 pulsation frequencies are higher. The dependence of W and R is weak.

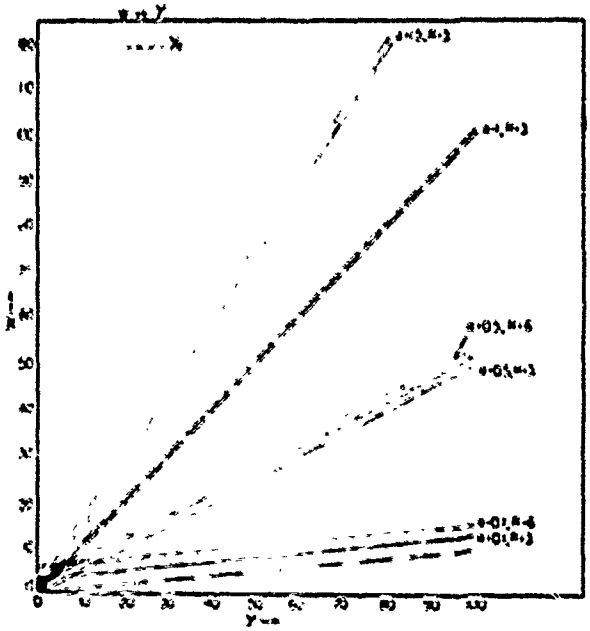

Fig. 2. The parameter W as defined in equation (19) in the text. This figure shows that except for almost zero closure ($\alpha = 0$) that $W = \gamma\alpha$ (denoted by solid lines) is a reasonable approximation. This graph indicates that the north-south surge dimensions generally determine the Pi 2 frequency characteristics.

As noted above, we solve for the inductive ($X > 0$) roots of (17). The resulting values of ω_r are inserted into the first term on the right-hand side of (18) and plotted in Figure 3*a*. The characteristic north-south dimension of the surge is taken as 500 km, and the quantities Σ_0/Z_0 and V_z/l are set to 10 and 0.005 s^{-1}, respectively. Note that a mode is excited whenever $X = 0$ or $\omega_r = (n + \frac{1}{2})\pi V_z/l$. This means that (17) has only physical solutions for frequencies less than $\pi V_z/\lambda_x$. Now the value of V_z increases with the energy of the precipitating electrons [*Rothwell et al.*, 1984]. Thus the energy of the zero-order component (dc) of the precipitating electrons controls the number of excited modes as seen from Figure 3*a*. More energetic precipitation is associated with higher magnetic activity. *Sakurai and McPherron* [1983] analyzed Pi 2 magnetic activity. *Sakurai and McPherron* [1983] analyzed Pi 2 magnetic pulsations observed at geosynchronous orbit on ATS 6. They found that as magnetic activity increased, the frequency spectrum became more complex with more spectral power at higher frequencies. This is consistent with Figure 3*a* in that a larger V_z is associated with more energetic electron precipitation and faster motion of the surge boundaries. As seen from Figure 3*a*, higher-frequency modes are excited at higher growth rates, implying a greater contribution to the spectral power. Figure 3*b* shows the corresponding mode frequencies for the same inputs as given for Figure 3*a*.

A horizontal line in Figure 3*a* would represent the damping due to electron-ion recombination. The net decay is the difference between this curve and the individual $\omega_r X$ curves. The present theory is applicable when the intersection of the V_z/λ_x line with the electron-ion loss rate is above the growth curves. If the intersection is below the growth curves, then continuous growth is predicted, which, of course, is unrealistic. Therefore this latter case should be treated by a more sophisticated non-

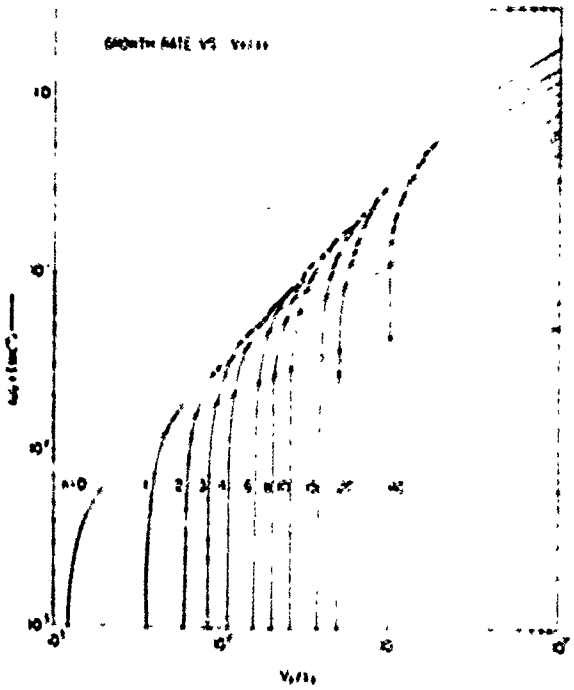

Fig. 3a. Growth rates for Σ_p/σ_0 and $l'_y/\lambda_x = 0.005$. The north-south dimension of the surge, λ_x, is taken as 500 km. The growth rates $\omega_r\lambda'$ of the various excited frequency modes are plotted as a function of l'_y/λ_x, where l'_y is the zero-order poleward surge velocity, neglecting electron-ion recombination effects. The value of this ratio determines the number of modes excited and the overall time profile of the resulting Pi 2 pulsation. A horizontal line equal to $2\alpha_r n$ would represent wave damping due to electron-ion recombination.

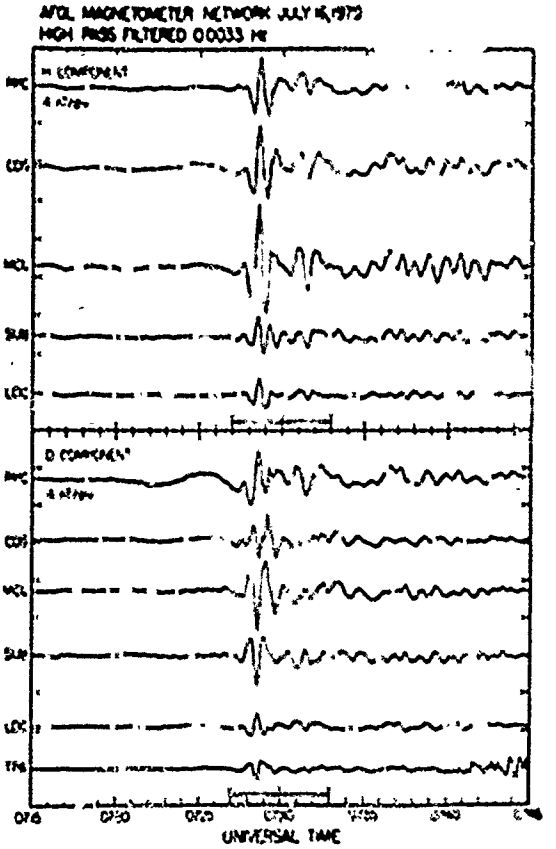

Fig. 4. AFGL magnetometer filtered Pi 2 data taken on July 16, 1979 (courtesy H. Singer AFGL).

linear approach. The sensitivity of the results to the variation parameters is as follows. Higher electron precipitation energy implies that higher-order modes are excited with faster growth rates and also that a higher ionospheric ionization density is attained. These two effects tend to offset each other in the sense that a higher ionization level implies faster electron-ion recombination and hence enhanced damping. The faster growth rates dominate however, so that the net effect is larger Pi 2 pulsations at higher incident electron energies. Higher incident flux at fixed incident energy can lead to overdamping. Lower flux causes more rapid growth. Smaller values of l'_y/λ_x (longer field lines) lead to the excitation of more modes shifted to lower frequencies.

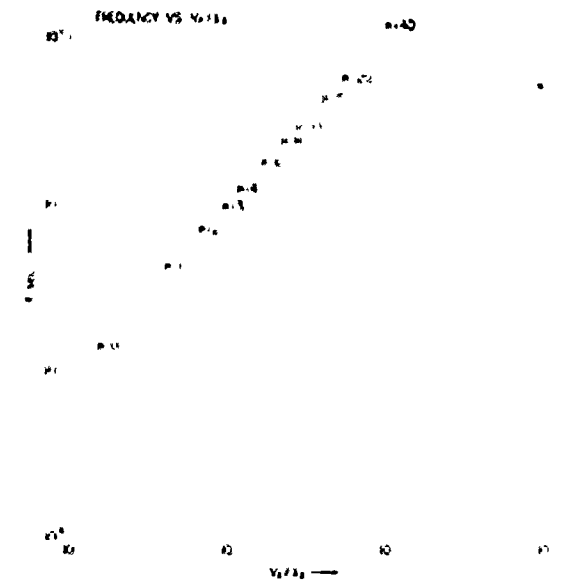

Fig. 3b. Frequencies of the various modes for the same input parameters as shown in Figure 3a.

In the present model an external condition is needed to relate the zero-order electron precipitation flux with the electron precipitation energy in order to ensure damped Pi 2 pulsations. We therefore took the results of *Fridman and Lemaire* [1980], who relate the field-aligned electron fluxes with the associated field-aligned potential drops. They consider five separate cases corresponding to different boundary conditions in the plasma sheet source. It was found that all five cases gave values for electron-ion recombination damping that were above the growth rate curves shown in Figure 3a. The *Fridman and Lemaire* [1980] results therefore are consistent with damped Pi 2 pulsations as derived from the present model.

Now in equation (23) of paper 1 we found that the model flux along the poleward boundary had to exceed some critical value in order for the surge to propagate. It turns out that this critical flux exceeds the required flux level inside the surge region to cause damped Pi 2 pulsations. Therefore from the present work one expects damped Pi 2 pulsations associated with poleward surge movements. This is an important consistency test between our theoretical approach and observational results.

Figure 4 shows a Pi 2 pulsation as measured by *Singer et al.* [1985], and Figure 5 shows the results of the present calcula-

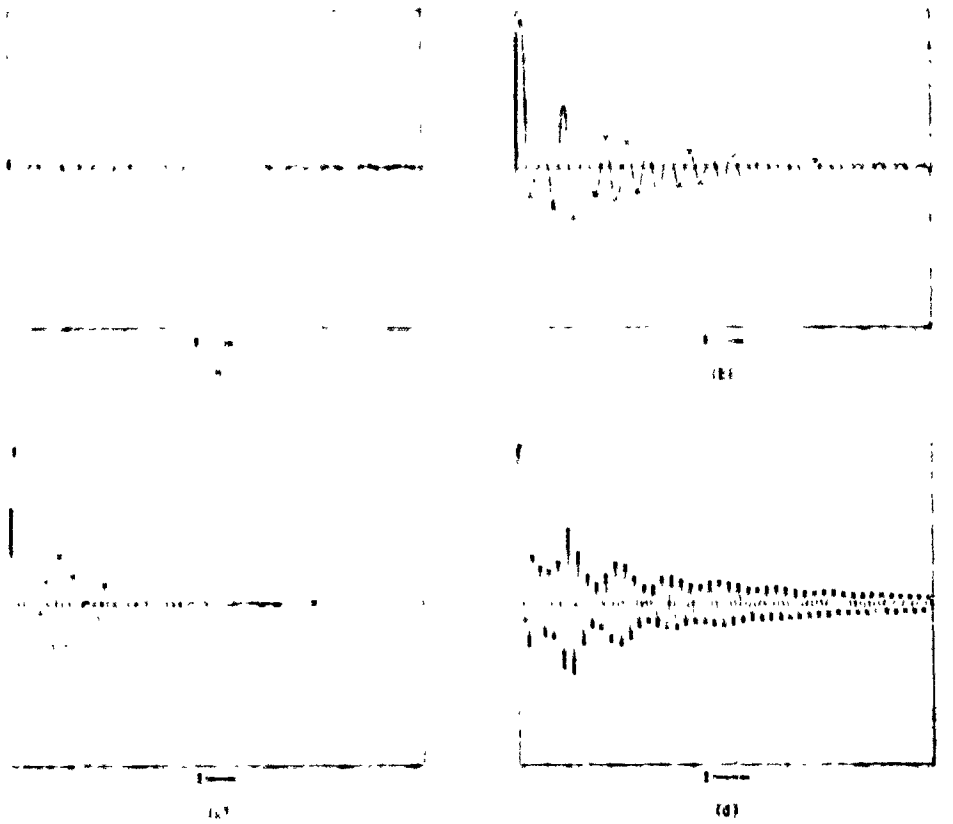

Fig. 5 The resulting model Pi 2 pulsation time profile based on the example shown in Figure 3a. This is a linear superposition of the individual modes assuming all are initially excited with an equal but arbitrary amplitude. Figures 5a–5d are the results for incident energies of 2 keV, 4 keV, 6 keV, and 8 keV, respectively. The corresponding precipitating electron fluxes used are 3.5×10^7, 7×10^7, 1.1×10^8, and 1.5×10^8 (cm^2 s)$^{-1}$. The equilibrium ionization level N_0 is given by $N_0 = (Q/\alpha_r)^{1/2}$ where Q is the ion production rate [*Rees*, 1963] and α_r is the electron-ion recombination rate. The damping term is given by $2\alpha_r N_0$ so that a minimum value of f is required in order to exceed the growth rates given in Figure 3a. Lower values of f lead to continued growth and to the nonlinear regime that is not covered in the present theory.

tion where the excited modes were considered initialized at equal amplitudes and all having a sinusoidal dependence. The four cases (*5a–5d*) correspond to incident energies of 2 keV, 4 keV, 6 keV, and 8 keV. The incident electron fluxes used in Figures *5a–5d* were 3.5×10^7, 7×10^7, 1.1×10^8, and 1.5×10^8 (cm^2 s)$^{-1}$, respectively. Note that the higher-frequency pulsations occur at higher incident energies. The agreement with *Singer et al.*'s [1985] data is seen to be quite good for Figure *5c*. The other cases (particularly Figures *5b* and *5d*) are not inconsistent with observations, although they are a little too regular and last too long. A slight increase in ionization (electron precipitation flux) would significantly decrease the pulsation duration. It is concluded that the different damping rates for the frequencies arising from the Sato formulation can lead to composite pulses which are very similar to the measured Pi 2 pulsations in shape and time duration. Therefore ionospheric generation of Alfvén waves could provide the primary signature for Pi 2 pulsations. The damping of the Pi 2's is very sensitive to increases in the precipitation current that enhances N_0.

The resulting physical model is as follows. The interruption of the dawn-dusk current in the plasma sheet causes electron precipitation, the collapse of tail field lines to a more dipolar configuration, and the formation of a substorm current wedge through the ionosphere. The impact of the initial precipitation electrons on the ionosphere triggers the feedback instability which has as a free energy source the east-west electric field E_{0y} in the substorm current wedge. The feedback instability fills the flux tubes from the ionosphere with Alfvén waves which form standing waves between conjugate ionospheres. Since the injected electrons are presumably on closed field lines, there is a simultaneous launching of Alfvén waves into the magnetosphere from comparable locations in the two ionospheres. The ionospheric conductivity is high inside the surge so that waves once injected into the magnetosphere are efficiently trapped between the conjugate ionospheres [*Hughes and Southwood*, 1976]. How do these standing Alfvén waves decay?

Sakurai and McPherron [1983] note Pi 2 polarization reversals in space similar to those observed by ground-based stations. They also point out that Pi 2's in space have a large compressional component and therefore can propagate across field lines as fast-mode hydromagnetic waves [*Singer et al.*, 1983]. The propagation speed is faster than the Alfvén speed since the fast-mode phase velocity is given as [*Akhiezer et al.*, 1975]

$$V_+ = (V_A^2 + C_s^2)^{1/2} \tag{20}$$

where C_s is the sound speed. It is argued that these waves still have a velocity component parallel to the magnetic field so that they impinge on the ionosphere outside the surge region. Outside the surge, however, the ionospheric conductivity is

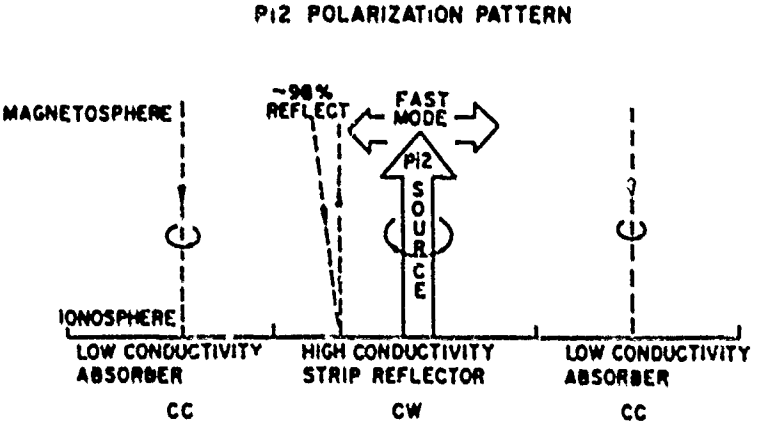

Fig. 6. Illustrates a possible explanation for the different Pi 2 polarization observed inside and outside the substorm current wedge. An incident Alfvén wave from the magnetosphere stimulates the feedback instability, as described in the text. The substorm wedge acts as an ionospheric source for Pi 2 pulsations with clockwise polarization. Farther out in the magnetosphere these couple to compressional waves that propagate perpendicular to B. Outside the substorm wedge region these compressional waves couple to Alfvén waves that are easily absorbed by the ionosphere in regions of low conductivity. As viewed from the ionosphere, these incident waves will have counterclockwise polarization consistent with observations.

much lower, and therefore wave reflection is much less efficient [*Hughes and Southwood*, 1976; *Ellis and Southwood*, 1983]. The magnetospheric Alfvén waves in these regions are rapidly damped by Joule heating [*Hughes and Southwood*, 1976].

The Alfvén wave created by the Sato feedback instability originates in the ionosphere and propagates into the magnetosphere. This wave is assumed to have clockwise polarization looking into the wave or counterclockwise polarization looking in the direction of propagation. It is also assumed that the sense of polarization is not affected by cross-field propagation via the fast-mode hydromagnetic wave. In the low-conductivity region outside the substorm current wedge the incident counterclockwise wave impinges on the ionosphere from the magnetosphere. If most of the incident wave in this region is absorbed by the ionosphere, then the polarization looking down is counterclockwise. In the high-conductivity region the launched waves are reflected in the conjugate ionosphere and return to the source region where they are highly reflected. Therefore the sense of polarization in the highly conductive region is determined by the ionospheric source characteristic of the feedback mechanism rather than by waves impinging from the magnetosphere. These concepts are illustrated in Figure 6.

In summary, the sense of polarization for ionospheric sources and sinks of Alfvén waves looking down at the ionosphere should be reversed. This interpretation is consistent with the observations of *Samson and Harrold* [1983] as described in the introduction.

The model has the following features.

1. The Pi 2 burst is a result of the sudden diversion of the tail current to the ionosphere [*Sakurai and McPherron*, 1983].

2. The feedback instability is an ionospheric source for Alfvén waves. Larger-amplitude components are generated at higher frequencies for more energetic precipitation.

3. Standing Alfven waves are created between conjugate ionospheres on field lines that connect the source locations. These standing waves propagate across B field lines via fast-mode hydromagnetic waves. Outside the surge region the waves are rapidly damped in the regions of lower ionospheric conductivity. This model therefore provides a possible energy path that Pi 2 pulsations could follow.

4. The present model is consistent with the results of paper 1 [*Rothwell et al.*, 1984] in that the electron precipitation fluxes required for surge propagation are also sufficiently high to damp the excited Pi 2 pulsations. The flux levels predicted by *Fridman and Lemaire* [1980] also ensure the presence of damped Pi 2 pulsations in the model given here.

The present work does not exclude the possibility of additional magnetospheric sources of Pi 2 pulsations. We assume, however, that these Pi 2's are easily reflected by the high-conductivity region and that the ground-based magnetometers most efficiently respond to the ionospheric source presented here.

Acknowledgments. We would like to acknowledge the many useful and insightful comments by Carl-Gunne Fälthammar and Göran Marklund of the Royal Institute of Technology, Stockholm, Sweden, and by W. J. Burke, Howard Singer, and Michael Heinemann at AFGL.

REFERENCES

Akhiezer, A. I., I. A. Akhiezer, R. V. Polovin, A. G. Sitenko, and K. N. Stepanov, *Plasma Electrodynamics*, vol. 1, *Linear Theory*, translated from Russian by D. ter Haar, Pergamon, New York, 1975.

Atkinson, G., Auroral arcs: Result of the interaction of a dynamic magnetosphere with the ionosphere, *J. Geophys. Res.*, *75*, 4746–4754, 1970.

Baumjohann, W., Ionospheric and field-aligned current systems in the auroral zone: A concise review, *Adv. Space Res.*, *2*, 55–62, 1983.

Baumjohann, W., and K.-H. Glassmeier, The transient response mechanism and Pi2 pulsations at substorm onset: Review and outlook, *Planet. Space Sci.*, *32*, 1361–1370, 1984.

Ellis, P., and D. J. Southwood, Reflection of Alfven waves by non-uniform ionospheres, *Planet. Space Sci.*, *31*, 107–111, 1983.

Fridman, M., and J. Lemaire, Relationship between auroral electron fluxes and field-aligned electric potential differences, *J. Geophys. Res.*, *85*, 664–670, 1980.

Glassmeier, K.-H., On the influence of ionospheres with non uniform conductivity distribution on hydromagnetic waves, *J. Geophys.*, *54*, 125–137, 1984.

Holzer, T. E., and T. Sato, Quiet auroral arcs and electrodynamic coupling between the ionosphere and magnetosphere, 2, *J. Geophys. Res.*, *78*, 7330–7339, 1973.

Hughes, W. J., and D. J. Southwood, The screening of micropulsation signals by the atmosphere and ionosphere, *J. Geophys. Res., 81*, 3234–3240, 1976.

Inhester, B. W., W. Baumjohann, R. W. Greenwald, and E. Nielsen, Joint two-dimensional observations of ground magnetic and ionospheric electric fields associated with auroral zone currents, 3, Auroral zone currents during the passage of a westward traveling surge, *J. Geophys., 49*, 155–162, 1981.

Kan, J. R., D. U. Longenecker, and J. V. Olson, A transient response model of Pi2 pulsations, *J. Geophys. Res., 87*, 7483–7488, 1982.

Lester, M., W. J. Hughes, and H. J. Singer, Polarization patterns of Pi2 pulsations and the substorm current wedge, *J. Geophys. Res., 88*, 7958–7966, 1983.

Lester, M., W. J. Hughes, and H. J. Singer, Longitudinal structure in Pi2 pulsations and the substorm current wedge, *J. Geophys. Res., 89*, 5489–5494, 1984.

Mallinckrodt, A. J., and C. W. Carlson, Relations between transverse electric fields and field-aligned currents, *J. Geophys. Res., 83*, 1426–1432, 1978.

Maltzev, Yu. P., S. V. Leontiev, and W. B. Lyatsky, Pi2 pulsations as a result of evolution of an Alfvén impulse originating in the ionosphere during a brightening of aurora, *Planet. Space Sci., 22*, 1519–1533, 1974.

Miura, A., and T. Sato, Numerical simulation of global formation of auroral arcs, *J. Geophys. Res., 85*, 73–91, 1980.

Miura, A., S. Ohtsuka, and T. Tamao, Coupling instability of the shear Alfvén wave in the magnetosphere with the ionospheric ion drift wave, 2, Numerical analysis, *J. Geophys. Res., 87*, 843–851, 1982.

Nishida, A., Possible origin of transient dusk-to-dawn electric field in the nightside magnetosphere, *J. Geophys. Res., 84*, 3409–3412, 1979.

Ogawa, T., and T. Sato, New mechanism of auroral arcs, *Planet. Space Sci., 19*, 1393–1412, 1971.

Pashin, A. B., K.-H. Glassmeier, W. Baumjohann, O. M. Raspopov, A. G. Yahnin, H. J. Opgenoorth, and R. J. Pellinen, Pi2 magnetic pulsations, auroral breakups, and the substorm current wedge: A case study, *J. Geophys., 51*, 223–233, 1982.

Rees, M. H., Auroral ionization and excitation by incident electron energetic electrons, *Planet. Space Sci., 11*, 1209–1218, 1963.

Rostoker, G., and J. C. Samson, Polarization characteristics of Pi2 pulsations and implications for their source mechanisms: Location of source regions with respect to the auroral electrojets, *Planet. Space Sci., 29*, 225–247, 1981.

Rothwell, P. L., M. B. Silevitch, and L. P. Block, A model for the propagation of the westward traveling surge, *J. Geophys. Res., 89*, 8941–8948, 1984.

Sakurai, T., and R. L. McPherron, Satellite observations of Pi 2 activity at synchronous orbit, *J. Geophys. Res., 88*, 7015–7022, 1983.

Samson, J. C., Pi 2 pulsation High latitude results, *Planet. Space Sci., 30*, 1239–1247, 1982.

Samson, J. C., and B. G. Harrold, Maps of the polarizations of high-latitude Pi 2's, *J. Geophys. Res., 88*, 9716–9744, 1983.

Samson, J. C., and G. Rostoker, Polarization characteristics of Pi2 pulsations and implications for their source mechanism: Influence of the westward travelling surge, *Planet. Space Sci., 31*, 435–458, 1983.

Sato, T., A theory of quiet auroral arcs, *J. Geophys. Res., 83*, 1042–1048, 1978.

Sato, T., Auroral physics, in *Magnetospheric Plasma Physics*, edited by A. Nishida, D. Reidel, Boston, Mass., 1982.

Sato, T., and T. E. Holzer, Quiet auroral arcs and electrodynamic coupling between the ionosphere and magnetosphere, 1, *J. Geophys. Res., 78*, 7314–7329, 1973.

Singer, H. J., W. J. Hughes, P. F. Fougere, and D. J. Knecht, The localization of Pi 2 pulsations: Ground-satelliteobservations, *J. Geophys. Res., 88*, 7029–7036, 1983.

Singer, H. J., W. J. Hughes, C. Gelpi, and B. G. Ledley, Magnetic disturbances in the vicinity of synchronous orbit and the substorm current wedge: A case study, *J. Geophys. Res., 90*, 9583–9589, 1985.

Southwood, D. J., and W. J. Hughes, Concerning the structure of Pi 2 pulsations, *J. Geophys. Res., 90*, 386–392, 1985.

Tamao, T., Magnetosphere-ionosphere interaction through hydromagnetic waves, Achievements of the International Magnetospheric Study (IMS), *Eur. Space Agency Spec. Publ., ESA SP-217*, 427–436, 1984.

Tamao, T., and A. Miura, Coupling instability of the shear Alfvén wave in the magnetosphere with the ionospheric ion drift wave, 1, Energetic consideration, *J. Geophys. Res., 87*, 905–911, 1982.

L. P. Block, Department of Plasma Physics, Royal Institute of Technology, Stockholm S 10044, Sweden.

P. L. Rothwell, Air Force Geophysics Laboratory/PHG, Hanscom Air Force Base, MA 01731.

M. B. Silevitch, Department of Electrical Engineering, Northeastern University, Boston, MA 02115.

(Received July 24, 1985;
revised November 18, 1985;
accepted November 18, 1985.)

JOURNAL OF GEOPHYSICAL RESEARCH, VOL. 94, NO. A3, PAGES 2717-2720, MARCH 1, 1989

Ionospheric Electron Acceleration by Electromagnetic Waves Near Regions of Plasma Resonances

ELENA VILLALÓN[1]

Center for Electromagnetics Research, Northeastern University, Boston, Massachusetts

Electron acceleration by electromagnetic fields propagating in the inhomogeneous ionospheric plasma is investigated. It is found that high-amplitude short wavelength electrostatic waves are generated by the incident electromagnetic fields that penetrate the radio window. These waves can very efficiently transfer their energy to the electrons if the incident frequency is near the second harmonic of the cyclotron frequency.

1. INTRODUCTION

Acceleration of ionospheric electrons by electromagnetic (EM) fields via irradiation either from ground-based microwave transmitters [*Wong et al.*, 1981; *Birkmayer et al.*, 1986], or from satellites or rockets [*James*, 1983], is a problem of very active research. This interest is motivated by observations of high-energy electrons by spacecraft in the ionosphere, and this fact can help to improve our understanding of basic properties of wave-particle plasma interactions [*Fejer*, 1979]. Artificially accelerated electrons can also be used as a probe of the potential coupling between the ionosphere and the magnetosphere. We consider an EM monochromatic plane wave of frequency ω and wave vector $\mathbf{k}$ and assume that the wave is launched near the ground at an arbitrary angle with respect to the constant, ambient magnetic field $\mathbf{B}_0$. We take $\mathbf{B}_0$ to be along the z direction, i.e., $\mathbf{B}_0 = B_0\mathbf{e}_z$, and $\mathbf{k} = k_x\mathbf{e}_x + k_z\mathbf{e}_z$. The wave electric field can be written as $\mathbf{E} = \mathbf{e}_x E_1 \cos\phi - \mathbf{e}_z E_2 \sin\phi - \mathbf{e}_z E_3 \cos\phi$, where $\phi = k_x x + k_z z - \omega t$, and E_i are real numbers. The motion of a relativistic electron of charge q and rest mass m is described by the Lorentz force equation

$$d\mathbf{p}/dt = q[\mathbf{E} + \mathbf{v} \times (\mathbf{B} + \mathbf{B}_0)] \tag{1}$$

where $\mathbf{B}$ is the wave magnetic field, $\mathbf{v}$ is the particle velocity, and $\mathbf{p} = m\gamma\mathbf{v}$ is the momentum. The relativistic factor is $\gamma = (1 + p_x^2/m^2c^2 + p_z^2/m^2c^2)^{1/2}$ where p_x and p_z are the momentum components perpendicular and parallel to $\mathbf{B}_0$, respectively. The particle gains energy if the resonance conditions

$$\omega - k_z v_z - n\Omega/\gamma = 0 \tag{2}$$

are closely satisfied. Here n is an integer and $\Omega = qB_0/mc$ is the electron cyclotron frequency.

Recently, *Villalón and Burke* [1987] have developed a theory in which EM superluminous (i.e., the refractive index, η, is smaller than one) cold plasma waves accelerate the electrons via resonant stochastic acceleration. That is, by taking ω near 2Ω, they show that the cyclotron resonances overlap at high power levels. It was shown that wave intensities of 10^6 mW/m^2 accelerate the electrons up to energies of about 100 keV. Numerical integration of (1) shows that for the electrons to reach large energies (in the MeV range) the power levels that are required exceed a value of 10^8 mW/m^2 [*Burke et al.*, 1988]. Nevertheless, such power levels are at least a factor of 10^6 times greater than what is currently available in ionospheric heating experiments. Thus other more feasible approaches to accelerate cold ionospheric electrons should be investigated.

In this article, we propose a far more effective acceleration mechanism based upon propagation characteristics of EM waves in nonuniform plasmas. If the incident frequency ω is near 2Ω, and if the plasma density is such that ω is between the local upper hybrid, ω_{uh}, and electron plasma, ω_p, frequencies, $\omega_p \lesssim \omega \lesssim \omega_{uh}$, coupling to electrostatic (ES) plasma waves of short wavelength is possible. We show that these waves very efficiently transfer energy to the electrons. We also report calculations relevant to present RF heating experiments by considering a power flux $P = 1$ mW/m^2. The energy gained by the electrons is obtained by applying the Hamiltonian potential wells theory of *Villalón and Burke* [1987]. At low pump field amplitudes we find that particles gain energy following trajectories in p_x, p_z phase space along the zero-order Hamiltonian H_0. For a relativistic particle we have

$$H_0 = mc^2\gamma - (\eta_z/\beta_z)p_z \tag{3}$$

where $\beta_z = \eta_z(1 + E_3k_x/E_1k_z)$ and η_z is the component of the refractive index, $\eta = ck/\omega$ along $\mathbf{B}_0$. For electrostatic waves we find that $\beta_z = 0$, and then that the zero-order trajectories are open and the particle gains energy in the direction perpendicular to the background magnetic field, i.e., p_z is constant.

2. ELECTROSTATIC WAVE GENERATION

We consider the propagation of EM waves in a nonuniform, ionospheric plasma. We assume that the density gradient is along the ζ (vertical) direction, that $\mathbf{B}_0$ forms an angle θ with respect to ζ, and that $\mathbf{k}$ is in the plane spanned by ζ and $\mathbf{B}_0$ (see Figure 1). The launching angle with respect to the vertical direction is denoted by ψ. The angle between $\mathbf{k}$ and $\mathbf{B}_0$ is called α and depends on the altitude. The refractive index η has a component Q along the vertical direction and a component S in the horizontal μ direction. We have the relation $\sin(\alpha + \pi/2 - \theta) = Q/\eta$. Because of the horizontally plane stratified ionospheric model considered here, the horizontal component of the refractive index S is a constant independent of the plasma density and then is given by $S = \sin\psi$. The vertical component Q depends on altitude (i.e., on the local plasma density) and is obtained by solving for the Booker quartic dispersion relation [*Budden*, 1961]. We may choose the angle

[1]Also at Air Force Geophysics Laboratory, Hanscom Air Force Base, Massachusetts.

Paper number 88JA04089.
0148-0227/89/88JA-04089$02.00

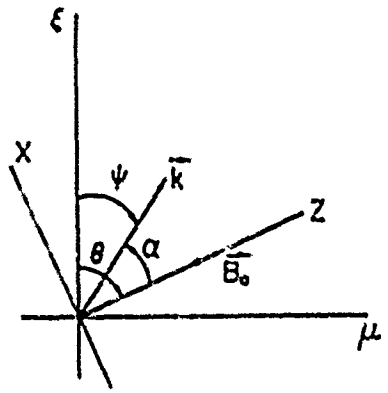

Fig. 1 Coordinate system as introduced in Section 2.

of incidence ψ such that

$$\sin \psi = Y^{1/2}(1 + Y)^{-1/2} \sin \theta \tag{4}$$

where $Y = \Omega/\omega$. If the ordinary (O) mode is launched near the ground at the critical angle given in (4), it will penetrate the radio window and will be transmitted near the coupling level where $\omega = \omega_p$ into the extraordinary mode (also called the Z mode). The transmission coefficient from O to Z modes has been obtained by *Mjolhus* [1984], and it is unity (total transmission) if $S = \sin \psi$ is given by (4). The Z mode propagates in the inhomogeneous plasma of the ionosphere until it falls into the region of high-frequency plasma resonances [*Mjolhus and Fld*, 1984]. Near the plasma resonance: (1) Q becomes very large ($Q \to \infty$), in fact, since $Q \gg S$ we find that $\alpha \to 0$, (2) the wave becomes electrostatic, i.e., $E_1/E_2 = -\tan \theta$ and $E_3 = 0$, and (3) the vertical group velocity component becomes very small. The plasma density in the resonance region is given by solving for $X = X_r$ where, because $\alpha = 0$, we have

$$X_r = (1 - Y^2)(1 - Y^2 \cos^2 \theta)^{-1} \tag{5}$$

and $X = \omega_p^2/\omega^2$. Near resonance, the vertical component of the refractive index Q must be calculated by considering a finite temperature plasma. In fact, by adding the lowest order thermal corrections to the coefficients of fourth and third degree of the Booker quartic, we find that Q is given by solving for the real root of the dispersion relation

$$(v_T/c)^2(AQ^3 + 2\kappa Q^2) - 2Y = 0 \tag{6}$$

where

$$A = 3\cos^4 \theta + \frac{3 \sin^4 \theta}{(1 - Y^2)(1 - 4Y^2)} + \frac{(6 - 3Y^2 + Y^4)}{(1 - Y^2)^3} \cos^2 \theta \sin^2 \theta$$

$$\kappa = S \sin \theta \cos \theta \left\{ \cos^2 \theta \frac{(-15Y^2 + 17Y^4 - 6Y^6)}{(1 - Y^2)^5} + \sin^2 \theta \frac{(-15Y^2 + 7Y^4 - 4Y^6)}{(1 - Y^2)^3(1 - 4Y^2)} \right\}$$

$$Y = S \sin \theta \cos \theta \frac{Y^2}{(1 - Y^2)}$$

and v_T, the electron thermal speed, is such that $v_T/c \ll 1$. A brief sketch on the derivation of (6) is presented in the appendix. The term proportional to A was calculated by *Golant and Piliya* [1972], and its contribution is much larger than that proportional to κ if $A \neq 0$. The case $A = 0$ has not received any attention yet. Nevertheless, we find that it is of interest, since the refractive indices are larger than when $A \neq 0$ by a factor of $(c/v_T)^{1/3}$. For a given value of θ, A is equal to zero at a certain frequency which is greater than Ω and smaller than 2Ω. In fact, we find that for $\theta \gtrsim 45°$, A becomes zero for ω very close to 2Ω. In Figure 2, we show the refractive indices as functions of the angle θ for two values of the incident frequency ω which are smaller than but close to 2Ω; we take $v_T/c = 0.25 \times 10^{-3}$. The largest Q are found near $\theta = \theta_r$, where θ_r is such that $A(\theta_r, \omega) = 0$. We have that for $\omega = 1.81\ \Omega$, $\theta_r = 43.6°$ and $Q = +563$, and that for $\omega = 1.92\ \Omega$, $\theta_r = 32.7°$ and $Q = +4060$.

The Landau damping rate Γ due to the Doppler shifted frequency at the second harmonic is (see the appendix)

$$\Gamma/\omega = -(1/16)(\pi/2)^{1/2}(v_T/c)^2(\sin^4 \theta \cos \theta)(\sigma/Y^4) \cdot \exp\left(-(\omega - 2\Omega)^2/2(k_1 v_T)^2\right) \tag{7}$$

where $\sigma = (1 - Y^2)/(X_r^{-1} - Y^2 \cos^2 \theta)$. We see that if $A \neq 0$, Γ/ω is of order $(v_T/c)^{1/2}$, but if $A = 0$, then $\Gamma/\omega \sim O(1)$.

The components of the group velocity along the vertical, v_{gz}, and horizontal, v_{gx}, directions are readily obtained from (6); we show

$$v_{gz}/c = \tfrac{1}{2}(v_T/c)^2(3AQ + 4\kappa)\sigma \tag{8}$$

$$v_{gx}/c = -\tfrac{1}{2}(v_T/c)^2 AQ^2 \sigma/S \tag{9}$$

If $A \neq 0$, we find that $v_{gz}/v_{gx} \sim O(Q^{-1})$, and then that the wave propagates in the direction perpendicular to the density gradient, but if $A = 0$, then $v_{gx} = 0$. However, by adding to (6) a third thermal correction of the form $(v_T/c)^3 \nu Q$, where ν is a function of θ and Y, we show that v_{gx} is proportional to $(v_T/c)^2 \nu$, when $A = 0$. Thus v_{gz} and v_{gx} become of the same order of magnitude and much smaller than v_{gx} for the case $A \neq 0$. The amplitude of the time-averaged electric field can be obtained solving for

$$P = (c/16\pi)(v_T/c)^2(3AQ + 4\kappa)X_r|E|^2 \tag{10}$$

Here P is the vertical component of the energy flux density. The highest energy concentration occurs when the group velocity is the smallest.

3 Electron Accelerations

Assuming that Γ is small, the energy that a single electron may gain interacting with a general EM plane wave of the

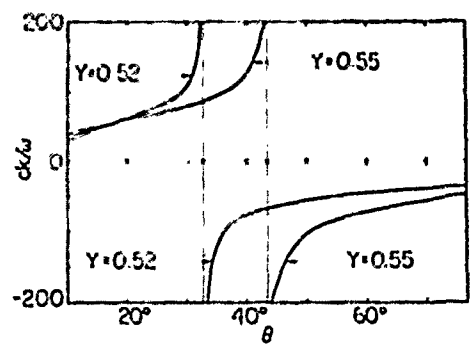

Fig. 2 Refractive indices in the plasma resonance regions, as functions of the angle θ between the ambient magnetic field and the vertical, for two values of $Y = \Omega/\omega$.

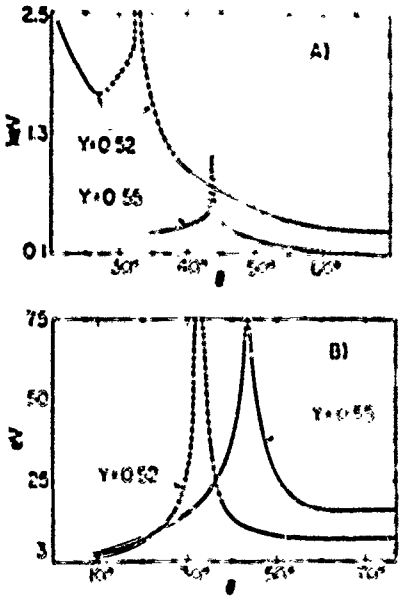

Fig. 3. Net energy gain as function of the angle θ between the ambient magnetic field and the vertical. We consider two values of $Y = \Omega/\omega$ and the interaction of cold electrons with (*a*) the $n = 2$, and (*b*) the $n = 1$ cyclotron resonances.

form given before (1), has been obtained as a function of time in the article by *Villalón and Burke* [1987]. It was found that the normalized particle energy U is obtained solving for

$$(U + 1)^2(dU/dt)^2 + V_n^2(U) = 0 \qquad (11)$$

where $U = \gamma - 1$, and time is normalized to number of wave-periods, $t = t\omega$. Here we consider the electron interaction with a single (isolated) cyclotron resonance of order n. For a particle initially ($t = 0$) at rest interacting with the ES waves ($E_1/E_3 = -\tan\theta$, and $E_2 = 0$) that are generated near resonance, the Hamiltonian potentials may be written as

$$V_n^2(U) = \tfrac{1}{2}U^2(U + 2r_n)^2 - \Sigma^2\cos^2\theta K_n(U) - \Sigma^2 2\sin^2\theta[K_{n+1}(U) + K_{n-1}(U)] \qquad (12)$$

with $r_n = 1 - nY$, $\Sigma = -q|E|/m\omega$, and

$$K_n(U) = \int_0^U J_n^2(k_n\rho')(U' + 1)\,dU'$$

Here $J_n(k_n\rho)$ are Bessel functions and ρ' is the Larmor radius evaluated at U', we have $\rho = c\Omega\,[2U + U^2]^{1/2}$. The allowable energies are restricted by the condition $V_n^2(U) \leq 0$. Note that the first term in (12) is always positive, and dominates over all the others at large values of U. Thus $V_n^2(U)$ can be regarded as a potential well within which the particle's energy oscillates in time. The kinetic energy slowly increases over many cyclotron and wave periods, and the net energy gained by the particle has always a finite value. If $V_n^2(U) < 0$ when $U = 0$, the potential can trap zero kinetic energy particles, these particles may increase their energy up to a value $U = U_0$ such that $V_n^2(U_0) = 0$. If $V_n^2(U) > 0$ when $U = 0$, then the potential cannot trap zero kinetic energy particles.

4. Numerical Calculations

In Figure 3*a*, we represent the net energy gained by the electrons (in keV) due to the interaction with the $n = 2$ cyclotron resonance, as function of θ. These energies are calculated by solving for the zeros of the Hamiltonian potentials. We consider two values of ω and a power flux $P = 1$ mW m^{-2}. The amplitudes of the ES fields are obtained from (10). We see that the $n = 2$ resonance can only trap cold electrons for angles greater than 20° if $\omega = 1.92\,\Omega$ ($Y = 0.52$), and 34° if $\omega = 1.81\,\Omega$ ($Y = 0.55$). The broken lines near the $\theta = \theta_c$, which makes $\Lambda = 0$, indicate that $\zeta = |\omega - 2\Omega|k_1v_T \geq 2$ and that $\Gamma/\omega \sim O(1)$. Thus the energy of the ES fields is strongly absorbed by the bulk distribution of plasma electrons. The kinetic energies reached by the electrons are very large due to the enhanced electric fields and large values of η near $\theta = \theta_c$. For larger values of ζ (solid lines), we find that Γ/ω is very small (i.e., $\Gamma/\omega < 2 \times 10^{-4}$), and hence that only a few electrons in the tail of the distribution function may interact with the waves. These electrons are accelerated in the direction perpendicular to the constant magnetic field up to energies of the order of hundreds of electron volts. Note that in the Earth's dipole magnetic field the mirroring force acting on the electrons will also accelerate them along geomagnetic field lines. The interaction of cold electrons with the $n = 1$ resonance takes place for all values of θ. The net energy gain (in eV) is represented in Figure 3*b*, and is quite small if $\theta \neq \theta_c$. This is because the resonance condition (2) is far from being satisfied for $\omega \cong 2\Omega$, $n = 1$, and initially cold electrons.

The time it takes to reach these energies can be calculated with the help of (11) and (12). We start with the $n = 1$ cyclotron resonance and cold electrons until the potential becomes positive, then, if there is overlapping with the $n = 2$ resonance, the particles are accelerated to high energies. For example, for $\omega = 1.92\,\Omega$ and $\theta = 23°$, it takes 168 wave periods (WP) to gain 2 keV, where half of this time is spent reaching the first 100 eV. If $\theta = 43°$ the electrons gain 800 eV over 86 WP (see Figure 4*a*). As a second example, we consider $\omega = 1.81\,\Omega$; if $\theta = 37°$, it takes 35 WP to gain 350 eV, but if $\theta = 46°$, then it only takes 25 WP to reach the same energy (see Figure 4*b*). Although the first and second cyclotron resonances may overlap over a broad range in energies, we find that we can neglect the contribution of the $n = 2$ resonance in the overlapping region. In fact, if $\omega = 1.81\,\Omega$ and $\theta = 37°$ it takes 43 WP to reach the first 28 eV with the $n = 2$ resonance, but it only takes 7 WP with the $n = 1$. On average we find that, in Gaussian units, the amplitude of the electric fields are about 0.005 times the ambient magnetic field.

5. Concluding Remarks

In this article, we have investigated the possibility of accelerating ionospheric electrons in intense electromagnetic (EM) fields. We have presented a very efficient acceleration and heating mechanism which consists in the generation of short-wavelength, high-amplitude electrostatic (ES) fields by the incident EM waves that penetrate the radio window. By including thermal effects, we have derived the dispersion relation for these ES fields, analytical expressions are given for their group velocities and damping rates. Because of the very small group velocity components in both the vertical and horizontal directions, the electromagnetic energy is highly concentrated in a region of plasma resonance. The effectiveness of this mechanism depends on the value of the incident frequency ω and on the angle θ that the background magnetic field forms with the vertical direction. Calculations on single particle acceleration show that the electrons can gain 1 or 2 keV for moderate (1 mW/m^2) power levels if, for small values of θ, ω is chosen slightly below the second gyroharmonic.

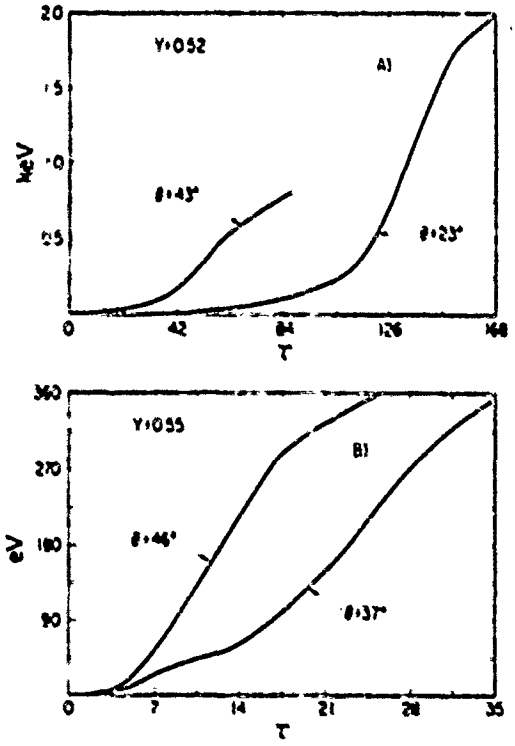

Fig. 4. Energy gain as function of time τ normalized to number of wave periods. Here θ is the angle between the ambient magnetic field and the vertical and $Y = \Omega/\omega$. The energy is given in (a) KeV, and (b) eV

APPENDIX

For electrostatic waves the dielectric response function is

$$\mathscr{S} = \eta^2(\varepsilon_{11}\sin^2\alpha + \varepsilon_{33}\cos^2\alpha + 2\varepsilon_{13}\cos\alpha\sin\alpha) \quad \text{(A1)}$$

where ε_{ij} are components of the dielectric tensor (the row is indicated by the subscript i and the column by j) which can be found elsewhere [*Ichimaru*, 1973]. Next, we expand ε_{ij} in powers of the small quantities $(k_\perp v_T/\Omega)^2$ and $[(\omega - n\Omega)/k_\parallel v_T]^{-1}$, where $n = 0, 1, 2$ and $k_\perp = k\sin\theta$, $k_\parallel = k\cos\theta$ are the perpendicular and parallel components to $\mathbf{B}_0$ of the wave vector. By keeping only first-order terms in $(v_T/c)^2$, we find

$$\varepsilon_{11} = 1 - \frac{X}{(1-Y^2)} - \eta^2\left(\frac{v_T}{c}\right)^2 X\left(\frac{3\sin^2\alpha}{(1-Y^2)(1-4Y^2)} + \cos^2\alpha\frac{(1+3Y^2)}{(1-Y^2)^3} - \frac{i}{2}\frac{\sin^2\alpha}{Y^3(1-2Y)}W_i\right) \quad \text{(A2)}$$

$$\varepsilon_{33} = 1 - X - \eta^2\left(\frac{v_T}{c}\right)^2 X\left(\frac{\sin^2\alpha}{(1-Y^2)} + 3\cos^2\alpha - \frac{i}{8}\frac{\sin^4\alpha}{\cos^2\alpha}\frac{(1-2Y)}{Y^4}W_i\right) \quad \text{(A3)}$$

$$\varepsilon_{13} = \eta^2\left(\frac{v_T}{c}\right)^2 X\left(-\frac{2\cos\alpha\sin\alpha}{(1-Y^2)^2} + \frac{i}{4}\frac{\sin^3\alpha}{Y^3\cos\alpha}W_i\right) \quad \text{(A4)}$$

where

$$W_i = \sqrt{\frac{\pi}{2}}\frac{(1-2Y)}{|k_\parallel|v_T/\omega}\exp\left(-\left(\frac{\omega-2\Omega}{2^{1/2}k_\parallel v_T}\right)^2\right)$$

By considering that $\cos\alpha = (S\sin\theta + Q\cos\theta)/\eta$ with $Q \gg S$, and by keeping the higher-order powers in Q, we may write $\mathscr{S} = \mathscr{S}_r + i\mathscr{S}_i$, where

$$\mathscr{S}_r = Q^4\left[\varepsilon_{zz} - \left(\frac{v_T}{c}\right)^2(AQ^2 + 2\kappa Q)X + \frac{2YX}{Q}\right] \quad \text{(A5)}$$

Here $\varepsilon_{zz} = 1 - X/N_r$, where N_r is given in (5) and A, κ, and Y are given after (6). By taking ε_{zz} very small and setting $\mathscr{S}_r = 0$, we obtain the dispersion relation (6). We also have

$$\mathscr{S}_i = \frac{1}{8}\left(\frac{\pi}{2}\right)^{1/2}\left(\frac{v_T}{c}\right)Q^5\frac{\sin^4\theta}{|\cos\theta|}\frac{X}{Y^4}\exp\left[-\left(\frac{\omega-2\Omega}{2^{1/2}k_\parallel v_T}\right)^2\right] \quad \text{(A6)}$$

The components of the group velocity v_{gz}, $v_{g\perp}$ in (8) and (9) are obtained by defining $\mathscr{K}_r = \mathscr{S}_r/Q^4$, and then

$$v_g = -\frac{(\partial\mathscr{K}_r/\partial k)}{(\partial\mathscr{K}_r/\partial\omega)} \quad \text{(A7)}$$

where recall that $ck_z/\omega = Q$ and $ck_\perp/\omega = S$. The Landau damping rate at the second cyclotron harmonic is also obtained by considering that $\mathscr{K}_i = \mathscr{S}_i/Q^4$ and then that $\Gamma = -\mathscr{K}_i[\partial\mathscr{K}_r/\partial\omega]$. Here $\partial\mathscr{K}_r/\partial\omega \simeq \partial\varepsilon_{zz}/\partial\omega = 2X/\omega\sigma$, where σ is defined after (7).

Acknowledgments. The author is grateful to A. Y. Wong for drawing her attention to the problem of propagation through the radio window, and for very helpful discussions. We also acknowledge helpful conversations with W. J. Burke and E. Mjolhus. This work has been supported by the U.S. Air Force under contract F19628-85-K-0053.

The Editor thanks I. Kimura and another referee for their assistance in evaluating this paper.

REFERENCES

Birkmayer, W., T. Hagfors, and W. Kofman, Small-scale plasma density depletions in Arecibo high-frequency modification experiments, *Phys. Rev. Lett.*, *57*, 1008, 1986.

Budden, K. G., *Radio Waves in the Ionosphere*, Cambridge University Press, New York, 1961.

Burke, W. J., G. Ginet, F. Villalón, and M. A. Heinemann, Electron acceleration in the ionosphere by obliquely propagating electromagnetic waves, *J. Geomagn. Geoelec.*, *40*, 1147, 1988.

Ieyer, J. A., Ionospheric modification and parametric instabilities, *Rev. Geophys.*, *17*, 135, 1979.

Golant, V. E., and A. D. Pilya, Linear transformation and absorption of waves in a plasma, *Sov. Phys. Usp.*, Engl. Transl., *14*, 413, 1972.

Ichimaru, S., *Basic Principles of Plasma Physics. A Statistical Approach*, W. A. Benjamin, Reading, Mass., 1973.

James, H. G., Sounder-accelerated particles observed in ISIS, *J. Geophys. Res.*, *88*, 4027, 1983.

Mjolhus, E., Coupling to Z mode near critical angle, *J. Plasma Phys.*, *31*, part 1, 7, 1984.

Mjolhus, E., and T. Flå, Direct access to plasma resonance in ionospheric radio experiments, *J. Geophys. Res.*, *89*, 3921, 1984.

Villalón, E., and W. J. Burke, Relativistic particle acceleration by obliquely propagating electromagnetic fields, *Phys. Fluids*, *30*, 3695, 1987.

Wong, A. Y., J. Santoru, and G. G. Sivjee, Active simulation on the auroral plasma, *J. Geophys. Res.*, *86*, 7718, 1981.

E. Villalón, Center for Electromagnetic Research, Northeastern University, Boston, MA 02115

(Received May 27, 1988;
revised November 14, 1988;
accepted November 14, 1988.)

Relativistic particle acceleration by obliquely propagating electromagnetic fields

Elena Villalón
Center for Electromagnetics Research, Northeastern University, Boston, Massachusetts 02115
William J. Burke
Air Force Geophysics Laboratory, Hanscom Air Force Base, Massachusetts 01731

(Received 4 December 1986; accepted 24 July 1987)

The relativistic equations of motion are analyzed for charged particles in a magnetized plasma and externally imposed electromagnetic fields $(\omega,\mathbf{k})$, which have wave vectors $\mathbf{k}$ that are at arbitrary angles. The particle energy is obtained from a set of nonlinear differential equations, as a function of time, initial conditions, and cyclotron harmonic numbers. For a given cyclotron resonance, the energy oscillates in time within the limits of a potential well; stochastic acceleration occurs if the widths of different Hamiltonian potentials overlap. The net energy gain for a given harmonic increases with the angle of propagation, and decreases as the magnitude of the wave magnetic field increases. Applications of these results to the acceleration of ionospheric electrons are presented.

I. INTRODUCTION

The interaction of high-power rf fields with plasma particles is a subject of very active research because of its richness in basic plasma processes and practical applications. It can be used as a method to increase the plasma temperature[1] and to accelerate some particles to high energies.[2] Particle acceleration by electrostatic waves is a well-explored area of research because of its application in laboratory plasmas.[3] Although less is known about acceleration processes by electromagnetic waves,[4,5] they may have greater relevance in space plasma physics. Recently, there has been an increasing effort to understand the basic ionospheric plasma processes and the nature of particle motion under the influence of high-power rf fields.[6] A number of nonlinear phenomena have been observed such as the formation of cavitons (local plasma density depletion) and parametric instabilities. In addition, particle acceleration has also been observed near the critical layer where the wave frequency matches the local plasma frequency.[7] In this paper, we concentrate on single particle rather than collective plasma motion.

The motion of a relativistic particle of charge q and rest mass m, under the influence of an external electromagnetic field and a uniform magnetic field $\mathbf{B}_0$ is described by the Lorentz force equation

$$\frac{d\mathbf{p}}{dt} = q\left(\mathbf{E} + \frac{\mathbf{v}}{c}\times(\mathbf{B} + \mathbf{B}_0)\right), \tag{1}$$

where c is the speed of light. Gaussian units are used throughout the paper. The wave propagates at an arbitrary angle with respect to $\mathbf{B}_0$, which we assume to be along the z direction. Without loss of generality, the wave propagation vector is given by $\mathbf{k} = k_x\hat{\mathbf{x}} + k_z\hat{\mathbf{z}}$, and the electric field is

$$\mathbf{E} = \hat{\mathbf{x}}E_1\cos\Phi - \hat{\mathbf{y}}E_2\sin\Phi - \hat{\mathbf{z}}E_3\cos\Phi, \tag{2}$$

where $\hat{\mathbf{x}}$, $\hat{\mathbf{y}}$, and $\hat{\mathbf{z}}$ are unit vectors, $\Phi = k_x x + k_z z - \omega t$, and ω is the wave frequency. The wave magnetic field is given by the Maxwell equation: $\mathbf{B} = c/\omega(\mathbf{k}\times\mathbf{E})$. The relativistic momentum is $\mathbf{p} = m\gamma\mathbf{v}$, where $\gamma = (1 - v_\perp^2/c^2 - v_z^2/c^2)^{-1/2}$ is the Lorentz factor, $\mathbf{v}$ is the particle velocity, and $v_\perp$, v_z are the components perpendicular and parallel to $\mathbf{B}_0$, respectively. This interaction is resonant at multiples of the relativistic cyclotron frequency Ω. The resonance conditions are

$$\omega - k_z v_z - n\Omega = 0, \tag{3a}$$

$$\Omega = -qB_0/mc\gamma, \tag{3b}$$

where n is an integer; the nonrelativistic cyclotron frequency is denoted by Ω_c, where $\Omega = \Omega_c/\gamma$. The case of a circularly polarized wave (i.e., $E_1 = E_2$ and $E_3 = 0$) which propagates along $\mathbf{B}_0$ has been studied in Refs. 8–10. It has been shown[8] that to all orders in the field amplitudes, particles can be accelerated indefinitely provided that (1) the index of refraction $\eta = ck/\omega$ is equal to 1 and (2) the particle is initially at resonance with the $n = 1$ harmonic.

In this paper we extend the analytical results of Roberts and Buchsbaum[9] to waves of arbitrary polarizations, propagation angles, and refractive indices, by assuming that the field amplitudes become small compared to $|\mathbf{B}_0|$ as the propagation angle increases. Our analysis is also applicable to electrostatic modes, which appear as a particular application of our general results. We show that the net energy gain for any given harmonic resonance is always finite except in the case of circularly polarized waves with $\eta = 1$. To lowest order in field amplitudes, particles gain energy following certain trajectories in $(p_z, p_\perp)$ phase space. These trajectories may be opened or closed according to the magnitude of the wave magnetic field, the angle of propagation, and the value of refractive index η. We find that they are closed for electromagnetic fields that propagate at large angles, and hence the net energy gain is restricted to finite values. They can be opened for em waves that propagate at small angles, if η is small or equal to 1. For electrostatic waves (i.e., for small values of $|\mathbf{B}|$) the energy trajectories are always opened, and if resonances overlap, the net energy gain can be very large.

The total energy H is obtained from a set of nonlinear differential equations which depend on time, initial conditions, and the harmonic number n. In deriving these equa-

 0031-9171/87/123695-08$01.90

tions, we assume that the particle undergoes many cyclotron orbits before its energy changes appreciably. The slow time evolution of H is found by averaging over time scales associated with the motion of the wave and gyromotion, and satisfies equations of the form $(dH/dt)^2 + V_n(H) = 0$. For a given harmonic n, H oscillates in time within the Hamiltonian potential wells, and the maximum allowed energy gain is given by setting the potentials $V_n(H) = 0$. The widths of the potential wells are also given as functions of $|B|$ and the angle of propagation. We find that the resonance widths increase with the angle and decrease as $|B|$ increases. Besides, they are larger for particles that initially satisfy the resonance condition, Eq. (3). The particle motion becomes stochastic when the widths of potentials for different harmonics overlap, and then the mean net momentum transfer to the particles can be very large.

We apply our results to the acceleration of electrons in the ionosphere by considering an extraordinary mode propagating into a region of increasing plasma density. For the purpose of illustration, calculations are presented with a mode frequency $\omega = 1.8\Omega_e$; here Ω_e is evaluated in the Earth's magnetic field ($\Omega_e = 1.6$ MHz). We show that, at large angles of propagation, initially cold particles can be accelerated to large energies at power levels ($P \simeq 0.25$ W/cm^2). This happens near the critical density (cutoff) where the wave vector k and group velocity along k are zero and the wave amplitude is greatly enhanced.[3] In addition, we also find that the mode becomes purely circularly polarized near the cutoff layer, and its magnetic field amplitude is very small. Because the first and second cyclotron harmonic resonances overlap near the cutoff, initially cold particles which gain some energy interacting with the first harmonic can be picked up by the second and boosted to still higher energies. For small angles of propagation and at the power levels considered in our calculations, we find that resonances do not overlap so that initially cold particles only interact with the first harmonic. Because the resonance condition, Eq. (3), is far from being satisfied for $n = 1$, cold particles $v_z = 0$, and $\omega \simeq 2\Omega_e$, then the net energy gain for small angles of propagation is very small.

II. BASIC EQUATIONS

We start by considering that Eq. (1) admits the following three constants of motion[11]:

$$\frac{d}{dt}\left(\mathbf{p} - \frac{q}{c}\mathbf{r}\times\mathbf{B}_0 - \frac{k}{\omega}H + \frac{q}{c}\mathbf{A}\right) = 0, \tag{4}$$

where $\mathbf{r} = (x,y,z)$ is the vector position, $H = \gamma mc^2$ is the total particle energy including the rest energy, and A, the vector potential, is

$$\mathbf{A} = \hat{\mathbf{x}}cE_1/\omega \sin\Phi + \hat{\mathbf{y}}cE_2/\omega \cos\Phi - \hat{\mathbf{z}}cE_3/\omega \sin\Phi .$$

After multiplying the x component of Eq. (4) by k_z and the z component by k_x, we easily obtain

$$\dot{p}_z - (K_z/\omega)\dot{H} + (E_3/E_1)(\dot{p}_x + \Omega p_y) = 0, \tag{5}$$

where $K_z = k_z(1 + E_1k_x/E_3k_z)$. Hereafter, dots signify differentiation with respect to time.

The equations of motion for the perpendicular components of the particle momentum can also be written in the form

$$\dot{p}_x + p_y[\Omega + (qE_2/mc\gamma)(k_z/\omega)\sin\Phi] - (qE_1/\omega)(\omega - K_z\dot{z})\cos\Phi , \tag{6}$$

$$\dot{p}_y - p_x[\Omega + (qE_2/mc\gamma)(k_z/\omega)\sin\Phi] = -(qE_2/\omega)(\omega - k_z\dot{z})\sin\Phi . \tag{7}$$

In our calculations, we shall neglect the correction to the cyclotron frequency in Eqs. (6) and (7) by assuming $B_z = E_2ck_z/\omega \ll B_0$ (i.e., we assume that either $k_z = 0$ or E_2/B_0 is very small).

The evolution in time of the particle energy is given by

$$\frac{\dot{H}}{c^2\omega} = \frac{qE_1}{\omega}p_x\cos\Phi - \frac{qE_2}{\omega}p_x\sin\Phi - \frac{qE_3}{\omega}p_z\cos\Phi . \tag{8}$$

Equations (5)–(8) are the foundations of our theoretical analysis.

Before going into a detailed mathematical derivation, it is useful to consider the lowest-order solutions in the electric field amplitudes to Eqs. (5)–(7). If the electric field amplitude is small we may approximate x by

$$x = \rho\cos(\sigma + \alpha), \tag{9}$$

where $\sigma = \int_0^t \Omega(t')dt'$, $\tan\alpha = -p_{x0}/p_{y0}$, and $\rho = v_\perp/\Omega$ is the particle gyroradius. Hereafter, the subscript zero refers to the initial conditions at $t = 0$. To zeroth order in the electric field amplitudes, Eq. (5) yields

$$p_z = p_{z0} + (K_z/\omega)(H - H_0). \tag{10}$$

In terms of $p_\parallel$ and $p_\perp$, the components parallel and perpendicular to $\mathbf{B}_0$, respectively, Eq. (10) can also be written as

$$\left(\frac{p_\parallel}{mc}\right)^2 = -1 + \gamma_0^2\left(1 - \frac{1}{\beta_\phi}\frac{v_{\perp 0}}{c}\right)^2 + \frac{2}{\beta_\phi}\frac{p_\perp}{mc}\gamma_0\left(1 - \frac{v_{\perp 0}}{c}\frac{1}{\beta_\phi}\right) + \left(\frac{p_\perp}{mc}\right)^2\left(\frac{1}{\beta_\phi^2} - 1\right), \tag{11a}$$

$$\beta_\phi = \frac{ck_z}{\omega}\left(1 + \frac{E_3}{E_1}\frac{k_x}{k_z}\right), \tag{11b}$$

where γ_0 is the Lorentz factor evaluated at $t = 0$, and $v_{\perp 0}$ is also evaluated at $t = 0$. Note that depending on the magnitude of β_ϕ, Eq. (11) describes families of elliptical ($|\beta_\phi| > 1$), parabolic ($|\beta_\phi| = 1$), or hyperbolic ($|\beta_\phi| < 1$) trajectories in $(p_\parallel, p_\perp)$ phase space.

III. SOLUTION OF THE EQUATION OF MOTION

Equations (6) and (7) can be solved to all orders in the field amplitudes as functions of $\Phi = k_x x + k_z z - \omega t$ and

$$Q = (qE_1/\omega)(\omega - K_z\dot{z}) - (qE_2/\omega)(\omega - k_z\dot{z}), \tag{12a}$$

$$R = (qE_1/\omega)(\omega - K_z\dot{z}) + (qE_2/\omega)(\omega - k_z\dot{z}). \tag{12b}$$

We find

$$p_x = \frac{1}{2}\int_0^t [Q'\cos(\sigma - \sigma' + \Phi') + R'\cos(\sigma - \sigma' - \Phi')]dt' - p_\perp \sin(\sigma + \alpha), \tag{13a}$$

$$p_y = \frac{1}{2}\int_0^t [Q'\sin(\sigma - \sigma' + \Phi') + R'\sin(\sigma - \sigma' - \Phi')]dt' + p_\perp \cos(\sigma + \alpha). \tag{13b}$$

Primed and unprimed quantities are evaluated at times t' and t, respectively. After substituting these equations into Eq. (5) and integrating, we obtain

$$p_z = p_{z0} + \frac{K_z}{\omega}(H - H_0) - \frac{1}{2}\frac{E_3}{E_1}\int_0^t (Q' + R')\cos\Phi'\,dt'. \tag{14}$$

Equations (13) and (14) together with Eq. (8) give the following expression for the rate of change of particle energy:

$$\frac{4\dot{H}H}{c^2\omega} = \frac{q}{\omega}(E_1 + E_2)\left(\int_0^t Q'\cos(\sigma + \Phi - \sigma' + \Phi')dt' + \int_0^t R'\cos(\sigma + \Phi - \sigma' - \Phi')dt' - 2p_\perp \sin(\sigma + \Phi + \alpha)\right)$$
$$+ \frac{q}{\omega}(E_1 - E_2)\left(\int_0^t Q'\cos(\Phi - \sigma + \sigma' - \Phi')dt' + \int_0^t R'\cos(\Phi - \sigma + \Phi' + \sigma')dt' + 2p_\perp \sin(\Phi - \sigma - \alpha)\right)$$
$$- \frac{q}{\omega}E_3\left[4\left(p_{z0} + \frac{K_z}{\omega}(H - H_0)\right)\cos\Phi - \frac{E_3}{E_1}\int_0^t (Q' + R')[\cos(\Phi + \Phi') + \cos(\Phi - \Phi')]dt'\right]. \tag{15}$$

We note that polarizations represented in Eq. (15) are related to terms multiplying electric fields in right-hand ($E_1 + E_2$), left-hand ($E_1 - E_2$), and parallel E_3 modes.

Next, we substitute for x using Eq. (9) and define $\Upsilon = \sigma + \alpha + \pi/2$ and $\Psi = k_z z - \omega t$, so that $\Phi = \Psi + k_\perp \rho \sin\Upsilon$. After expanding the sine and cosine terms in Eq. (15) in the series of Bessel functions $J_n(\lambda)$, we obtain

$$\frac{4\dot{H}H}{c^2\omega} = \sum_n I_n, \tag{16a}$$

where

$$I_n = \frac{q}{\omega}(E_1 + E_2)J_{n-1}(\lambda)\left(\sum_m \int_0^t [Q'J_{m+1}(\lambda')\cos(n\Upsilon + m\Upsilon' + \Psi + \Psi') + R'J_{m-1}(\lambda')\cos(n\Upsilon - m\Upsilon' + \Psi - \Psi')]dt' + 2p_\perp \cos(n\Upsilon + \Psi)\right) + \frac{q}{\omega}(E_1 - E_2)J_{n+1}(\lambda)$$
$$\times\left(\sum_m \int_0^t [Q'J_{m+1}(\lambda')\cos(n\Upsilon - m\Upsilon' + \Psi - \Psi') + R'J_{m-1}(\lambda')\cos(n\Upsilon + m\Upsilon' + \Psi + \Psi')]dt' + 2p_\perp \cos(n\Upsilon + \Psi)\right) - \frac{qE_3}{\omega}J_n(\lambda)\left[4\left(p_{z0} + \frac{K_z}{\omega}(H - H_0)\right)\cos(n\Upsilon + \Psi) - \frac{E_3}{E_1}\sum_m \int_0^t (Q' + R')J_m(\lambda')[\cos(n\Upsilon + m\Upsilon' + \Psi + \Psi') + \cos(n\Upsilon - m\Upsilon' + \Psi - \Psi')]dt'\right], \tag{16b}$$

where $\lambda = k_\perp \rho$, and the summations are over all integer values from $-\infty$ to $+\infty$. Note that H can be split into rapidly fluctuating parts, which depend on the time scales associated with the motion of the wave (through the function Ψ) and with the gyromotion (through the function Υ), and a slowly time-varying part H^S. If $f(H)$ is any given function of the total energy, the slow time variation of f is obtained as

$$f(H)^S = \int_0^{2\pi}\frac{d\Upsilon}{2\pi}\int_0^{\pi}\frac{d\Psi}{\pi}f(H).$$

Our next step is to approximate $v_z \simeq (c^2/H)p_z$ in Q and R by the zeroth-order solution to Eq. (10). Here, every H function appearing in the definitions of v_z and p_z is given to lowest order by the slow time energy function H^S. The argument of the Bessel functions λ and the momentum p_z are also given in terms of H^S and initial conditions by means of Eqs. (10) and (11),

$$\lambda = \frac{ck_\perp}{\Omega_0}\left[1 - \frac{v_{\perp 0}^2}{c^2} - \frac{1}{\gamma_0^2} + 2U\left(1 - \beta_z\frac{v_{z0}}{c}\right) + U^2(1 - \beta_z^2)\right]^{1/2}, \tag{17}$$

where $\Omega_0 = -qB_0/mc\gamma_0$ is the relativistic cyclotron frequency evaluated at $t = 0$, and $U = (H^S - H_0^S)/H_0^S$ is the slow time evolution of the normalized particle energy. Differentiating Eq. (16b) with respect to time, we obtain the following:

$$I_n = \frac{q}{\omega}(E_1 + E_2)J_{n+1}(\lambda)\sum_m\{QJ_{m+n+1}(\lambda)\cos[(n+m)\Upsilon + 2\Psi] + RJ_{m-n-1}(\lambda)\cos[(n-m)\Upsilon]\}$$

$$+ \frac{q}{\omega}(E_1 - E_2)J_{n-1}(\lambda)\sum_m\{QJ_{m-n-1}(\lambda)\cos[(n-m)\Upsilon] + RJ_{m+n+1}(\lambda)\cos[(n+m)\Upsilon + 2\Psi]\}$$

$$+ \frac{q}{\omega}\frac{E_3^2}{E_1}J_n(\lambda)\sum_m(Q+R)J_m(\lambda)\{\cos[(n+m)\Upsilon + 2\Psi] + \cos[(n-m)\Upsilon]\} - (n\dot{\Upsilon} + \dot{\Psi})P_n\,. \tag{18}$$

where $n\dot{\Upsilon} + \dot{\Psi} = n\dot{\Omega} + k_z v_z = \omega$. The function P_n is defined by

$$P_n = \frac{q}{\omega}(E_1 + E_2)J_{n+1}(\lambda)\left(\sum_m\int_0^t[Q'J_{m-n-1}(\lambda')\sin(n\Upsilon + m\Upsilon' + \Psi + \Psi')\right.$$

$$\left. + R'J_{m+n+1}(\lambda')\sin(n\Upsilon - m\Upsilon' + \Psi - \Psi')]dt' + 2p_z\sin(n\Upsilon + \Psi)\right) + \frac{q}{\omega}(E_1 - E_2)J_{n-1}(\lambda)$$

$$\times\left(\sum_m\int_0^t[Q'J_{m-n+1}(\lambda')\sin(n\Upsilon - m\Upsilon' + \Psi - \Psi') + R'J_{m+n-1}(\lambda')\sin(n\Upsilon + m\Upsilon' + \Psi + \Psi')]dt'\right.$$

$$\left. + 2p_z\sin(n\Upsilon + \Psi)\right) + \frac{qE_3}{\omega}J_n(\lambda)\left[4\left(p_{z0} + \frac{K_z}{\omega}(H' - H_0^S)\right)\sin(n\Upsilon + \Psi)\right.$$

$$\left. - \frac{E_3}{E_1}\sum_m\int_0^t(Q' + R')J_m(\lambda')[\sin(n\Upsilon + m\Upsilon' + \Psi + \Psi') + \sin(n\Upsilon - m\Upsilon' + \Psi - \Psi')]dt'\right].$$

Differentiating P_n with respect to time, we obtain

$$\dot{P}_n = \frac{q}{\omega}(E_1 + E_2)J_{n+1}(\lambda)\sum_m\{QJ_{m+n+1}(\lambda)\sin[(n+m)\Upsilon + 2\Psi] + RJ_{m-n-1}(\lambda)\sin[(n-m)\Upsilon]\}$$

$$+ \frac{q}{\omega}(E_1 - E_2)J_{n-1}(\lambda)\sum_m\{QJ_{m-n-1}(\lambda)\sin[(n-m)\Upsilon] + RJ_{m+n+1}(\lambda)\sin[(n+m)\Upsilon + 2\Psi]\}$$

$$+ \frac{q}{\omega}\frac{E_3^2}{E_1}J_n(\lambda)\sum_m(Q+R)J_m(\lambda)\{\sin[(n+m)\Upsilon + 2\Psi] + \sin[(n-m)\Upsilon]\} + (n\dot{\Upsilon} + \dot{\Psi})I_n\,. \tag{19}$$

Since we are only interested in the slow time evolution of the total particle energy, we can average Eqs. (18) and (19) over the fast time dependencies (i.e., over Υ and Ψ) to find that only terms with $n = m$ give a nonzero contribution.[12] We also consider the contribution of a single (isolated) resonance, and then for each harmonic n, we find that the particle energy ($4H\dot{H}/c^2\omega = I_n^S$) obeys the following coupled differential equations:

$$\dot{I}_n^S = \frac{q}{\omega}(E_1 + E_2)RJ_{n+1}^2(\lambda) + \frac{q}{\omega}(E_1 - E_2)QJ_{n-1}^2(\lambda)$$

$$+ \frac{q}{\omega}\frac{E_3^2}{E_1}(Q+R)J_n^2(\lambda) - (n\dot{\Upsilon} + \dot{\Psi})P_n^S\,, \tag{20a}$$

$$\dot{P}_n^S = (n\dot{\Upsilon} + \dot{\Psi})I_n^S\,. \tag{20b}$$

The superscript S refers to the slow time contributions. Here, P_n^S is such that at $t = 0$ one has $P_n^S(0) = 4(H_0/c)^2\xi_n(0)\sin\delta_n$, where

$$\xi_n(0) = (v_{z0}/2c)\{-(\Sigma_1 + \Sigma_2)J_{n+1}(\lambda_0) + (\Sigma_2 - \Sigma_1)J_{n-1}(\lambda_0)] + (v_{z0}/c)\Sigma_3 J_n(\lambda_0)\,,$$

$$\delta_n = n(\alpha + \pi/2) + k_z z_0\,,$$

$$\Sigma_l = -(qE_l/\omega)(c/H_0)\,, \quad l = 1,2,3,$$

and all quantities with the subscript 0 are evaluated at $t = 0$. Combining Eqs. (10), (17), and (20) leads to a nonlinear equation for H as a function of time and initial conditions. Hereafter we shall drop the S on the function H, knowing that by H we always mean the slow time evolution of the particle energy. After multiplying by $H\dot{H}$, integrating once over time, and writing all expressions in terms of normalized quantities, we find (see the Appendix),

$$(U+1)^2\left(\frac{1}{\omega}\frac{dU}{dt}\right)^2 + V_n(U) = 0, \tag{21a}$$

$$V_n(U) = \frac{d_1^2}{4}U^2\left(U + \frac{2r_1}{d_1}\right)^2 - \xi_n(0)d_1U\left(U + \frac{2r_n}{d_1}\right)\sin\delta_n + \left(\frac{\Sigma_2 - \Sigma_1}{2}\right)$$

$$\times\{-(\Sigma_2 - \Sigma_1)[F_{n+1}(U) + G_{n+1}(U)] + (\Sigma_2\eta_z - \Sigma_1\beta_z)[(v_{z0}/c)F_{n+1}(U) + \beta_z G_{n+1}(U)]\}$$

$$- [(\Sigma_1+\Sigma_2)/2]\{(\Sigma_1+\Sigma_2)[F_{n-1}(U)+G_{n-1}(U)]$$
$$-(\beta_t\Sigma_1+\Sigma_2\eta_t)[(v_{t0}/c)F_{n-1}(U)+\beta_t G_{n-1}(U)]\}$$
$$-\Sigma_3^2\{G_n(U)+F_n(U)-\beta_t[(v_{t0}/c)F_n(U)+\beta_t G_n(U)]\}=[\xi_n(0)\cos\delta_n]^2, \quad (21b)$$

where $d_1\equiv 1-\eta_t\beta_t$, $\eta_t=ck_z/\omega$, β_t is defined in Eq. (11b), $r_n\equiv 1-k_z v_{z0}/\omega-n\Omega_e/\omega$, and

$$G_n(U)\equiv\int_0^U J_n^2[\lambda(U')]U'\,dU',$$
$$F_n(U)\equiv\int_0^U J_n^2[\lambda(U')]\,dU',$$

with $\nu\equiv n,n\pm 1$. This is just a differential equation describing the motion of trapped particles within the Hamiltonian potential well V_n. Under the limit $k_z\to 0$, Eqs. (21) reduce to the equations derived by Roberts and Buchsbaum[9] for the cases $n=\pm 1$. Note that in the limit $k_z\to 0$, Eqs. (21) and the Hamiltonian trajectories as defined in Eq. (10) are exact integrals to the equation of motion (i.e., they are valid to all orders in the field amplitudes).

IV. THE HAMILTONIAN POTENTIAL WELLS

We note that the first term of Eq. (21b) does not depend on the wave amplitude and is always positive for $d_1\neq 0$. The case $d_1=0$ corresponds to a circularly polarized wave with a refractive index $\eta=1$. If, in addition, $r_n=0$, then this term is zero and we are in the case of unlimited acceleration. For $d_1\neq 0$ and at large values of U, this first term dominates over all the others, and its contribution can be diminished by taking $r_n=0$ (i.e., particles initially at resonance with the wave). Thus V_n can be regarded as a potential well within which H oscillates as a function of time. The maximum value that H can attain for a given resonance and field amplitude can be found by setting the potentials $V_n(U)=0$. At wave amplitudes and propagation angles where the widths of potentials for different harmonics overlap, the particle motion becomes stochastic and at the net momentum transfer to the particle can be very large. Nevertheless, since λ (the argument of the Bessel functions) is given by the lower-order solution, Eq. (17), the amount of energy the particle can gain is limited according to the value of β_t. In fact, recall that the Hamiltonian trajectories as defined in Eqs. (11) are open hyperbolas for $|\beta_t|<1$ in a (p_z,p_t) phase space. For $\beta_t<-1$ they are closed ellipses and the range of accessible energy gain is restricted to finite values.

In order to better understand the physical meaning of β_t, let us consider the time average of the wave magnetic field

$$\langle B^2\rangle=(E_1^2/2)(\eta^2E_z^2/E_t^2+\beta_t^2). \quad (22)$$

Electrostatic waves are characterized by small values of β_t and of the product $\eta E_z/E_t$. Thus, the zeroth-order trajectories associated with electrostatic fields are open in a (p_z,p_t) phase space. For electromagnetic waves, β_t is large, in general. However, if the angle of propagation is small and if the refractive index is such that $\eta<1$, then $\beta_t\sim\eta_t$ and the Hamiltonian trajectories can also be open as is the case for circularly polarized waves with $\eta\lesssim 1$. If the angle of propagation is large, the allowable energy gain is limited even for $\eta<1$.

It is also instructive to study the behavior of V_n with respect to β_t. We consider only the case of particles which are initially at rest, i.e., $v_{z0}=v_{t0}=0$. Hence $U=\lambda-1$ and the potential well becomes

$$V_n(U)=(d_1^2U^2/4)(U+2r_n/d_1)^2+[(\Sigma_2-\Sigma_1)/2]\{(\Sigma_2-\Sigma_1)[G_{n+1}(U)+F_{n+1}(U)]$$
$$+\beta_t(\Sigma_2\eta_t-\Sigma\beta_t)G_{n+1}(U)\}-[(\Sigma_1+\Sigma_2)/2]\{(\Sigma_1+\Sigma_2)[G_{n-1}(U)+F_{n-1}(U)]$$
$$-\beta_t(\Sigma\beta_t+\Sigma_2\eta_t)G_{n-1}(U)\}-\Sigma_3^2[G_n(U)+F_n(U)-\beta_t^2G_n(U)] \quad (23)$$

Terms multiplying β_t in the right-hand and parallel polarization fields are always positive for any $\beta_t\neq 0$. Although the β_t term in the left-hand component may be negative, its contribution is small because the order of the Bessel function is higher. Therefore, we conclude that the larger β_t is, the smaller the widths of potential wells.

Finally, some comment should be made regarding the dependence of V_n on propagation angles. For initially cold particles with small gyroradii, all but the zeroth-order Bessel functions are very small. Since the argument of the Bessel functions is the perpendicular component of the wave vector k_z times the particle's gyroradius, increasing the propagation angle increases the value of the Bessel functions terms. Thus, for all but the first- and zeroth-order harmonics, the potential may not trap low-energy particles unless the propagation angle is large. The behavior of the potential for small values of k_z is as follows. For $k_z\to 0$ and $|n|>2$, only the first term of Eq. (23) is nonzero, and therefore no particles can be trapped. For $k_z\to 0$ and $n=\pm 1$, the right-hand polarization field may accelerate cold particles.

V. ELECTRON ACCELERATION IN THE IONOSPHERE

We consider an extraordinary mode propagating in a cold plasma at an angle θ with respect to $\mathbf{B}_0$. The dispersion relation is[11]

$$\eta^2=1-X/D, \quad (24a)$$
$$D=1-[Y^2/2(1-X)]\sin^2\theta$$
$$-\{[Y^2/2(1-X)]^2\sin^4\theta+Y^2\cos^2\theta\}^{1/2}, \quad (24b)$$

where $X=\omega_p^2/\omega^2$, ω_p is the electron plasma frequency, $Y=\Omega_e/\omega$, and $\Omega_e=eB_0/cm$. The electric field component ratios are given by

$$\frac{E_2}{E_1} = \frac{iXY}{(1-Y^2)(1-\eta^2)-X^2} \tag{25a}$$

$$\frac{E_3}{E_1} = \frac{\eta_x \eta_z}{1-X-\eta_z^2} . \tag{25b}$$

Combining Eqs. (25b) and (11b) we find

$$\beta_z = \eta_z(1-X)/(1-X-\eta_z^2) . \tag{26}$$

where η_x, η_z are the x and z components of the refractive index.

The magnitude of the electric field Σ_1 is given as a function of the power flow density P along k by solving for the following equation:

$$P = \frac{\omega^2 H_0^2}{q^2 c}\frac{v_g}{c}\frac{\Sigma_1^2}{16\pi}\left[\left(\frac{E_2}{E_1}\right)^2(1+\eta^2)+1+\left(\frac{E_3}{E_1}\right)^2+\beta_z^2\right] , \tag{27a}$$

where v_g, the group velocity along k, is given by

$$\frac{v_g}{c} = \frac{\eta}{1+\frac{1}{2}(D'\omega/D)(1-\eta^2)} . \tag{27b}$$

and $D' \equiv dD/d\omega$.

In our numerical calculations we assume that $\omega = 1.8\Omega_e$, where $\Omega_e \simeq 1.6$ MHz is the electron cyclotron frequency in the Earth's magnetic field. The wave propagates into a region of increasing plasma density until it reaches the cutoff point where k and v_g are zero. At the reflection point we find the following.

(i) The electron density is given by solving for $1-X=Y$, which in our case is $n = 4.65\times10^4$ cm^{-3} and corresponds to $\omega_{pe}/\Omega_e = 1.22$.

(ii) The electromagnetic mode becomes circularly polarized, i.e., $\Sigma_1 = \Sigma_2$, and $\Sigma_3 = 0$.

(iii) The magnetic field is zero because k, the propagation vector, is zero.

(iv) The electric field amplitude Σ_1 is very large because $v_g \simeq 0$.

(v) The resonance widths as obtained solving for $V_n(U) = 0$ are also large because β_z is zero.

We conclude that electron acceleration should be most effective near the turning point. In the following calculations we show that significant acceleration can indeed only take place near the cutoff layer.

Figure 1 shows the zeroth-order Hamiltonian trajectories for a low plasma density ($n = 3\times10^3$ cm^{-3}) at different angles of propagation. These trajectories are open (hyperbolic) for $\theta < \theta_T \simeq 14°$ and closed (elliptical) for larger angles. In all cases the refractive index is smaller than, but close to, unity ($\eta \simeq 0.95$). The ratio between the magnitudes of the wave magnetic and electric fields is also close to unity. For $\omega \simeq 2\Omega_e$ and for the power levels that are used in our calculations ($P \simeq 0.25$ W/cm^2), we find that the potentials are positive so that acceleration cannot take place. If the density is increased to 3.14×10^4 cm^{-3}, we find that electrons can gain about 12 keV through the interaction with the $n = 1$ harmonic.

In Figs. 2 and 3, the plasma density is 4.5×10^4 cm^{-3} which corresponds to $\omega_{pe}/\Omega_e = 1.2$, and the Hamiltonian

FIG. 1. Hamiltonian trajectories for different propagation angles to the magnetic field. The chosen parameters are $\omega_{pe}/\Omega_e = 0.3$ and $\omega = 1.8\Omega_e$. If $\theta = \theta_T$ the trajectory is a parabola, and it represents the transition angle between closed elliptical ($\theta < \theta_T$) and opened hyperbola ($\theta > \theta_T$) orbits.

trajectories are open for all angles of propagation. The net energy gain, as given by solving for the zeros of $V_n(U)$, is represented by the shaded regions as a function of θ. We consider the first two cyclotron harmonic resonances and assume that the particle is initially at rest. The first harmonic resonance interacts with cold particles through the contribution of the right-hand polarization field. The second harmonic does not interact with cold electrons even for the largest θ, because η, the refractive index, is very small ($\eta \simeq 0.25$). The energy that a particle can gain from the first harmonic is very limited because the resonance condition is far from being satisfied ($r_1 = 0.45$) for $v_{z0} = 0$ and $\omega \simeq 2\Omega_e$. For the second harmonic $r_2 = -0.1$, and the net energy gain can be larger. In Fig. 2, $P = 0.15$ W/cm^2, and the first and second harmonics barely overlap. In Fig. 3 where $P = 0.25$ W/cm^2, they fully overlap (double shaded region) for angles greater than 40°. The second harmonic may trap those electrons that have already gained some energy interacting with the first harmonic, and boost them to still higher energies. In fact, since $U \simeq \gamma - 1$, we see that the net energy gain can be as much as 150 keV.

In Fig. 4, we show the Hamiltonian potential wells as a function of the normalized particle energy U. We represent the inverse of the function W_n,

$$W_n(U) = -\mathrm{sgn}(V_n)\log[|V_n(U)|/(U+1)^2] . \tag{28}$$

The plasma parameters are those of Fig. 3, and we consider

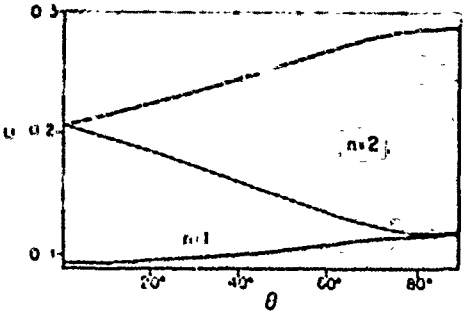

FIG. 2. Range of allowed energy gain (shaded regions) for the resonance harmonic numbers $n = 1,2$, as a function of wave propagation angle to magnetic field. The plasma frequency is such that $\omega_{pe}/\Omega_e = 1.2$, $\omega = 1.8\Omega_e$, and the total power flux is $P = 0.15$ W/cm^2.

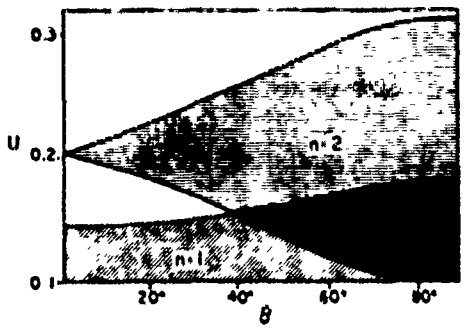

FIG. 3. The same as in Fig. 2 but with $P = 0.25$ W/cm^2.

two different angles of propagation: (a) $\theta = 80°$ and (b) $\theta = 20°$. The magnitudes of the potential wells, $|V_n(U)|$, are very small. For $\theta = 80°$ and $n = 2$ the maximum value of $|V_n|$ is of order 10^{-5}, and for $n = 1$ the maximum value is 2×10^{-3}. This is consistent with the assumption that the particle energy changes slowly over the gyro and wave periods. In fact, by normalizing time to Ω^{-1} in Eqs. (21) we see that $|V_n|(\omega/\Omega)^2$ must be much smaller than 1 if the changes in energy occur over many gyroperiods.

In the theory presented in Sec. III, we assume that the magnitude of the wave magnetic field is much smaller than that of the background magnetic field B_0 for increasing propagation angles. This allows us to use the zeroth-order solutions, Eqs. (9) and (10), in the perturbative analysis at large angles. In order to verify the validity of this approximation we have calculated the following dimensionless quantities:

$$B_x/B_0 = \eta_x(\omega/\Omega)\Sigma_2\gamma_0\,, \quad B_z/B_0 = \eta_z(\omega/\Omega)\Sigma_2\gamma_0\,,$$
$$B_y/B_0 = \beta_y(\omega/\Omega)\Sigma_1\gamma_0\,.$$

In the case of Fig. 4, we find that for $\theta = 80°$, $B_x/B_0 = 7\times10^{-2}$, $B_z/B_0 = 9\times10^{-4}$, and $B_y/B_0 = 1.3\times10^{-2}$. For $\theta = 20°$ these values are 1.5×10^{-2}, 4×10^{-2}, and 4×10^{-2}, respectively. The magnitude of the wave electric field as given by Σ_1 (recall that near the cutoff we have $\Sigma_1 \simeq \Sigma_2$ and $\Sigma_3 \simeq 0$) is found to be closed to 0.14 for all cases of Fig. 4.

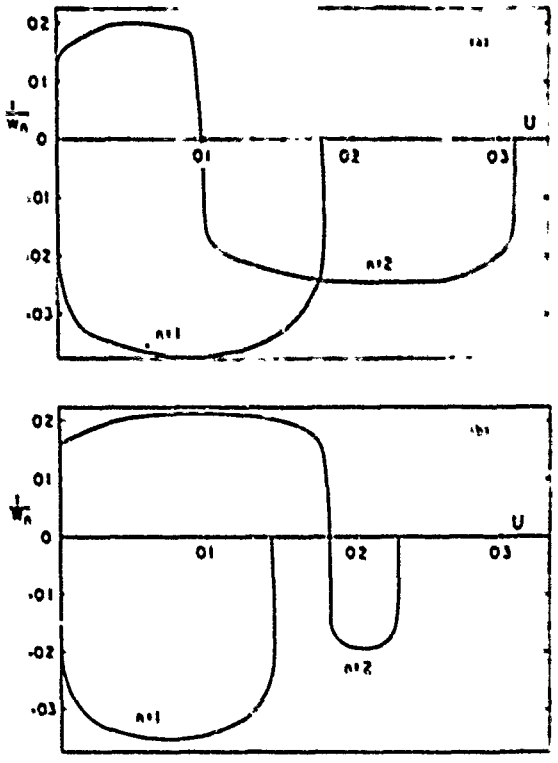

FIG. 4. Hamiltonian potential wells as represented by the functions $1/W_n$ [see Eq. (28)] as a function of particle energy for the plasma parameters of Fig. 3, and for two different angles of propagation: (a) $\theta = 80°$ and (b) $\theta = 20°$.

VI. CONCLUSION

In this paper, we have presented a theoretical analysis of the energy gained by relativistic charged particles in obliquely propagating electromagnetic waves. The main results of our analysis are as follows.

(1) To lower order in the field amplitudes, particles gain energy following certain trajectories in a $(p_\parallel, p_\perp)$ phase space. Because these trajectories are closed for large values of the magnetic field amplitude $|\mathbf{B}|$ and the propagation angle θ, the net energy is restricted to finite values. They are, however, open for large values of $|\mathbf{B}|$ and small values of θ if the refractive index η is smaller or equal to 1. For sufficiently small values of $|\mathbf{B}|$ they are always open.

(2) For a given harmonic resonance, the range of the allowed particle energies is obtained by solving for the zeros of the Hamiltonian potentials V_n. The resonance widths are always finite except for the case of circularly polarized waves with $\eta = 1$ and for particles that are initially in resonance with the $n = 1$ harmonic.

(3) Resonance widths are larger for particles that initially most closely satisfy the resonance condition. They increase as θ increases and decrease as $|\mathbf{B}|$ increases.

(4) The onset of stochasticity occurs when the widths of potentials for different harmonics overlap.

This analysis is limited to small field amplitudes in comparison with the dc magnetic field $\mathbf{B}_0$ at large values of θ, which is a good approximation for the calculations we have presented on the acceleration of ionospheric electrons. It is valid to all orders in the field amplitudes for small values of θ. We have shown that electrons can be accelerated by extraordinary-mode waves which propagate into a plasma of increasing density. At moderate power levels, acceleration occurs near the cutoff point for large angles. This is because of the following results.

(5) The extraordinary mode becomes purely circularly polarized and its magnetic field is zero.

(6) The electric field amplitude is largest at the turning point.

(7) The resonance widths are also larger.

(8) The first and second cyclotron harmonic resonances overlap for large propagation angles.

Depending on the location in the plasma where one wishes to accelerate electrons, the wave frequency should be chosen so that the cutoff point falls within that region. For continuous acceleration over large regions of the plasma, a

broad spectrum of waves should be considered. As the resonance widths overlap,[14] the electrons may gain considerable energy for different frequencies and harmonics. However, near the turning point the electric fields are so large that other nonlinear effects may also be important, and may affect both the acceleration and propagation processes. In addition, linear mode conversion into electrostatic waves[15] of large refractive indices can also be very relevant and may enhance the acceleration process by allowing initially cold particles to be picked up by the second- or higher-order harmonics. Questions related to the propagation of large-amplitude waves in the ionosphere and the consequent heating of plasma electrons deserve further attention.

ACKNOWLEDGMENTS

We are very grateful to Dr. A. Drobot and Dr. K. Papadopoulos for introducing us to this problem and for useful discussions. We also acknowledge helpful conversations with Dr M. Silevitch.

This work was supported by the U.S. Air Force under Contract No. F19628-85-K-0053.

APPENDIX: DERIVATION OF EQS. (21)

From Eq. (10) we obtain

$$1 - k_z v_z/\omega = d_1 + (H_0/H)d_2, \tag{A1}$$

$$1 - K_z v_z/\omega = h_1 + (H_0/H)h_2, \tag{A2}$$

$$n\dot{\Upsilon} + \dot{\Psi} = -[d_1 + (H_0/H)(d_2 - n\Omega_0/\omega)], \tag{A3}$$

where $d_1 = 1 - \eta_z\beta_z$, $d_2 = \eta_z(\beta_z - v_{z0}/c)$, $h_1 = 1 - \beta_z^2$, and $h_2 = \beta_z(\beta_z - v_{z0}/c)$.

By using Eq. (A3), integrating Eq. (20b) over time from zero to t, and recalling that $I_n^S = 4H\dot{H}/c^2\omega$, we find that the function $\chi = (n\dot{\Upsilon} + \dot{\Psi})P_n^S(t)/H$ is given by

$$\chi = -(H_0\omega/H^2)\{r_n P_n^S(0) + [d_1 P_n^S(0) - 4r_n^2 H_0^2/c^2]U - 6r_n(H_0^2/c^2)d_1U^2 - 2(H_0^2/c^2)d_1^2U^3\}. \tag{A4}$$

By substituting Eqs. (A1) and (A2) into Eqs. (12), we find Q and R as functions of H and initial conditions. Combining this with Eqs. (A4) and (20a), we obtain

$$H\ddot{H} - \frac{d}{dt}(H\dot{H}) - \frac{c^2\omega^2}{4}H\left(\frac{q}{\omega}(E_1 + E_2)(b_1H + H_0b_2)J_{n+1}^2(\lambda) + \frac{q}{\omega}(E_1 - E_2)(a_1H + H_0a_2)J_{n+1}^2(\lambda) + 2\frac{q^2}{\omega^2}E_1^2(b_1H + H_0b_2)J_n^2(\lambda)\right) - \frac{c^2\omega}{4}H^2H_0, \tag{A5}$$

where

$$a_1 = \frac{qE_1}{\omega}h_1 - \frac{qE_2}{\omega}d_1, \quad a_2 = \frac{qE_1}{\omega}h_2 - \frac{qE_2}{\omega}d_2,$$

$$b_1 = \frac{qE_1}{\omega}h_1 + \frac{qE_2}{\omega}d_1, \quad b_2 = \frac{qE_1}{\omega}h_2 + \frac{qE_2}{\omega}d_2.$$

Equation (A5) can be integrated once over time from 0 to t. The left-hand side becomes $\frac{1}{2}(H^2\dot{H}^2 - H_0^2\dot{H}_0^2)$. The contribution of the term $H_0\dot{H}_0$ can be calculated by means of Eq. (8). By considering that at $t = 0$, $\Phi_0 = k_x\rho_0\cos\alpha + k_z z_0$ and that $p_{x0} = -p_{10}\sin\alpha$, $p_{y0} = p_{10}\cos\alpha$, and expanding in terms of Bessel functions, we obtain

$$\frac{\dot{H}_0}{\omega H_0} = \sum_n \zeta_n(0)\cos\delta_n, \tag{A6}$$

where $\zeta_n(0)$ and δ_n are defined after Eqs. (20). Using Eq. (A6) and after a good deal of tedious but straightforward algebra, we arrive at Eqs. (21).

[1] D. B. Batchelor and R. C. Goldfinger, Nucl. Fusion 20, 403 (1980).
[2] T. Katsouleas and J. M. Dawson, Phys. Rev. Lett. 51, 392 (1983).
[3] G. R. Smith and A. N. Kaufman, Phys. Rev. Lett. 34, 1613 (1975); P. J. Palmadesso, Phys. Fluids 15, 2006 (1972).
[4] P. C. Clemmow and R. D. Harding, J. Plasma Phys. 23, 71 (1980).
[5] A. B. Kitsenko, I. M. Pankratov, and K. N. Stepanov, Sov. Phys. Tech. Phys. 20, 575 (1976).
[6] A. Y. Wong, J. Santoru, C. Darrow, L. Wang, and J. G. Roederer, Radio Sci. 18, 815 (1983).
[7] A. Y. Wong, J. Santoru, and G. G. Sivjee, J. Geophys. Res. 86, 7718 (1981).
[8] V. Ya. Davydovskii, Zh. Eksp. Teor. Fiz. 43, 886 (1962) [Sov. Phys. JETP 16, 629 (1963)]; A. A. Kolomenskii and A. N. Lebedev, Sov. Phys. Dokl. 7, 745 (1963).
[9] C. S. Roberts and S. J. Buchsbaum, Phys. Rev. A 135, 381 (1964).
[10] H. Motz and C. J. H. Watson, Adv. Electron Phys. 23, 153 (1967).
[11] M. L. Woolley, Plasma Phys. 13, 1141 (1971).
[12] Similar calculations can be found in the theory of quasilinear diffusion of particles; see, for instance, C. F. Kennel and F. Engelmann, Phys. Fluids 12, 2377 (1966).
[13] P. C. Clemmow and J. P. Dougherty, *Electrodynamics of Particles and Plasmas* (Addison-Wesley, London, 1969).
[14] B. V. Chirikov, Phys. Rep. 52, 263 (1979).
[15] V. E. Golant and A. D. Piliya, Sov. Phys. Usp. 14, 413 (1972).

Some Consequences of Intense Electromagnetic Wave Injection into Space Plasmas

By

William J. Burke[1], Elena Villalon[2], Paul L. Rothwell[1], and Michael Silevitch[2]

I Introduction

The past decade has been marked by an increasing interest in performing active experiments in space. These experiments involve the artificial injections of beams, chemicals, or waves into the space environment. Properly diagnosed, these experiments can be used to validate our understanding of plasma processes, in the absence of wall effects. Sometimes they even lead to practical results. For example, the plasma-beam device on SCATHA became the prototype of an automatic device now available for controlling spacecraft charging at geostationary orbit.

In this paper we discuss the future possibility of actively testing our current understanding of how energetic particles may be accelerated in space or dumped from the radiation belts using intense electromagnetic energy from ground based antennas. The ground source of radiation is merely a convenience. A space station source for radiation that does not have to pass through the atmosphere and lower ionosphere, is an attractive alternative. The text is divided into two main sections addressing the possibilities of (1) accelerating electrons to fill selected flux tubes above the Kennel-Petscheck limit for stably trapped fluxes and (2) using an Alfven maser to cause rapid depletion of energetic protons or electrons from the radiation belts. Particle acceleration by electrostatic waves have received a great deal of attention over the last few years (Wong et al., 1981; Katsouleas and Dawson, 1983). However, much less is known about acceleration using electromagnetic waves. The work described herein is still in evolution. We only justify its presentation at this symposium based on the novelty of the ideas in the context of space plasma physics and the excitement they have generated among several groups as major new directions for research in the remaining years of this century.

1. Air Force Geophysics Laboratory, Hanscom AFB, MA 01731

2. Center for Electromagnetic Research,
Northeastern University, Boston, MA 02115

II Electron Acceleration by Electromagnetic Waves

One of the first things we were mistaught in under graduate physics is that electromagnetic (em) waves can't accelerate charged particles. If the particle gains energy in the first half cycle, it loses it in the second half. Teachers are, of course, clever people who want graduate students. So they hold off discussing gyroresonance, in which case, all bets are off. The resonance condition is:

$$(1) \qquad \omega - k_z v_z - n \Omega_o / \gamma = 0$$

Here ω is the frequency of the driving wave, k_z the component of the wave vector along the zero order magnetic field $\underline{B_o} = B_o \hat{z}$, v_z the particle's component of velocity along $\underline{B_o}$ and n is an integer representing an harmonic of the gyrofrequency $\Omega_o = q B_o/m$, γ is the relativistic correction $(1 - v^2/c^2)^{-1/2}$, q is the charge, and m the rest mass of the electron.

Before going into a detailed mathematical analysis it is obvious that there are going to be problems accelerating cold ionospheric electrons to high energies. Higher than first gyroharmonics will have Bessel function multipliers where the argument of the Bessel function is the perpendicular component of the wave vector and the gyroradius. For cold electrons with small gyroradii, all but the zero index Bessel function terms will be small. The second concern can be understood by considering the motion of a charged particle in a circularly polarized wave. Roberts and Buchsbaum (1964) have shown that with an electron in gyroresonance according to eq.(1) and $\underline{v}_\perp$ initially antiparallel to the wave electric field $\underline{E}$ and perpendicular to the wave magnetic field $\underline{B}$, two effects combine to drive it away from resonance. As the electric field accelerates the electron, γ increases, changing the gyrofrequency. The magnetic component of the wave changes v_z and thus, the Doppler shift term. It is only in the case of the index of refraction $n = ck/\omega = 1$ that unrestricted acceleration occurs. In all other cases the electron goes through cycles gaining and losing kinetic energy.

Recently, the SAIC group (Menyuk et al. 1986) has devised a conceptually simple way to understand acceleration by em waves as a stochastic process. In terms of the relativistic momenta p_z and $p_\perp$, eq.(1) can be rewritten as

$$p_\perp^2 = (n_z^2 - 1) p_z^2 + 2 n_z p_z mc (n \Omega_o/\omega) + [(n \Omega_o/\omega)^2 - 1] mc^2$$

Depending on the phase velocity of the waves, equation (2) represents a family of ellipses ($n_z = ck_z/\omega < 1$), hyperbolae ($n_z > 1$) and parabolae ($n_z = 1$) in a $p_\perp$, p_z phase space. The zero order Hamiltonian can also be written in the form

$$(2) \qquad H_o/mc^2 = [1 + (p_z/mc)^2 + (p_\perp/mc)^2]^{1/2} - (p_z/mc)(\omega/ck_z)$$

Thus, in $p_\perp$, p_z space constant Hamiltonian surfaces represent families of hyperbolae ($n_z < 1$) ellipses ($n_z > 1$) and parabolae ($n_z = 1$). Hamiltonian surfaces have open topologies for indices of refraction $n_z < 1$. The case $n_z = 1$ in which resonance and Hamiltonian surfaces are overlying parabolae is that of unlimited acceleration studied by Roberts and Buschbaum (1964).

In the case of small amplitude waves the intersections of resonance and Hamiltonian surfaces in $p_\perp$, p_z space are very sharp. As the amplitudes of the waves grow so too do the widths of resonance. For sufficiently large amplitudes, resonance widths may extend down to low kinetic energies allowing cold electrons to be stochastically accelerated to relativistic energies.

It should be pointed out that although this model heuristically explains the main conceptual reasons for stochastic acceleration to occur, its validity extends only to small angles θ between $\underline{k}$ and $\underline{B}_0$. At large angles, it is not clear that the zero-order Hamiltonian topologies described above will still hold.

Over the past several months we have developed a rigorous extension of the analytical model of Roberts and Buchsbaum by letting $\underline{k} = k_x \hat{x} + k_z \hat{z}$ assume an arbitrary angle to $\underline{B}_0$. We begin with the Lorentz equation.

$$(3) \qquad \frac{d\underline{p}}{dt} = q \left[\underline{E} + \underline{v} \times (\underline{B}_0 + \underline{B}) \right]$$

The relativistic momentum and Hamiltonian are given by $\underline{p} = m \gamma \underline{v}$ and $H = mc^2 \gamma$, respectively. The magnetic field of the wave $\underline{B}$ is related to the electric $\underline{E}$ through Maxwell's equation $\underline{B} = (c/\omega)\underline{k} \times \underline{E}$. The time rate of change of the Hamiltonian is

$$(4) \qquad \dot{H} = q \underline{E} \cdot \underline{v} = qc^2 \underline{E} \cdot \underline{p}/H$$

If we define $E_x = E_1 \cos \phi$, $E_y = - E_2 \sin \phi$ and $E_z = - E_3 \cos \phi$, where $\phi = k_x x + k_z z - \omega t$ then equation (4) may be rewritten in the form

$$(5) \qquad \frac{H \dot{H}}{c^2 \omega} = \frac{qE_1}{\omega} p_x \cos \phi - \frac{qE_2}{\omega} p_y \sin \phi - \frac{qE_3}{\omega} p_z \cos \phi$$

The Lorentz force equation can also be rewritten as

$$(6)\quad \dot{p}_x + p_y \left[\Omega + \frac{qE_2}{m\gamma} \frac{k_x}{\omega} \sin\phi \right] = \frac{qE_1}{\omega} (\omega - K_z \dot{z}) \cos\phi$$

$$(7)\quad \dot{p}_y - p_x \left[\Omega + \frac{qE_2}{m\gamma} \frac{k_x}{\omega} \sin\phi \right] = -\frac{qE_2}{\omega} (\omega - k_z \dot{z}) \sin\phi$$

$$(8)\quad \dot{p}_z - \frac{K_z}{\omega} \dot{H} + \frac{E_3}{E_1} (\dot{p}_x + \Omega p_y) = 0$$

where $K_z = k_z (1 + E_3 k_x / E_1 k_z)$. Equations (5-8) are exact. Our first simplification is to assume $E_2 k_x / \omega = B_z << B_0$, then eqs. (6-8) may be combined to give

$$(9)\quad \frac{4\dot{H}H}{c^2 \omega} = \frac{q}{\omega} (E_1 + E_2) \left[\int_0^t Q' \cos(\sigma + \phi - \sigma' + \phi')\, dt' + \right.$$

$$+ \int_0^t R' \cos (\sigma + \phi - \sigma' - \phi') dt' - 2p_\perp \sin (\sigma + \phi + \alpha) \Big]$$

$$+ \frac{q}{\omega} (E_1 - E_2) \left[\int_0^t Q' \cos (\phi - \sigma + \sigma' - \phi')\, dt' \right.$$

$$+ \int_0^t R' \cos(\phi - \sigma + \phi' + \sigma')\, dt' + 2p_\perp \sin (\phi - \sigma - \alpha) \Big]$$

$$- \frac{q}{\omega} E_3 \left[4 \left(p_{zo} + \frac{K_z}{\omega} (H - H_0) \right) \cos\phi \right.$$

$$- \frac{E_3}{E_1} \int_0^t (Q' + R') \left[\cos(\phi + \phi') + \cos (\phi - \phi') \right] dt' \Big]$$

where $\sigma(t) = \int_0^t \Omega(t')\, dt'$, $\tan\alpha = -(p_{xo}/p_{yo})$,

(the subscript o refers to the initial conditions at $t = 0$), and

$$Q = \frac{qE_1}{\omega} (\omega - K_z \dot{z}) - \frac{qE_2}{\omega} (\omega - k_z \dot{z})$$

$$R = \frac{qE_1}{\omega} (\omega - K_z \dot{z}) + \frac{qE_2}{\omega} (\omega - k_z \dot{z})$$

Primed and unprimed quantities are evaluated at times t' and t, respectively. We note that accelarations represented in Eq. (9) are related to terms multiplying electric fields in right-hand ($E_1 + E_2$), left-hand ($E_1 - E_2$) and parallel E_3 modes.

Our next simplification is to substitute for x and $\dot{z}$ in eq.(9) the zero order solutions (in the electric field amplitude) of eqs. (6-8). That is, we take $x = \rho \cos(\sigma + \alpha)$ where $\rho = v_\perp / \Omega$ is the electron gyroradius and

$$(10) \qquad p_z = \left[p_{zo} + \frac{K_z}{\omega} (H - H_o) \right] .$$

We note that eq.(10) reduces to eq.(2) by taking $K_z = k_z$, which is only valid for small angles between $\underline{k}$ and $\underline{B}_o$. In fact, Figure 1 shows that Hamiltonians with open (hyperbolic or parabolic) topologies in p_z, $p_\perp$ space at small angles between $\underline{k}$ and $\underline{B}_o$ become closed (elliptical) as the angle increases. The practical implication is that cases of potentially infinite acceleration with $k = k_z$ become restricted to finite values at other direction of wave propagation.

By taking $x = \rho \cos(\sigma + \alpha)$ and expanding terms with $\sin k_x x$ and $\cos k_x x$ in series of Bessel functions, eq. (9) becomes

$$(11) \quad \frac{4H\dot{H}}{c^2 \omega} = \sum_n T_n$$

$$T_n = \frac{q}{\omega} (E_1 + E_2) J_{n-1} (k_x \rho) \left\{ \sum_m \int_o^t \left[Q' J'_{m+1} \cos(n\theta + m\theta' + \psi + \psi') + R' J'_{m-1} \cos(n\theta - m\theta' + \psi - \psi') \right] d\tau' + 2p_\perp \cos(n\theta + \Psi) \right\}$$

$$+ \frac{q}{\omega} (E_1 - E_2) J_{n+1} (k_x \rho) \left\{ \sum_m \int_o^t \left[Q' J'_{m+1} \cos(n\theta - m\theta' + \psi - \psi') + R' J'_{m-1} \cos(n\theta + m\theta' + \psi + \psi') \right] d\tau' + 2p_\perp \cos(n\theta + \Psi) \right\}$$

$$- \frac{qE_3}{\omega} J_n (k_x \rho) \left\{ 4 \left(p_{zo} + \frac{K_z}{\omega} (H - H_o) \right) \cos(n\theta + \Psi) - \frac{E_3}{E_1} \sum_m \int_o^t (Q' + R') J'_m \left[\cos(n\theta + m\theta' + \psi + \psi') + \cos(n\theta - m\theta' + \psi - \psi') \right] d\tau' \right\}$$

where $\theta = \int_o^t \Omega(\tau') d\tau' + \alpha + \pi/2$, $J'_\nu \equiv J_\nu (k_x \rho')$, $(\nu = m, m \pm 1)$
and $\psi = k_z z - \omega t$.

After averaging over the fast (gyroperiod) time dependencies and a good deal of tedious algebra, we obtain that, for each n, the particle energy obeys the following differential equation:

$$(12) \quad (U + 1)^2 \left(\frac{1}{\omega} \frac{dU}{dt} \right)^2 + V_n (U) = 0$$

where $U = (H - H_o)/H_o$ and

$$V_n(U) = \frac{d_1^2}{4} U^2 \left(U + 2 r_n/d_1 \right)^2 - \psi(o)\sin\phi_n \; d_1 U \left(U + 2r_n/d_1 \right)$$

$$+ \frac{\Sigma_1 - \Sigma_2}{2} \left[\left(\Sigma_2 d_1 - \Sigma_1 h_1 \right) \left(G_{n+1}(U) + F_{n+1}(U) \right) + \left(\Sigma_2 d_2 - \Sigma_1 h_2 \right) F_{n+1}(U) \right]$$

$$- \frac{\Sigma_1 + \Sigma_2}{2} \left[\left(\Sigma_1 h_1 + \Sigma_2 d_1 \right) \left(G_{n-1}(U) + F_{n-1}(U) \right) + \left(\Sigma_1 h_2 + \Sigma_2 d_2 \right) F_{n-1}(U) \right]$$

$$- \Sigma_3^2 \left[h_1 \left(G_n(U) + F_n(U) \right) + h_2 F_n(U) \right] - \left(\psi(0)\cos\phi_n \right)^2$$

where $\Sigma_i = -(q E_i/\omega)\, c/B_o \quad (i=1,2,3), \qquad d_1 = 1 - K_z k_z c^2/\omega^2$

$d_2 = K_z k_z c^2/\omega^2 - k_z \dot{z}_o/\omega, \qquad h_1 = 1 + K_z/k_z \,(d_1 - 1)$

$r_n = 1 - k_z \dot{z}_o/\omega - n\Omega_o/\omega, \qquad h_2 = K_z/k_z \; d_2$

$\psi(0) = v_{\perp o}/2c \left[-(\Sigma_1 + \Sigma_2) J_{n-1}(k_x \rho_o) + (\Sigma_2 - \Sigma_1) J_{n+1}(k_x \rho_o) \right] + v_{zo}/c \; \Sigma_3 J_n(k_x \rho_o),$

$\phi_n = n\left(\alpha + \frac{\pi}{2}\right) + k_z z_o$

and $G_\nu(U) = \int_o^U J_\nu^2 \left[k_x \rho(U') \right] U' \, dU'$

$F_\nu(U) = \int_o^U J_\nu^2 \left[k_x \rho(U') \right] dU', \quad (\nu = n, n \pm 1).$

Eq.(12) is in the form of the equations of a harmonic oscillator. Under the limit $\theta = 0$, Eq. (12) becomes the equation derived by Robert and Buchsbaum (1964). The limits of the particles excursion in energy for a given resonance n and electric field E can be found by setting the potentials $V_n(U) = 0$. At wave amplitudes where the range of potentials for different harmonics overlap, we have the onset of stochasticity.

At the present time we have just begun to explore the numerical solutions of equation (12). In Figure 2, we show some of our preliminary results. We assume that $\omega_{pe}/\Omega_o = 0.3$, the electric field amplitude is such that $\Sigma 1 = 0.1$, and the wave frequency is $\omega = 1.8\,\Omega_o$. We consider only the second cyclotron harmonic since this is the closest to satisfying the resonance condition, eq.(1), for initially cold electrons. The components of the wave electric field and the refractive index n are calculated from the cold plasma dispersion relation for electromagnetic waves at any arbitrary angle θ to B_o. It turns out that n is always smaller than, but very close to 1 ($n = 0.97$). The maximum allowed

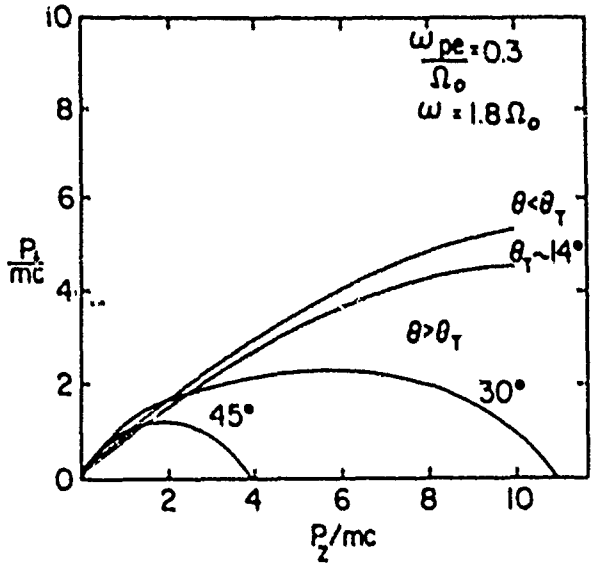

Fig. 1. Surfaces of zero order Hamiltonians with different propagation angles to magnetic field.

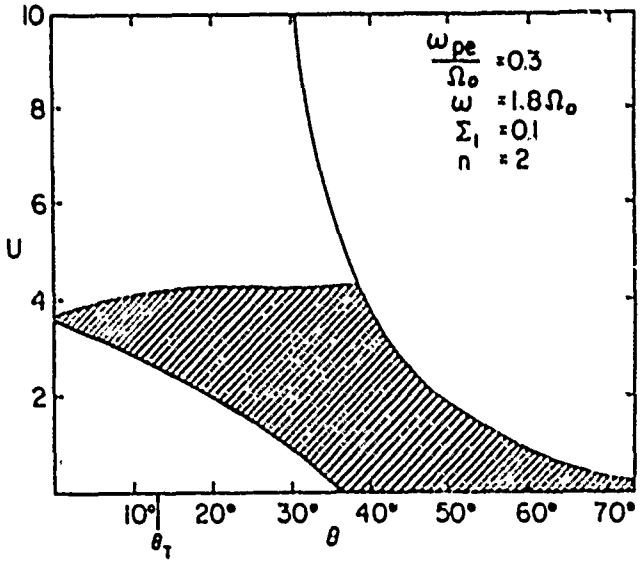

Fig. 2. Range of allowed electron energy gain (shaded) as a function of wave propagation angle to magnetic field. The solid line represents maximum energy excursion for elliptical topologies.

energy gain, as given by the zero order Hamiltonian topologies, is represented by the solid lines . The shaded region represents the actual energy gain as obtained by requiring V_n (U) < 0. We see that for $\theta = 35^\circ$, initially cold electrons can be accelerated to very high energies. In fact, for cold electrons we find that U = γ − 1 and that the particle can gain as much as 2.5 Mev. As θ decreases more initial kinetic energy is required for any acceleration to take place. For large θ , the elliptical hamiltonian topologies severely restrict the energy gain.

III The Alfven Maser

Active control of energetic particle fluxes in the radiation belts has maintained a continuing interest in both the United States and the Soviet Union. Electron dumping experiments concluded by the Stanford University and Lockheed groups using VLF transmissions are well known (Inan et al. 1982, Imhof et al. 1983). Perhaps less known is a theoretical paper by Trakhtengerts (1983) entitled "Alfven Masers" in which he proposes a theoretical scheme for dumping both electrons and protons from the belts. The basic idea is to use RF energy to heat the ionosphere at the foot of a flux tube to raise the height integrated conductivity. The conductivity is then modulated at VLF or ELF frequencies which modulates the reflection of waves that cause pitch angle diffusion in the equatorial plane. The artificially enhanced conductivity of the ionosphere thus maintains high wave energy densities in the associated flux tube, thereby, producing a masing effect.

In addition to external ionospheric perturbations particle precipitation also raises ionospheric conductivity. The masing of the VLF waves causes further precipitation which, in principle, results in an explosive instability. The purpose of this section is to establish the basic equations and to present the results of a preliminary computer simulation.

The fundamental equations derived by Trakhtengerts (1983) are based on quasilinear theory and relate only to the weak diffusion regime. It is useful to use similar set of equations derived by Schulz (1974) based on phenomenological arguments that includes strong pitch angle diffusion. The key variables are N, the number of trapped particles per unit area on a flux tube and c the wave intensity averaged over the flux tube. In this we assume that c is directly proportioned to the pitch angle diffusion coefficient. The time rate of change for N is

$$(13) \quad \frac{dN}{dt} = \frac{-A\, c\, N}{1 + c\, \tau} + S.$$

where the first term represent losses due to pitch angle scattering with A a constant and S accounts for represents particle source terms in the magnetospheric equatorial plane. τ is a parameter that characterizes lifetimes against strong pitch angle diffusion. The time rate of change of c is given by

$$(14) \quad \frac{d\, c}{dt} = \frac{\left(2\, \gamma\, {}^*N/N^* \right)}{1 + c\tau}\, c + \frac{V_g\, c}{L R_e} \ln R + W$$

The first term represents wave growth near the equatorial plane, the second term gives the wave losses in and through the ionosphere and the third accounts for any wave energy sources. The terms γ^* and N^* are used to denote the weak diffusion growth rate and column density of a flux tube at the Kennel and Petschek (1966) limit for stably trapped particles. In the second term, v_g/LR_e approximates bounce frequency of waves where v_g is the group velocity of the wave LR_e the approximate length of a flux tube; R is the reflection coefficient of the ionosphere. Since $R < 1$ the second term is always negative. The $(1 + c\ \tau)$ term empirically lowers growth rate due to the pitch angle distribution becoming more isotropic under strong diffusion conditions.

In our present study we have examined numerical solutions of equations (13) and (14) using non-equilibrium initial conditions. The first case is represented by Figure 3 in which we started initial wave energy densities which are a factor of 3 (top panel) and 0.1 (bottom panel) above the Kennel-Petschek limit. In both cases we ignored associated enhancements in ionospheric coupling that lead to increased reflectivity. We see that the wave energy density quickly damps to the Kennel-Petschek equilibrium represented by the solid line.

In the second level of simulation the wave energy density is initially set at a factor of three above the Kennel-Petschek equilibrium value but includes a coupling factor to the ionosphere ζ. We find that for values of $\zeta \geq 10\%$ the oscillations become spike-like. The top panel of Figure 4 represents the normalized wave energy density for $\zeta = 10\%$ after the waves have evolved into periodic spikes. The middle and bottom panels of Figure 4 represent the normalized energetic particle density (cm^{-2}) contained on a flux tube and the normalized height integrated density of the ionosphere. Attention is directed to the phase relationship between the maxima of the three curves. The maximum, energetic particle flux leads the wave term and goes through the Kennel-Petschek value as the wave growth changes from positive to negative.

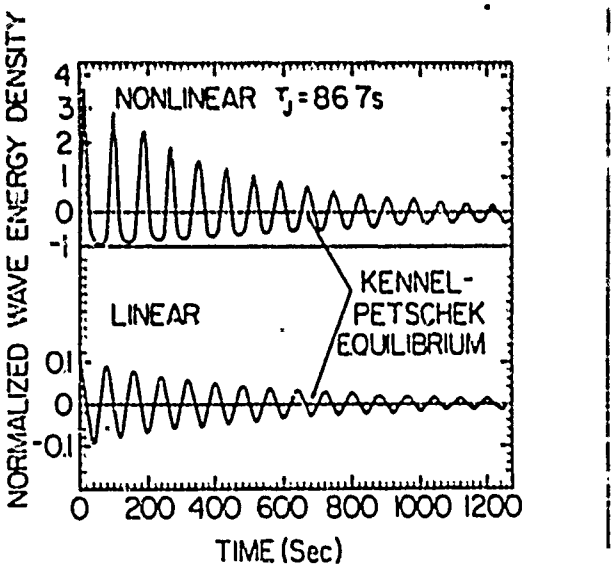

Fig. 3. Example of wave energy densities initially set at factors of 3.0 and 0.1 above Kennel Petschek equilibrium value.

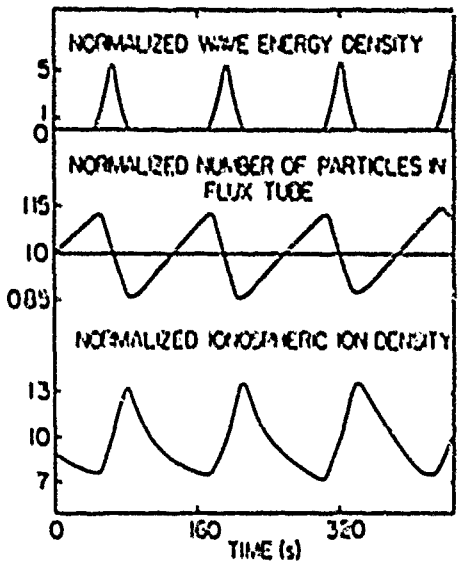

Fig. 4. Example of spike-like wave structures as well as energetic particle losses and ionospheric density changes with magnetosphereionosphere coupling.

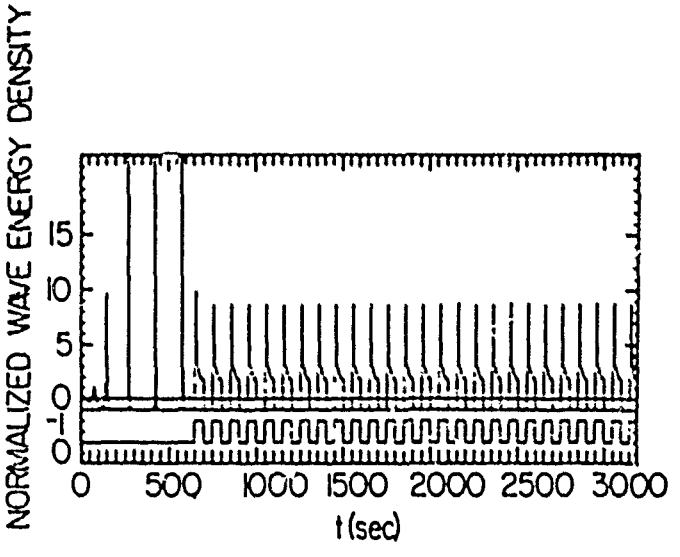

Fig. 5. Simulated, normalized wave energy density with magnetosphere-ionosphere coupling. A VLF source is turned on at t = 650s.

The maximum ionospheric effect occurs after the wave spike maximum. Our physical interpretation of Figure 4 is as follows. A spike in the wave energy density causes a depletion of electrons trapped in the belts to levels well below the Kennel-Petschek limit. The subsequent drop of precipitating electron flux allows the ionospheric conductivity to decrease. Thus, VLF waves are less strongly reflected back into the magnetosphere. This effectively raises the Kennel-Petschek limit as higher particle fluxes are necessary to offset increased ionospheric VLF absorbtion. In the presence of equatorial sources of particles, the similations show flux levels building to 1.15 times the Kennel-Petschek limit. The enhanced fluxes in the magnetosphere, even with weak pitch angle diffusion, allows the ionospheric conductivity to rise, eventually leading to another masing spike.

Figure (5) shows the effect of an external VLF signal. The first few spikes result from the masing effect of the ionosphere due to particle precipitation. At t = 650 seconds a VLF square wave source is turned on with a 50 second duration. The spikes now are modulated at the driving frequency at a reduced amplitude. The amplitude is reduced since the fluxes are more frequently dumped with the VLF signal present than in its absence.

Iversen et al. (1984) using simultaneous ground and satellite measurements, have recently observed the modulation of precipitating electron at pulsation frequencies. In terms of our simulations these would be close to the situation shown in Figure 4 in which natural masing occurs in a flux tube. The observed frequencies are consistent with those expected from the linear theory. Detailed comparison with experimental data necessitates knowing the efficiency with which VLF waves reach the ionosphere.

IV Conclusion

Although the work presented in this paper is still in a very preliminary stage of development it appears that significant space effects can be produced by the injection of intense electromagnetic waves into ionospheric plasmas. In the coming months we expect that as calculations mature we will grow in the ability to translate mathematical representation into physical understanding. If the results of our analyses live up to early promise then a series of ground-based wave emission experiments will be developed to measure injection effects in space. The upcoming ECHO-7 experiment presents a well instrumented target of opportunity for electron acceleration experiments with the HIPAS system. After the launch of the CRRES satellite it will be possible to make simultaneous in situ measurements of wave and particle fluxes in artificially excited Alfven Masers. Looking forward to the 1990's it appears that WISP experiment planned for the Space Station will make an ideal source for both electron acceleration and radiation belt depletion experiments. Recently a Soviet experiment measured electrons accelerated to kilovolt energies using a low power telemetry system (Babaev et al., 1983). Just imagine what could be done with the specifically designed, high power WISP!

References

Babaev, A.P., S.B. Lyakhov, G.G. Managadze, A.A. Martinson and P.P. Timofeev, Plasma particle acceleration due to emission of ground-based and onboard transmitters, in Active Experiments in Space, ESA SP-195 61-65, 1983.

Imhof, W.L., J.B. Reagan, H.D. Voss, E.E. Gaines, D.W. Datlowe, J. Mobilia, R.A. Helliwell, U.S. Inan, J. Katsufrakis, and R.G. Joiner, Direct observation of radiation belt electrons precipitated by the controlled injection of VLF signals from a ground based transmitter, Geophys. Res. Lett., 4, 361 - 364, 1983.

Imhof, W.L., H.D. Voss, J.B. Reag[illegible] D.S. Evans, Relativistic electron and energetic ion precipita[illegible] the magnetopause, J. Geophys. Res., 91, 3077 - 3088, 1986

Inan, U.S., T.F. Bell and H. C[illegible] precipitation induced by short duration VLF waves in the magneto[illegible], 87, 6243 - 6264, 1982.

Iversen, I.B., L.P. Block, K. Bronstad, A. Grad, G. Haerendel, H. Junginger, A Korth, G. Kremser M. Madsen, J. Niskanen, W. Riedler, P. Tanskanen, K.M. Torkar, and S. Ullaland, Simultaneous observations of a pulsation event from the ground with balloons and with a geostationary satellite on August 12, 1978, J. Geophys. Res., 89, 6775 - 6785, 1984.

Katsouleas, T., and J.M. Dawson, Unlimited electron acceleration in laser driven plasma waves, Phys. Rev. Lett., 51, 392 - 395, 1983.

Kennel, C.F., and H.E. Petschek, Limit on stably trapped particle fluxes, J. Geophys. Res., 71, 1 - 28, 1966.

Menyuk, C.R., A.T. Drobot, K. Papadopoulos and H. Karimabadi, Stochastic electron acceleration in obliquely propagating electromagnetic waves, SAIC Preprint, 1986

Roberts, C.S., and S.J. Buchsbaum, Motion of a charged particle in a constant magnetic field and a transverse electromagnetic field, Phys. Rev., 135, A381, 1964.

Schulz, M., Particle saturation of the outer zone: a nonlinear model, Astrophys. and Space Sci., 29, 232 - 242, 1974.

Trakhtengerts, V.Yu., Alfven masers, in Active Experiments in Space, ESA SP-195, 67 - 74, 1983.

Wong, A.Y., J. Santoru, and G.G. Sivjee, Active stimulation of the auroral plasma, J. Geophys. Res., 86, 7718 - 7732, 1981.